

POLITECNICO DI TORINO
Department of Energy
Master Thesis in Electrical Engineering



Comparison of Models and Implementation of Virtual Synchronous Generators

Author: Vincenzo Mallemaci

Supervisor: Prof. Radu Bojoi

Advisor: Fabio Mandrile

October 2020

Acknowledgements

Nonostante la tesi sia redatta in lingua inglese, ritengo corretto porgere i miei ringraziamenti in lingua italiana.

Prima di tutto vorrei davvero ringraziare il mio co-relatore Fabio Mandrile e il mio relatore Radu Bojoi per il loro aiuto e la loro disponibilità. Grazie alla loro guida ho appreso molto, anche oltre l'argomento di questa tesi.

A conclusione di questo percorso quinquennale mi sento in dovere di ringraziare tutte le persone che mi sono state vicine. A cominciare dalla mia famiglia, a chi c'è e chi non c'è più, perchè mi ha trasmesso il senso del dovere e del lavoro, credendo sempre in me. Grazie mamma, papà e Salvo, per avermi supportato in ogni scelta e in ogni istante.

Trasferirsi dalla Sicilia a Torino 5 anni fa non è stato facile, ma grazie a Dino e Sonia ha pesato un po' di meno.

Ringrazio i colleghi e gli amici conosciuti nel corso degli anni, perchè da tutti ho potuto imparare qualcosa di nuovo.

Grazie Domenica, inesauribile fonte di forza e affetto. Grazie per i consigli, la fiducia e la pazienza con cui mi sei sempre stata accanto.

Vincenzo

Abstract

In the last years, the issue of global warming and emission of greenhouse gases led to a major interest and exploitation of renewable energy sources (RESs). The most promising renewable power generators (RPGs) are based on solar and wind energy. To interface them with the grid, power electronics converters, in particular inverters, are needed.

The scientific and technological progresses in this field are enabling their integration into the grid. So, in the next future, it is expected to reach a higher and higher penetration of them.

The grid stability is strictly linked with the presence of the synchronous generators (SGs) of hydro/thermal plants, because they can provide ancillary services and support the grid. Static converters do not embed such features and conventional control techniques are not suitable to solve this problem. Therefore, the spread of RPGs is limited because it would lead the grid to become more and more unstable.

To solve this issue, many solutions were proposed in literature, under the name of Virtual Synchronous Generator (VSG). With this different approach, it is possible to make static converters mimic synchronous generators or even outdo them, limiting the problem of grid instability.

The goal of my master thesis is to implement and compare VSG models available in the literature by means of PLECS simulations and experimental tests using a specific laboratory setup at the Power Electronics Innovation Center (PEIC), in order to highlight advantages and disadvantages of each technique.

Contents

1	Introduction	1
1.1	Climate Change	1
1.2	Renewable Energy Sources and Grid Converters	4
1.3	Stability of the Electric Grid	6
1.4	Regulations and Grid Codes	7
1.4.1	General Aspects	7
1.4.2	Active Power Regulation	8
1.4.3	Voltage Regulation	9
1.5	The Concept of Virtual Synchronous Generator	10
1.6	Goal of the Thesis and My Contributions	11
2	General Aspects of VSGs	13
2.1	General Structure	13
2.2	Grid Synchronization	16
2.2.1	Phase Locked Loop: PLL	17
2.3	The Role of Inertia	20
2.4	Droop Control	22
2.5	Implementation of VSG Solutions	24
2.5.1	List of VSGs Solutions	24
2.5.2	PLECS Models	25
2.5.3	C-code Realisation	26
2.5.4	Current-Output Models	28
2.5.5	Voltage-Output Models	30
2.5.6	Linearised Model for Active Control	32
2.5.7	Linearised Model of the Excitation Control	35
2.6	List of Tests	38
3	Synchronverter	42
3.1	Base version of Synchronverter	42
3.2	Enhanced version of Synchronverter	45

4	Osaka	48
4.1	Model Description and Implementation	48
5	VISMA	51
5.1	Model Description and Implementation	51
6	VISMA1	58
6.1	Model Description and Implementation	58
7	VISMA2	61
7.1	Model Description and Implementation	61
8	SPC	65
8.1	Model Description and Implementation	65
8.2	Power Loop Controller	67
8.2.1	Synchronous Generator Emulation	67
8.2.2	PI Regulator	68
8.2.3	Lead-Lag	68
9	VSYNC	70
9.1	Model Description and Implementation	70
10	Kawasaki	74
10.1	Model Description and Implementation	74
11	CVSM	77
11.1	Model Description and Implementation	77
12	Experimental Tests and Outcomes	82
12.1	Experimental Setup	82
12.2	Synchronverter	87
12.2.1	Active and Reactive Power References	87
12.2.2	Inertial Response	89
12.2.3	Harmonic Distortion	90
12.2.4	Voltage Dips	91
12.3	Osaka	95
12.3.1	Active and Reactive Power References	95
12.3.2	Inertial Response	97
12.3.3	Harmonic Distortion	98
12.3.4	Voltage Dips	99
12.4	VISMA	104
12.4.1	Active and Reactive Power References	104

12.4.2	Inertial Response	106
12.4.3	Harmonic Distortion	106
12.4.4	Voltage Dips	107
12.5	VISMA1	113
12.5.1	Stability Analysis	113
12.5.2	Active and Reactive Power References	114
12.5.3	Inertial Response	116
12.5.4	Harmonic Distortion	117
12.5.5	Voltage Dips	118
12.6	VISMA2	122
12.6.1	Active and Reactive Power References	122
12.6.2	Inertial Response	124
12.6.3	Harmonic Distortion	125
12.6.4	Voltage Dips	126
12.7	SPC	130
12.7.1	Active and Reactive Power References	130
12.7.2	Inertial Response	135
12.7.3	Harmonic Distortion	137
12.7.4	Voltage Dips	139
12.8	VSYNC	149
12.8.1	Active and Reactive Power References	149
12.8.2	Inertial Response	151
12.8.3	Harmonic Distortion	152
12.8.4	Voltage Dips	153
12.9	Kawasaki	157
12.9.1	Stability Analysis	157
12.9.2	Active and Reactive Power References	158
12.9.3	Inertial Response	159
12.9.4	Harmonic Distortion	160
12.9.5	Voltage Dips	161
12.10	CVSM	165
12.10.1	Active and Reactive Power References	165
12.10.2	Inertial Response	166
12.10.3	Harmonic Distortion	167
12.10.4	Voltage Dips	168
13	Comparison of VSG Solutions	176
13.1	Active Power Reference	176
13.2	Reactive Power Reference	177
13.3	Inertial Response	179
13.4	Harmonic Distortion	181

13.5 Voltage Dips	182
13.6 Final Result	184
14 Conclusions	185
Appendix A Base Values	191
Bibliography	193

List of Tables

2.1.1	LCL Filter Parameters.	15
2.2.1	PLL Parameters.	20
2.5.1	List of VSG solutions module.	24
2.5.2	PI Parameters.	29
2.5.3	Parameters for Active Control.	35
2.5.4	Parameters for Excitation Control.	38
2.6.1	Voltage Dips chosen for tests.	41
12.1.1	Main data of the experimental setup.	83
13.1.1	Active Power Reference: comparison.	177
13.2.1	Reactive Power Reference: comparison.	179
13.3.1	Inertial Response: comparison.	181
13.4.1	Harmonic Distortion: comparison.	182
13.5.1	Voltage Dips: comparison.	184
13.6.1	Final comparison.	184
14.0.1	Main pros and cons of the analysed VSG solutions.	186

List of Figures

1.1.1	Land-ocean temperature index, change from 1880 to 2019. Source: NASA.	1
1.1.2	Land-ocean temperature index, 1880 to present. Source: NASA.	2
1.1.3	Cumulative ice mass loss from the Greenland and Antarctic ice sheets. Source: EEA.	2
1.1.4	Observed change in global mean sea level. Source: EEA.	3
1.1.5	Global anthropogenic CO ₂ emissions. Source: IPCC.	4
1.2.1	Renewable electricity generation by Wind and Solar PV, World 1995-2017. Source: IEA.	5
1.2.2	Electricity generation by fuel and scenario, 2018-2040. Source: IEA [2].	5
1.2.3	Conventional scheme of connection between PV plant and grid.	6
1.4.1	Active Power Regulation Curve for Wind and PV plants. Source: [6, 7]	9
1.4.2	FRT Curves for Wind and PV plants. Source: [6, 7]	10
1.5.1	General structure for VSG concept.	11
2.1.1	Hardware block diagram adopted for every VSG solution.	14
2.1.2	LCL Filter.	15
2.2.1	Scheme of connection between inverter and grid.	16
2.2.2	Vectorial representation during: (a) transient; (b) steady state.	17
2.2.3	Basic Structure of PLL.	17
2.2.4	PLL block scheme.	19
2.5.1	Simplified scheme with average model.	25
2.5.2	Block scheme for PI regulator tuning.	28
2.5.3	Equivalent circuit for current-output models.	29
2.5.4	Equivalent circuit for voltage-output models.	30

2.5.5	Simplified circuit of connection between VSG's stator and grid for active control tuning.	32
2.5.6	Linearised model in pu of VSG's stator connected to the grid.	33
2.5.7	Simplified circuit of connection between VSG's stator and grid for excitation control tuning.	36
2.5.8	Linearised model in pu of VSG's excitation control [30]. . .	36
2.6.1	Frequency profile to evaluate the inertial response of VSGs.	40
2.6.2	Voltage Dips incidence in mixed networks according to PD IEC/TR 61000-2-8:2002.	41
3.1.1	Synchronverter's control scheme for the base version in Laplace domain.	42
3.2.1	Synchronverter's control scheme for the enhanced version in the Laplace domain.	45
4.1.1	Osaka's control scheme in Laplace domain.	48
5.1.1	VISMA's control scheme in Laplace domain: general structure.	51
5.1.2	VISMA's control scheme in Laplace domain: stator windings.	52
5.1.3	VISMA's control scheme in Laplace domain: damper winding on the d-axis (top) and q-axis (bottom).	54
5.1.4	VISMA's control scheme in Laplace domain: excitation winding.	55
5.1.5	VISMA's control scheme in Laplace domain: swing equation.	56
6.1.1	VISMA1's control scheme in Laplace domain.	58
6.1.2	VISMA1's excitation block.	60
7.1.1	VISMA2's control scheme in Laplace domain.	61
7.1.2	VISMA2's excitation block.	63
7.1.3	VISMA2's equivalent circuit.	64
8.1.1	SPC's control scheme in Laplace domain.	65
8.2.1	SPC SG: Block scheme of swing equation.	67
8.2.2	SPC PI's governor.	68
9.1.1	VSYNC's control scheme in Laplace domain.	70
10.1.1	Kawasaki's control scheme in Laplace domain.	74
11.1.1	CVSM's control scheme in Laplace domain.	77

11.1.2	CVSM's control scheme: Measuring Processing (top) and Active Damping (bottom).	78
11.1.3	CVSM's control scheme: Reactive Power Droop Controller (top); Virtual Inertia and Power Control (bottom).	79
11.1.4	CVSM's control scheme: Virtual Impedance.	80
11.1.5	CVSM's control scheme: Voltage Control.	80
11.1.6	CVSM's control scheme: Current Control.	81
12.1.1	From left to right: (a) Block scheme of the experimental setup; (b) Experimental setup at the laboratory of PEIC.	82
12.1.2	From left to right: (a) Regatron Grid Emulator; (b) PLECS RT Box and PLECS grid model.	84
12.1.3	From left to right: (a) Grid-side filters; (b) three phase inverter.	85
12.1.4	Delta Elektronika AD/DC power supply.	85
12.1.5	From left to right: (a) dSPACE module; (b) Oscilloscope and dSPACE interface.	86
12.2.1	Synchronverter's response to active power reference step from 0.3 to 0.4 pu, from left to right: (a) Grid-side currents; (b) Active power (top) and Synchronverter's frequency (bottom).	87
12.2.2	Synchronverter's response to reactive power reference step from 0.3 to 0.4 pu with droop control disabled, from left to right: (a) Grid-side currents; (b) Reactive power (top) and electromotive force (bottom).	88
12.2.3	Synchronverter's response to reactive power reference step from 0.3 to 0.4 pu with droop control enabled, from left to right: (a) Grid-side currents; (b) Reactive power (top) and electromotive force (bottom).	89
12.2.4	Synchronverter's response to grid frequency variation of -0.42 Hz, from left to right: (a) Grid-side currents; (b) Active power (top) and Synchronverter's frequency (bottom).	90
12.2.5	From left to right: (a) PCC Phase Voltage with 5% of fifth harmonic (top) and its FFT (bottom) with Synchronverter's current references disabled; (b) PCC Phase Voltage with 5% of fifth harmonic (top) and grid-side currents (bottom) with Synchronverter's current references disabled.	90

12.2.6	From left to right: (a) PCC Phase Voltage with 5% of fifth harmonic (top) and its FFT (bottom) with Synchronverter's current references enabled; (b) PCC Phase Voltage with 5% of fifth harmonic (top) and grid-side currents (bottom) with Synchronverter's current references enabled.	91
12.2.7	Synchronverter's response to voltage dip type 1, with reactive droop control disabled, from left to right: (a) PCC line voltages (top) and grid-side currents (bottom); (b) Reactive power (top) and electromotive force (bottom).	92
12.2.8	Synchronverter's response to voltage dip type 1, with reactive droop control enabled, from left to right: (a) PCC line voltages (top) and grid-side currents (bottom); (b) Reactive power (top) and electromotive force (bottom).	92
12.2.9	Synchronverter's response to voltage dip type 2, with reactive droop control disabled, from left to right: (a) PCC line voltages (top) and grid-side currents (bottom); (b) Reactive power (top) and electromotive force (bottom).	93
12.2.10	Synchronverter's response to voltage dip type 2, with reactive droop control enabled, from left to right: (a) PCC line voltages (top) and grid-side currents (bottom); (b) Reactive power (top) and electromotive force (bottom).	93
12.2.11	Synchronverter's response to voltage dip type 3, with reactive droop control disabled, from left to right: (a) PCC line voltages (top) and grid-side currents (bottom); (b) Reactive power (top) and electromotive force (bottom).	94
12.2.12	Synchronverter's response to voltage dip type 3, with reactive droop control enabled, from left to right: (a) PCC line voltages (top) and grid-side currents (bottom); (b) Reactive power (top) and electromotive force (bottom).	94
12.3.1	Osaka's response to active power reference step from 0.3 to 0.4 pu, from left to right: (a) Grid-side currents; (b) Active power (top), Osaka's frequency (center) and PCC voltage amplitude (bottom).	96
12.3.2	Osaka's response to reactive power reference step from 0.3 to 0.4 pu with reactive droop control disabled, from left to right: (a) Grid-side currents; (b) Reactive power (top) and electromotive force (bottom).	97
12.3.3	Osaka's response to reactive power reference step from 0.3 to 0.4 pu with reactive droop control enabled, from left to right: (a) Grid-side currents; (b) Reactive power (top) and electromotive force (bottom).	97

12.3.4	Osaka's response to grid frequency variation of -0.42 Hz, from left to right: (a) Grid-side currents; (b) Active power (top), Osaka's frequency (center) and PCC voltage amplitude (bottom).	98
12.3.5	From left to right: (a) PCC Phase Voltage with 5% of fifth harmonic (top) and its FFT (bottom) with Osaka disabled; (b) PCC Phase Voltage with 5% of fifth harmonic (top) and grid-side currents (bottom).	99
12.3.6	From left to right: (a) PCC Phase Voltage with 5% of fifth harmonic (top) and its FFT (bottom) with Osaka enabled; (b) PCC Phase Voltage with 5% of fifth harmonic (top) and grid-side currents (bottom).	99
12.3.7	Osaka's response to voltage dip type 1, with reactive droop control disabled, from left to right: (a) PCC line voltages (top) and grid-side currents (bottom); (b) Reactive power (top) and electromotive force (bottom).	101
12.3.8	Osaka's response to voltage dip type 1, with reactive droop control enabled, from left to right: (a) PCC line voltages (top) and grid-side currents (bottom); (b) Reactive power (top) and electromotive force (bottom).	101
12.3.9	Osaka's response to voltage dip type 2, with reactive droop control disabled, from left to right: (a) PCC line voltages (top) and grid-side currents (bottom); (b) Reactive power (top) and electromotive force (bottom).	102
12.3.10	Osaka's response to voltage dip type 2, with reactive droop control enabled, from left to right: (a) PCC line voltages (top) and grid-side currents (bottom); (b) Reactive power (top) and electromotive force (bottom).	102
12.3.11	Osaka's response to voltage dip type 3, with reactive droop control disabled, from left to right: (a) PCC line voltages (top) and grid-side currents (bottom); (b) Reactive power (top) and electromotive force (bottom).	103
12.3.12	Osaka's response to voltage dip type 3, with reactive droop control enabled, from left to right: (a) PCC line voltages (top) and grid-side currents (bottom); (b) Reactive power (top) and electromotive force (bottom).	103
12.4.1	VISMA's response to active power reference step from 0.3 to 0.4 pu, from left to right: (a) Grid-side currents; (b) Active power (top) and VISMA's frequency (bottom).	104

12.4.2	VISMA's response to reactive power reference step from 0.3 to 0.4 pu with reactive droop control disabled, from left to right: (a) Grid-side currents; (b) Reactive power (top) and electromotive force (bottom).	105
12.4.3	VISMA's response to reactive power reference step from 0.3 to 0.4 pu with reactive droop control enabled, from left to right: (a) Grid-side currents; (b) Reactive power (top), excitation flux linkage (center), voltages (bottom).	105
12.4.4	VISMA's response to grid frequency variation of -0.42 Hz, from left to right: (a) Grid-side currents; (b) Active power (top) and VISMA's frequency (bottom).	106
12.4.5	From left to right: (a) PCC Phase Voltage with 5% of fifth harmonic (top) and its FFT (bottom) with VISMA's current references disabled; (b) PCC Phase Voltage with 5% of fifth harmonic (top) and grid-side currents (bottom) with VISMA's current references disabled.	107
12.4.6	From left to right: (a) PCC Phase Voltage with 5% of fifth harmonic (top) and its FFT (bottom) with VISMA's current references enabled; (b) PCC Phase Voltage with 5% of fifth harmonic (top) and grid-side currents (bottom) with VISMA's current references enabled.	107
12.4.7	VISMA's response to voltage dip type 1, with reactive droop control disabled, from left to right: (a) PCC line voltages (top) and grid-side currents (bottom); (b) Reactive power (top), excitation flux linkage (center), voltages (bottom).	108
12.4.8	VISMA's response to voltage dip type 1, with reactive droop control enabled, from left to right: (a) PCC line voltages (top) and grid-side currents (bottom); (b) Reactive power (top), excitation flux linkage (center), voltages (bottom).	109
12.4.9	VISMA's response to voltage dip type 2, with reactive droop control disabled, from left to right: (a) PCC line voltages (top) and grid-side currents (bottom); (b) Reactive power (top), excitation flux linkage (center), voltages (bottom).	110
12.4.10	VISMA's response to voltage dip type 2, with reactive droop control enabled, from left to right: (a) PCC line voltages (top) and grid-side currents (bottom); (b) Reactive power (top), excitation flux linkage (center), voltages (bottom).	110

12.4.11	VISMA's response to voltage dip type 3, with reactive droop control disabled, from left to right: (a) PCC line voltages (top) and grid-side currents (bottom); (b) Reactive power (top), excitation flux linkage (center), voltages (bottom).	111
12.4.12	VISMA's response to voltage dip type 3, with reactive droop control enabled, from left to right: (a) PCC line voltages (top) and grid-side currents (bottom); (b) Reactive power (top), excitation flux linkage (center), voltages (bottom).	112
12.5.1	VISMA1's response to reactive power reference equal to 0.1 pu, from left to right: (a) Grid-side currents with $l_v = 0.1$ pu; (b) inverter currents with $l_v = 0.2$ pu.	114
12.5.2	VISMA1's response to active power reference step from 0.1 to 0.2 pu, with $l_v = 0.1$ from left to right: (a) Grid-side currents before the step; (b) Active power (top) and currents (bottom).	114
12.5.3	VISMA1's response to active power reference step from 0.3 to 0.4 pu: (a) Grid-side currents; (b) Active power (top) and VISMA1's frequency (bottom).	115
12.5.4	VISMA1's response to reactive power reference step from 0.3 to 0.4 pu with reactive droop control disabled, from left to right: (a) Grid-side currents; (b) Reactive power (top) and electromotive force (bottom).	116
12.5.5	VISMA1's response to reactive power reference step from 0.3 to 0.4 pu with reactive droop control enabled, from left to right: (a) Grid-side currents; (b) Reactive power (top) and electromotive force (bottom).	116
12.5.6	VISMA1's response to grid frequency variation of -0.42 Hz, from left to right: (a) Grid-side currents; (b) Active power (top) and frequency (bottom).	117
12.5.7	From left to right: (a) PCC Phase Voltage with 5% of fifth harmonic (top) and its FFT (bottom) with VISMA1's current references disabled; (b) PCC Phase Voltage with 5% of fifth harmonic (top) and grid-side currents (bottom) with VISMA1's current references disabled.	117
12.5.8	From left to right: (a) PCC Phase Voltage with 5% of fifth harmonic (top) and its FFT (bottom) with VISMA1's current references enabled; (b) PCC Phase Voltage with 5% of fifth harmonic (top) and grid-side currents (bottom) with VISMA1's current references enabled.	118

12.5.9	VISMA1's response to voltage dip type 1, with reactive droop control disabled, from left to right: (a) PCC line voltages (top) and grid-side currents (bottom); (b) Reactive power (top) and electromotive force (bottom).	119
12.5.10	VISMA1's response to voltage dip type 1, with reactive droop control enabled, from left to right: (a) PCC line voltages (top) and grid-side currents (bottom); (b) Reactive power (top) and electromotive force (bottom).	119
12.5.11	VISMA1's response to voltage dip type 2, with reactive droop control disabled, from left to right: (a) PCC line voltages (top) and grid-side currents (bottom); (b) Reactive power (top) and electromotive force (bottom).	120
12.5.12	VISMA1's response to voltage dip type 2, with reactive droop control enabled, from left to right: (a) PCC line voltages (top) and grid-side currents (bottom); (b) Reactive power (top) and electromotive force (bottom).	120
12.5.13	VISMA1's response to voltage dip type 3, with reactive droop control disabled, from left to right: (a) PCC line voltages (top) and grid-side currents (bottom); (b) Reactive power (top) and electromotive force (bottom).	121
12.5.14	VISMA1's response to voltage dip type 3, with reactive droop control enabled, from left to right: (a) PCC line voltages (top) and grid-side currents (bottom); (b) Reactive power (top) and electromotive force (bottom).	121
12.6.1	VISMA2's response to active power reference step from 0.3 to 0.4 pu: (a) Grid-side currents; (b) Active power (top) and VISMA2's frequency (bottom).	122
12.6.2	VISMA2's response to reactive power reference step from 0.3 to 0.4 pu with reactive droop control disabled, from left to right: (a) Grid-side currents; (b) Reactive power (top) and electromotive force (bottom).	123
12.6.3	VISMA2's response to reactive power reference step from 0.3 to 0.4 pu with reactive droop control enabled, from left to right: (a) Grid-side currents; (b) Reactive power (top) and electromotive force (bottom).	124
12.6.4	VISMA2's response to grid frequency variation of -0.42 Hz, from left to right: (a) Grid-side currents; (b) Active power (top) and frequency (bottom).	125

12.6.5	From left to right: (a) PCC Phase Voltage with 5% of fifth harmonic (top) and its FFT (bottom) with VISMA2 disabled; (b) PCC Phase Voltage with 5% of fifth harmonic (top) and grid-side currents (bottom) with VISMA2 disabled.	125
12.6.6	From left to right: (a) PCC Phase Voltage with 5% of fifth harmonic (top) and its FFT (bottom) with VISMA2 enabled; (b) PCC Phase Voltage with 5% of fifth harmonic (top) and grid-side currents (bottom) with VISMA2 enabled.	126
12.6.7	VISMA2's response to voltage dip type 1, with reactive droop control disabled, from left to right: (a) PCC line voltages (top) and grid-side currents (bottom); (b) Reactive power (top) and electromotive force (bottom).	127
12.6.8	VISMA2's response to voltage dip type 1, with reactive droop control enabled, from left to right: (a) PCC line voltages (top) and grid-side currents (bottom); (b) Reactive power (top) and electromotive force (bottom).	127
12.6.9	VISMA2's response to voltage dip type 2, with reactive droop control disabled, from left to right: (a) PCC line voltages (top) and grid-side currents (bottom); (b) Reactive power (top) and electromotive force (bottom).	128
12.6.10	VISMA2's response to voltage dip type 2, with reactive droop control enabled, from left to right: (a) PCC line voltages (top) and grid-side currents (bottom); (b) Reactive power (top) and electromotive force (bottom).	128
12.6.11	VISMA2's response to voltage dip type 3, with reactive droop control disabled, from left to right: (a) PCC line voltages (top) and grid-side currents (bottom); (b) Reactive power (top) and electromotive force (bottom).	129
12.6.12	VISMA2's response to voltage dip type 3, with reactive droop control enabled, from left to right: (a) PCC line voltages (top) and grid-side currents (bottom); (b) Reactive power (top) and electromotive force (bottom).	129
12.7.1	SPC SG's response to active power reference step from 0.3 to 0.4 pu, from left to right: (a) Grid-side currents; (b) Active power (top) and frequency (bottom).	131
12.7.2	SPC PI's response to active power reference step from 0.3 to 0.4 pu, from left to right: (a) Grid-side currents; (b) Active power (top) and frequency (bottom).	131
12.7.3	SPC LL's response to active power reference step from 0.3 to 0.4 pu, from left to right: (a) Grid-side currents; (b) Active power (top) and frequency (bottom).	132

12.7.4	SPC SG's response to reactive power reference step from 0.3 to 0.4 pu with reactive droop control disabled, from left to right: (a) Grid-side currents; (b) Reactive power (top) and electromotive force (bottom).	133
12.7.5	SPC PI's response to reactive power reference step from 0.3 to 0.4 pu with reactive droop control disabled, from left to right: (a) Grid-side currents; (b) Reactive power (top) and electromotive force (bottom).	133
12.7.6	SPC LL's response to reactive power reference step from 0.3 to 0.4 pu with reactive droop control disabled, from left to right: (a) Grid-side currents; (b) Reactive power (top) and electromotive force (bottom).	134
12.7.7	SPC SG's response to reactive power reference step from 0.3 to 0.4 pu with reactive droop control enabled, from left to right: (a) Grid-side currents; (b) Reactive power (top) and electromotive force (bottom).	134
12.7.8	SPC PI's response to reactive power reference step from 0.3 to 0.4 pu with reactive droop control enabled, from left to right: (a) Grid-side currents; (b) Reactive power (top) and electromotive force (bottom).	135
12.7.9	SPC LL's response to reactive power reference step from 0.3 to 0.4 pu with reactive droop control enabled, from left to right: (a) Grid-side currents; (b) Reactive power (top) and electromotive force (bottom).	135
12.7.10	SPC SG's response to grid frequency variation of -0.42 Hz, from left to right: (a) Grid-side currents; (b) Active power (top) and frequency (bottom).	136
12.7.11	SPC PI's response to grid frequency variation of -0.42 Hz, from left to right: (a) Grid-side currents; (b) Active power (top) and frequency (bottom).	137
12.7.12	SPC LL's response to grid frequency variation of -0.42 Hz, from left to right: (a) Grid-side currents; (b) Active power (top) and frequency (bottom).	137
12.7.13	From left to right: (a) PCC Phase Voltage with 5% of fifth harmonic (top) and its FFT (bottom) with SPC's current references disabled; (b) PCC Phase Voltage with 5% of fifth harmonic (top) and grid-side currents (bottom).	138
12.7.14	From left to right: (a) PCC Phase Voltage with 5% of fifth harmonic (top) and its FFT (bottom) with SPC SG's current references enabled; (b) PCC Phase Voltage with 5% of fifth harmonic (top) and grid-side currents (bottom).	138

12.7.15	From left to right: (a) PCC Phase Voltage with 5% of fifth harmonic (top) and its FFT (bottom) with SPC PI's current references enabled; (b) PCC Phase Voltage with 5% of fifth harmonic (top) and grid-side currents (bottom).	139
12.7.16	From left to right: (a) PCC Phase Voltage with 5% of fifth harmonic (top) and its FFT (bottom) with SPC LL's current references enabled; (b) PCC Phase Voltage with 5% of fifth harmonic (top) and grid-side currents (bottom).	139
12.7.17	SPC SG's response to voltage dip type 1, with reactive droop control disabled, from left to right: (a) PCC line voltages (top) and grid-side currents (bottom); (b) Reactive power (top) and electromotive force (bottom).	140
12.7.18	SPC PI's response to voltage dip type 1, with reactive droop control disabled, from left to right: (a) PCC line voltages (top) and grid-side currents (bottom); (b) Reactive power (top) and electromotive force (bottom).	140
12.7.19	SPC LL's response to voltage dip type 1, with reactive droop control disabled, from left to right: (a) PCC line voltages (top) and grid-side currents (bottom); (b) Reactive power (top) and electromotive force (bottom).	141
12.7.20	SPC SG's response to voltage dip type 1, with reactive droop control enabled, from left to right: (a) PCC line voltages (top) and grid-side currents (bottom); (b) Reactive power (top) and electromotive force (bottom).	141
12.7.21	SPC PI's response to voltage dip type 1, with reactive droop control enabled, from left to right: (a) PCC line voltages (top) and grid-side currents (bottom); (b) Reactive power (top) and electromotive force (bottom).	142
12.7.22	SPC LL's response to voltage dip type 1, with reactive droop control enabled, from left to right: (a) PCC line voltages (top) and grid-side currents (bottom); (b) Reactive power (top) and electromotive force (bottom).	142
12.7.23	SPC SG's response to voltage dip type 2, with reactive droop control disabled, from left to right: (a) PCC line voltages (top) and grid-side currents (bottom); (b) Reactive power (top) and electromotive force (bottom).	143
12.7.24	SPC PI's response to voltage dip type 2, with reactive droop control disabled, from left to right: (a) PCC line voltages (top) and grid-side currents (bottom); (b) Reactive power (top) and electromotive force (bottom).	143

12.7.25	SPC LL's response to voltage dip type 2, with reactive droop control disabled, from left to right: (a) PCC line voltages (top) and grid-side currents (bottom); (b) Reactive power (top) and electromotive force (bottom).	144
12.7.26	SPC SG's response to voltage dip type 2, with reactive droop control enabled, from left to right: (a) PCC line voltages (top) and grid-side currents (bottom); (b) Reactive power (top) and electromotive force (bottom).	144
12.7.27	SPC PI's response to voltage dip type 2, with reactive droop control enabled, from left to right: (a) PCC line voltages (top) and grid-side currents (bottom); (b) Reactive power (top) and electromotive force (bottom).	145
12.7.28	SPC LL's response to voltage dip type 2, with reactive droop control enabled, from left to right: (a) PCC line voltages (top) and grid-side currents (bottom); (b) Reactive power (top) and electromotive force (bottom).	145
12.7.29	SPC SG's response to voltage dip type 3, with reactive droop control disabled, from left to right: (a) PCC line voltages (top) and grid-side currents (bottom); (b) Reactive power (top) and electromotive force (bottom).	146
12.7.30	SPC PI's response to voltage dip type 3, with reactive droop control disabled, from left to right: (a) PCC line voltages (top) and grid-side currents (bottom); (b) Reactive power (top) and electromotive force (bottom).	146
12.7.31	SPC LL's response to voltage dip type 3, with reactive droop control disabled, from left to right: (a) PCC line voltages (top) and grid-side currents (bottom); (b) Reactive power (top) and electromotive force (bottom).	147
12.7.32	SPC SG's response to voltage dip type 3, with reactive droop control enabled, from left to right: (a) PCC line voltages (top) and grid-side currents (bottom); (b) Reactive power (top) and electromotive force (bottom).	147
12.7.33	SPC PI's response to voltage dip type 3, with reactive droop control enabled, from left to right: (a) PCC line voltages (top) and grid-side currents (bottom); (b) Reactive power (top) and electromotive force (bottom).	148
12.7.34	SPC LL's response to voltage dip type 3, with reactive droop control enabled, from left to right: (a) PCC line voltages (top) and grid-side currents (bottom); (b) Reactive power (top) and electromotive force (bottom).	148

12.8.1	VSYNC's response to active power reference step from 0.3 to 0.4 pu: (a) Grid-side currents; (b) Active power (top) and VSYNC's frequency (bottom).	149
12.8.2	VSYNC's response to reactive power reference step from 0.3 to 0.4 pu with reactive droop control disabled, from left to right: (a) Grid-side currents; (b) Reactive power (top) and voltage reference amplitude (bottom).	150
12.8.3	VSYNC's response to reactive power reference step from 0.3 to 0.4 pu with reactive droop control enabled, from left to right: (a) Grid-side currents; (b) Reactive power (top) and voltage reference amplitude (bottom).	151
12.8.4	VSYNC's response to grid frequency variation of -0.42 Hz, from left to right: (a) Grid-side currents; (b) Active power (top) and frequency (bottom).	151
12.8.5	From left to right: (a) PCC Phase Voltage with 5% of fifth harmonic (top) and its FFT (bottom) with VSYNC's current references disabled; (b) PCC Phase Voltage with 5% of fifth harmonic (top) and grid-side currents (bottom) with VSYNC's current references disabled.	152
12.8.6	From left to right: (a) PCC Phase Voltage with 5% of fifth harmonic (top) and its FFT (bottom) with VSYNC's current references enabled; (b) PCC Phase Voltage with 5% of fifth harmonic (top) and grid-side currents (bottom) with VSYNC's current references enabled.	152
12.8.7	VSYNC's response to voltage dip type 1, with reactive droop control disabled, from left to right: (a) PCC line voltages (top) and grid-side currents (bottom); (b) Reactive power (top) and voltage reference amplitude (bottom).	153
12.8.8	VSYNC's response to voltage dip type 1, with reactive droop control enabled, from left to right: (a) PCC line voltages (top) and grid-side currents (bottom); (b) Reactive power (top) and voltage reference amplitude (bottom).	154
12.8.9	VSYNC's response to voltage dip type 2, with reactive droop control disabled, from left to right: (a) PCC line voltages (top) and grid-side currents (bottom); (b) Reactive power (top) and voltage reference amplitude (bottom).	154
12.8.10	VSYNC's response to voltage dip type 2, with reactive droop control enabled, from left to right: (a) PCC line voltages (top) and grid-side currents (bottom); (b) Reactive power (top) and voltage reference amplitude (bottom).	155

12.8.11	VSYNC's response to voltage dip type 3, with reactive droop control disabled, from left to right: (a) PCC line voltages (top) and grid-side currents (bottom); (b) Reactive power (top) and voltage reference amplitude (bottom).	155
12.8.12	VSYNC's response to voltage dip type 3, with reactive droop control enabled, from left to right: (a) PCC line voltages (top) and grid-side currents (bottom); (b) Reactive power (top) and voltage reference amplitude (bottom).	156
12.9.1	Kawasaki's response to reactive power reference step from 0.2 to 0.3 pu, with $x = 0.1$ from left to right: (a) Grid-side currents before the step; (b) Reactive power (top) and currents (bottom).	157
12.9.2	Kawasaki's response to active power reference step from 0.3 to 0.4 pu: (a) Grid-side currents; (b) Active power (top) and Kawasaki's frequency (bottom).	158
12.9.3	Kawasaki's response to reactive power reference step from 0.3 to 0.4 pu with reactive droop control enabled, from left to right: (a) Grid-side currents; (b) Reactive power (top) and electromotive force (bottom).	159
12.9.4	Kawasaki's response to grid frequency variation of -0.42 Hz, from left to right: (a) Grid-side currents; (b) Active power (top) and frequency (bottom).	160
12.9.5	From left to right: (a) PCC Phase Voltage with 5% of fifth harmonic (top) and its FFT (bottom) with Kawasaki's current references disabled; (b) PCC Phase Voltage with 5% of fifth harmonic (top) and grid-side currents (bottom) with Kawasaki's current references disabled.	160
12.9.6	From left to right: (a) PCC Phase Voltage with 5% of fifth harmonic (top) and its FFT (bottom) with Kawasaki's current references enabled; (b) PCC Phase Voltage with 5% of fifth harmonic (top) and grid-side currents (bottom) with Kawasaki's current references enabled.	161
12.9.7	Kawasaki's response to voltage dip type 1, with reactive droop control disabled, from left to right: (a) PCC line voltages (top) and grid-side currents (bottom); (b) Reactive power (top) and electromotive force (bottom).	162
12.9.8	Kawasaki's response to voltage dip type 1, with reactive droop control enabled, from left to right: (a) PCC line voltages (top) and grid-side currents (bottom); (b) Reactive power (top) and electromotive force (bottom).	162

12.9.9	Kawasaki's response to voltage dip type 2, with reactive droop control disabled, from left to right: (a) PCC line voltages (top) and grid-side currents (bottom); (b) Reactive power (top) and electromotive force (bottom).	163
12.9.10	Kawasaki's response to voltage dip type 2, with reactive droop control enabled, from left to right: (a) PCC line voltages (top) and grid-side currents (bottom); (b) Reactive power (top) and electromotive force (bottom).	163
12.9.11	Kawasaki's response to voltage dip type 3, with reactive droop control disabled, from left to right: (a) PCC line voltages (top) and grid-side currents (bottom); (b) Reactive power (top) and electromotive force (bottom).	164
12.9.12	Kawasaki's response to voltage dip type 3, with reactive droop control enabled, from left to right: (a) PCC line voltages (top) and grid-side currents (bottom); (b) Reactive power (top) and electromotive force (bottom).	164
12.10.1	CVSM's response to active power reference step from 0.3 to 0.4 pu: (a) Grid-side currents; (b) Active power (top) and CVSM's frequency (bottom).	165
12.10.2	CVSM's response to reactive power reference step from 0.3 to 0.4 pu with reactive droop control enabled, from left to right: (a) Grid-side currents; (b) Reactive power (top) and electromotive force (bottom).	166
12.10.3	CVSM's response to grid frequency variation of -0.42 Hz, from left to right: (a) Grid-side currents; (b) Active power (top) and CVSM's frequency (bottom).	167
12.10.4	From left to right: (a) PCC Phase Voltage with 5% of fifth harmonic (top) and its FFT (bottom) with CVSM disabled; (b) PCC Phase Voltage with 5% of fifth harmonic (top) and grid-side currents (bottom) with CVSM disabled.	168
12.10.5	From left to right: (a) PCC Phase Voltage with 5% of fifth harmonic (top) and its FFT (bottom) with CVSM enabled; (b) PCC Phase Voltage with 5% of fifth harmonic (top) and grid-side currents (bottom) with CVSM enabled.	168
12.10.6	CVSM's response to voltage dip type 1, with reactive droop control disabled, from left to right: (a) PCC line voltages (top) and grid-side currents (bottom); (b) Reactive power (top) and electromotive force (bottom).	169

12.10.7	CVSM's response to voltage dip type 1, with reactive droop control enabled, from left to right: (a) PCC line voltages (top) and grid-side currents (bottom); (b) Reactive power (top) and voltage amplitude (bottom).	170
12.10.8	CVSM's response to voltage dip type 1, from left to right: (a) Active power with reactive droop control disabled; (b) Active power with reactive droop control enabled.	170
12.10.9	CVSM's response to voltage dip type 2, with reactive droop control disabled, from left to right: (a) PCC line voltages (top) and grid-side currents (bottom); (b) Reactive power (top) and voltage amplitude (bottom).	171
12.10.10	CVSM's response to voltage dip type 2, with reactive droop control enabled, from left to right: (a) PCC line voltages (top) and grid-side currents (bottom); (b) Reactive power (top) and electromotive force (bottom).	171
12.10.11	CVSM's response to voltage dip type 2, from left to right: (a) Active power with reactive droop control disabled; (b) Active power with reactive droop control enabled.	172
12.10.12	CVSM's response to voltage dip type 3, with reactive droop control disabled, from left to right: (a) PCC line voltages (top) and grid-side currents (bottom); (b) Reactive power (top) and electromotive force (bottom).	172
12.10.13	CVSM's response to voltage dip type 3, with reactive droop control enabled, from left to right: (a) PCC line voltages (top) and grid-side currents (bottom); (b) Reactive power (top) and electromotive force (bottom).	173
12.10.14	CVSM's response to voltage dip type 3, from left to right: (a) Active power with reactive droop control disabled; (b) Active power with reactive droop control enabled.	173
12.10.15	CVSM's response to the fourth case, with reactive droop control disabled, from left to right: (a) PCC line voltages (top) and grid-side currents (bottom); (b) Reactive power (top) and electromotive force (bottom).	174
12.10.16	CVSM's response to the fourth case, with reactive droop control enabled, from left to right: (a) PCC line voltages (top) and grid-side currents (bottom); (b) Reactive power (top) and electromotive force (bottom).	174
12.10.17	CVSM's response to the fourth case, from left to right: (a) Active power with reactive droop control disabled; (b) Active power with reactive droop control enabled.	175

Chapter 1

Introduction

1.1 Climate Change

Over the last century, Earth's climate system has undergone a profound change. The main aspect regards the phenomenon known as Global Warming, the increase of the average surface temperature. As can be seen from Fig. 1.1.1 and Fig. 1.1.2, nearly every part of the planet is interested by these anomalies, with a intense concentration in the colder zones. The effects of this change represent one of the most important issues of our era.

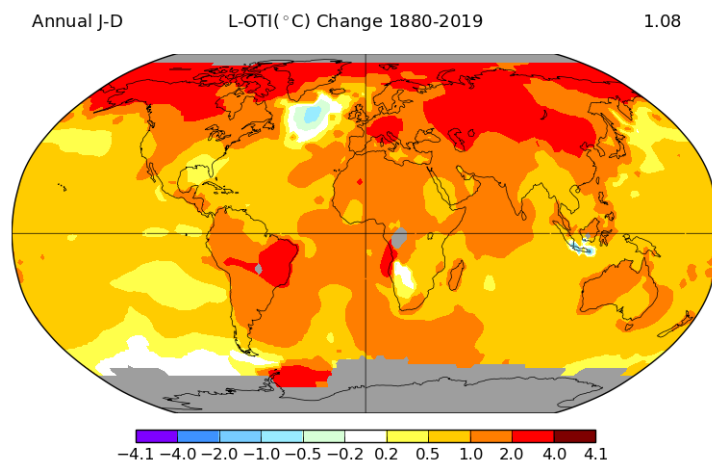


Figure 1.1.1: Land-ocean temperature index, change from 1880 to 2019.
Source: NASA.

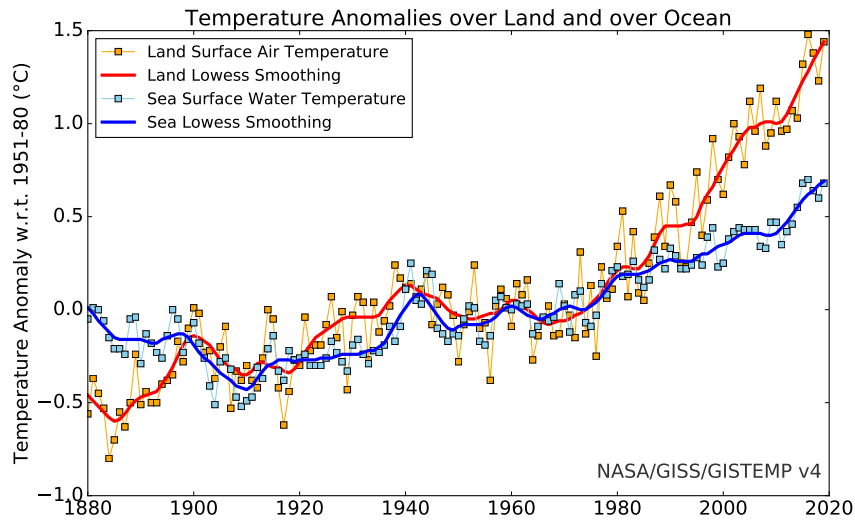


Figure 1.1.2: Land-ocean temperature index, 1880 to present. Source: NASA.

The direct consequence of global warming is the melting of glaciers and permafrost and the successive rise of the sea level, as can be noticed in Fig. 1.1.3 and Fig. 1.1.4. Moreover, the rise of the number and intensity of extreme weather phenomena have been observed, such as storms, hurricanes and changes in rainfall patterns.

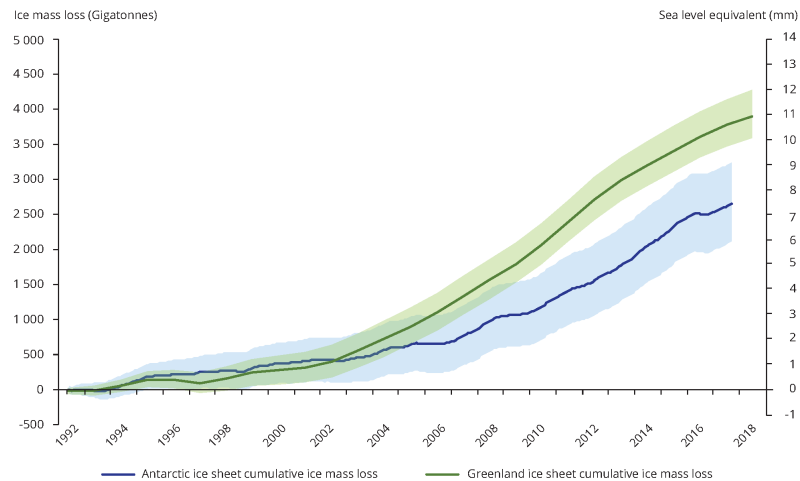


Figure 1.1.3: Cumulative ice mass loss from the Greenland and Antarctic ice sheets. Source: EEA.

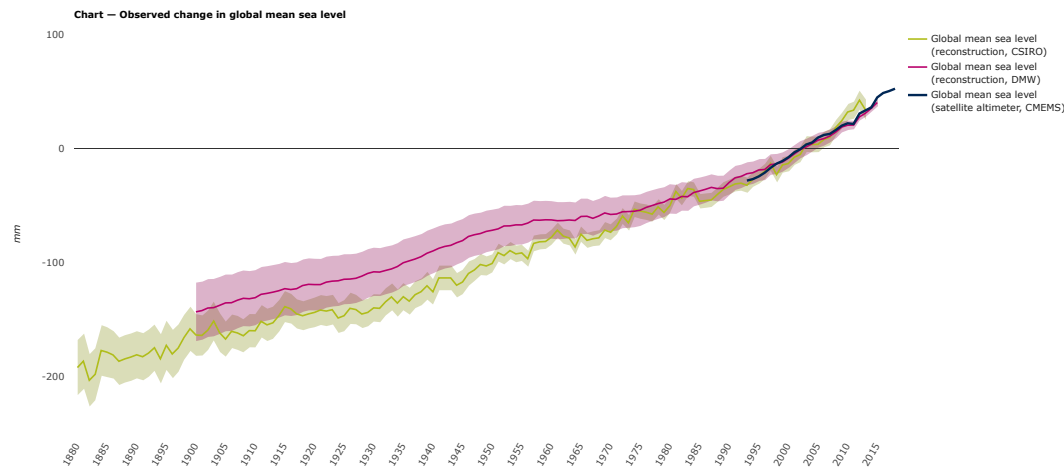


Figure 1.1.4: Observed change in global mean sea level. Source: EEA.

In order to assess the phenomena related to climate change, the World Meteorological Organization (WMO) and United Nations Environment Programme (UNEP) set up the intergovernmental body called Intergovernmental Panel on Climate Change (IPCC), in 1988. This agency provides regular assessments of the scientific basis of climate change, its impacts, future risks and options for adaptation and mitigation.

According to the Fifth Assessment Report (AR5) of IPCC, realized in 2014 [1]: *"Human influence on the climate system is clear, and recent anthropogenic emissions of greenhouse gases are the highest in history. Recent climate changes have had widespread impacts on human and natural systems"*.

The main cause of climate change can be found in the increase of emission of greenhouses gases (GHGs). These are atmospheric gases located in the atmosphere able to absorb and reflect part of the Earth's infrared radiation, realizing the phenomenon called greenhouse effect. The main GHGs are: water vapor (H_2O), carbon dioxide (CO_2), methane (CH_4), nitrous oxide (N_2O), and ozone (O_3). On one hand, they are necessary to life on Earth, because without them the average surface temperature should be around $-18^\circ C$, against the current $+15^\circ C$. However, their excessive concentration represents an issue.

The higher concentration of GHGs in the atmosphere, the larger the intensity of the greenhouse effect and the consequent average temperature of the planet increase. The main source of GHGs is the human activity: mainly fossil fuel (i.e. carbon and oil) combustion, but also deforestation and agriculture

represent the most important anthropogenic GHGs sources, in particular of CO_2 , as demonstrated in Fig. 1.1.5.

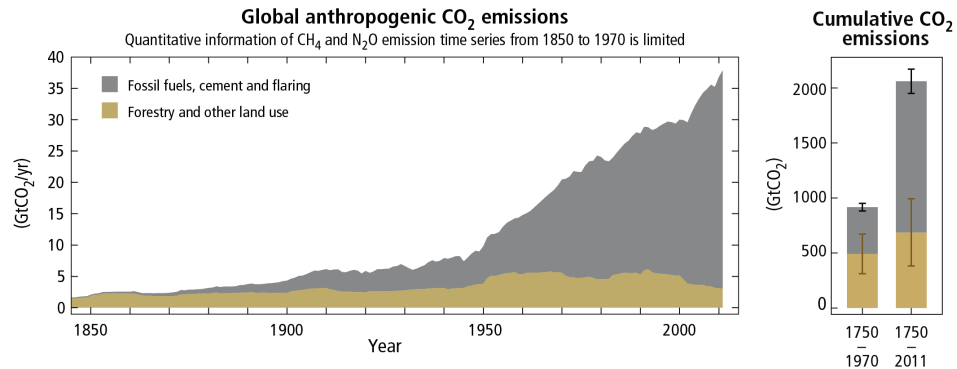


Figure 1.1.5: Global anthropogenic CO_2 emissions. Source: IPCC.

1.2 Renewable Energy Sources and Grid Converters

In order to limit the emissions of greenhouse gases, renewable energy sources (RESs) can play a fundamental role. In fact, these do not require fossil fuel burning and so they do not contribute to GHGs emission. In particular, photovoltaic and wind plants represent the most promising solutions. The former can convert solar energy in electrical energy, whereas the latter transform wind kinetic energy in mechanical and then in electrical energy.

In the last decade, the amount of energy produced from wind and solar sources has grown exponentially and it is supposed to spread more and more, as can be observed from analysis of Fig. 1.2.1 and forecast of Fig. 1.2.2.

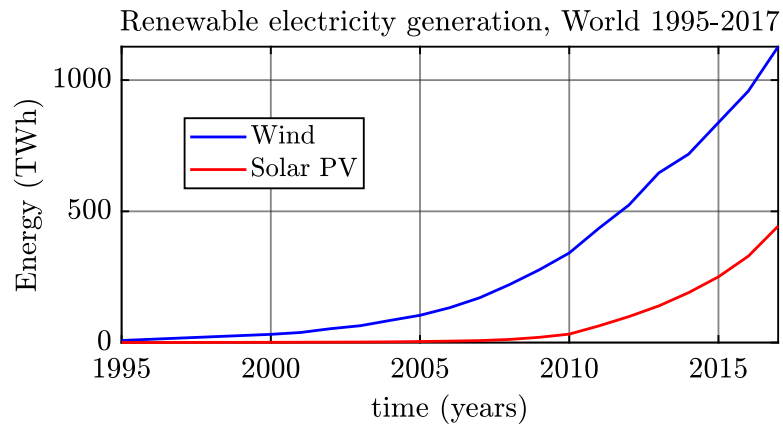


Figure 1.2.1: Renewable electricity generation by Wind and Solar PV, World 1995-2017. Source: IEA.

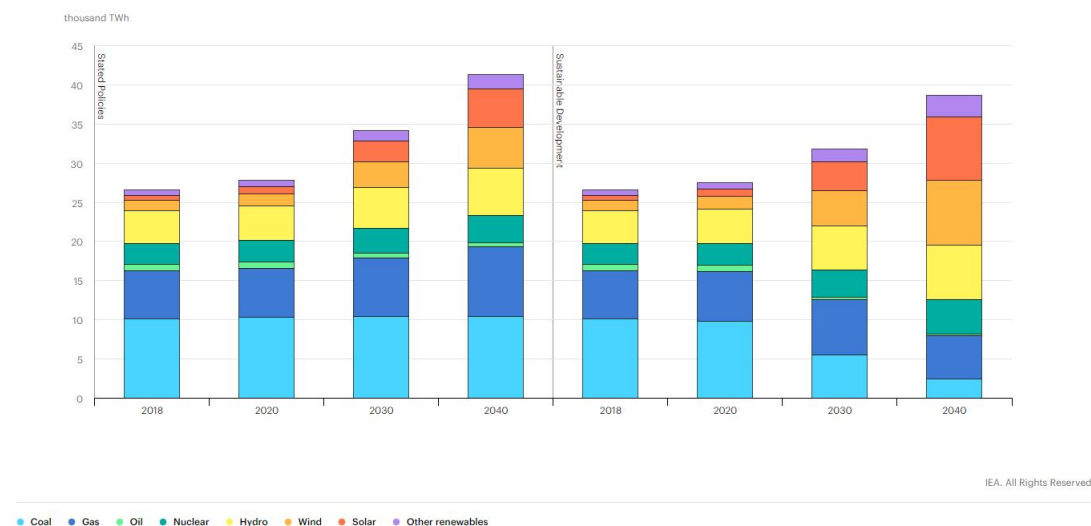


Figure 1.2.2: Electricity generation by fuel and scenario, 2018-2040. Source: IEA [2].

In order to interface solar and wind generators with the electric grid, power electronics converters are mandatory. These are devices able to transform electrical energy from a form to another. For instance, photovoltaic plants produce electrical energy in the DC form, whereas the grid works in AC. In this case two conversion stages are used: adaptation of the DC power, thanks to a DC/DC converter and a conversion from DC to AC power, by means of DC/AC converter, called inverter. These devices have to be controlled implementing a specific algorithm. The most used technique for photovoltaic

application is *Maximum Power Point Tracking* (MPPT) control algorithm [3]. Thanks to it, the maximum energetic exploitation of the source is guaranteed with an efficiency around 98%. The conventional simplified scheme is proposed in Fig. 1.2.3.

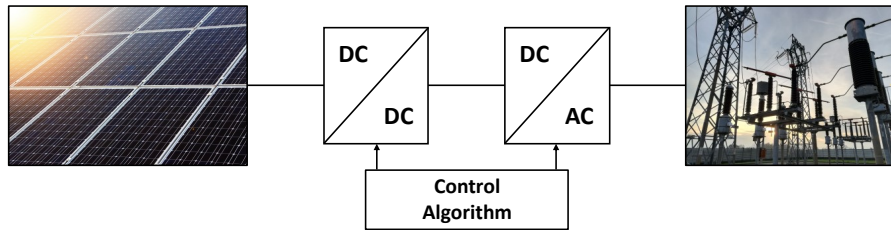


Figure 1.2.3: Conventional scheme of connection between PV plant and grid.

1.3 Stability of the Electric Grid

The working principle of the electric grid is to guarantee instant by instant the balance between demand and response of the electric power.

The grid as we know was designed to rely on alternators of hydroelectric and thermoelectric plants. This guarantees several advantages. First of all, the power balance is transiently guaranteed by means of rotors' mechanical inertia: if the power demand increases, rotors will slow down and inject inertial active power into the grid. Then a regulation of power and frequency is needed to restore the previous working condition.

This is just one of the several fundamental functions required by the grid, called ancillary services. They are:

- Frequency regulation (in terms of inertia and frequency control);
- Reactive support (voltage regulation);
- Support during faults (with injection of short circuit currents);
- Harmonics compensation;
- Imbalance compensation.

Renewable power generators (RPGs) cannot provide such features, because power converters are static, without rotating mechanical parts. Moreover, the conventional control techniques are not suitable to overcome this issue. It means that, for now, RPGs can only inject power according to the MPPT algorithm and the ancillary services are provided by conventional

synchronous generators. Consequently, it implies that the exploitation of renewable sources is limited, because it would lead to a lower grid stability.

1.4 Regulations and Grid Codes

Electric System is going through a revolutionary phase, where the penetration of RPGs and the thickening of the distributed generation are the main actors. Year by year, at international level, authorities and entities are updating the guidelines for the integration of the RESs.

A milestone was reached in 2016, when the European Commission established a network code on requirements for grid connection of generators [4], for both conventional and renewable energy sources.

In this context, frequency and voltage regulations hold a central position. For each of them, the main guidelines defined in Italy will be described.

1.4.1 General Aspects

Terna, the Italian Transmission System Operator (TSO), has acknowledged the European regulation, updating their grid code in 2018 and then in December 2019 [5]. The main aspects about RESs can be found in the annexes A18 (for wind power plants) [6] and A68 (photovoltaic power plants) [7].

Since Terna is a TSO, the guide lines refer to plants either directly connected to the transmission power system, or indirectly connected by means of a portion of grid with a nominal voltage equal or higher than 110 kV.

The main topics of the annexes are:

- the general features of the plant and the needed operating range for the connection to the high voltage (HV) power system;
- the characteristics of the managing and regulation systems which plants have to provide in normal and emergency conditions.

According to Terna Grid Code's annexes, inverters have to be designed, built and employed in order to stay connected to the grid even during emergency conditions and grid restore, within specific operating limits. They are defined in terms of voltage, frequency and the rate of change of frequency (ROCOF):

$$85 \%V_n \leq V \leq 115 \%V_n \quad (1.4.1)$$

$$47.5 \text{ Hz} \leq f \leq 51.5 \text{ Hz} \quad (1.4.2)$$

$$\frac{df}{dt} \leq 2.5 \text{ Hz/s} \quad (1.4.3)$$

where:

- V_n is the nominal voltage (V_{rms});
- V is the voltage at the connection point (V_{rms});
- f is the grid frequency (Hz).
- $\frac{df}{dt}$ is the derivative of frequency, measured at least on 5 cycles (100 ms).

1.4.2 Active Power Regulation

The active power regulation is necessary to control the frequency of the electric system. The active power regulation curve for wind and PV plants is proposed in Fig. 1.4.1. According to the Terna's grid code, the wind and PV plants must be suitable to provide a frequency regulation as performed by conventional synchronous generators. Three kinds of modalities are defined:

- Frequency Sensitive Mode (FSM);
- Limited Frequency Sensitive Mode Under-Frequency (LFSM-U);
- Limited Frequency Sensitive Mode Over-Frequency (LFSM-O).

The frequency regulation law is the following:

$$f - f_n = -s \cdot (P - P_n)$$

$$\Delta f = -s \cdot \Delta P \quad (1.4.4)$$

where:

- f is the output frequency (Hz);
- f_n is the nominal frequency (Hz);
- s is the active droop coefficient (Hz/W);
- P is the output active power (W);
- P_n is the nominal active power (W).

According to the frequency range, s assumes a different value.

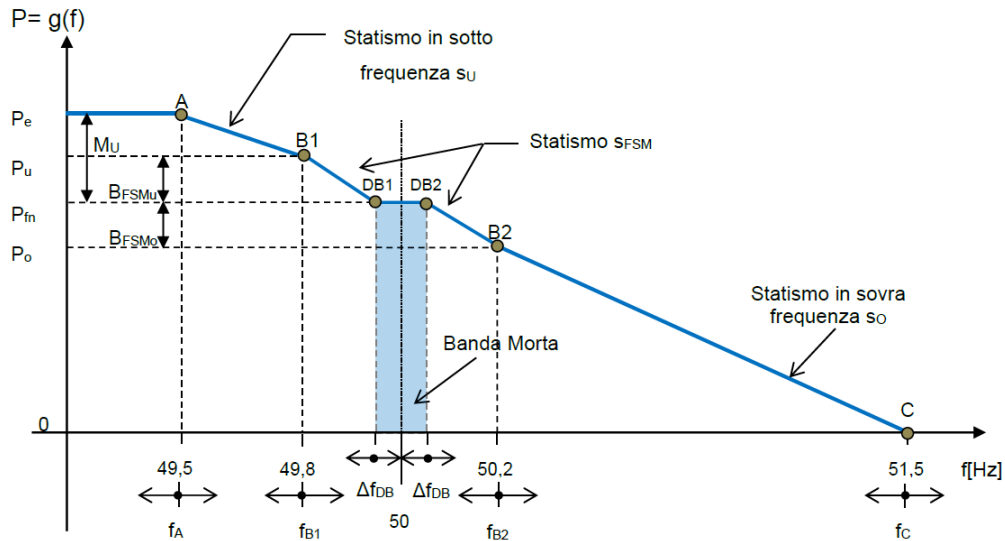


Figure 1.4.1: Active Power Regulation Curve for Wind and PV plants.
Source: [6, 7]

FSM is the frequency regulation performed around the nominal frequency value. It is implemented in the interval $[f_{B1}, f_{B2}]$ shown in Fig. 1.4.1. It is actuated according to an active droop coefficient indicated with s_{FSM} . In this case maximum insensibility value must be 10 mHz. Moreover, a dead band in the interval $[0, 500 \text{ mHz}]$ is requested.

LFSM-U is the law to follow when the frequency is lower than the nominal value, in the interval $[f_A, f_{B1}]$. In this case the active droop coefficient is s_U .

LFSM-O is the modality actuated when the frequency is in the interval $[f_{B2}, f_C]$. Here the active droop coefficient is s_O and it is chosen in order to zero the injected active power when the upper limit of frequency (51.5 Hz) is reached.

1.4.3 Voltage Regulation

The capability to be insensible to voltage variations is requested, within specific limits. The common expression of this feature is Fault Ride Through (FRT). In Fig. 1.4.2, two curves are proposed with the time limits: Under Fault Ride Through (UFRT) curve and Over Fault Ride Through (OFRT) curve. The allowed and forbidden working areas are highlighted.

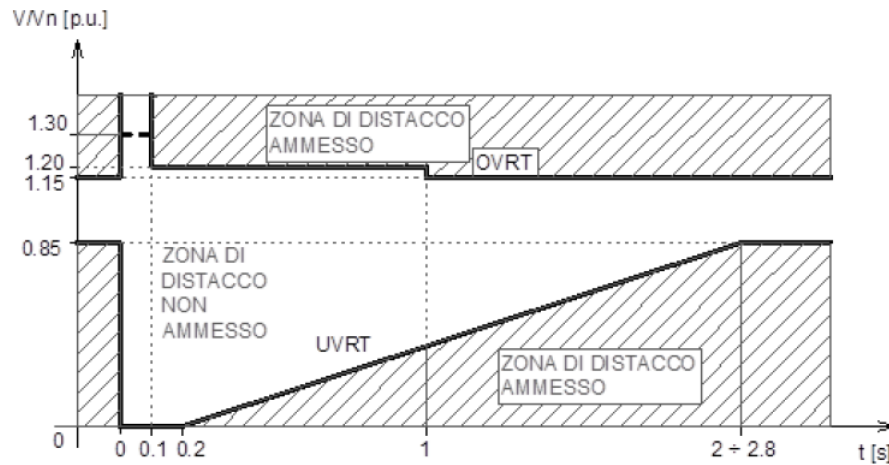


Figure 1.4.2: FRT Curves for Wind and PV plants. Source: [6, 7]

1.5 The Concept of Virtual Synchronous Generator

In order to enable power converters to follow the directions of new grid codes and provide ancillary services, more advanced control structures have to be implemented. In the technical literature different solutions have been proposed during the last 15 years. Many of them converge to a common solution: controlling the power converter in order to mimic the behaviour of conventional synchronous generators, leading to the concept of *Virtual Synchronous Generator* (VSG).

If a converter worked as an alternator, it could provide ancillary services inheriting all the positive features of synchronous generators. Moreover, it could outdo them, limiting their negative aspects. For instance, inertia is a physical property of a generator and it is not tunable. For a converter mimicking an alternator, the inertia constant is virtual, so it is a parameter tunable according to the application.

The general scheme in which the VSG takes part is proposed in Fig. 1.5.1. The only difference with respect to the conventional structure seen in Fig. 1.2.3 lies in the control algorithm: MPPT is substituted by VSG.

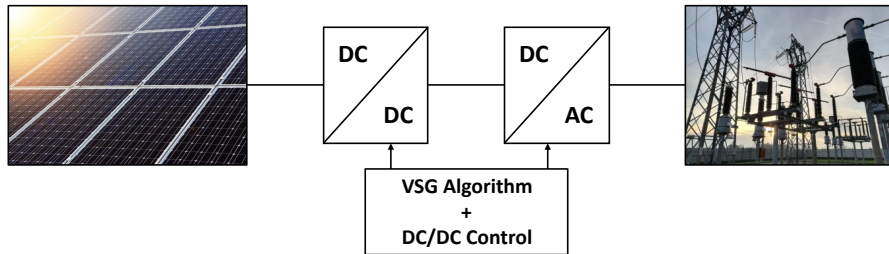


Figure 1.5.1: General structure for VSG concept.

1.6 Goal of the Thesis and My Contributions

The goal of this master thesis is to study, implement and compare VSG models available in literature. At first, they will be simulated by means of the software PLECS. This is a preliminary phase useful to understand the working principles and to verify their C-code implementation. Then, experimental tests can be performed with the laboratory setup at the Power Electronics Innovation Center (PEIC). At the end, the advantages and disadvantages of each technique will be highlighted.

My contributions can be summarized in the following main activities:

- Bibliography research and study of VSG solutions available in literature;
- Realization of PLECS simulations for each VSG solution;
- C-code implementation of the discrete-time version of each solution;
- Adaptation of C-codes for dSPACE environment and the experimental setup;
- Experimental evaluation of each considered VSG model by means of a setup composed by the following main elements:
 - battery emulator;
 - inverter;
 - grid emulator;
 - dSPACE module.

The analysed VSG solutions are:

- Synchronverter [8, 9, 10];
- Osaka [11, 12];
- VISMA [13, 14];
- VISMA 1 [15, 16];
- VISMA 2 [17];
- SPC [18, 19];
- VSYNC [20, 21];
- Kawasaki [22];
- CVSM [23, 24].

Chapter 2

General Aspects of VSGs

As mentioned before, VSGs aim to reproduce the behaviour of real synchronous generators. Each VSG solution embeds a control algorithm to reach the same goal, with some analogies and differences. Independently on the type, some aspects are in common and they are described in this Chapter.

2.1 General Structure

The scheme adopted to study and implement VSG solutions is proposed in Fig.2.1.1, where:

- \bar{v}_{abc} is the three phase inverter voltage:

$$\bar{v}_{abc} = \begin{bmatrix} v_a \\ v_b \\ v_c \end{bmatrix}$$

- \bar{v}_{PCC} is the measured three phase PCC phase voltage:

$$\bar{v}_{PCC} = \begin{bmatrix} v_{PCC,a} \\ v_{PCC,b} \\ v_{PCC,c} \end{bmatrix}$$

- \bar{i}_{abc} is the measured three phase inverter current:

$$\bar{i}_{abc} = \begin{bmatrix} i_a \\ i_b \\ i_c \end{bmatrix}$$

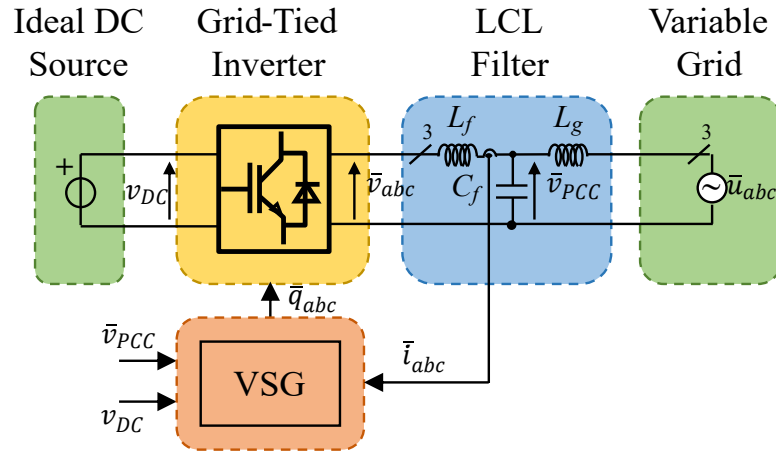


Figure 2.1.1: Hardware block diagram adopted for every VSG solution.

This structure is composed by five main elements: Ideal DC Source, Grid-tied Inverter, LCL Filter, Variable Grid and VSG block. The values used in simulations are the same of the laboratory setup.

- Ideal DC Source: as already seen in Fig.1.5.1, the DC source is not directly connected with the inverter, but there is a DC/DC converter which regulates the input voltage of the DC/AC converter. Between them is located a capacitor, called DC-link. The control of the DC/DC converter is out of the scope of this thesis, therefore the DC-link can be treated as an ideal voltage source DC. The value is set to $380 V_{DC}$.
- Grid-Tied Inverter is a two-level, three phase, voltage source inverter, composed by six IGBTs modules. Losses are neglected. The nominal power is $S_N = 15 \text{ kVA}$.
- LCL Filter is interposed between the inverter and the grid to reduce the impact of noise produced by the Pulse Width Modulation (PWM) technique. The grid voltage is measured at the Point of Common Coupling (PCC). A more detailed representation of the filter is given in Fig.2.1.2, whereas the values of its elements are listed in Table 2.1.1.

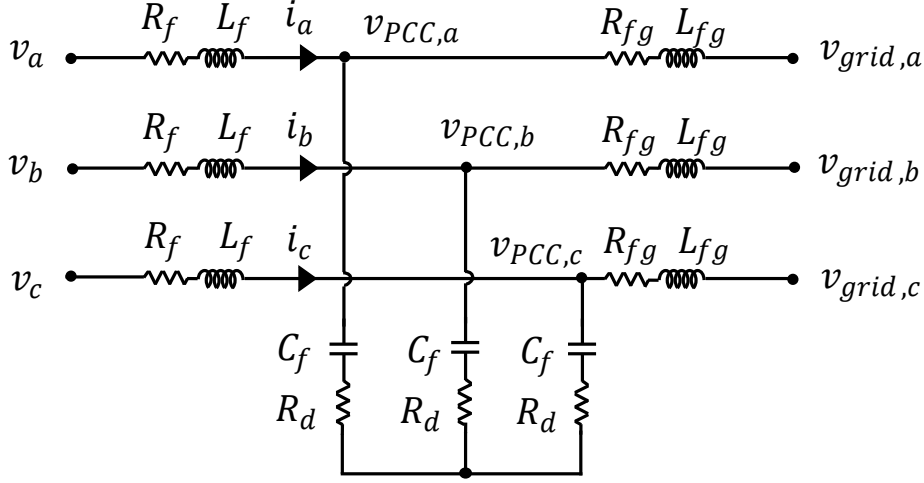


Figure 2.1.2: LCL Filter.

Table 2.1.1: LCL Filter Parameters.

Parameter	Value	Meas. Unit
L_f	545	μH
C_f	22	μF
L_{fg}	120	μH

- Variable Grid is a block used to emulate the behaviour of an ideal grid. The grid inductance and resistance are respectively $L_g = 300 \mu\text{H}$ and $R_g = 10 \text{ m}\Omega$. Moreover, it is built to simulate frequency variations, symmetrical and asymmetrical voltage dips and outages, harmonic distortions and phase perturbations. The nominal voltage is set to $120 \text{ V}_{\text{rms}}$. There are switches between grid and LCL filter as well as a precharge circuitry composed by resistors.
- The VSG block is the part of the scheme devoted to the implementation of the whole control algorithm, including the VSG technique as well as PLL, PWM modulation, AD conversion and sampling emulation. Switching frequency is set to $f_s = 10 \text{ kHz}$.

2.2 Grid Synchronization

In order to interface inverters with the grid, a process of synchronization has to be performed. A detailed representation of the circuit on study is shown in Fig.2.2.1.

The grid imposes the three phase sinusoidal voltage \bar{u}_{abc} , whereas converter creates the three phase voltages \bar{v}_{abc} . They are produced by means of the PWM technique, which introduces switching harmonics. In order to reduce them, a LCL filter is located between inverter and grid.

The voltage is measured at the PCC, so the three phase voltage of interest for the synchronization is \bar{v}_{PCC} , not \bar{u}_{abc} .

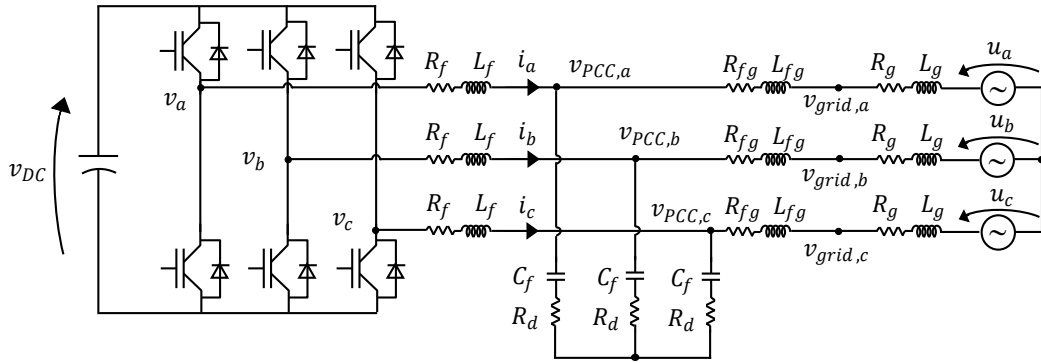


Figure 2.2.1: Scheme of connection between inverter and grid.

Sinusoidal quantities can be represented as vectors in several frames: three phase stationary frame (a, b, c) , two phase stationary frame (α, β) , two phase synchronous frame (d, q) .

Synchronization means retrieving the amplitude of the PCC voltage vector and its phase θ . The connection must occur when the difference between the PCC phase voltage and the inverter voltage is as small as possible. Even the minimum discrepancy can lead to the circulation of large currents. Therefore, there is the need to use a strategy to synchronize the inverter with the grid.

In Fig.2.2.2 the vectors \bar{v}_{abc} and \bar{v}_{PCC} are represented in two different conditions: during transient, when there is an error in terms of angle and/or amplitude between \bar{v}_{abc} and \bar{v}_{PCC} (Fig.2.2.2a); in steady state, when the synchronization process is completed and so they coincide (Fig.2.2.2b).

Notice that the two phase stationary frame (α, β) is the same for both, whereas each of vectors has their own two phase synchronous frame: (d_G, q_G) for grid and (d_I, q_I) for inverter.

Many control algorithms (included several VSGs) work on the synchronous frame $((d, q))$. Therefore, the phase θ is useful to define the correct reference frame $((d, q))$ on which represent the quantities used in control.

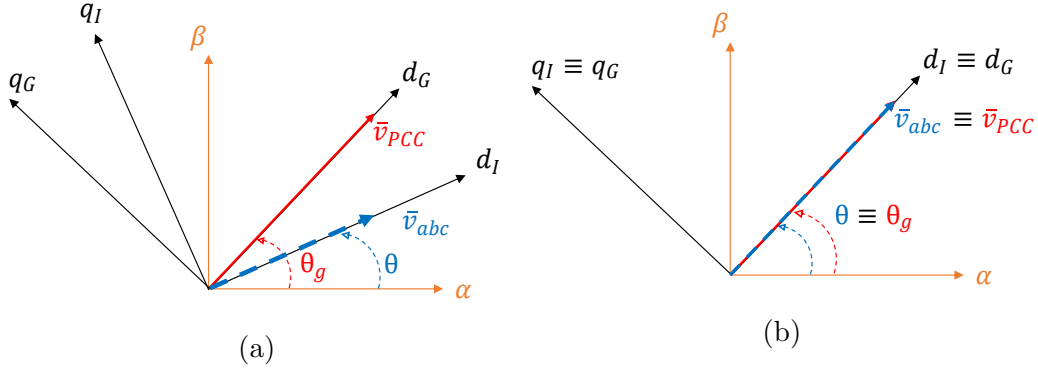


Figure 2.2.2: Vectorial representation during: (a) transient; (b) steady state.

These concepts are independent of the control algorithm and so they are valid for both conventional techniques and VSG solutions.

2.2.1 Phase Locked Loop: PLL

Many grid synchronization strategies have been studied and proposed in the literature. For the scope of this master thesis, the most popular technique has been chosen: the Phase Locked Loop (PLL) [25, 26].

The basic structure of the PLL is proposed in Fig.2.2.3. It has been decided to use the normalized form, in order to have a regulator independent of the voltage amplitude. It is composed by three parts: phase detector, loop filter and voltage controller oscillator.

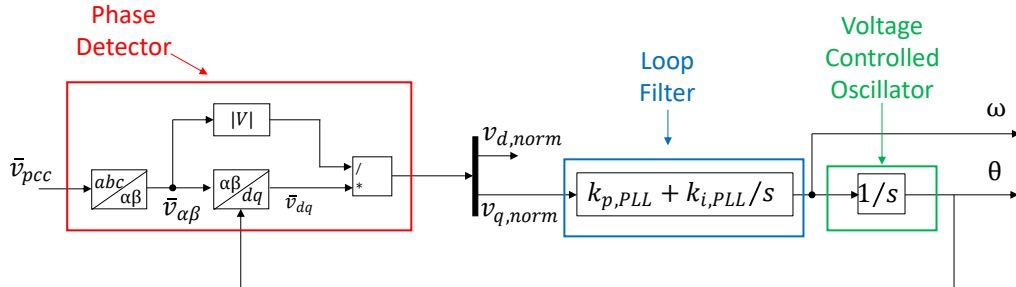


Figure 2.2.3: Basic Structure of PLL.

- Phase Detector receives the three phase PCC voltages $v_{PCC,a}$, $v_{PCC,b}$, $v_{PCC,c}$. The first step is the transformation into the two phase voltages v_α , v_β , applying the Clarke Transformation by means of the matrix $T_{\alpha\beta}$. The operation is shown in (2.2.1).

$$\begin{aligned} \begin{bmatrix} v_\alpha \\ v_\beta \end{bmatrix} &= T_{\alpha\beta} \cdot \begin{bmatrix} v_{PCC,a} \\ v_{PCC,b} \\ v_{PCC,c} \end{bmatrix} \\ \begin{bmatrix} v_\alpha \\ v_\beta \end{bmatrix} &= \begin{bmatrix} \frac{2}{3} & -\frac{1}{3} & -\frac{1}{3} \\ 0 & \frac{1}{\sqrt{3}} & -\frac{1}{\sqrt{3}} \end{bmatrix} \cdot \begin{bmatrix} v_{PCC,a} \\ v_{PCC,b} \\ v_{PCC,c} \end{bmatrix} \end{aligned} \quad (2.2.1)$$

Then, the rotation transformation is performed to retrieve the two voltages v_d , v_q , by means of the matrix T_{dq} . It defines the frame (d, q) , rotating the frame (α, β) with an angle equal to θ .

$$\begin{aligned} \begin{bmatrix} v_d \\ v_q \end{bmatrix} &= T_{dq} \cdot \begin{bmatrix} v_\alpha \\ v_\beta \end{bmatrix} \\ \begin{bmatrix} v_d \\ v_q \end{bmatrix} &= \begin{bmatrix} \cos(\theta) & \sin(\theta) \\ -\sin(\theta) & \cos(\theta) \end{bmatrix} \cdot \begin{bmatrix} v_\alpha \\ v_\beta \end{bmatrix} \end{aligned} \quad (2.2.2)$$

The union between the Clarke and the rotation transformation is the Park Transformation.

- Loop Filter is a PI regulator which receives as input the normalised grid voltage component $v_{q,norm}$. This can be written as follows:

$$v_{q,norm} = \sin(\theta_g - \theta) \quad (2.2.3)$$

The working principle of the controller brings $v_{q,norm}$ to zero. Therefore, in steady state θ will be equal to θ_g , the grid voltage will be aligned with the d -axis and $v_{d,norm}$ will coincide with the amplitude \widehat{V}_{norm} . The output of the regulator is the frequency ω .

For a small difference between the two angles, Equation (2.2.3) can be approximated:

$$v_{q,norm} = \sin(\theta_g - \theta) \approx \theta_g - \theta \quad (2.2.4)$$

From this observation, the Laplace block scheme of Fig.2.2.4 can be retrieved.

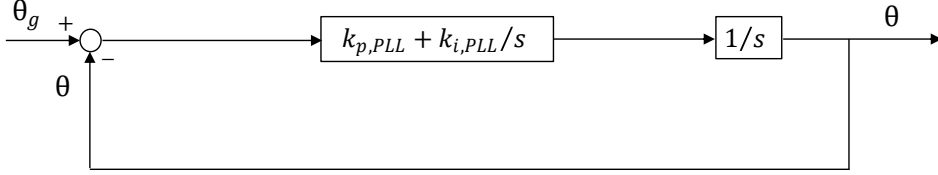


Figure 2.2.4: PLL block scheme.

This scheme is useful to properly design the PI regulator. The open-loop and closed-loop transfer functions are expressed respectively in (2.2.5) and (2.2.6):

$$H_{OL,PLL} = \frac{k_{p,PLL}s + k_{i,PLL}}{s^2} \quad (2.2.5)$$

$$H_{CL,PLL} = \frac{k_{p,PLL}s + k_{i,PLL}}{s^2 + k_{p,PLL}s + k_{i,PLL}} \quad (2.2.6)$$

Now, the characteristic equation (2.2.7a) can be compared with the canonic formulation (2.2.7b), obtaining the expressions (2.2.8a) and (2.2.8b) for PI regulator's gains.

$$\begin{cases} s^2 + k_{p,PLL}s + k_{i,PLL} = 0 & (2.2.7a) \\ s^2 + 2\zeta\omega_{bw,PLL}s + \omega_{bw,PLL}^2 = 0 & (2.2.7b) \end{cases}$$

where:

$-\zeta_{PLL}$ is the desired damping factor;

$-\omega_{bw,PLL}$ is the bandwidth frequency, equal to $2\pi f_{bw,PLL}$ (rad/s).

$$\begin{cases} k_{p,PLL} = 2\zeta\omega_{bw,PLL} & (2.2.8a) \\ k_{i,PLL} = \omega_{bw,PLL}^2 & (2.2.8b) \end{cases}$$

where:

$-k_{p,PLL}$ is the proportional gain (1/s);

$-k_{i,PLL}$ is the integral gain ($1/s^2$).

$f_{bw,PLL}$ is imposed to 5 Hz and the damping factor ζ_{PLL} equal to $1/\sqrt{2}$. All PLL parameters are listed in Table 2.2.1.

Table 2.2.1: PLL Parameters.

Parameter	Value	Meas. Unit
$f_{bw,PLL}$	5	Hz
ζ_{PLL}	0.707	-
$k_{p,PLL}$	44.4	1/s
$k_{i,PLL}$	987	$1/s^2$

- Voltage Controlled Oscillator gives as output the phase angle θ integrating the frequency. Finally $\sin(\theta)$ and $\cos(\theta)$ are calculated and used as feedbacks to perform the rotation transformation.

This is the working principle of the standard PLL. Others and more complex structures exists in literature. The main disadvantage of this solution is the negative impact on the dynamic of the total system. Nevertheless, for many VSGs it is essential.

2.3 The Role of Inertia

Synchronous generators provides electrical power converting the mechanical power of a prime motor. It rotates and drag the generator's rotor imposing a speed ω which defines the voltage electrical frequency f_{el} , according to (2.3.1).

$$\omega = 2\pi f_{el} \quad (2.3.1)$$

The link between the two kind of powers, neglecting losses, can be found in the swing equation (2.3.2) [27]:

$$P_m - P_e = \frac{d}{dt} \left(\frac{1}{2} J \omega^2 \right) = J \omega \frac{d\omega}{dt} \quad (2.3.2)$$

where:

- P_m is the mechanical power (W);
- P_e is the electrical power (W);
- J is the generator inertia ($\text{kg} \cdot \text{m}^2$);

- ω is the rotor speed (rad/s);
- $\frac{1}{2}J\omega^2$ is the kinetic energy of the generator (J).

Working with per unit (pu) quantities is useful to have a better sensibility on both parameters and their variation effect. Therefore base values are needed and they are listed in Appendix A.

In order to express the swing equation in pu, the first step is to define the inertia constant H , as follows:

$$H = \frac{1}{2}J \frac{\omega_b^2}{S_b} \quad (2.3.3)$$

Here, ω_b and S_b are, respectively, the base value of speed and power. Substituting (2.3.3) in (2.3.2) an alternative form of swing equation can be obtained:

$$P_m - P_e = \frac{2HS_b}{\omega_b^2} \cdot \omega \cdot \frac{d\omega}{dt} \quad (2.3.4)$$

Assuming $\omega \simeq \omega_b$, the swing equation in pu can be finally defined:

$$\begin{aligned} \frac{P_m}{S_b} - \frac{P_e}{S_b} &= 2H \cdot \frac{\omega}{\omega_b} \cdot \frac{1}{\omega_b} \frac{d\omega}{dt} \\ P_{m,pu} - P_{e,pu} &= 2H \frac{d\omega_{pu}}{dt} \end{aligned} \quad (2.3.5)$$

where:

- $P_{m,pu}$ is the mechanical power (pu);
- $P_{e,pu}$ is the electrical power (pu);
- H is the inertia constant (s);
- ω_{pu} is the rotor speed (pu).

In steady state condition, speed is constant and the electrical power is equal to the mechanical one. The former depends on the loads' requests, the latter is imposed by the prime motor.

To understand how generators exchange power with the grid, the following example is considered: with a load insertion, P_e increases immediately, whereas P_m needs some seconds to reach P_e and establish the new balance. It means that, in the first instants of the transient, the power required by the load is provided by the kinetic energy stored in the rotor. It decelerates, satisfying the load's request. If speed decreases, electrical frequency does the same. With a regulation process, P_m increases so that the speed and the frequency come back to their steady state values.

This procedure regards conventional generators, which have rotating parts. In order to emulate this process with VSGs, the swing equation is reproduced, defining a virtual inertia coefficient. The electrical power has the same meaning, whereas the mechanical term is the power produced by the renewable source. The advantage of this approach is the possibility to tune the inertia coefficient, choosing the best value for the application, whereas SGs are constrained to their physical value. VSG must be able to both inject and absorb active power, in the same way of SGs. It means that is impossible to exploit the source as with MPPT techniques, since a margin has to be guaranteed. In many solutions an energy storage system can be used to manage the flow of power and normally its nominal state of charge (SOC) is about 50% of its total capacity [28].

Finally, a more complete definition of swing equation takes the damping windings effect into account as well, as shown in (2.3.6):

$$P_m - P_e = J\omega \frac{d\omega}{dt} + K_d \cdot \Delta\omega \quad (2.3.6)$$

where:

- K_d is the damping factor $\left(\text{kg} \cdot \frac{\text{m}^2}{\text{s}^2}\right)$;
- $\Delta\omega$ is the difference between the actual speed and its reference (rad/s).

Substituting (2.3.3) in (2.3.6) the following relationship can be obtained:

$$P_m - P_e = J \frac{2HS_b}{\omega_b^2} \omega \frac{d\omega}{dt} + K_d \cdot \Delta\omega \quad (2.3.7)$$

In per unit it becomes:

$$P_{m,pu} - P_{e,pu} = 2H \frac{d\omega_{pu}}{dt} + k_d \cdot \Delta\omega_{pu} \quad (2.3.8)$$

where k_d is the damping factor in pu:

$$k_d = K_d \cdot \frac{\omega_b}{S_b} \quad (2.3.9)$$

2.4 Droop Control

Two fundamental ancillary services are the frequency and the voltage regulation. Droop control consists in the voltage and frequency control according to the active and reactive power. In fact, in case of mostly inductive lines,

there is a close link between frequency and active power as well as between voltage and reactive power. This can be noticed from, respectively, (2.4.1) and (2.4.2).

$$\begin{aligned}\frac{f - f_n}{f_n} &= -b_p \cdot \frac{P - P_n}{P_n} \\ \frac{\Delta f}{f_n} &= -b_p \cdot \frac{\Delta P}{P_n}\end{aligned}\tag{2.4.1}$$

where:

- f is the output frequency (Hz);
- f_n is the nominal frequency (Hz);
- b_p is the active droop coefficient (pu);
- P is the output active power (W);
- P_n is the nominal active power (W).

$$\begin{aligned}\frac{\widehat{V} - \widehat{V}_n}{\widehat{V}_n} &= -b_q \cdot \frac{Q - Q_n}{Q_n} \\ \frac{\Delta \widehat{V}}{\widehat{V}_n} &= -b_q \cdot \frac{\Delta Q}{Q_n}\end{aligned}\tag{2.4.2}$$

where:

- \widehat{V} is the output voltage amplitude (V);
- \widehat{V}_n is the nominal voltage amplitude (V);
- b_q is the reactive droop coefficient (pu);
- Q is the output reactive power (var);
- Q_n is the nominal reactive power (var).

In case of resistive lines (such as low voltage systems) the two relationships must be inverted: active power is strictly linked with the voltage just like reactive power with the frequency.

(2.4.1) shows that output power must increase with the decrease of the output frequency, and vice versa. The same happens from reactive droop control. Implementing these laws into the control algorithm of a converter, it can provide these ancillary services.

A typical value for b_p is 0.05 (5%) [27]. It means that (assuming $f_n = 50$ Hz) a frequency reduction of 1 Hz determines a power variation of 40%:

$$\begin{aligned}\frac{f - f_n}{f_n} &= -b_p \cdot \frac{P - P_n}{P_n} \\ -\frac{1}{50} &= -0.05 \cdot \frac{\Delta P}{P_n} \\ \Delta P &= 0.4P_n\end{aligned}$$

Some VSG solutions inherently embed active droop control, whereas the others have dedicated part to it. For the second category, the active droop coefficient will be set to 0.05.

Finally, the values for the reactive droop coefficients chosen for the VSG solutions will be defined in Subsection 2.5.7.

2.5 Implementation of VSG Solutions

2.5.1 List of VSGs Solutions

The VSG solutions studied and implemented in this master thesis are listed in Table 2.5.1.

Table 2.5.1: List of VSG solutions.

Model	Output Type	Synchronization
Synchronverter [8, 9, 10]	Current	Power based
Osaka [11, 12]	Voltage	PLL based
VISMA [13, 14]	Current	PLL based
VISMA 1 [15, 16]	Current	PLL based
VISMA 2 [17]	Voltage	PLL based
SPC [18, 19]	Current	Power based
VSYNCR [20, 21]	Current	Power based
Kawasaki [22]	Current	PLL based
CVSM [23, 24]	Current	Power based

As can be noticed from Table 2.5.1 two categories of VSG can be distinguished: current and voltage output references.

The former needs a regulator (PI controller is the most popular choice) to generate the voltage references which will be provided to the PMW modulator. The latter gives directly its output to the modulator.

2.5.2 PLECS Models

The whole system already shown in Fig.2.1.1 has been implemented by means of the software PLECS. Two different PLECS models have been realised for each VSG solution. The only difference between them regards how the VSG block is built.

- Average Model: the PWM modulator is bypassed and the inverter is substituted by an ideal three phase voltage source. Therefore, it is a simplified structure where the voltage references are used directly as inverter voltages, as shown in Fig.2.5.1. The VSG block is built in the Laplace domain by means of a block scheme. This solution has been adopted for the following reasons:
 - it is a simple and fast way to understand, tune and test the VSG's control algorithm;
 - the absence of commutations allows to study the behaviour of the system in a large time scale (tens of seconds) with a reasonable computational burden;
 - it is a useful starting point for the C-code implementation.

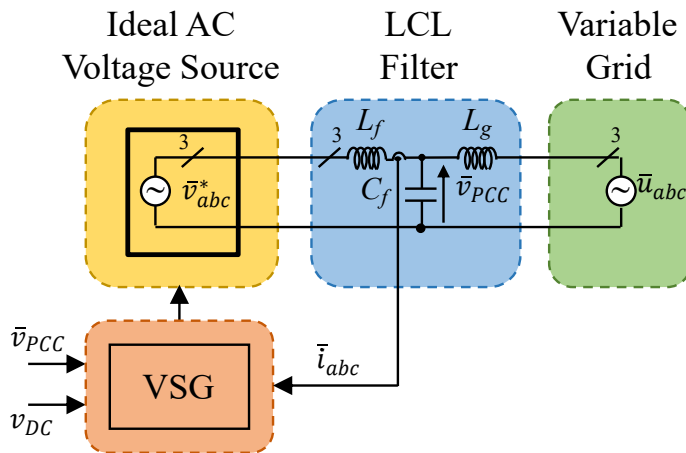


Figure 2.5.1: Simplified scheme with average model.

- Complete Model: a C-code embeds VSG's control algorithm in the discrete-time domain and the PWM technique. Inverter is composed

by six IGBTs, which receive the commands provided by the VSG block. With this solution the C-code can be validated before the experimental tests.

2.5.3 C-code Realisation

For each VSG control algorithm, the structure of the C-code is the same. The execution of the algorithm follows the rules of Interrupt Service Routine (ISR), in order to emulate a digital control. A periodical pulse train is built, with a frequency of 10 kHz. When the positive edge occurs the code is executed and then it waits until the new occurrence.

The ISR execution is based on the concept of state machine, realised by means of the switch-case construct.

State Machine

The state machine is organised with several states. Some of them are maintained until an external input occurs (from now called User Button). The others, instead, have a defined time permanence: when their function is completed, the transition to the following state happens autonomously.

States are the following:

- **ERROR**: this is the first state of the code. It can be considered the safe state, because the modulation is disabled and the references are set to zero. Moreover, it is the condition reached when a fault (e.g. overcurrent or overvoltage) occurs. The switches between the grid and the rest of the system are open.
- **PRECHARGE**: the enter condition is the User Button occurrence during state **ERROR**. In this state the modulation is still disabled, but the switches between the grid and the LCL filter are closed, in order to charge the capacitors. This procedure is performed using precharge resistors, avoiding abrupt voltage variations. This state is temporary. Therefore, at the end of the process, the resistors are bypassed and the following state can be reached.
- **SYNC**: this is a temporary state, dedicated to the synchronization procedure by means of PLL. This state is absent for Synchronverter, SPC, VSYNC and CVSM, because they actuate the synchronization without PLL, as shown in Table 2.5.1. Modulation is still disabled.
- **READY**: this is a stable state. The only function is waiting until the User Button occurrence.

- **START**: the modulation is now enabled. For each VSG solution the control algorithm is written in a dedicated function, which is called in this state. The output of the function can be either current or voltage references (see Table 2.5.1). In the first case, references are given to a PI Regulator which provide the voltage references used to compute duty cycles by means of the BEM (Balanced Enveloped Modulation) technique and then switches commands are obtained. In the second case the PI regulator is not needed and references are directly used to retrieve duty cycles.

Discrete-Time Equations

In the discrete time domain, there is the need to transform differential equations into discrete difference equations. The starting point is the well known continuous time state space model:

$$\begin{cases} \dot{x}(t) = Ax(t) + Bu(t) & (2.5.1a) \\ y(t) = Cx(t) + Du(t) & (2.5.1b) \end{cases}$$

The exact discretized expression is:

$$\begin{cases} x(k+1) = A_d x(k) + B_d u(k) & (2.5.2a) \\ y(k+1) = C_d x(k) + D_d u(k) & (2.5.2b) \end{cases}$$

where:

$$\begin{cases} A_d = e^{AT_s} & (2.5.3a) \end{cases}$$

$$\begin{cases} B_d = \left(\int_0^{T_s} e^{AT_s} d\tau \right) B & (2.5.3b) \end{cases}$$

$$\begin{cases} C_d = C & (2.5.3c) \end{cases}$$

$$\begin{cases} D_d = D & (2.5.3d) \end{cases}$$

T_s is sampled time (the inverse of switching frequency f_s) equal to 100 μ s in this thesis.

In case of complex systems, the matrix exponential and the integral can lead to heavy computational burden. For time steps sufficiently low, (2.5.3a) can be approximated as follows:

$$e^{AT_s} \approx I + AT_s$$

Where I is the identity matrix.

Applying this approximation to (2.5.2a), the well-known Euler equation can be retrieved:

$$x(k+1) \approx (I + AT_s)x(k) + T_sBu(k) \quad (2.5.4)$$

Each VSG solution will be described by means of block schemes in the Laplace domain. The equations will be written in the Laplace domain as well. Then, for the C-code implementation, all differential equations of VSG algorithms have been discretized using the Euler's method, except for SPC solution, since in this case the Euler's method is not sufficient.

2.5.4 Current-Output Models

Many VSG solutions belongs to the voltage-input current-output category. They provide as output the current references \vec{i}_{abc}^* . Then, a closed loop current control is implemented to retrieve the voltage references which will be used to obtain the commands for the inverter by means of the PWM algorithm. The control is performed by means of a conventional PI regulator, which allows to actuate a reliable current limitation. This controller is characterised by a proportional gain k_p and an integral gain k_i , which must be tuned.

The model of the converter used for the tuning is depicted in Fig. 2.5.2.

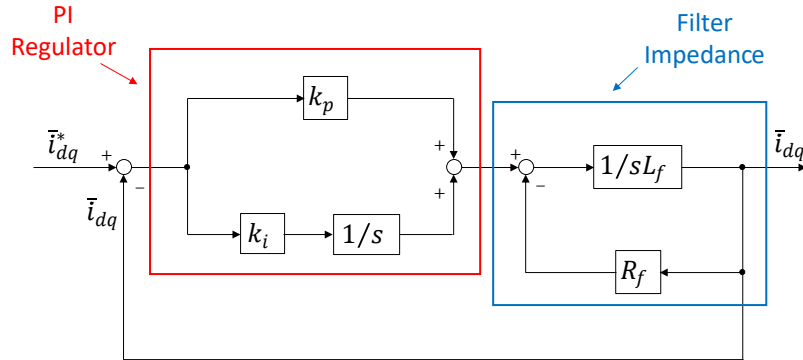


Figure 2.5.2: Block scheme for PI regulator tuning.

The switching frequency f_s in this thesis is equal to 10 kHz. According to control theory, in order to guarantee the stability of the system, the bandwidth frequency f_{bw} must be:

$$f_{bw} < \frac{1}{10} f_s$$

A reasonable value is $f_{bw} = 500$ Hz.

PI regulator's gains have been tuned applying (2.5.5a) and (2.5.5b):

$$\begin{cases} k_p = 2\pi f_{bw} \cdot L_f & (2.5.5a) \\ k_i = 0.2 \cdot 2\pi f_{bw} \cdot k_p & (2.5.5b) \end{cases}$$

where:

- k_p is the proportional gain (Ω);
- k_i is the integral gain (Ω/s);
- f_{bw} is the bandwidth frequency (Hz);
- L_f is the filter inductance (H).

All parameters are listed in Table 2.5.2.

Table 2.5.2: PI Parameters.

Parameter	Value	Meas. Unit
f_{bw}	500	Hz
L_f	545	μH
k_p	1.712	V/A
k_i	1076	V/(A · s)

The equivalent circuit which properly represents the connection between this kind of model and the grid is shown in Fig. 2.5.3.

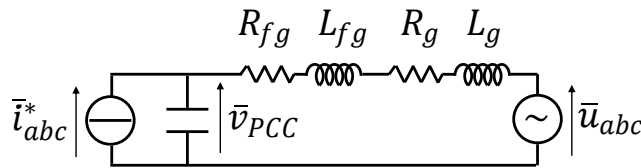


Figure 2.5.3: Equivalent circuit for current-output models.

Independently on the concept of VSG, this model is the typical configuration for current source inverters. The ideal current generator is equivalent to the series of an ideal voltage generator (which provides the electromotive force of the VSG) and a virtual impedance. This structure represents the virtual stator of the VSG. The parameters of the virtual impedance can be arbitrarily chosen. It has been decided to use the following values in per unit, similar for the real SGs [27]:

$$\begin{cases} r_v = 0.02 \text{ pu} & (2.5.6a) \\ l_v = 0.1 \text{ pu} & (2.5.6b) \end{cases}$$

Almost every current-output VSG uses this virtual impedance to retrieve the current references. The difference between the electromotive force \bar{e}_{abc} and the PCC phase voltage \bar{v}_{PCC} multiplied by the virtual admittance leads to current references.

The definition of current references in the Laplace domain and three phase reference frame is the following:

$$\begin{aligned} \bar{i}_{abc}^* &= \frac{1}{R_v + sL_v} (\bar{e}_{abc} - \bar{v}_{PCC}) \\ \bar{i}_{abc}^* &= \begin{bmatrix} i_a^* \\ i_b^* \\ i_c^* \end{bmatrix} = \frac{1}{R_v + sL_v} \cdot \left(\begin{bmatrix} e_a \\ e_b \\ e_c \end{bmatrix} - \begin{bmatrix} v_{PCC,a} \\ v_{PCC,b} \\ v_{PCC,c} \end{bmatrix} \right) \end{aligned} \quad (2.5.7)$$

All quantities are in absolute values. The current reference \bar{i}_{abc}^* is then represented in $((d, q))$ reference frame by means of the Park Transformation, defining the vector \bar{i}_{dq}^* . Successively, it is compared with the measured phase currents and the error is provided to PI regulator, obtaining the voltage references for the PWM modulator.

2.5.5 Voltage-Output Models

The current-input voltage-output models are two: Osaka and VISMA2. For these models, voltage references are the electromotive forces produced by VSG and directly provided to the PWM Modulator, without using an inner controller.

For this category, the equivalent circuit which describes the connection between the VSG and the grid is illustrated in Fig. 2.5.4.

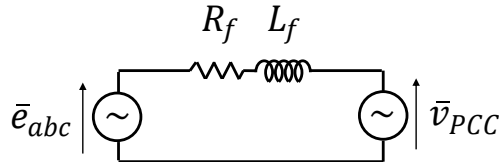


Figure 2.5.4: Equivalent circuit for voltage-output models.

This is the typical configuration of voltage-source inverters. In this case the impedance between inverter and PCC is the real filter impedance:

$$\begin{cases} R_f = 0.1 \Omega & (2.5.8a) \\ L_f = 545 \mu\text{H} & (2.5.8b) \end{cases}$$

The per unit values are:

$$\begin{cases} r_f = 0.035 \text{ pu} & (2.5.9a) \\ l_f = 0.059 \text{ pu} & (2.5.9b) \end{cases}$$

For this kind of model, the open loop voltage control does not embed a current saturation system. This is the most important disadvantage of this solution, since during voltage dips or frequency variations, currents could be larger than the nominal value, leading to an overcurrent fault. The algorithm must be modified in order to limit the circulation of currents, guaranteeing the safety of the system.

The VSG model does not change. The output is still the electromotive force, but it is not provided directly to the PWM modulator.

The adopted solution recalls what is made by current-output models. The chosen values for the parameters of the virtual admittance are the same of the physical filter:

$$\begin{cases} R_v = R_f = 0.1 \Omega & (2.5.10a) \\ L_v = L_f = 545 \mu\text{H} & (2.5.10b) \end{cases}$$

Current references are retrieved as described for current-output models:

$$\vec{i}_{abc}^* = \begin{bmatrix} i_a^* \\ i_b^* \\ i_c^* \end{bmatrix} = \frac{1}{R_v + sL_v} \cdot \left(\begin{bmatrix} e_a \\ e_b \\ e_c \end{bmatrix} - \begin{bmatrix} v_{PCC,a} \\ v_{PCC,b} \\ v_{PCC,c} \end{bmatrix} \right) \quad (2.5.11)$$

Even here the current reference \vec{i}_{abc}^* is transformed in the $((d, q))$ reference frame, defining the vector \vec{i}_{dq}^* . Then the same PI regulator for current output models is used.

The critical aspect of this modification is the transition between one technique and the other. It has been chosen to define a current threshold, whose value depends on the test performed.

When the threshold is reached, the control switches from the conventional form to the current one. Then, it comes back to the voltage type when inverter current stays continuously lower than 5 A for 0.5 s.

Moreover, when the transition to current mode occurs, feedback powers are not measured any more, but calculated using the current references.

2.5.6 Linearised Model for Active Control

In order to tune parameters useful for the active control of several VSG solutions, a common, linearised model in per unit is described here.

The connection between a generic voltage source (like the VSG's stator) and the grid can be represented with the circuit shown in Fig.2.5.5 [27].

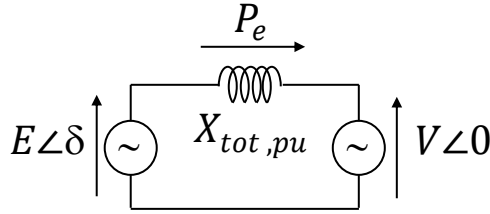


Figure 2.5.5: Simplified circuit of connection between VSG's stator and grid for active control tuning.

This representation is valid for mostly inductive connection (e.g. medium and high voltage lines), where the resistive term is negligible compared to the inductive one. The quantities of this model in per unit are:

- grid voltage, expressed in the polar notation $V\angle 0$ (pu);
- VSG voltage $E\angle\delta$ (pu);
- $X_{tot,pu}$, the equivalent reactance between the two voltage sources (pu);
- P_e , the active power transferred from one side to another in pu:

$$P_e = \frac{EV}{X_{tot,pu}} \sin(\delta) = K_s \sin(\delta) \quad (2.5.12)$$

Here K_s is the synchronizing power in pu, equal to theoretical maximum transferable power between the two voltage sources.

The equivalent reactance is given by the sum of three terms:

$$X_{tot} = \omega_b(L^{VSG} + L_{fg} + L_g) \quad (2.5.13)$$

where:

- L_g is the grid inductance (H);

- L_{fg} is the grid-side filter inductance (H);
- L^{VSG} is the inductance which depends on the model (H):
 - equal to the real filter L_f for voltage-output models;
 - equal to the virtual inductance L_v for current-output models.

Using the per unit notation, the equation becomes:

$$\begin{aligned}
 X_{tot,pu} &= \frac{\omega_b}{Z_b} \cdot (L^{VSG} + L_{fg} + L_g) \\
 X_{tot,pu} &= l^{VSG} + l_{fg} + L_{g,pu} \\
 X_{tot,pu} &= X_{pu}^{VSG} + X_{fg,pu} + X_{g,pu}
 \end{aligned} \tag{2.5.14}$$

By means of (2.3.8) and (2.5.12), and considering a small deviation (denoted by the prefix Δ) from the nominal working point, the Equation (2.5.15) and the linearised model in Laplace domain of Fig.2.5.6 can be retrieved.

$$\Delta P_e = K_s \sin(\Delta\delta) \simeq K_s \Delta\delta \tag{2.5.15}$$

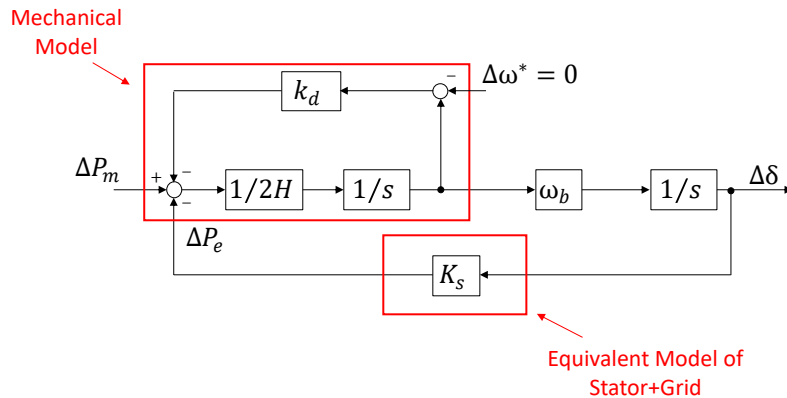


Figure 2.5.6: Linearised model in pu of VSG's stator connected to the grid.

Now, the characteristic equation of the control scheme can be obtained:

$$s^2 + \frac{k_d}{2H}s + \frac{\omega_b K_s}{2H} = 0 \tag{2.5.16}$$

Finally, it can be compared with the canonic equation illustrated in (2.5.17):

$$s^2 + 2\zeta\omega_N s + \omega_N^2 = 0 \tag{2.5.17}$$

where:

- ζ is the desired damping factor;

$-\omega_N$ is the natural frequency (rad/s).

The results, useful for some VSG solutions, can be obtained from the comparison:

$$\begin{cases} k_d = 2\zeta\sqrt{2H\omega_b K_s} & (2.5.18a) \\ \omega_N = \sqrt{\frac{\omega_b K_s}{2H}} & (2.5.18b) \end{cases}$$

In some cases, the frequency ω_{PLL} retrieved by PLL is used, instead of ω^* . In this circumstance, the linearised model changes and a corrective factor k_c has to be multiplied to k_d [29]:

$$\begin{cases} k_c = \frac{L^{VSG} + L_{fg} + L_g}{L^{VSG}} & (2.5.19a) \\ k'_d = k_d \cdot k_c & (2.5.19b) \end{cases}$$

The damping factor and inertia constant are set to typical values [27], whereas K_s depends on the total reactance. These values, together with the results of tuning, are listed in Table 2.5.3. Table is divided into three parts: the first one is dedicated for the common parameters of the output-current and the voltage-output models; the second one is for parameters of output-current models; the third one for voltage-output models.

Table 2.5.3: Parameters for Active Control.

Parameter	Value	Meas. Unit
Common Parameters		
V	1	pu
E	1	pu
ω_b	314	rad/s
Z_b	2.88	Ω
l_{fg}	0.013	pu
$L_{g,pu}$	0.033	pu
ζ	0.7	pu
H	4	s
Current-Output Parameters		
l_v	0.1	pu
$X_{tot,pu}$	0.146	pu
K_s	6.85	pu
k_d	184	pu
ω_N	16.4	rad/s
k_c	1.46	pu
k'_d	269	pu
Voltage-Output Parameters		
l_f	0.059	pu
$X_{tot,pu}$	0.105	pu
K_s	9.5	pu
k_d	216	pu
ω_N	19.31	rad/s
k_c	1.77	pu
k'_d	383	pu

2.5.7 Linearised Model of the Excitation Control

If the active parts of the VSGs solutions are very similar with each others, the same is not true for the reactive one.

Some models embed a PI regulator, others a pure integrator or a simple droop control. Nevertheless, a comprehensive tuning method for the excitation control can be performed [30].

The system on study is, obviously, the same already described for the active control in Fig.2.5.5 and shown here in Fig.2.5.7.

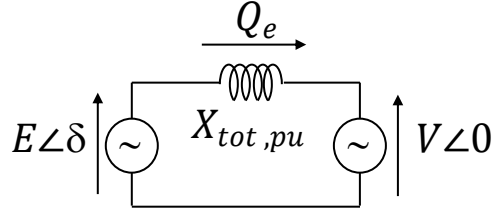


Figure 2.5.7: Simplified circuit of connection between VSG’s stator and grid for excitation control tuning.

All quantities have been already described, except for Q_e , the reactive power transferred from one side to another. It can be obtained from (2.5.20).

$$Q_e = \frac{V \cdot (E - V)}{X_{tot,pu}} \quad (2.5.20)$$

As made for the active control, a linearisation around the nominal working point is actuated and the prefix Δ denotes the small deviation from it. The model on study is realised in the Laplace domain in pu, and it is depicted in Fig. 2.5.8.

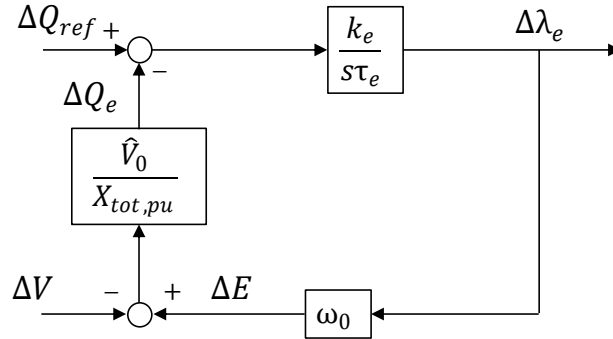


Figure 2.5.8: Linearised model in pu of VSG’s excitation control [30].

The quantities which take part into this model are:

- ΔQ_{ref} , the variation of the reactive power reference (pu);
- ΔQ_e , the variation of the reactive power transferred from the VSG’s stator to the grid (pu);
- ΔV , the variation of the grid voltage (pu);
- ΔE , the variation of the VSG voltage (pu);
- ω_0 , the nominal speed equal to 1 pu;
- \hat{V}_0 , the nominal voltage equal to 1 pu;
- $X_{tot,pu}$, the equivalent reactance between the two voltages sources (pu);

- $\Delta\lambda_e$, the variation of the VSG excitation flux linkage (pu);
- τ_e , the time constant of the excitation control (s);
- k_e , the gain of the excitation control (pu).

The error between the reactive power reference and the VSG reactive power is provided to a pure integrator to obtain the excitation flux linkage. Then this is used to retrieve the VSG voltage. The difference between it and the grid voltage leads to the reactive power.

The characteristic equation of the system can be now retrieved:

$$s\tau_e X_{tot,pu} + \omega_0 k_e = 0 \quad (2.5.21)$$

The system is characterized by a single pole, with the following time constant:

$$\tau = \frac{\tau_e X_{tot,pu}}{\omega_0 k_e} \quad (2.5.22)$$

τ can be imposed by the user and set equal to τ_e . The excitation gain k_e becomes:

$$k_e = \frac{X_{tot,pu}}{\omega_0} \quad (2.5.23)$$

The inverse of k_e is chosen as reactive droop coefficient defined in (2.4.2):

$$b_q = \frac{1}{k_e} \quad (2.5.24)$$

Finally, the constant K_{ecc} is defined as follows:

$$K_{ecc} = \frac{k_e}{\tau_e} \quad (2.5.25)$$

All values are listed in Table 2.5.4.

Table 2.5.4: Parameters for Excitation Control.

Parameter	Value	Meas. Unit
Common Parameters		
V	1	pu
E	1	pu
\hat{V}_0	1	pu
ω_0	1	pu
l_{fg}	0.013	pu
$L_{g,pu}$	0.033	pu
Current-Output Parameters		
l_v	0.1	pu
$X_{tot,pu}$	0.146	pu
τ_e	1	s
k_e	0.146	pu
b_q	6.85	pu
K_{ecc}	0.146	1/s
Voltage-Output Parameters		
l_f	0.059	pu
$X_{tot,pu}$	0.105	pu
τ_e	1	s
k_e	0.105	pu
b_q	9.52	pu
K_{ecc}	0.105	1/s

2.6 List of Tests

For each VSG solution, a series of tests has been performed to highlight all their advantages and disadvantages:

- Active and Reactive Power References;
- Inertial Response;
- Harmonic Distortion;
- Voltage Dips.

Chapter 12 is dedicated to experimental outcomes, whereas in Chapter 13 the final comparison can be found.

For all tests the quantities will be expressed in pu, in order to facilitate the comparison. The only exception is for frequency, measured in Hz.

Finally, for many VSG solutions a distinction between two kinds of powers must be defined:

- P_i and Q_i are respectively the real active and reactive power flowing between the inverter and the grid. They can be calculated measuring voltages and currents at the PCC, expressed in the (α, β) frame, by means of Clarke Transformation. P_i and Q_i in pu are obtained as follows:

$$P_i = \frac{3}{2} \cdot \frac{1}{S_b} \cdot (v_\alpha \cdot i_\alpha + v_\beta \cdot i_\beta) \quad (2.6.1)$$

$$Q_i = \frac{3}{2} \cdot \frac{1}{S_b} \cdot (v_\beta \cdot i_\alpha - v_\alpha \cdot i_\beta) \quad (2.6.2)$$

where S_b is the base value of power, set to 15 kVA.

- P_e and Q_e are respectively the VSG's active and reactive power, retrieved according to the algorithm.

They can coincide or not, according to the cases. For each solution a detailed description will be provided.

Active and Reactive Power References

The active power reference starts from 0.3 pu and then a step variation of 0.1 pu is applied. This test is useful to observe the VSG active power response, in terms of damping and time to reach the set point. The same is performed for reactive power, with and without reactive droop control.

Inertial Response

Maintaining the active and reactive power references to zero, a grid frequency variation of -0.42 Hz is applied. Thanks to this test, an evaluation of the active power injection during the transient can be performed. Moreover, the damping-droop coupling of each solution can be analysed. Frequency variation will follow the typical profile obtained by a conventional power system after the lost a generator, as shown in Fig.2.6.1 [31].

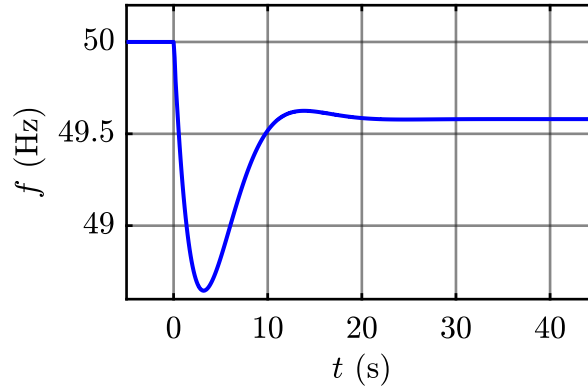


Figure 2.6.1: Frequency profile to evaluate the inertial response of VSGs.

The minimum value of the grid frequency (commonly known as nadir) will be around 48.6 Hz.

Harmonic Distortion

Grid starts from the ideal condition of 50 Hz symmetrical three phase system, with a nominal voltage of $120 V_{\text{rms}}$. Then 5% of fifth harmonic is added and the grid-side current waveforms are observed. This test is useful to understand if VSG helps or not the grid in case of harmonic distortion, featuring an active filter behaviour. The Fast Fourier Transform (FFT) will be used on the oscilloscope to evaluate the contribution of harmonics.

Voltage Dips

Grid starts from the ideal condition of 50 Hz symmetrical three phase system, with a nominal voltage of $120 V_{\text{rms}}$. Then a symmetrical voltage dip is applied. In this way the grid support of VSG during faults can be quantified.

Voltage dips are classified in different categories according to their depth (difference between the reference voltage and the residual voltage) and duration.

It has been chosen to study the VSG response in three cases, which belongs to the three more common categories in mixed networks. Data come from the measurements results collected in the international standard IEC PD IEC/TR 61000-2-8:2002 [32]. In this report can be found the table in Fig. 2.6.2, where the three categories chosen are highlighted in red.

Table 8 – Mixed networks: voltage dip incidence – 95th percentile

Residual voltage u % of reference voltage	Duration t					
	$10 \leq t < 100$ ms	$100 \leq t < 500$ ms	$0,5 \leq t < 1$ s	$1 \leq t < 3$ s	$3 \leq t < 20$ s	$20 \leq t < 60$ s
$90 > u \geq 70$	61	68	12	6	1	0
$70 > u \geq 40$	8	38	4	1	0	0
$40 > u \geq 0$	2	20	4	2	1	0
$u = 0$ (interruptions)	0	18	26	5	4	9
95th percentile of dips/site: 256						

Figure 2.6.2: Voltage Dips incidence in mixed networks according to PD IEC/TR 61000-2-8:2002.

The three types of dip chosen are listed in Table 2.6.1.

Table 2.6.1: Voltage Dips chosen for tests.

Dip Type	Residual Voltage (%)	Duration (ms)
1	80	60
2	80	300
3	50	300

Voltage dips will be test with and without reactive droop control.

Chapter 3

Synchronverter

3.1 Base version of Synchronverter

Synchronverter is a solution proposed in 2009 by Qing-Chang Zhong and George Weiss [8, 9]. The control scheme is illustrated in Fig. 3.1.1. All quantities are expressed in absolute values.

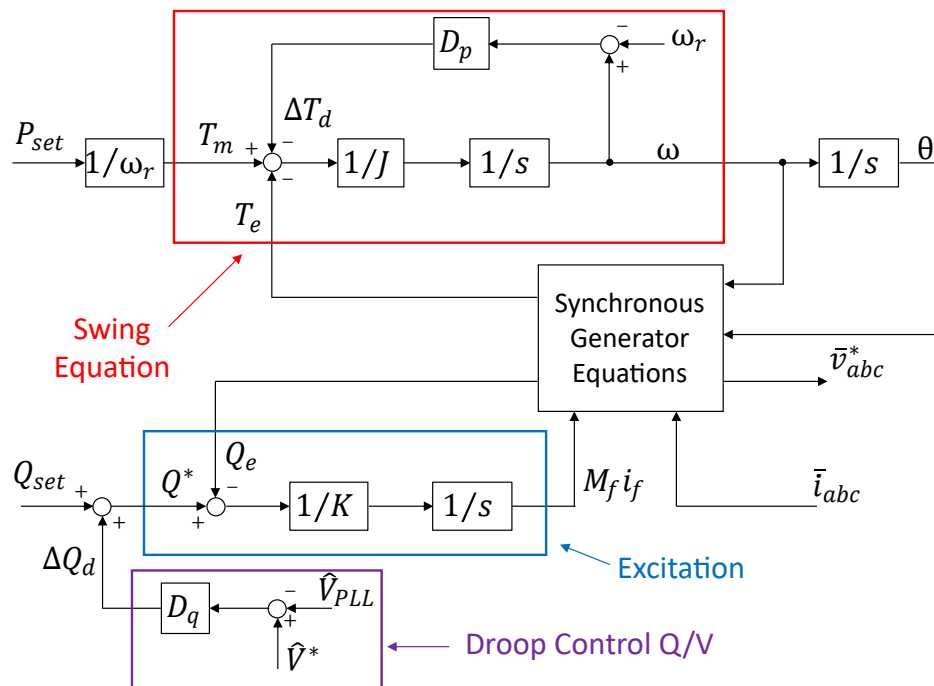


Figure 3.1.1: Synchronverter's control scheme for the base version in Laplace domain.

Synchronverter belongs to the current-input voltage-output models: starting from the measure of inverter currents, the voltage references are calculated and provided to the PWM modulator. There is not a closed-loop current or voltage control. Therefore, there is no current saturation system and it is necessary to implement additional blocks to limit currents.

A grid synchronization process is needed and the PLL is employed for this purpose.

The core of this structure is the Synchronous Generator Equations block, which contains the equations of the electromechanical synchronous generator model:

$$\begin{cases} T_e = M_f i_f \cdot \langle \bar{i}_{abc}, \widetilde{\sin(\theta)} \rangle & (3.1.1a) \\ Q_e = -\omega \cdot M_f i_f \cdot \langle \bar{i}_{abc}, \widetilde{\cos(\theta)} \rangle & (3.1.1b) \\ \bar{v}_{abc}^* = \omega \cdot M_f i_f \cdot \widetilde{\sin(\theta)} & (3.1.1c) \end{cases}$$

where:

- \bar{i}_{abc} is the three phase inverter current (A);
- $\widetilde{\sin \theta}$ and $\widetilde{\cos \theta}$ are the vectors:

$$\widetilde{\sin \theta} = \begin{bmatrix} \sin(\theta) \\ \sin\left(\theta - \frac{2\pi}{3}\right) \\ \sin\left(\theta + \frac{2\pi}{3}\right) \end{bmatrix}, \quad \widetilde{\cos \theta} = \begin{bmatrix} \cos(\theta) \\ \cos\left(\theta - \frac{2\pi}{3}\right) \\ \cos\left(\theta + \frac{2\pi}{3}\right) \end{bmatrix} \quad (3.1.2)$$

- $\langle \cdot, \cdot \rangle$ denotes the conventional inner product in \mathbb{R}^3 ;
- $M_f i_f$ is the excitation flux linkage of the Synchronverter (Vs);
- T_e is the virtual torque of the Synchronverter (Nm);
- ω is the virtual speed of the Synchronverter (rad/s);
- Q_e is the virtual reactive power of the Synchronverter (var);
- \bar{v}_{abc}^* is the three phase reference voltage (V).

The mechanical part of Synchronverter is based on the complete swing equation already seen in (2.3.6), but written in terms of torque and not power:

$$T_m - T_e = J \cdot \frac{d\omega}{dt} + D_p \cdot (\omega - \omega_r) \quad (3.1.3)$$

In the Laplace domain it becomes:

$$T_m - T_e = Js\omega + D_p \cdot (\omega - \omega_r) \quad (3.1.4)$$

T_m is the fictitious mechanical torque of the virtual generator, expressed in Nm. It is obtained from the ratio between the real power P_{set} coming from the source and the speed, assumed equal to the reference speed ω_r .

D_p is the damping factor, expressed in $\text{kg} \cdot \frac{\text{m}^2}{\text{s}}$. The damping torque is defined as follows:

$$\Delta T_d = D_p \cdot (\omega - \omega_r) = D_p \cdot \Delta\omega \quad (3.1.5)$$

Its main role is to provide damping to the electromechanical part. Moreover, it actually behaves as a frequency droop coefficient, not differently from what described with (2.4.1) in Section 2.4. It means that Synchronverter solution inherently embeds frequency droop control, but the coefficient is strictly dependent on the damping effect and the vice versa is also true: there is a coupling between the droop control and the damping factor. Using (2.4.1) and (3.1.5) the relationship, in module, can be retrieved:

$$D_p = \frac{S_b}{\omega_b^2 k_p} \quad (3.1.6)$$

Then, the swing equation is used to obtain the speed of the Synchronverter. Next, it is integrated to retrieve the angular position θ .

The last portion of the scheme regards the reactive one. It is divided into two parts: Droop Control Q/V and Excitation. The first one embeds the law of voltage droop control already seen and described in Section 2.4:

$$\Delta Q_d = D_q \cdot (\widehat{V}^* - \widehat{V}_{PLL}) \quad (3.1.7)$$

where:

- D_q is the reactive droop coefficient (var/V);
- \widehat{V}^* is the voltage reference amplitude, equal to $120\sqrt{2}$ V_{pk};
- \widehat{V}_{PLL} is the voltage amplitude measured at the PCC (V).

The reactive power reference is defined by the sum of ΔQ_d and the external power Q_{set} :

$$Q^* = Q_{set} + \Delta Q_d \quad (3.1.8)$$

The second part is based on a pure integrator and it is used to retrieve the excitation flux linkage of the Synchronverter, starting from the difference between the reference Q^* and Q_e :

$$M_f i_f = \frac{1}{s} \cdot \frac{1}{K} (Q^* - Q_e) \quad (3.1.9)$$

Here, K is the inverse of K_{ecc} of Equation (2.5.25), expressed in the absolute form.

Finally, it is also useful to define virtual active power:

$$P_e = T_e \cdot \omega_r \quad (3.1.10)$$

3.2 Enhanced version of Synchronverter

In the literature, an enhanced version of Synchronverter is proposed [10].

The control scheme is shown in Fig. 3.2.1.

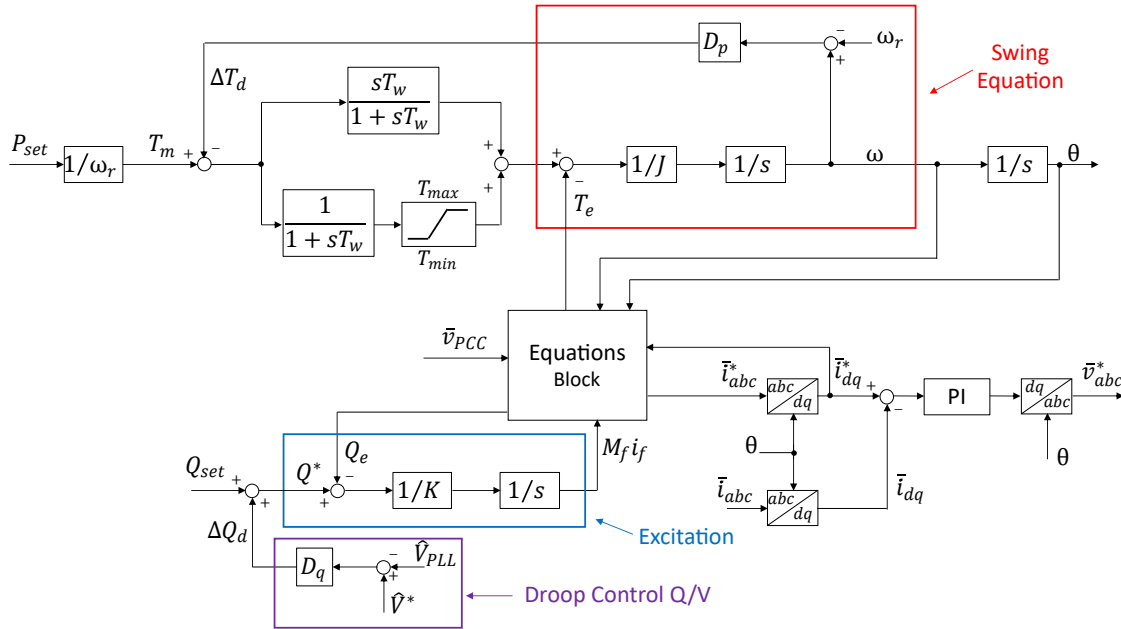


Figure 3.2.1: Synchronverter's control scheme for the enhanced version in the Laplace domain.

Differently from the base version, it belongs to the voltage-input current-output category. Therefore its output is the current reference \bar{i}_{abc}^* . Then, a closed-loop current control is performed. The error between the current reference and the measured current feeds a conventional PI regulator, used to retrieve the voltage reference \bar{v}_{abc}^* . It is built in the (d, q) reference frame and tuned as shown in Subsection 2.5.4. This enhanced version has been proposed to overcome the limits of the base one. In fact, the employment of a PI regulator guarantees the possibility to easily limit the current.

The other difference lies in the synchronization process with the grid. This

model can synchronize with the grid on its own, avoiding the employment of the PLL.

This is the version used for experimental tests and comparison.

There are some analogies and differences respect to the base version.

The reactive portion of the model (Excitation and Droop Control Q/V) are exactly the same.

The active one is modified. As can be noticed from Fig. 3.2.1, the difference between the mechanical torque T_m and the damping torque ΔT_d divides into two paths: in the first one the error passes through a high pass filter, whereas in the second one there is a low pass filter. Then, the sum between these two contributions is compared to the virtual torque T_e and the conventional swing equation block can be completed.

The other difference lies in the Equations Block, which substitutes the Synchronous Generator Equations block. It includes:

- the Park Transformation used to transform the PCC phase voltage \bar{v}_{PCC} in the \bar{v}_{dq} on the (d, q) reference frame;
- the computation of the virtual torque T_e , the virtual reactive power Q_e and electromotive force \bar{e}_{abc} :

$$\begin{cases} T_e = -M_f i_f \cdot i_q^* & (3.2.1a) \\ Q_e = \frac{3}{2}(v_q i_d^* - v_d i_q^*) & (3.2.1b) \\ \bar{e}_{abc} = \omega \cdot M_f i_f \cdot \widetilde{\sin(\theta)} & (3.2.1c) \end{cases}$$

- the implementation of the virtual impedance to retrieve the current reference \bar{i}_{abc}^* . As this model belongs to the voltage-input current-output category, the equivalent circuit which defines its connection with the grid is the one shown in Fig. 2.5.3. The difference between the electromotive force \bar{e}_{abc} and the PCC phase voltage \bar{v}_{PCC} is the voltage drop on the virtual impedance. The current reference \bar{i}_{abc}^* can be retrieved as seen in (2.5.7):

$$\bar{i}_{abc}^* = \begin{bmatrix} i_a^* \\ i_b^* \\ i_c^* \end{bmatrix} = \frac{1}{R_v + sL_v} \cdot \left(\begin{bmatrix} e_a \\ e_b \\ e_c \end{bmatrix} - \begin{bmatrix} v_{PCC,a} \\ v_{PCC,b} \\ v_{PCC,c} \end{bmatrix} \right) \quad (3.2.2)$$

Finally the PI regulator on the (d, q) reference frame can be used to retrieve the voltage reference for the PWM modulator.

In order to facilitate the comparison with the other solutions, the results will be provided in terms of powers in per unit and no torque.

$$\left\{ \begin{array}{l} P_m = \frac{\omega T_m}{S_b} \\ P_e = \frac{\omega T_e}{S_b} \end{array} \right. \quad \begin{array}{l} (3.2.3a) \\ (3.2.3b) \end{array}$$

Chapter 4

Osaka

4.1 Model Description and Implementation

Osaka is a solution realised by Osaka University in 2011 [11, 12]. Its control scheme in the Laplace domain is depicted in Fig. 4.1.1.

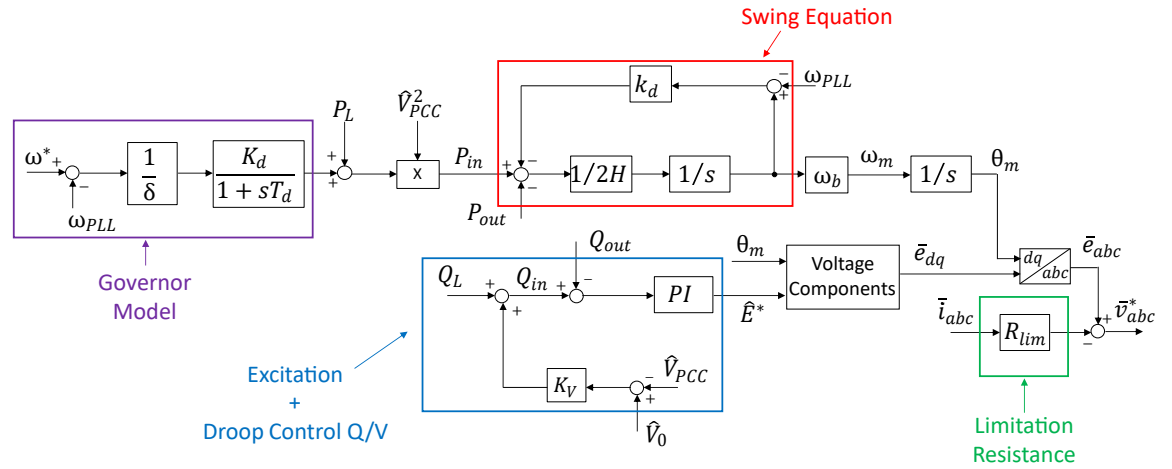


Figure 4.1.1: Osaka’s control scheme in Laplace domain.

This VSG solution belongs to the current-input voltage-output category. Therefore, it directly creates the voltage reference \bar{v}_{abc} which are used by the PWM modulator to create the commands for the inverter.

The synchronization with the grid is performed by means of a PLL, as described in Subsection 2.2.1.

The main blocks are: Governor Model, Swing Equation and Excitation +

Droop Control Q/V. They are expressed in pu.

The first block on analysis is the Governor Model. It is used to actuate the primary regulation of the frequency. It compares the reference frequency ω^* with the PLL frequency ω_{PLL} . The error is divided by the droop coefficient δ and then it passes through a low pass filter, obtaining the active power contribution P_ω :

$$P_\omega = \frac{K_d}{1 + sT_d} \cdot \frac{1}{\delta} \cdot (\omega^* - \omega_{PLL}) \quad (4.1.1)$$

where:

- K_d is the gain of the low pass filter (pu);
- T_d is the time constant of the low pass filter (pu).

Then the active power reference P_{in} can be computed, as shown in Equation (4.1.2):

$$P_{in} = \widehat{V}_{PLL}^2 \cdot (P_\omega + P_L) \quad (4.1.2)$$

where:

- P_L is the external active power reference (pu);
- \widehat{V}_{PLL} is the PCC voltage amplitude (pu).

For inductive lines, it has been already shown that active power can be calculated using (2.5.12). Therefore, Equation (4.1.2) aims to take the influence of the PCC voltage variability into account.

The successive block is constituted by the swing equation in pu already seen in (2.3.8) and written in the Laplace domain.

$$P_{in} - P_{out} = 2Hs \cdot \omega_m + k_d \cdot \Delta\omega \quad (4.1.3)$$

Here, P_{out} is the real active power measured at the PCC (pu). The damping term $k_d \cdot \Delta\omega$ is obtained as follows:

$$k_d \cdot \Delta\omega = k_d(\omega_m - \omega_{PLL})$$

where ω_{PLL} is the PLL frequency in pu.

The swing equation gives as output the Osaka's speed ω_m which is integrated to retrieve the position θ_m . This is the first piece of the model needed to create the voltage references.

The other one is the electromotive force amplitude \widehat{E}^* . It is obtained by the

Excitation+Droop Control Q/V block.

The reactive power reference Q_{in} is obtained by the sum of two terms:

$$Q_{in} = Q_L + \Delta Q_d \quad (4.1.4)$$

where:

- Q_L is the external reactive power reference (pu);

- ΔQ_d is the reactive droop term in pu, obtained as seen in Section 2.4:

$$\Delta Q_d = K_v(\widehat{V}_0 - \widehat{V}_{PCC}) \quad (4.1.5)$$

where:

- \widehat{V}_0 is the voltage reference amplitude (pu);

- K_v is the reactive droop coefficient (pu).

For Osaka, the Excitation block is built using a PI regulator, which receives the error between the reactive power reference Q_{in} and the measured power Q_{out} . Its output is \widehat{E}^* .

The integral gain is equal to K_{ecc} of Table 2.5.4, whereas the proportion gain is experimentally tuned.

With the electromotive force amplitude \widehat{E}^* and the angular position θ_m , the electromotive force vector \bar{e}_{dq} can be created. Using Park Transformation, it is converted in the three phase vector \bar{e}_{abc} .

Finally, the three phase reference voltage \bar{v}_{abc}^* is obtained as follows:

$$\bar{v}_{abc}^* = \bar{e}_{abc} - R_{lim} \bar{i}_{abc}$$

$$\bar{v}_{abc}^* = \begin{bmatrix} v_a^* \\ v_b^* \\ v_c^* \end{bmatrix} = \begin{bmatrix} e_a \\ e_b \\ e_c \end{bmatrix} - R_{lim} \cdot \begin{bmatrix} i_a \\ i_b \\ i_c \end{bmatrix} \quad (4.1.6)$$

where:

- \bar{i}_{abc} is three phase measured current (A);

- R_{lim} is a virtual resistance which can be tune to reduce the inrush currents (Ω).

Chapter 5

VISMA

5.1 Model Description and Implementation

VISMA is a model proposed for the first time in 2007 by Hans-Peter Beck and Ralf Hesse [13, 14]. This solution fully emulates the behaviour of a synchronous generator. In fact, it is realised using the complete electromechanical model of a SG. The general structure is shown in Fig. 5.1.1.

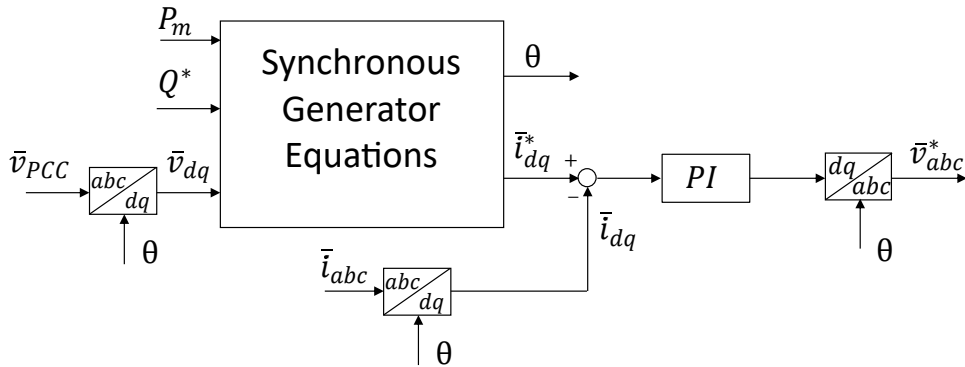


Figure 5.1.1: VISMA's control scheme in Laplace domain: general structure.

As can be noticed from the scheme, this model belongs to the voltage-input current-output category. Starting from the external active and reactive power references (respectively P_m and Q^*) and the measurement of PCC phase voltage \bar{v}_{PCC} , VISMA creates the current references on the (d, q) reference frame by means of the synchronous generators equations. Then, a conventional PI regulator is used to retrieve the voltage reference \bar{v}_{dq}^* . Finally, by means of the Park Transformation, the three phase voltage reference \bar{v}_{abc}^* is obtained.

PWM modulator will use it to define the commands for the inverter. The angle θ used for the Park Transformation is the angular position of VISMA.

Now the main blocks of the model can be singularly described. All equations are written in per unit, in the (d, q) reference frame and in the Laplace domain. The synchronization with the grid is actuated by means of PLL, as described in Subsection 2.2.1.

The first block on analysis is shown in Fig. 5.1.2. It is realised combining the electrical and the magnetic stator equations of a conventional synchronous generator, including the presence of damper windings.

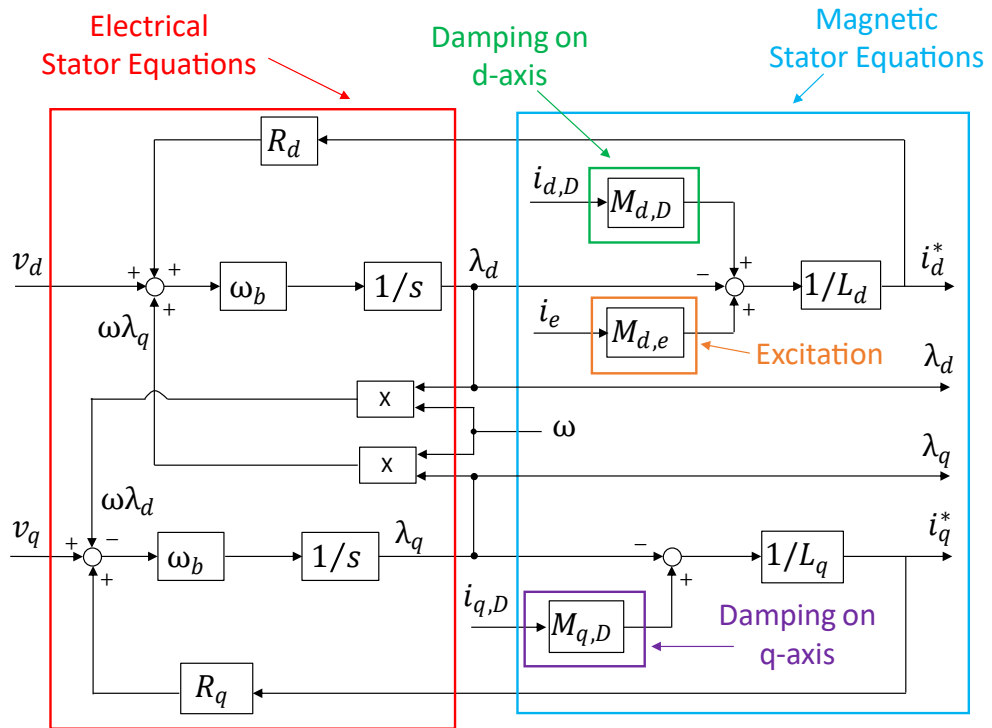


Figure 5.1.2: VISMA's control scheme in Laplace domain: stator windings.

Current references can be retrieved by means of the magnetic equations of

VISMA:

$$\begin{cases} i_d^* = \frac{1}{L_d} \cdot (M_{d,D}i_{d,D} + M_{d,e}i_e - \lambda_d) & (5.1.1a) \\ i_q^* = \frac{1}{L_q} \cdot (M_{q,D}i_{q,D} - \lambda_q) & (5.1.1b) \end{cases}$$

where:

- i_d^* is the stator current reference on the d-axis (pu);
- i_q^* is the stator current reference on the q-axis (pu);
- λ_d is the stator flux linkage on the d-axis (pu);
- λ_q is the stator flux linkage on the q-axis (pu);
- L_d is the stator inductance on the d-axis (pu);
- L_q is the stator inductance on the q-axis (pu);
- i_e is the current of the excitation winding on the d-axis (pu);
- $i_{d,D}$ is the current of the damper winding on the d-axis (pu);
- $i_{q,D}$ is the current of the damper winding on the q-axis (pu);
- $M_{d,e}$ is the mutual inductance between the stator winding and the excitation winding on the d-axis (pu);
- $M_{d,D}$ is the mutual inductance between the stator winding and the damper winding on the d-axis (pu);
- $M_{q,D}$ is the mutual inductance between the stator winding and the damper winding on the q-axis (pu).

Fluxes are calculated using the electrical equations:

$$\begin{cases} \lambda_d = \frac{1}{s} \cdot \omega_b \cdot (v_d + R_d i_d^* + \omega \lambda_q) & (5.1.2a) \\ \lambda_q = \frac{1}{s} \cdot \omega_b \cdot (v_q + R_q i_q^* - \omega \lambda_d) & (5.1.2b) \end{cases}$$

where:

- v_d is the PCC voltage on the d-axis (pu);
- v_q is the PCC voltage on the q-axis (pu);
- R_d is the stator resistance on the d-axis (pu);
- R_q is the stator resistance on the q-axis (pu);
- ω is the speed of VISMA (pu);
- ω_b is the base value of speed (rad/s).

The Laplace block schemes for the damper windings are proposed in Fig. 5.1.3.

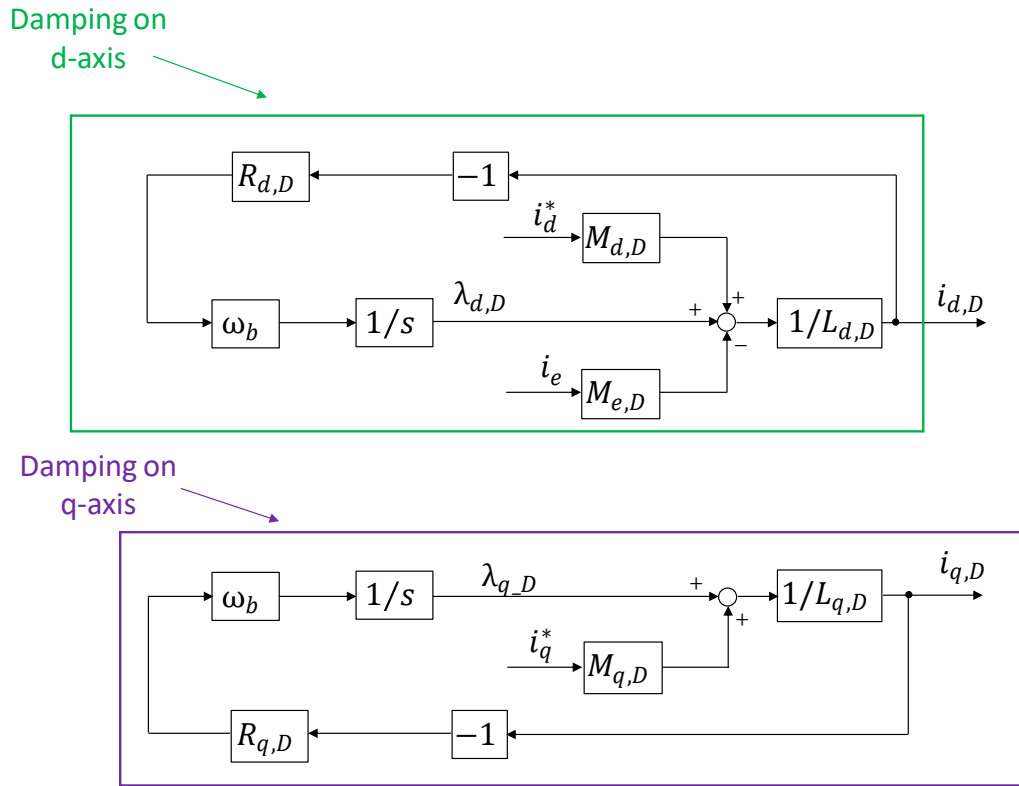


Figure 5.1.3: VISMA's control scheme in Laplace domain: damper winding on the d-axis (top) and q-axis (bottom).

The damping current on the d-axis $i_{d,D}$ is retrieved by means of the combination between the electrical equation and the magnetic equation of damper winding on the d-axis. They are respectively (5.1.3a) and (5.1.3b):

$$\begin{cases} \lambda_{d,D} = \frac{1}{s} \cdot \omega_b \cdot (-R_{d,D} i_{d,D}) & (5.1.3a) \\ i_{d,D} = \frac{1}{L_{d,D}} \cdot (\lambda_{d,D} + M_{d,D} i_d^* - M_{e,D} i_e) & (5.1.3b) \end{cases}$$

where:

- $\lambda_{d,D}$ is the flux linkage of the damper winding on d-axis (pu);
- $R_{d,D}$ is the resistance of the damper winding on d-axis (pu);
- $L_{d,D}$ is the inductance of the damper winding on d-axis (pu);
- $M_{e,D}$ is the mutual inductance between the excitation winding and the damper winding on the d-axis (pu).

The same is valid for the damping current on the q-axis $i_{q,D}$, where the electrical and the magnetic equations are respectively (5.1.4a) and (5.1.4b):

$$\begin{cases} \lambda_{q,D} = \frac{1}{s} \cdot \omega_b \cdot (-R_{q,D} i_{q,D}) & (5.1.4a) \\ i_{q,D} = \frac{1}{L_{q,D}} \cdot (\lambda_{q,D} + M_{q,D} i_q^*) & (5.1.4b) \end{cases}$$

where:

- $\lambda_{q,D}$ is the flux linkage of the damper winding on q-axis (pu);
- $R_{q,D}$ is the resistance of the damper winding on q-axis (pu);
- $L_{q,D}$ is the inductance of the damper winding on q-axis (pu).

The last quantity is the excitation current i_e . It is the output of the excitation block of Fig. 5.1.5.

VISMA has an excitation part different from the other solution, because it is the only model which aims to completely emulate the behaviour of a synchronous generator. It is proposed in Fig. 5.1.4.

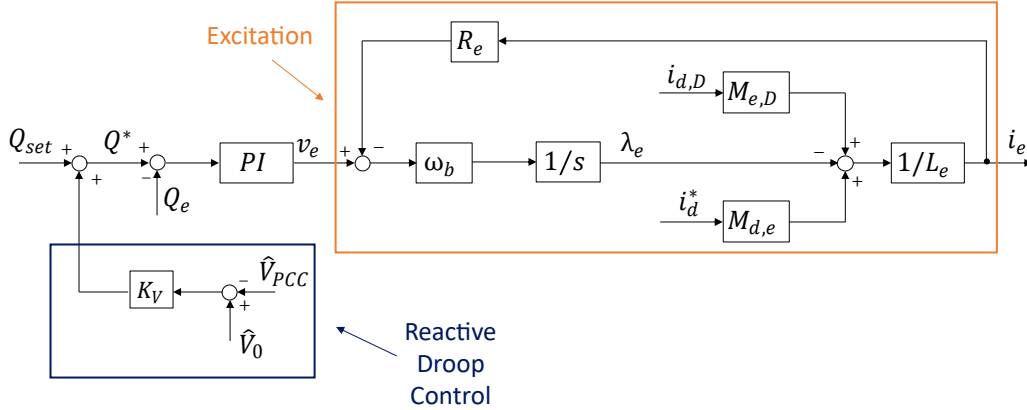


Figure 5.1.4: VISMA's control scheme in Laplace domain: excitation winding.

The excitation system embeds a reactive power controller, which is based on a PI regulator. It uses the error between the reactive power reference Q^* and the virtual reactive power Q_e to retrieve the excitation voltage v_e .

The virtual reactive power is computed as follows:

$$Q_e = v_q \cdot i_d^* - v_d \cdot i_q^* \quad (5.1.5)$$

The reactive power reference Q^* is obtained by the sum of two terms:

$$Q^* = Q_{set} + \Delta Q_d \quad (5.1.6)$$

where:

- Q_{set} is the external reactive power reference (pu);

- ΔQ_d is the reactive droop term in pu, obtained as seen in Section 2.4:

$$\Delta Q_d = K_v(\widehat{V}_0 - \widehat{V}_{PCC}) \quad (5.1.7)$$

where:

- \widehat{V}_0 is the voltage reference amplitude (pu);

- K_v is the reactive droop coefficient (pu).

Then, like for the other currents of this model, the merging of the electrical and the magnetic equations of the excitation winding leads to obtain the excitation current i_e . The two equations are respectively (5.1.8a) and (5.1.8b):

$$\begin{cases} \lambda_e = \frac{1}{s} \cdot \omega_b \cdot (-R_e i_e) & (5.1.8a) \\ i_e = \frac{1}{L_e} \cdot (M_{d,e} i_d^* + M_{e,D} i_{d,D} - \lambda_e) & (5.1.8b) \end{cases}$$

where:

- λ_e is the flux linkage of the excitation winding (pu);

- R_e is the resistance of the excitation winding (pu);

- L_e is the inductance of the excitation winding (pu).

What is described until now is the electromagnetic model of VISMA. The last part is the mechanical part, shown in Fig. 5.1.5.

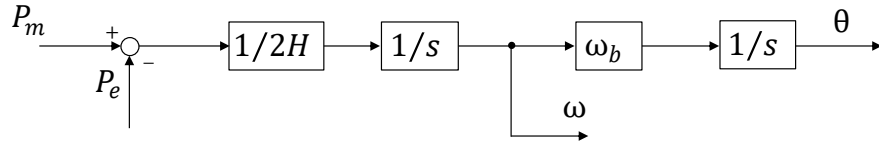


Figure 5.1.5: VISMA's control scheme in Laplace domain: swing equation.

It is characterised by the typical swing equation in per unit without the damping term, as already seen in (2.3.5):

$$P_m - P_e = 2Hs\omega \quad (5.1.9)$$

Here P_e is the virtual active power obtained by equation (5.1.10) in pu:

$$P_e = v_d \cdot i_d^* + v_q \cdot i_q^* \quad (5.1.10)$$

The damping term of the swing equation is used to take the effect of damper windings into account. In this case it is not necessary, thanks to the presence of the damper windings.

The swing equation gives as output the VISMA speed ω and its angular position θ . The former is used to define the electromotive terms $\omega\lambda_d$ and $\omega\lambda_q$ of the previous equations. The latter allows to perform the Park Transformation.

Chapter 6

VISMA1

6.1 Model Description and Implementation

VISMA1 is a simplified version of VISMA, designed by Yong Chen, Ralf Hesse, Dirk Turschner and Hans-Peter Beck in 2011 [15]. The control block scheme of the model is depicted in Fig. 6.1.1.

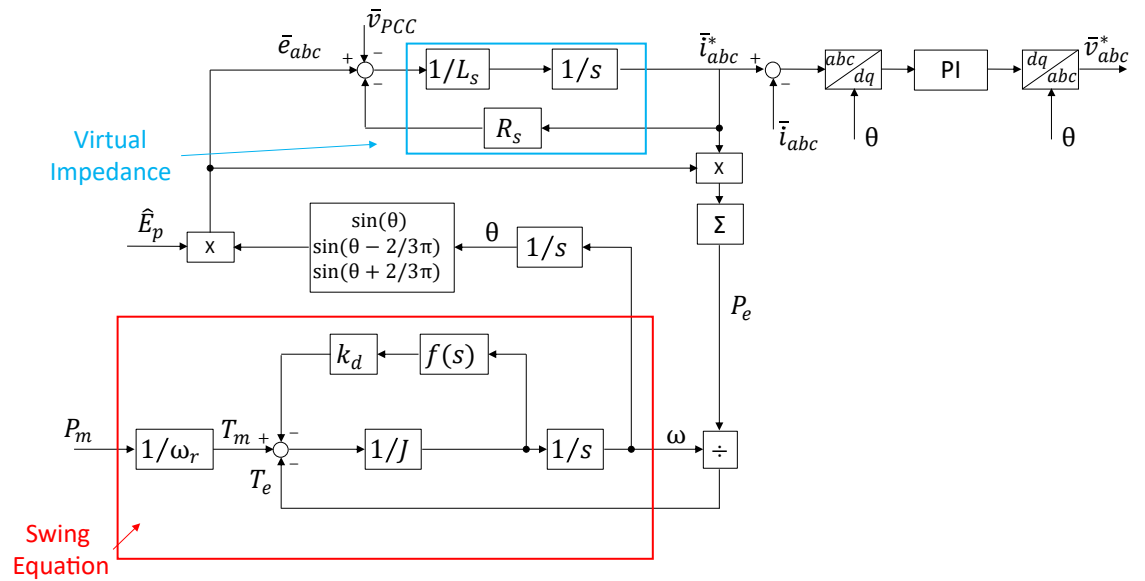


Figure 6.1.1: VISMA1's control scheme in Laplace domain.

It is a voltage-input current-output model. Therefore, it gives current references as output. In the version proposed in the literature, a hysteresis regulator is used to retrieve the commands for the inverter. This kind of

control introduces not negligible noise, therefore it has been decided to implement VISMA1 using the conventional PI regulator designed in Subsection 2.5.4. It is used to actuate a closed loop current control in the (d, q) reference frame and retrieve the voltage reference \bar{v}_{abc}^* for the PWM modulator. A reliable current limitation can be easily performed.

The synchronization with the grid is actuated by means of the PLL, as seen in Subsection 2.2.1.

As previously said, this is a simplified version of VISMA. Therefore it does not embed all the equations of a synchronous generator. Three main blocks can be distinguished: the active part, the reactive part and the virtual impedance block.

The active part is constituted by a slight different form of the swing equation described in (2.3.6):

$$T_m - T_e = J \frac{d\omega}{dt} + k_d f(s) \frac{d\omega}{dt} \quad (6.1.1)$$

where:

- T_m is the mechanical torque, which emulates the mechanical torque of a primary motor for conventional SGs;

- T_e is the virtual torque of VISMA1;

- $f(s)$ is the phase compensation term, defined as follows:

$$f(s) = \frac{1}{1 + s\tau} \quad (6.1.2)$$

It is a low pass filter with a time constant τ . In this case the feedback in the swing equation is not the speed but its derivative.

The swing equation is used to retrieve the speed of VISMA1 ω and its angular position θ .

In order to facilitate the comparison with the other solutions, this model has been implemented with powers instead of torques:

$$\left\{ \begin{array}{l} P_m = \frac{\omega T_m}{S_b} \\ P_e = \frac{\omega T_e}{S_b} \end{array} \right. \quad (6.1.3a)$$

$$(6.1.3b)$$

where the virtual active power in pu P_e can be computed by means of the following equation:

$$P_e = v_\alpha \cdot i_\alpha^* + v_\beta \cdot i_\beta^* \quad (6.1.4)$$

The excitation block of VISMA1 is shown in Fig. 6.1.2.

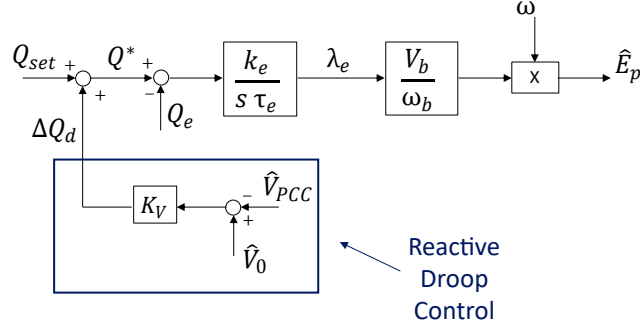


Figure 6.1.2: VISMA1's excitation block.

It embeds a reactive power controller in per unit. It provides the error between the reactive power reference Q^* and the virtual reactive power Q_e to a pure integrator, in order to retrieve the amplitude of the electromotive force \hat{E}_p of VISMA1. The pure integrator is characterised by a gain k_e and a excitation time constant τ_e . The values are in Table 2.5.4.

Reactive droop control is also embedded. In fact, the reference Q^* is defined by the sum of the external reactive reference Q_{set} and the reactive droop term ΔQ_d . It is obtained as seen in Section 2.4:

$$\Delta Q_d = K_v(\hat{V}_0 - \hat{V}_{PCC}) \quad (6.1.5)$$

where:

- \hat{V}_0 is the voltage reference amplitude (pu);

- K_v is the reactive droop coefficient (pu).

With the electromotive force amplitude \hat{E}_p and the angular position θ , the three phase electromotive force \bar{e}_{abc} can be retrieved. Finally, as described in Subsection 2.5.4, the equivalent circuit for this kind of model is the one shown in Fig. 2.5.3. The difference between the electromotive force \bar{e}_{abc} and the PCC phase voltage \bar{v}_{PCC} is the voltage drop on this impedance. Knowing its value, current reference \bar{i}_{abc}^* can be retrieved:

$$\bar{i}_{abc}^* = \begin{bmatrix} i_a^* \\ i_b^* \\ i_c^* \end{bmatrix} = \frac{1}{R_v + sL_v} \cdot \left(\begin{bmatrix} e_a \\ e_b \\ e_c \end{bmatrix} - \begin{bmatrix} v_{PCC,a} \\ v_{PCC,b} \\ v_{PCC,c} \end{bmatrix} \right) \quad (6.1.6)$$

Chapter 7

VISMA2

7.1 Model Description and Implementation

VISMA2 is the second simplified version of VISMA, proposed by Yong Chen, Ralf Hesse, Dirk Turschner and Hans-Peter Beck in 2012 [17]. Its control scheme in the Laplace domain is proposed in Fig. 7.1.1.

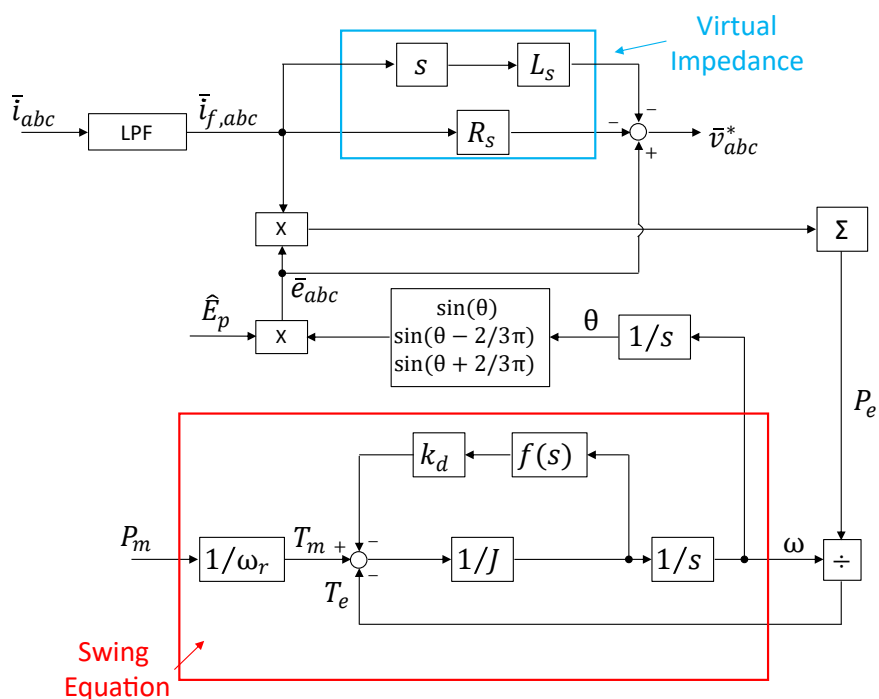


Figure 7.1.1: VISMA2's control scheme in Laplace domain.

Differently from VISMA and VISMA1, it belongs to the current-input voltage-

output category. Therefore, it directly produces the voltage reference \bar{v}_{abc}^* for the PWM modulator. As mentioned in its Chapter, VISMA1 has been originally designed with a hysteresis controller. Consequently, the current waveform is characterized by high noise. VISMA2 has been proposed in order to overcome this issue. Since it directly produces the voltage reference, no regulator is employed.

Comparing the control scheme of VISMA1 in Fig. 6.1.1 with the scheme of VISMA2, it can be noticed that they are very similar. Also for VISMA2 the synchronization with the grid is performed by means of PLL, as described in Sybsection 2.2.1.

VISMA2 is constituted by three blocks: active part, reactive part and virtual impedance block.

The active part is the same of VISMA1. It is a revised version of the swing equation seen in (2.3.6):

$$T_m - T_e = J \frac{d\omega}{dt} + k_d f(s) \frac{d\omega}{dt} \quad (7.1.1)$$

where:

- T_m is the mechanical torque, which emulates the mechanical torque of a primary motor for conventional SGs;
- T_e is the virtual torque of VISMA2;
- $f(s)$ is the phase compensation term, defined as follows:

$$f(s) = \frac{1}{1 + s\tau} \quad (7.1.2)$$

By means of the swing equation, VISMA2 speed ω and its angular position θ can be retrieved.

In order to facilitate the comparison with the other solutions, even this model has been implemented with powers in pu and no torques:

$$\left\{ \begin{array}{l} P_m = \frac{\omega T_m}{S_b} \end{array} \right. \quad (7.1.3a)$$

$$\left\{ \begin{array}{l} P_e = \frac{\omega T_e}{S_b} \end{array} \right. \quad (7.1.3b)$$

where P_e in pu can be computed by means of the following equation:

$$P_e = i_\alpha \cdot v_\alpha^* + i_\beta \cdot v_\beta^* \quad (7.1.4)$$

Virtual active power P_e is computed using the voltage references $\bar{v}_{\alpha\beta}^*$ and the measured current $\bar{i}_{\alpha\beta}$ in the (α, β) reference frame. It means that it is computed before the voltage drop on the filter impedance. The real active power, in stead, is measured at PCC. There will be a difference between virtual active power and real active power, constituted by the contribution of the filter resistance.

Also for the reactive part, all the concepts described for VISMA1 are valid for VISMA2. The excitation block of VISMA2 is proposed in Fig. 7.1.2.

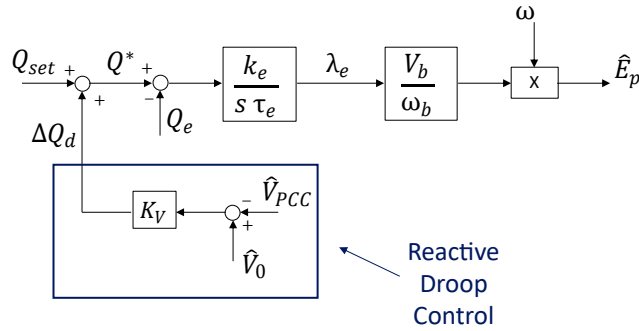


Figure 7.1.2: VISMA2's excitation block.

A reactive power controller is used to obtain the electromotive force amplitude \hat{E}_p . To do this, the reactive power reference Q^* is compared with the virtual reactive power Q_e . The error passes through a pure integrator which gives \hat{E}_p as output. The values of the gain k_e and the excitation time constant τ_e are listed in Table 2.5.4. Even in this case, the reactive droop control is embedded. Q^* is defined as the sum between the external reactive power Q_{set} and the reactive droop term ΔQ_d . This is obtained as seen in Section 2.4:

$$\Delta Q_d = K_v(\hat{V}_0 - \hat{V}_{PCC}) \quad (7.1.5)$$

where:

- \hat{V}_0 is the voltage reference amplitude (pu);

- K_v is the reactive droop coefficient (pu).

With the amplitude \hat{E}_p and the angular position θ the three phase electromotive force \bar{e}_{abc} can be retrieved.

As VISMA2 is a current-input voltage-output model, the connection between this kind of VSG and the PCC is performed as described in the Subsection

2.5.5. But, differently from Synchronverter base form and Osaka, the electromotive force \bar{e}_{abc} does not correspond to the voltage reference \bar{v}_{abc}^* . In fact, there is an additional stage constituted by the virtual stator impedance, as shown in Fig. 7.1.3.

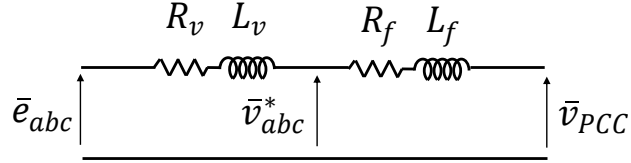


Figure 7.1.3: VISMA2's equivalent circuit.

In this case, the inverter current is measured and the voltage drop on the virtual impedance can be computed. Now, one of the two main problems of this model rises. A derivation of current is performed. This operation strongly amplifies the noise of the waveform. Therefore it is necessary to filter the current before to use it for measurement. The filter is a low pass filter with the following transfer function:

$$LPF(s) = \frac{1}{1 + s/\omega_f} \quad (7.1.6)$$

where ω_f is the cut-off frequency of the filter (rad/s).

Finally, the voltage reference \bar{v}_{abc}^* can be obtained as follows:

$$\bar{v}_{abc}^* = \bar{e}_{abc} - (R_v + sL_v) \cdot \bar{i}_{abc}$$

$$\bar{v}_{abc}^* = \begin{bmatrix} v_a^* \\ v_b^* \\ v_c^* \end{bmatrix} = \begin{bmatrix} e_a \\ e_b \\ e_c \end{bmatrix} - (R_v + sL_v) \cdot \begin{bmatrix} i_a \\ i_b \\ i_c \end{bmatrix} \quad (7.1.7)$$

Here the second main problem of VISMA2 can be highlighted.

Since it is a voltage-output model, voltage reference \bar{v}_{abc}^* is directly provided to a PWM modulator. It is an open loop control, where currents are measured but not controlled. Therefore, there is no current limitation system. Additional blocks must be implemented to perform a safe and reliable saturation.

Chapter 8

SPC

8.1 Model Description and Implementation

SPC is a voltage-input current-output model proposed by Abengoa Research in 2011. Its control block scheme in the Laplace domain is shown in Fig.8.1.1.

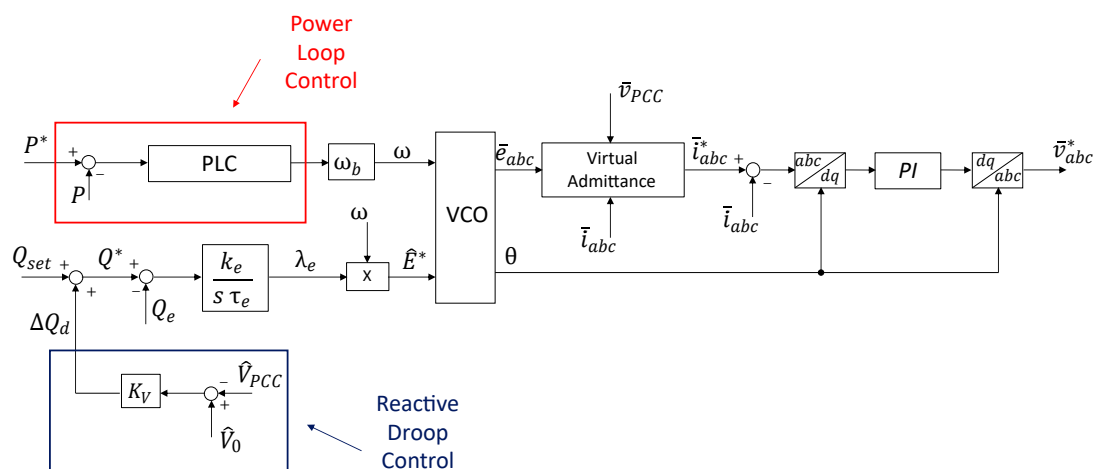


Figure 8.1.1: SPC's control scheme in Laplace domain.

SPC is a self-synchronizing model. It autonomously synchronizes with the grid, avoiding the employment of a PLL.

The main blocks are: Power Loop Controller (PLC), reactive block, Voltage Controller Oscillator (VCO) and virtual admittance block. All of them are expressed in per unit.

The PLC will be accurately described in the following Section. It is used to provide the SPC speed ω in per unit, starting from the error between the active power reference P^* and the measured active power P in pu. It is computed as shown in (2.6.1) in the (α, β) reference frame:

$$P = v_\alpha \cdot i_\alpha + v_\beta \cdot i_\beta \quad (8.1.1)$$

As regards the reactive part, the error between the reactive power reference Q^* and the real reactive power Q feeds a pure integrator. The values for the gain k_e and the excitation time constant τ_e are proposed in Table 2.5.4. The output of the integrator is the amplitude of the electromotive force \hat{E}^* . The reactive droop control is also implemented. In fact, the reactive power reference Q^* is obtained by the sum between the external reference Q_{set} and the reactive droop term ΔQ_d . It is obtained as seen in Section 2.4:

$$\Delta Q_d = K_v(\hat{V}_0 - \hat{V}_{PCC}) \quad (8.1.2)$$

where:

$-\hat{V}_0$ is the voltage reference amplitude (pu);

$-K_v$ is the reactive droop coefficient (pu).

The VCO provides two output. The former is the angular position θ of SPC, obtained from the integration of the speed ω . Then, θ and \hat{E}^* are used to retrieve the three phase electromotive force \bar{e}_{abc} .

Since SPC is a voltage-input current-output model, the corresponding circuit model is the one depicted in Fig. 2.5.3.

Current references \bar{i}_{abc}^* can be finally computed, by means of the multiplication between the virtual admittance and the difference between the electromotive force and the PCC voltage:

$$\bar{i}_{abc}^* = \frac{1}{R_v + sL_v} \cdot (\bar{e}_{abc} - \bar{v}_{PCC})$$

$$\bar{i}_{abc}^* = \begin{bmatrix} \bar{i}_a^* \\ \bar{i}_b^* \\ \bar{i}_c^* \end{bmatrix} = \frac{1}{R_v + sL_v} \cdot \left(\begin{bmatrix} e_a \\ e_b \\ e_c \end{bmatrix} - \begin{bmatrix} v_{PCC,a} \\ v_{PCC,b} \\ v_{PCC,c} \end{bmatrix} \right) \quad (8.1.3)$$

After that, Park Transformation is applied and then the PI regulator in the (d, q) reference frame is used to retrieve the voltage reference \bar{v}_{dq}^* . Finally, the Park Transformation allows to obtain the voltage reference \bar{v}_{abc}^* for the PWM modulator.

8.2 Power Loop Controller

Three different types of PLC have been studied: Synchronous Generator Emulation, PI Regulator and Lead-Lag.

8.2.1 Synchronous Generator Emulation

The first type of PLC on analysis is the Synchronous Generator (SG). Its transfer function is the following:

$$PLC_{SG}(s) = \frac{S_b}{\omega_b} \frac{k\omega_c}{s + \omega_c} \quad (8.2.1)$$

It is based on the conventional swing equation, already described in (2.3.8):

$$P^* - P = 2H \frac{d\omega}{dt} + k_d \cdot \Delta\omega \quad (8.2.2)$$

The block scheme related to (8.2.2) is shown in Fig. 8.2.1.

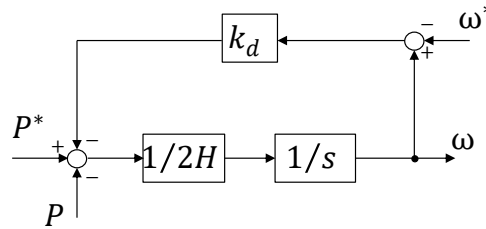


Figure 8.2.1: SPC SG: Block scheme of swing equation.

In Fig. 8.2.1 ω^* is the reference speed (pu).

The transfer function retrievable from the scheme in Fig. 8.2.1 is:

$$PLC_{SG}(s) = \frac{1}{2Hs + k_d} \quad (8.2.3)$$

Comparing (8.2.1) with (8.2.3), the following relationships can be defined:

$$\begin{cases} k = \frac{\omega_b}{S_b \cdot k_d} & (8.2.4a) \\ \omega_c = \frac{k_d}{2H} & (8.2.4b) \end{cases}$$

With this kind of PLC, SPC emulates the behaviour of the conventional synchronous generators. There is no dedicated part for the frequency droop

control. Therefore, there is a strict coupling between the damping factor k_d and the frequency droop coefficient: the former is the inverse of the latter. When a grid frequency occurs, SPC SG injects active power according to the tuning of the damping factor k_d .

The active power reference P^* is equal to the external active power reference P_{set} .

8.2.2 PI Regulator

The second type of PLC is a conventional PI regulator. Its transfer function is the following:

$$PLC_{PI}(s) = \frac{S_b k_p s + ki}{\omega_b s} \quad (8.2.5)$$

A PI regulator guarantees a reliable active power control, with no steady state error. On the other hand, in case of grid frequency variations, the droop control cannot be actuated. Therefore, an additional dedicated governor model can be added. It is shown in Fig. 8.2.2.

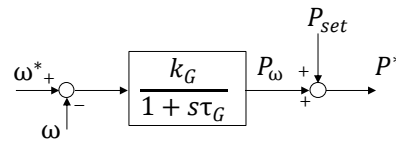


Figure 8.2.2: SPC PI's governor.

The governor model is used to perform the active droop control, as described in Section 2.4. It compares the reference frequency ω^* with the SPC frequency ω . The error is multiplied by k_G , which is the inverse of the droop coefficient. It can be arbitrarily tuned. Then, the product passes through a low pass filter obtaining the active droop term P_ω . The filter has a time constant τ_G and it is used to avoid abrupt variations of active power when grid frequency changes.

In this case the total active power reference P^* is the sum between the external active power reference P_{set} and the active droop term P_ω .

8.2.3 Lead-Lag

The third type of PLC is a Lead-Lag. Its transfer function is the following:

$$PLC_{LL}(s) = \frac{S_b}{\omega_b} \frac{k_p s + k_i}{s + k_g} \quad (8.2.6)$$

This structure guarantees no steady state error as happens for SPC PI. Moreover, it has an additional freedom degree given by k_g . A properly tuning of this parameter leads to the damping-droop decoupling. Therefore, SPC LL can actuate an active droop control, which will depend only on the tuning of k_g . No additional blocks are needed.

In this case the active power reference P^* is equal to the external active power reference P_{set} .

Chapter 9

VSYNC

9.1 Model Description and Implementation

VSYNC is a model proposed by M.P.N van Wessenbeek, S.W.H. de Haan, P. Varela and K. Visscher in 2009 [21]. Its control scheme in the Laplace domain is illustrated in Fig. 9.1.1.

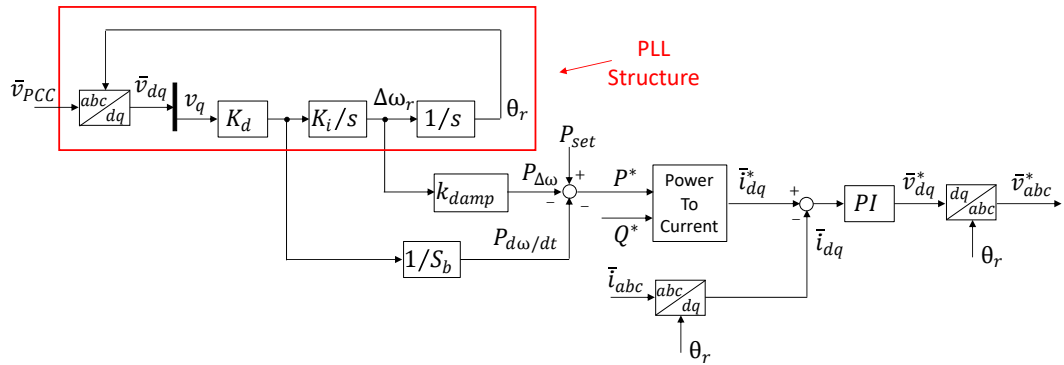


Figure 9.1.1: VSYNC's control scheme in Laplace domain.

As can be observed from the control scheme, it is a voltage-input current-output model. It provides as output the current reference \vec{i}_{dq}^* in the (d, q) reference frame.

VSYNC is a peculiar model because, differently from many other solutions, its core is constituted by a PLL structure, highlighted in red in Fig. 9.1.1. It can be noticed that there are many elements in common with the conventional structure of PLL, described in Subsection 2.2.1 and shown in Fig. 2.2.3. Since it is based on a PLL structure, the VSYNC model can synchronize with

the grid on its own, without the use of external elements.

Differently from the conventional PLL of Fig. 2.2.3, this model is built in absolute value and the PI regulator is substituted by a pure integrator, but the working principle is the same. Even here in fact, a synchronization process with the grid is performed. The PCC phase voltage \bar{v}_{PCC} is measured and transformed in the vector \bar{v}_{dq} by means of the Park Transformation. The angle used to actuate the rotation and define the (d, q) reference frame is the VSYNC angular position θ_r . The difference between the grid phase voltage θ_g and θ_r is indicated with δ . The q-axis component of \bar{v}_{dq} will be:

$$v_q = V_b \sin(\theta_g - \theta) = V_b \sin(\delta) \quad (9.1.1)$$

where V_b is the base value of voltage.

v_q is provided to a pure integrator to retrieve the speed variation $\Delta\omega_r$. Integrating $\Delta\omega_r$, the angular position θ_r is obtained. In steady state, the integrator zeroes the q-axis component v_q and consequently even the difference between the VSYNC angle θ_r and the grid phase θ_g . The synchronization is completed.

VSYNC is based on the PLL structure because a strict analogy between it and the swing equation can be retrieved. The active power reference P^* in per unit can be written as follows:

$$P^* = P_{set} - P_{\Delta\omega} - P_{d\omega/dt} \quad (9.1.2)$$

where:

- P_{set} is the external active power reference (pu);
- $P_{\Delta\omega}$ is the inertial term (pu);
- $P_{d\omega/dt}$ is the derivative term (pu).

$P_{\Delta\omega}$ and $P_{d\omega/dt}$ can be retrieved thanks to the analogy between the PLL structure and the swing equation.

The starting point is the conventional swing equation described in (2.3.4):

$$P^* - P_e = \frac{2HS_b}{\omega_b^2} \cdot \omega \cdot \frac{d\omega}{dt} \quad (9.1.3)$$

where P_e is the active power flowing from the inverter to the grid.

As actuated in Subsection 2.5.6, a linearised model can be realised to define the needed parameters. In the Laplace domain, considering a small deviation (denoted by the prefix Δ) around the nominal working point, and assuming $\omega \simeq \omega_b$, (9.1.3) becomes:

$$\Delta P_e = \frac{2HS_b}{\omega_b} \cdot s\Delta\omega \quad (9.1.4)$$

ΔP_e in absolute value is obtainable as seen in (2.5.15), applying the base value S_b :

$$\Delta P_e = \frac{3}{2} \frac{V_b^2}{X_{tot}} \sin(\Delta\delta) \quad (9.1.5)$$

Substituting (9.1.1) in (9.1.5), an alternative form for the active power P_e can be retrieved:

$$\Delta P_e = \frac{3}{2} \frac{V_b}{X_{tot}} \cdot V_b \sin(\Delta\delta) = \frac{3}{2} \frac{V_b}{X_{tot}} \Delta v_q = K_d \Delta v_q \quad (9.1.6)$$

This first comparison leads to the definition of the gain K_d :

$$K_d = \frac{3}{2} \frac{V_b}{X_{tot}} \quad (9.1.7)$$

the first gain on the direct chain in Fig. 9.1.1 expressed in V/Ω . Finally, the derivative term $P_{d\omega/dt}$ in pu is retrieved:

$$P_{d\omega/dt} = \frac{K_d}{S_b} v_q \quad (9.1.8)$$

From the Fig. 9.1.1 it can be noticed that:

$$s\Delta\omega = K_i K_d \Delta v_q = K_i \Delta P_e \quad (9.1.9)$$

Comparing (9.1.9) with (9.1.4) the integral gain K_i can be defined:

$$K_i = \frac{\omega_b}{2HS_b} \quad (9.1.10)$$

Finally the damping term $P_{\Delta\omega}$ can be retrieved as follows:

$$P_{\Delta\omega} = k_{damp} \Delta\omega_r \quad (9.1.11)$$

where k_{damp} corresponds to k_d of Table 2.5.3.

All the contributions for the active power reference P^* have been defined.

As regards the reactive power reference Q^* , no excitation part is implemented. Q^* is constituted by two contributions: the external reactive power reference Q_{set} and the reactive droop term ΔQ_d . The reactive droop control is used to balance the voltage variation by means of reactive droop term ΔQ_d ,

as described in Section 2.4.

The two power references in per unit are used to compute the current reference \bar{i}_{dq}^* in per unit. No active or reactive power loop control is used. The PCC phase voltage \bar{v}_{PCC} is measured and transformed in \bar{v}_{dq} by means of Park Transformation, using the VSYNC angular position θ_r . The two current reference components in per unit can be finally computed:

$$\left\{ \begin{array}{l} i_d^* = \frac{P^* v_d + Q^* v_q}{\sqrt{v_d^2 + v_q^2}} \\ i_q^* = \frac{P^* v_q - Q^* v_d}{\sqrt{v_d^2 + v_q^2}} \end{array} \right. \quad (9.1.12a)$$

$$\left\{ \begin{array}{l} i_d^* = \frac{P^* v_d + Q^* v_q}{\sqrt{v_d^2 + v_q^2}} \\ i_q^* = \frac{P^* v_q - Q^* v_d}{\sqrt{v_d^2 + v_q^2}} \end{array} \right. \quad (9.1.12b)$$

Then, a conventional PI regulator is used to retrieve the voltage reference \bar{v}_{dq}^* . Successively, the three phase voltage reference \bar{v}_{abc}^* is retrieved by means of the Park Transformation. By means of the PI regulator the current limitation can be easily actuated.

Chapter 10

Kawasaki

10.1 Model Description and Implementation

Kawasaki is a model proposed by Y. Hirase, K. Abe, K. Sugimoto and Y. Shindo in 2012 [22]. The block scheme in the Laplace domain is illustrated in Fig. 10.1.1.

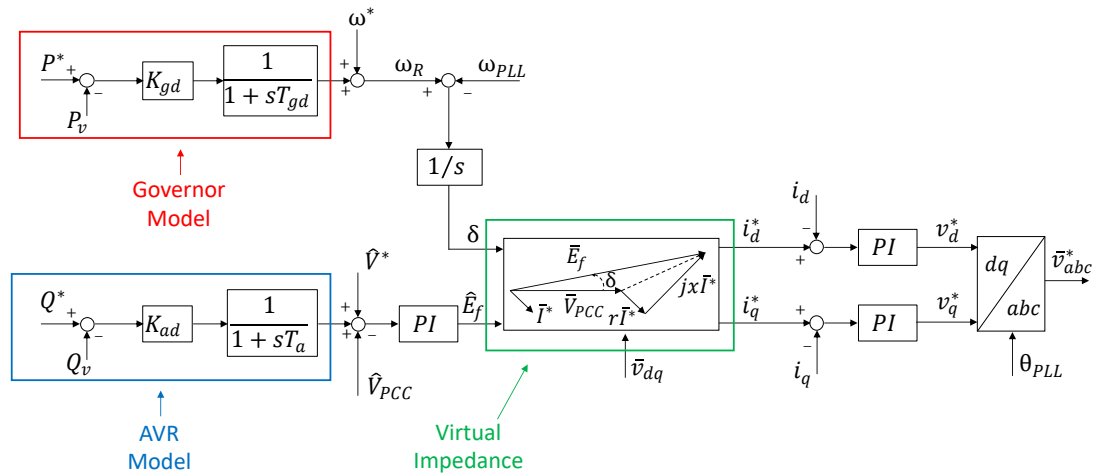


Figure 10.1.1: Kawasaki's control scheme in Laplace domain.

It is a voltage-input current-output model, which provides the current reference \vec{i}_{dq}^* in the (d, q) reference frame.

The synchronization with the grid is performed by means of PLL, as described in Subsection 2.2.1.

It is composed by three main blocks: Governor Model, AVR Model and Virtual Impedance Block. Each of them is implemented in per unit.

The Governor Model compares the active power reference P^* with the virtual active power P_v , computed as follows:

$$P_v = v_d i_d^* + v_q i_q^* \quad (10.1.1)$$

where v_d and v_q are the components of the PCC phase voltage \bar{v}_{PCC} transformed in \bar{v}_{dq} by means of Park Transformation. It is performed using the PLL phase angle θ_{PLL} .

The active power error is multiplied by the active droop coefficient K_{gd} and then it passes through a low pass filter characterized by an unitary gain and a time constant T_{gd} . The output is the frequency variation $\Delta\omega_{gd}$ related to the active power error. This is the principle of frequency droop control described in Section 2.4. When a grid frequency variation occurs, Kawasaki can inject active power according to the tuning of K_{gd} .

Then, the sum between the frequency variation $\Delta\omega_{gd}$ and the reference frequency ω^* defines the Kawasaki frequency ω_R .

The Kawasaki model belongs to the voltage-input current-output category. Therefore, its connection with the grid can be described by the equivalent circuit in Fig. 2.5.3. The electromotive force \bar{e}_{abc} and the PCC phase voltage \bar{v}_{abc} can be respectively represented as the vectors \bar{E}_f and \bar{V}_{PCC} . The phase angle between them is indicated with δ . Integrating the difference between Kawasaki frequency ω_R and the PLL frequency ω_{PLL} , δ can be retrieved. This is the phase angle of the electromotive force vector \bar{E}_f .

The amplitude of \bar{E}_f can be obtained by the AVR model.

It shares the same structure with the governor model: the error between the reactive power reference Q^* and the virtual reactive power Q_v is multiplied by the gain K_a and the result passes through a low pass filter characterised by the time constant T_a . The outcome is the voltage variation $\Delta\hat{V}$. Q_v is calculated as follows:

$$Q_v = v_q i_d^* - v_d i_q^* \quad (10.1.2)$$

Then, the voltage error ϵ_v is retrieved as follows:

$$\epsilon_v = \Delta\hat{V} + \hat{V}^* - \hat{V}_{PCC} \quad (10.1.3)$$

where:

- \hat{V}_{PCC} is the amplitude of the PCC phase voltage in pu;

- \hat{V}^* is the reference voltage in pu.

This error feeds a PI regulator which provides the electromotive force amplitude \widehat{E}_f . The integral gain of the regulator is equal to K_{ecc} of Table 2.5.4, whereas k_p is experimentally tuned.

By means of the amplitude \widehat{E}_f and the phase angle δ , the components of the vector \overline{E}_f on the (d, q) reference frame can be retrieved:

$$\begin{cases} e_d = \widehat{E}_f \cos(\delta) & (10.1.4a) \\ e_q = \widehat{E}_f \sin(\delta) & (10.1.4b) \end{cases}$$

The Kawasaki model is based on the concept of virtual admittance as other VSG solutions. The difference between \overline{E}_f and \overline{V}_{PCC} multiplied by the virtual admittance defines the current reference vector \overline{I}_{dq}^* . But, differently from what is described in (2.5.7), the Kawasaki's virtual impedance is algebraically implemented. Therefore, no integration is performed and the two components of \overline{I}_{dq}^* in pu can be computed as follows:

$$\begin{bmatrix} i_d^* \\ i_q^* \end{bmatrix} = Y \cdot \left(\begin{bmatrix} e_d \\ e_q \end{bmatrix} - \begin{bmatrix} v_d \\ v_q \end{bmatrix} \right) \quad (10.1.5)$$

where Y is the virtual admittance matrix defined in (10.1.6):

$$Y = \frac{1}{r_v^2 + l_v^2} \begin{bmatrix} r_v & l_v \\ -l_v & r_v \end{bmatrix} \quad (10.1.6)$$

Here r_v and l_v are the parameters defined in (2.5.6).

Finally the current reference \overline{i}_{dq}^* is compared with the measured current i_{dq} and the error feeds a PI regulator, which produces the voltage reference for the PWM modulator. With the employment of a PI regulator the limitation of current can be easily performed.

Chapter 11

CVSM

11.1 Model Description and Implementation

CVSM is a model proposed by S. D'Arco, J. A. Suul and O. B. Fosso in 2013 [23]. The general block scheme is illustrated in Fig. 11.1.1. It shows the main blocks of this control algorithm.

CVSM can autonomously synchronize with the grid, avoiding the employment of a PLL.

The model is built on the (d, q) reference frame, defined by the CVSM angular position θ_{VSM} .

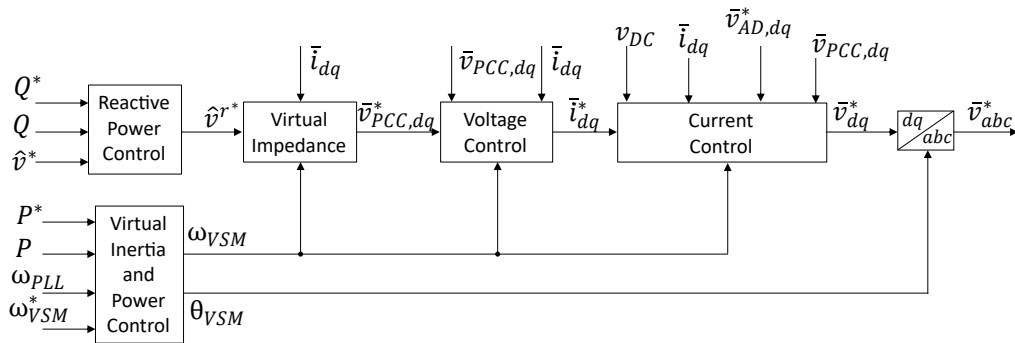


Figure 11.1.1: CVSM's control scheme in Laplace domain.

The first step is the measurement processing. As shown in Fig. 11.1.2, PCC phase voltage \bar{v}_{PCC} and the inverter current \bar{i}_{abc} are measured to obtain:

- inverter current \bar{i}_{dq} in pu;
- PCC phase voltage $\bar{v}_{PCC,dq}$ in pu;

-active power P and reactive power Q in pu:

$$\begin{cases} P = v_{PCC,d}i_d + v_{PCC,q}i_q & (11.1.1a) \\ Q = v_{PCC,q}i_d - v_{PCC,d}i_q & (11.1.1b) \end{cases}$$

Moreover, the active damping algorithm in pu is implemented to reduce the oscillations caused by the filter between the inverter and the grid. The block scheme is proposed on the bottom of Fig. 11.1.2. A low pass filter is used to eliminate all the oscillations on the PCC phase voltage $\bar{v}_{PCC,dq}$, obtaining ϕ_{dq} . The cut-off frequency ω_{AD} is set to 5 Hz. Then, the difference between $\bar{v}_{PCC,dq}$ and ϕ_{dq} contains only the undesired components of $\bar{v}_{PCC,dq}$. The active damping voltage $\bar{v}_{AD,dq}^*$ can be finally defined, setting the gain K_{AD} to 1 pu.

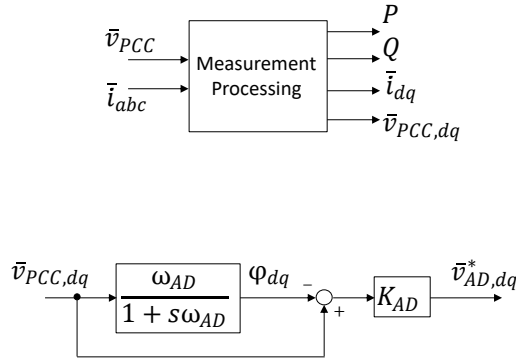


Figure 11.1.2: CVSM's control scheme: Measuring Processing (top) and Active Damping (bottom).

In Fig. 11.1.3 the two external power control loops in pu are shown. On the top there is the Reactive Power Droop Controller. It is used to retrieve the amplitude of the electromotive force amplitude \hat{v}^{r*} . The gain k_q is the reactive droop coefficient. It multiplies the difference between the reactive power reference Q^* and the filtered reactive power Q_m . The result of the reactive droop control is the voltage variation Δv . The concept is the same of what seen in Section 2.4. Finally, the electromotive force amplitude \hat{v}^{r*} is:

$$\hat{v}^{r*} = \hat{v}^* + \Delta v \quad (11.1.2)$$

On the bottom of the Fig. 11.1.3 the active part of the model is also proposed. It is divided into two parts: Frequency Droop and Swing Equation. The former block is used to actuate the active droop control as described in

Section 2.4. The active power reference P^{r*} is the sum of two contributions: the external active power reference P^r and the active droop term P_ω defined as follows:

$$P_\omega = k_\omega(\omega_{VSM}^* - \omega_{VSM}) \quad (11.1.3)$$

where k_ω is the active droop coefficient in pu.

Then, the conventional swing equation is implemented, as already seen in (2.3.8):

$$P^{r*} - P = T_a \frac{d\omega_{VSM}}{dt} + k_d \cdot (\omega_{VSM} - \omega_{PLL}) \quad (11.1.4)$$

where $T_a = 2H$. CVSM does not need PLL to synchronize with the grid, but PLL is used to perform the damping as can be seen from (11.1.4).

By means of the swing equation, the CVSM speed ω_{VSM} and the CVSM angular position θ_{VSM} can be retrieved.

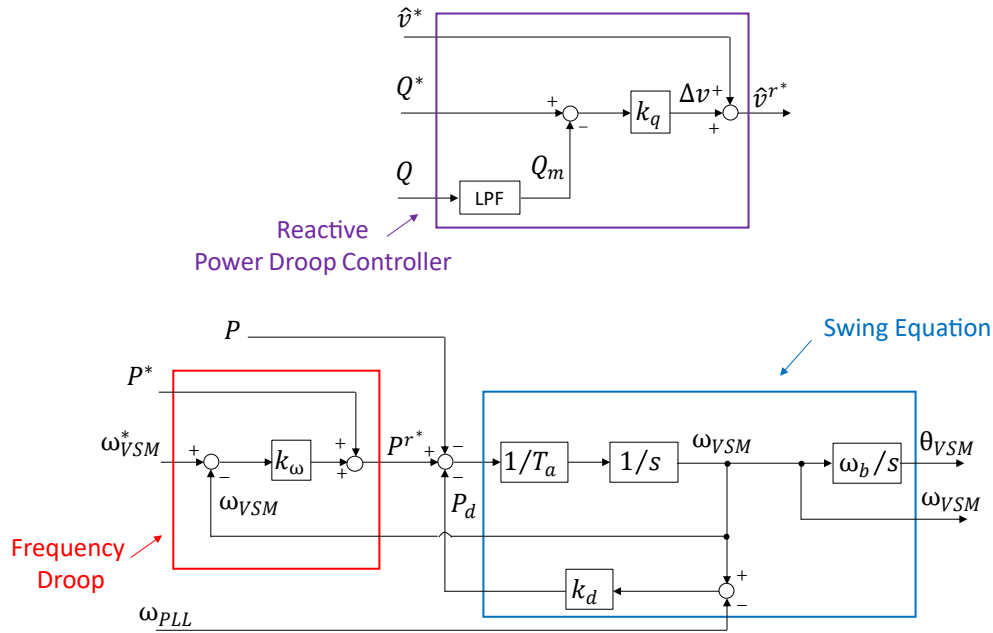


Figure 11.1.3: CVSM's control scheme: Reactive Power Droop Controller (top); Virtual Inertia and Power Control (bottom).

The core of the CVSM model is constituted by two cascaded voltage and current controllers in the (d, q) reference frame. The equivalent circuit which describes the connection between the CVSM and the PCC is shown in Fig 2.5.3.

Differently from the other current-output models, in this case there is a higher voltage controller. Therefore, here, the circuit of Fig 2.5.3 is valid for the PCC reference voltage $\bar{v}_{PCC,dq}^*$, instead of $\bar{v}_{PCC,dq}$.

The electromotive force on the (d, q) reference frame is constituted by the two components: v^{r*} and 0. The parameters of virtual impedance are the same of (2.5.6).

The difference between the electromotive force and the voltage drop on the virtual impedance defines the PCC reference voltage $\bar{v}_{PCC,dq}^*$, as shown in Fig. 11.1.4.

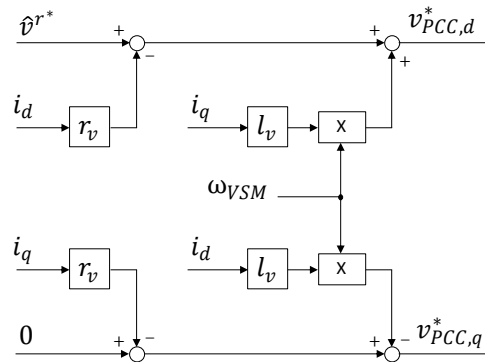


Figure 11.1.4: CVSM's control scheme: Virtual Impedance.

Here, no integration is performed. The implementation of the virtual impedance is simplified respect to the general case shown in (2.5.7).

Next, the closed loop voltage control can be performed. The block scheme is proposed in Fig. 11.1.5. It is a conventional control actuated in the (d, q) reference frame using PI regulators. The result is the current reference \bar{i}_{dq}^* .

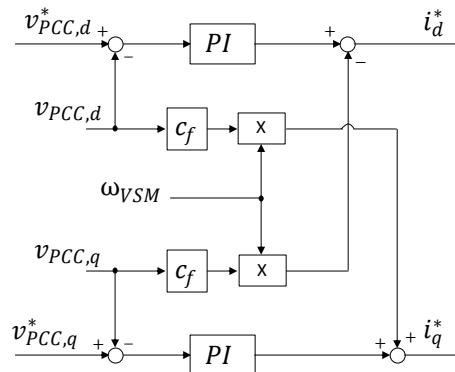


Figure 11.1.5: CVSM's control scheme: Voltage Control.

Finally, the closed loop current control can be actuated, as shown in Fig. 11.1.6. Even here conventional PI regulators are used. They guarantee a reliable current limitation. The output of the PI regulator is compensated by the damping voltage as well as the cross electromotive force term. The result is the voltage reference \bar{v}_{dq}^* . Park Transformation is used to obtain the three phase voltage reference \bar{v}_{abc}^* for the PWM modulator.

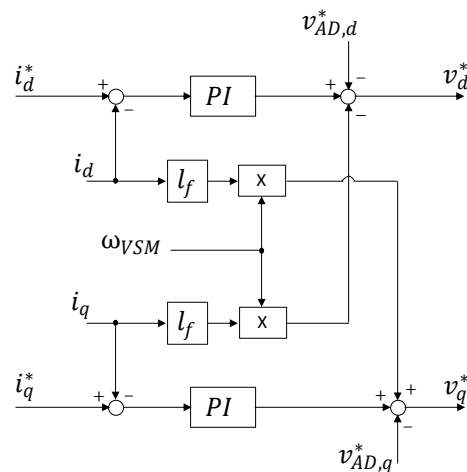


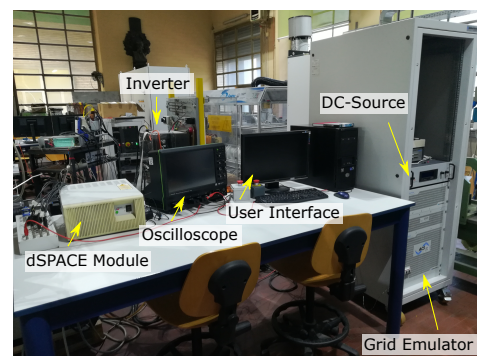
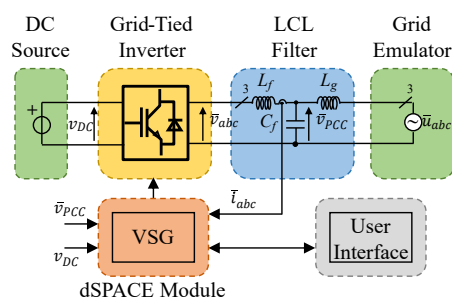
Figure 11.1.6: CVSM's control scheme: Current Control.

Chapter 12

Experimental Tests and Outcomes

12.1 Experimental Setup

In the realization of this master thesis, the first milestone has been the implementation of each VSG solution by means of PLECS simulations. Then, experimentally tests have been conducted to verify the validity of each model. In Fig. 12.1.1a a block scheme of the experimental setup used for the tests is proposed. The setup, shown in Fig. 12.1.1b, is located in the laboratory of the Power Electronics Innovation Center (PEIC) of the Politecnico di Torino.



(a)

(b)

Figure 12.1.1: From left to right:

- (a) Block scheme of the experimental setup;
- (b) Experimental setup at the laboratory of PEIC.

In Table 12.1.1 the main data of the experimental setup are summarised.

Table 12.1.1: Main data of the experimental setup.

Regatron Grid Emulator		
Nominal Grid Phase Voltage	$120\sqrt{2}$	V
Nominal Frequency	50	Hz
Grid-side Filters		
Filter Inductance	120	μH
Inverter		
Nominal Power	15	kVA
Nominal Current	60	A
Limit Current	36	A
Switching Frequency	10	kHz
Inverter-side Filters		
Filter Inductance	545	μH
DC-link		
DC Voltage Set-Point	380	V
DC-link Capacity	1.8	mF
Delta AC/DC Power Supply		
DC Voltage	300	V

The experimental setup is composed by the following main elements:

- Grid Emulator: the Regatron Grid Emulator is used to create an ideal three phase voltage to emulate the grid. It is shown in Fig. 12.1.2a. Moreover, a grid model on the software PLECS is used to actuate:
 - frequency variations;
 - voltage dips;
 - harmonic distortions.

Regatron is interfaced with the software by means of the PLECS RT Box, shown in Fig. 12.1.2b;



(a)

(b)

Figure 12.1.2: From left to right:
(a) Regatron Grid Emulator;
(b) PLECS RT Box and PLECS grid model.

- Filtering stage: the filters interfacing between the inverter to the grid emulator are shown in Fig. 12.1.3a;
- Inverter: the three phase inverter, illustrated in Fig. 12.1.3b, is controlled by dSPACE according to the VSG algorithms;

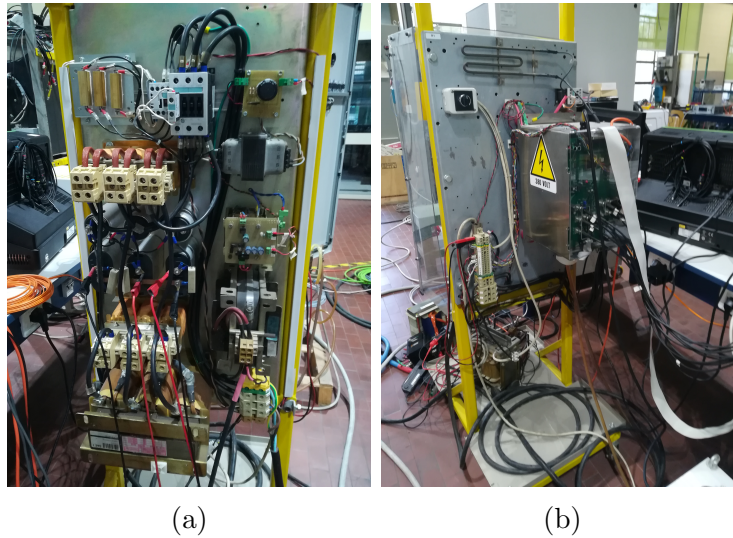


Figure 12.1.3: From left to right:
 (a) Grid-side filters;
 (b) three phase inverter.

- DC stage: a DC/DC converter is used to control the current injected by the DC source as well as the voltage on the DC-link of the inverter;
- DC source: the Delta Elektronika AD/DC power supply, shown in Fig. 12.1.4, is the primary DC-source, representing e.g. a battery storage system.

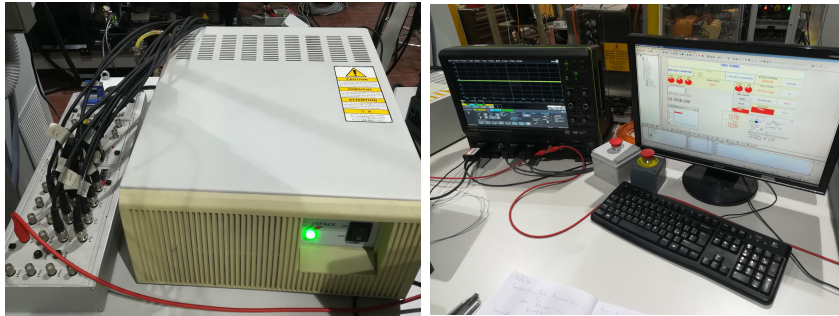


Figure 12.1.4: Delta Elektronika AD/DC power supply.

- dSPACE Module: the dSPACE Module of Fig. 12.1.5a is used to implement the VSG control algorithms on the control board of the inverter.

Moreover, it provides a useful user interface displaying the measurements of the needed quantities and save data (shown in Fig. 12.1.5b)

- Measurement system: the oscilloscope of Fig. 12.1.5b is used to observe the grid-side currents and the grid phase voltage as well as to save results.



(a)

(b)

Figure 12.1.5: From left to right:
(a) dSPACE module;
(b) Oscilloscope and dSPACE interface.

12.2 Synchronverter

The base version of Synchronverter belongs to the current-input voltage-output category, together with Osaka and VISMA2. As described in Subsection 2.5.5, the main disadvantage of these solutions is the absence of an inherent current limitation system. For this solution, it has been decided to avoid the implementation of the modification described in Subsection 2.5.5 because the enhanced version of Synchronverter was made exactly to overcome this issue. In fact, it is a voltage-input current-output model, where the current references are provided to a PI regulator, which generates the voltage references for the PWM modulator. Now the limitation of current can be easily actuated by means of the regulator.

As this enhanced version is more reliable, experimental tests have been conducted only for it.

12.2.1 Active and Reactive Power References

Active Power Reference Step

In this test the active power reference P_{set} is modified from 0.3 pu to 0.4 pu and the response of the Synchronverter is evaluated. As can be seen in Fig. 12.2.1b, active power quickly reaches the new value with a negligible overshoot. In this case the virtual power is circa equal to the real one.

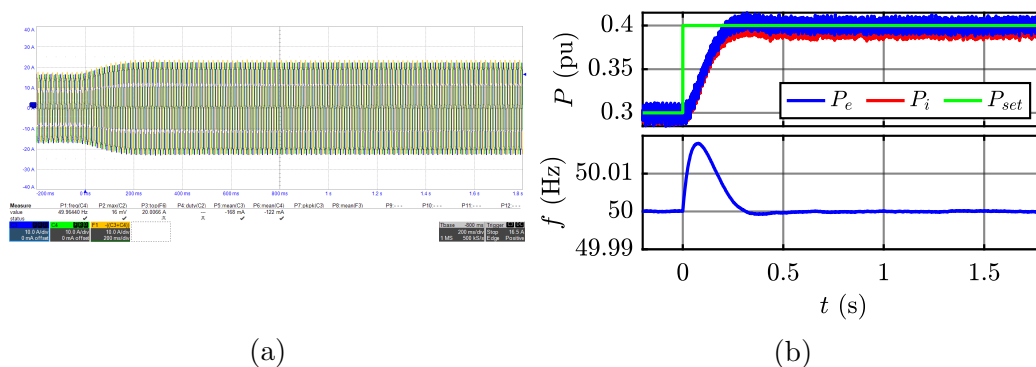


Figure 12.2.1: Synchronverter's response to active power reference step from 0.3 to 0.4 pu, from left to right:

- (a) Grid-side currents;
- (b) Active power (top) and Synchronverter's frequency (bottom).

Reactive Power Reference Step

The excitation constant τ_e has been set to 1 s. According to control theory, the steady state condition must be reached after $4\tau_e - 5\tau_e$. It can be noticed that both with and without reactive droop control, the transient takes circa 5 s, coherently with the tuning. In steady state $Q_e = Q^*$.

The reference Q^* is the sum of the two terms:

$$Q^* = Q_{set} + \Delta Q_d$$

In case of droop control disabled, Q^* is obviously equal to Q_{set} , because the droop control term is zero. Therefore the virtual reactive power reaches the value of 0.4 pu, as shown in Fig. 12.2.2b.

When the droop control is enabled, the difference between the reference voltage \hat{V}^* and the PCC voltage amplitude \hat{V}_{PCC} , leads to the circulation of reactive power. \hat{V}^* is equal to 0.98 pu, because it is the value of \hat{V}_{PCC} when all references are zero. It allows to have ΔQ_d when $Q_{set} = 0$.

When $Q_{set} \neq 0$, inverter starts to inject reactive power and the PCC voltage grows. Consequently, the droop control begins to work as well, with a $\Delta Q_d < 0$. The result is that the reference Q^* is lower than 0.4 pu, as can be noticed in Fig. 12.2.3b.

Finally, in both cases, the difference between the virtual reactive power and the real one is negligible.

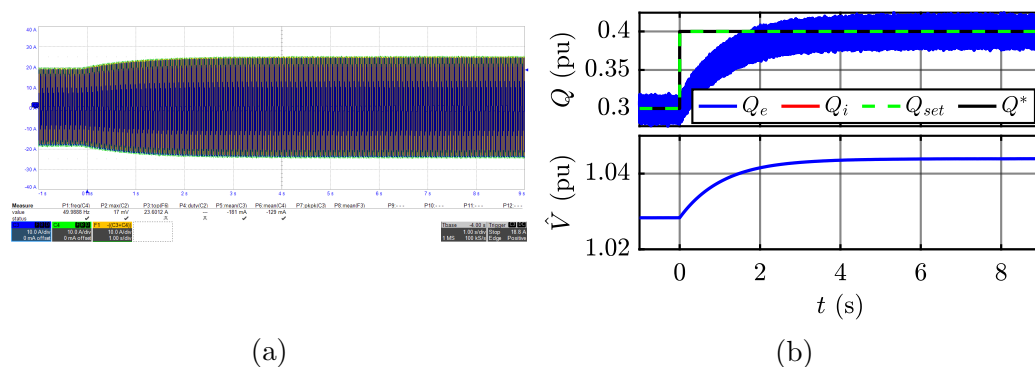


Figure 12.2.2: Synchronverter's response to reactive power reference step from 0.3 to 0.4 pu with droop control disabled, from left to right: (a) Grid-side currents; (b) Reactive power (top) and electromotive force (bottom).

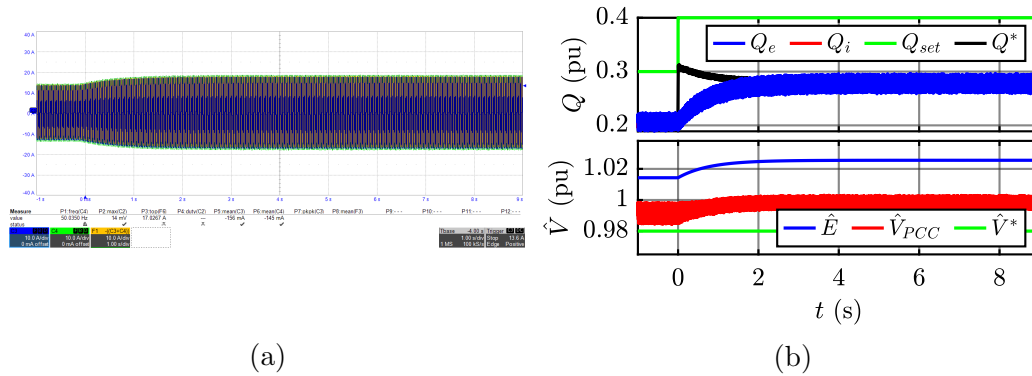


Figure 12.2.3: Synchronverter's response to reactive power reference step from 0.3 to 0.4 pu with droop control enabled, from left to right:

- (a) Grid-side currents;
 (b) Reactive power (top) and electromotive force (bottom).

12.2.2 Inertial Response

When the frequency variation occurs, the Synchronverter injects active power into the grid. The difference between the reference frequency and the Synchronverter's one passes through a high pass filter and a low pass filter, retrieving the two terms P_{HF} and P_{LF} . The former has no limitation and operates during the transient. On the other hand, in steady state it is equal to zero. The latter, instead, prevails in steady state and it is saturated with a droop coefficient of 5%. This is the classic case where the virtual active power and the real one cannot coincide. In fact, as can be seen in Fig. 12.2.4b, the frequency decreases and leads to a virtual active power of almost 3 pu. Obviously, the real power is saturated, because the inverter current limitation is set to 36 A. The PI regulator allows to perform it easily.

Then, when the steady state is reached, $P_{HF} = 0$ and only P_{LF} contributes to the active power injection. The value of power depends on the droop coefficient and the frequency variation, according to the following equation:

$$\Delta P = -\frac{\Delta f}{b_p} = \frac{0.42}{50 \cdot 0.05} = 0.168 \text{ pu}$$

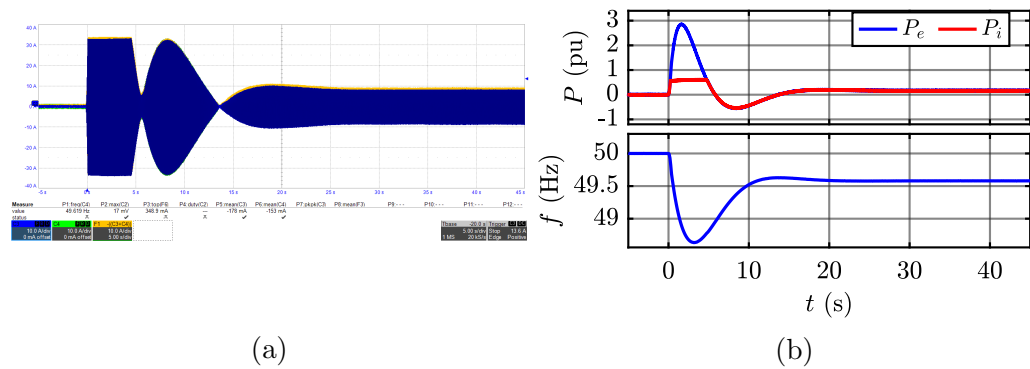


Figure 12.2.4: Synchronverter's response to grid frequency variation of -0.42 Hz, from left to right:
 (a) Grid-side currents;
 (b) Active power (top) and Synchronverter's frequency (bottom).

12.2.3 Harmonic Distortion

In this test, 5% of fifth harmonic is added to the three phase grid voltage provided by the grid emulator. The FFT of Fig. 12.2.5a shows that PCC voltage has a contribution of circa 8.5 V of fifth harmonic, with reference currents disabled. When they are enabled, inverter currents are distorted, but they actuate a filtering action: in fact they introduce a voltage drop on the grid impedance, which allows to reduce the distortion of PCC voltage. In fact, as can be noticed from Fig. 12.2.6a, the contribution of fifth harmonic decreases to circa 4.5 V.

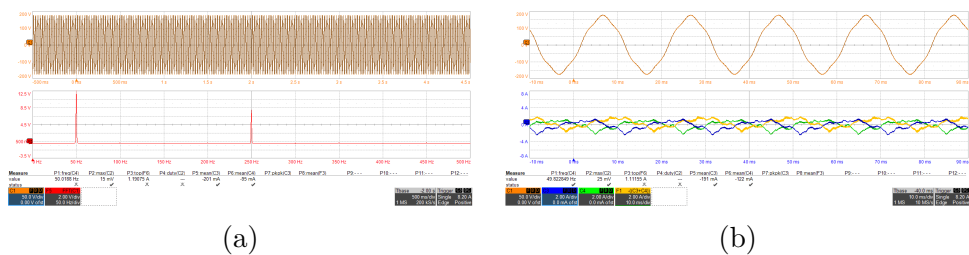


Figure 12.2.5: From left to right:
 (a) PCC Phase Voltage with 5% of fifth harmonic (top) and its FFT (bottom) with Synchronverter's current references disabled;
 (b) PCC Phase Voltage with 5% of fifth harmonic (top) and grid-side currents (bottom) with Synchronverter's current references disabled.

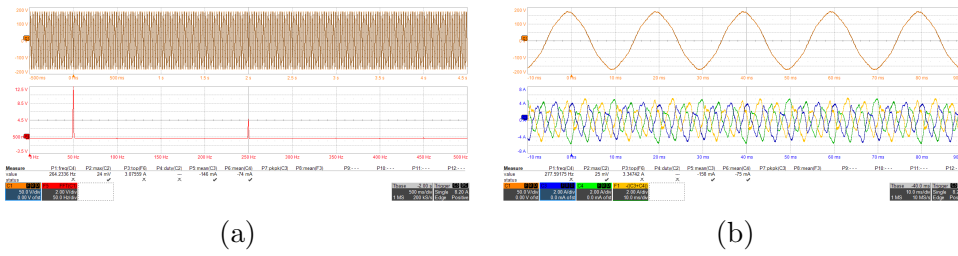


Figure 12.2.6: From left to right:
 (a) PCC Phase Voltage with 5% of fifth harmonic (top) and its FFT (bottom) with Synchronverter's current references enabled;
 (b) PCC Phase Voltage with 5% of fifth harmonic (top) and grid-side currents (bottom) with Synchronverter's current references enabled.

12.2.4 Voltage Dips

In the following charts, \hat{U} is the amplitude of the voltage provided by the grid emulator. It is not a physical measured quantity, but it is inserted to show the shape of the generated voltage dip.

Each dip is tested with and without reactive droop control.

Independently on the type and the droop control, when the voltage dip occurs, the virtual reactive power exceeds the limit of 1 pu and currents are saturated to the limit of 36 A. Therefore, Synchronverter can inject reactive power to support the grid during the fault, as demonstrated by the results shown from Fig. 12.2.7 to Fig. 12.2.12.

Dip Type 1

It can be noticed from Fig. 12.2.7b that the electromotive force decreases when reactive droop control is disabled, whereas it remains circa constant when it is enabled, as shown in Fig. 12.2.8b.

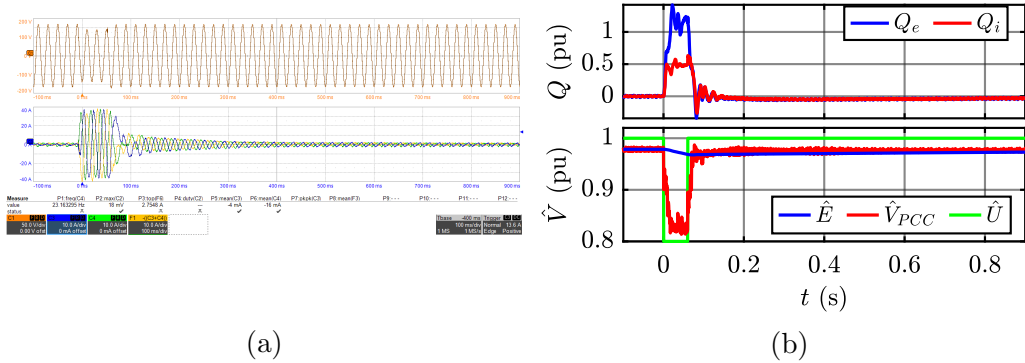


Figure 12.2.7: Synchronverter’s response to voltage dip type 1, with reactive droop control disabled, from left to right:
 (a) PCC line voltages (top) and grid-side currents (bottom);
 (b) Reactive power (top) and electromotive force (bottom).

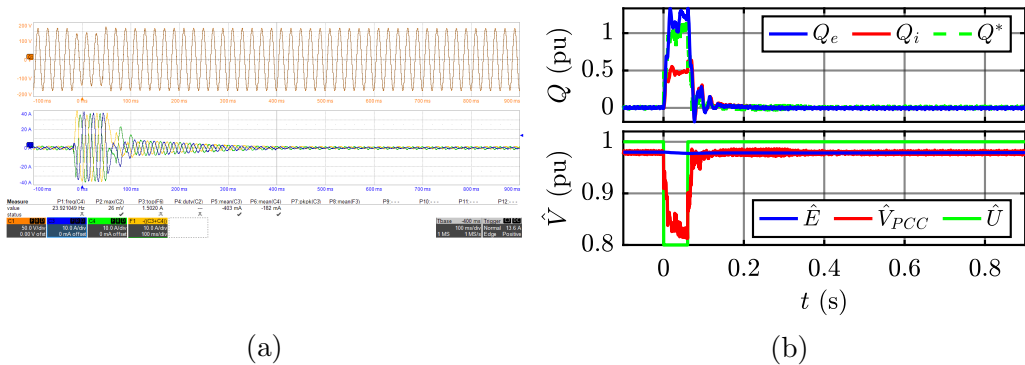


Figure 12.2.8: Synchronverter’s response to voltage dip type 1, with reactive droop control enabled, from left to right:
 (a) PCC line voltages (top) and grid-side currents (bottom);
 (b) Reactive power (top) and electromotive force (bottom).

Dip Type 2

If the reactive droop control is disabled, Fig. 12.2.9b shows that at the end of the voltage dip there is a transient governed by the time constant τ_e , set to 1 s. The electromotive force takes circa 4 s to restore the previous value and the same transient can be seen in reactive power and so currents. Whereas, when the droop control is enabled, the dynamic is faster, as can be noticed from Fig. 12.2.10b.

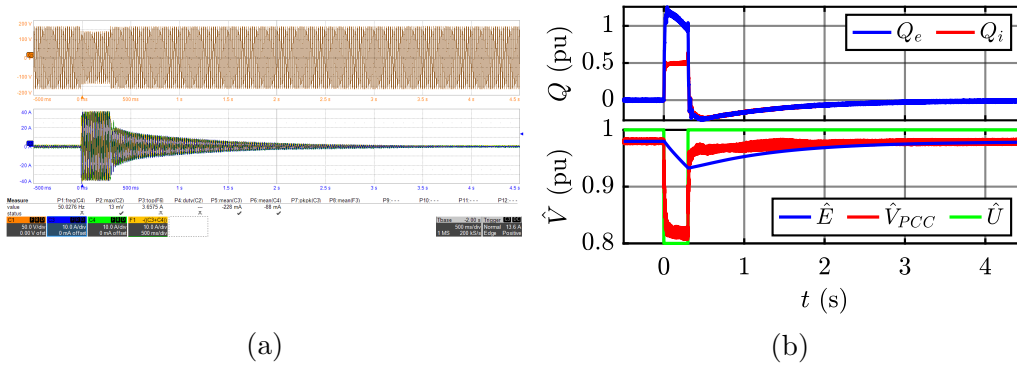


Figure 12.2.9: Synchronverter’s response to voltage dip type 2, with reactive droop control disabled, from left to right:
 (a) PCC line voltages (top) and grid-side currents (bottom);
 (b) Reactive power (top) and electromotive force (bottom).

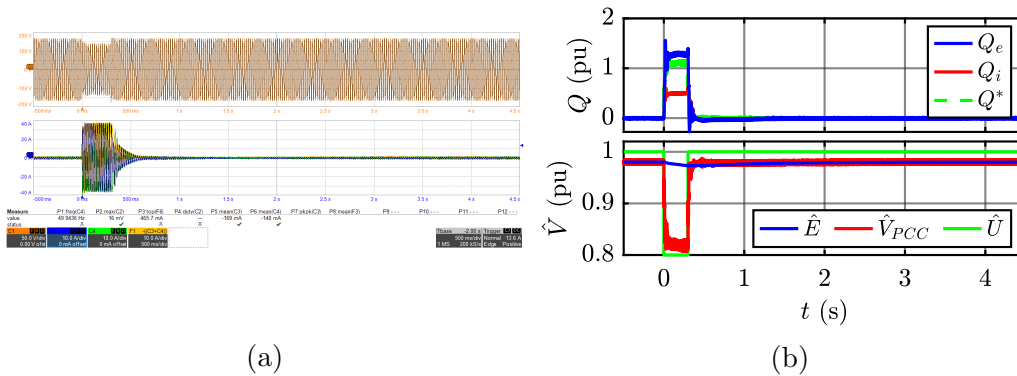


Figure 12.2.10: Synchronverter’s response to voltage dip type 2, with reactive droop control enabled, from left to right:
 (a) PCC line voltages (top) and grid-side currents (bottom);
 (b) Reactive power (top) and electromotive force (bottom).

Dip Type 3

The same observations of dip 2 are valid for dip 3 as well. In this case the only difference lies in the depth of voltage dip and consequently on the larger value of reactive power and electromotive force’s variation. Results without and with reactive droop control are shown respectively in Fig. 12.2.11 and Fig. 12.2.12.

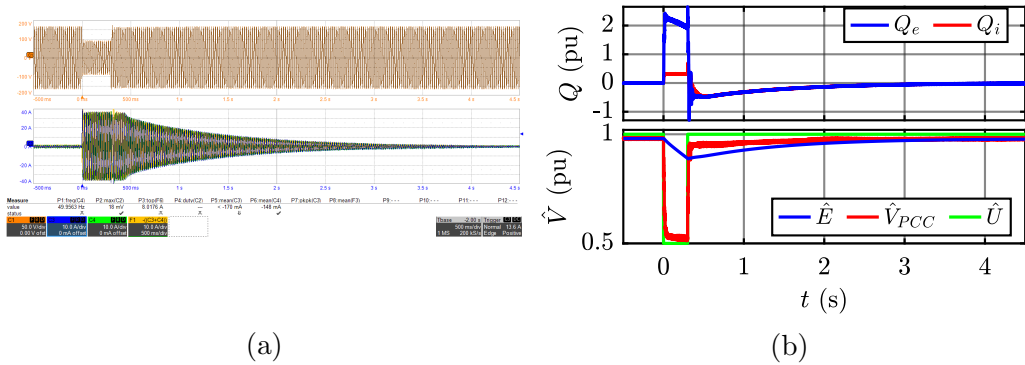


Figure 12.2.11: Synchronverter's response to voltage dip type 3, with reactive droop control disabled, from left to right:
 (a) PCC line voltages (top) and grid-side currents (bottom);
 (b) Reactive power (top) and electromotive force (bottom).

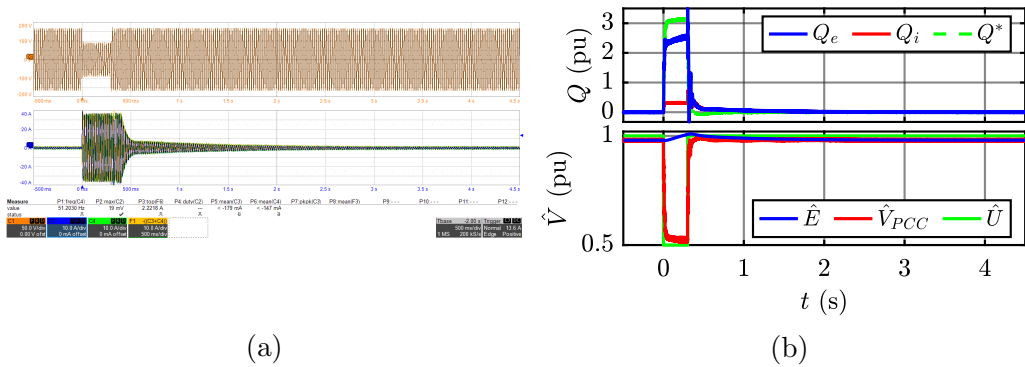


Figure 12.2.12: Synchronverter's response to voltage dip type 3, with reactive droop control enabled, from left to right:
 (a) PCC line voltages (top) and grid-side currents (bottom);
 (b) Reactive power (top) and electromotive force (bottom).

12.3 Osaka

Osaka is a current-input voltage-output model, like Synchronverter (base form) and VISMA2. Voltage references are directly provided to the PWM modulator, without the employment of a PI regulator. Differently from the other two models of its category, for Osaka there is not an alternative version where the current limitation can be easily performed. For this reason, in order to safely perform the tests listed in Section 2.6, it has been necessary to introduce an additional part to the model.

This adaptation has been described in Subsection 2.5.5.

12.3.1 Active and Reactive Power References

For this tests, currents are very far from the limit of 36 A. The threshold is set to 30 A for safety reasons, but it will be never reached and so only the conventional algorithm will be used.

Active Power Reference Step

The peculiarity of this model is the choice to take the influence of PCC voltage into account. In fact, the difference between P_L and P_{in} is due to the amplitude of \widehat{V}_{PCC} . In steady state, when $P_\omega \cong 0$:

$$P_{in} = \widehat{V}_{PCC}^2 \cdot (P_L + P_\omega) = 0.984^2 \cdot (0.4 + 0) \cong 0.387 \text{ pu}$$

This statement justifies the difference between P_{in} and P_L of Fig. 12.3.1. Moreover, it shows that the response to the step variation of active power reference is fast and overdamped.

Finally, it can be noticed that, since the saturation limit is not reached, $P_{out} \equiv P_i$.

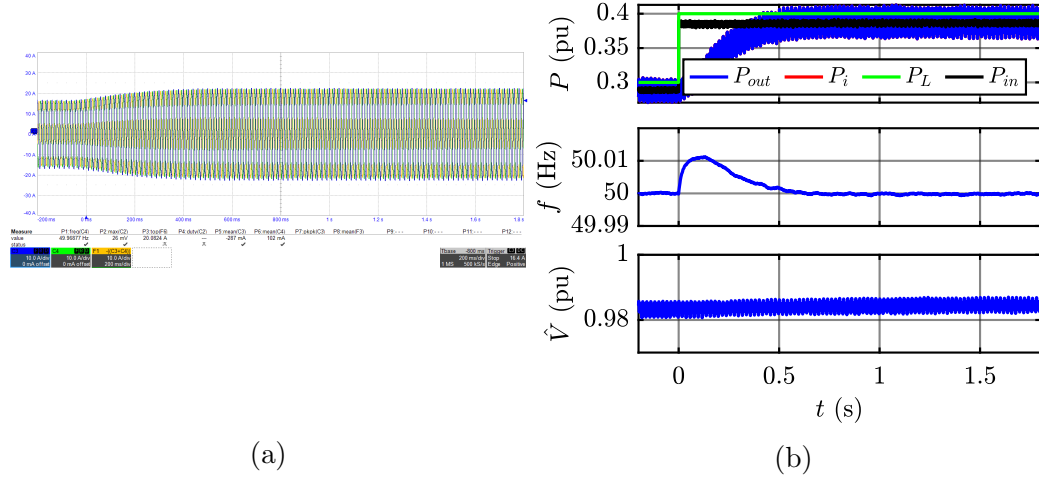


Figure 12.3.1: Osaka's response to active power reference step from 0.3 to 0.4 pu, from left to right:

- (a) Grid-side currents;
- (b) Active power (top), Osaka's frequency (center) and PCC voltage amplitude (bottom).

Reactive Power Reference Step

The excitation time constant τ_e has been set to 1 s. Therefore, electromotive force and reactive power need circa 5 s to complete the transient and reach the steady state value, according to the control theory. The experimental outcome is in compliance with this statement, both with and without reactive droop control, as demonstrated in Fig. 12.3.2 and Fig. 12.3.3. Moreover, as the current limit is not reached, $Q_{out} \equiv Q_i$.

When the reactive droop control is disabled, $Q_{in} = Q_L$ and the virtual reactive power reaches the value of 0.4 pu, as shown in Fig. 12.3.2b.

For the second case, the voltage reference \hat{V}_0 is equal to 0.98 pu. This is the value of \hat{V}_{PCC} when all references are zero. In this way, $\Delta Q_d = 0$ when $Q_L = 0$. Applying an external reference $Q_L \neq 0$, currents starts to flowing from the inverter to the grid, and PCC voltage increases. Consequently, the reactive droop control starts to work, with $\Delta Q_d < 0$. This results in a total reactive power reference:

$$Q_{in} = Q_L + \Delta Q_d$$

Applying the step variation of Q_L from 0.3 pu to 0.4 pu, Q_{in} is around 0.25 pu and the real reactive power reaches this value. This result is illustrated in Fig. 12.3.3b.

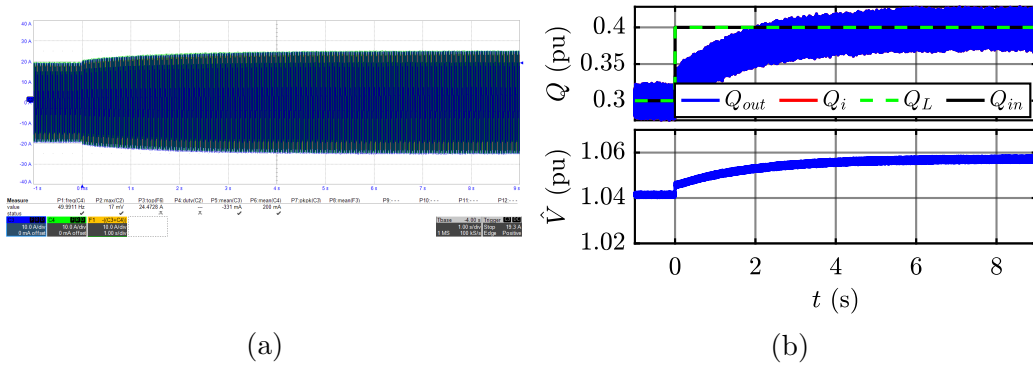


Figure 12.3.2: Osaka’s response to reactive power reference step from 0.3 to 0.4 pu with reactive droop control disabled, from left to right:
 (a) Grid-side currents;
 (b) Reactive power (top) and electromotive force (bottom).

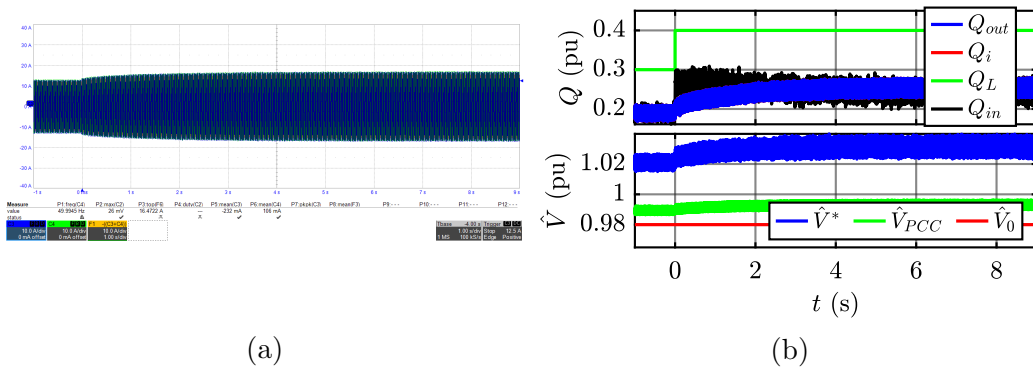


Figure 12.3.3: Osaka’s response to reactive power reference step from 0.3 to 0.4 pu with reactive droop control enabled, from left to right:
 (a) Grid-side currents;
 (b) Reactive power (top) and electromotive force (bottom).

12.3.2 Inertial Response

As described in Section 12, the inverter current is limited to 36 A for safety reasons, but the nominal value is 80 A. PLECS simulations demonstrated that the maximum current would have been around 50 A. For this reason, only for this test, it has been decided to increase the current limit and the threshold to 60 A. In this way, the transition between the voltage and current control does not occur, and the behaviour of the original version of Osaka

can be observed.

Even in this case, the virtual and the real power coincide, because P_{out} is calculated starting from the PCC voltage and inverter currents.

Fig. 12.3.4 shows that, after a transient where power reaches a peak of 0.76 pu and current is almost 53 A, in steady state the governor leads to an injection of active power which depends on the frequency variation and droop coefficient:

$$P_{\omega} = 100 \cdot \frac{\omega^* - \omega_{PLL,pu}}{\delta} = 100 \cdot \frac{1 - \left(1 - \frac{0.42}{50}\right)}{5} = 0.168 \text{ pu}$$

Finally, even here PCC voltage gives its contribution:

$$P_{in} = \hat{V}_{PCC}^2 \cdot (P_L + P_{\omega}) = 0.98^2 \cdot (0 + 0.168) = 0.161 \text{ pu}$$

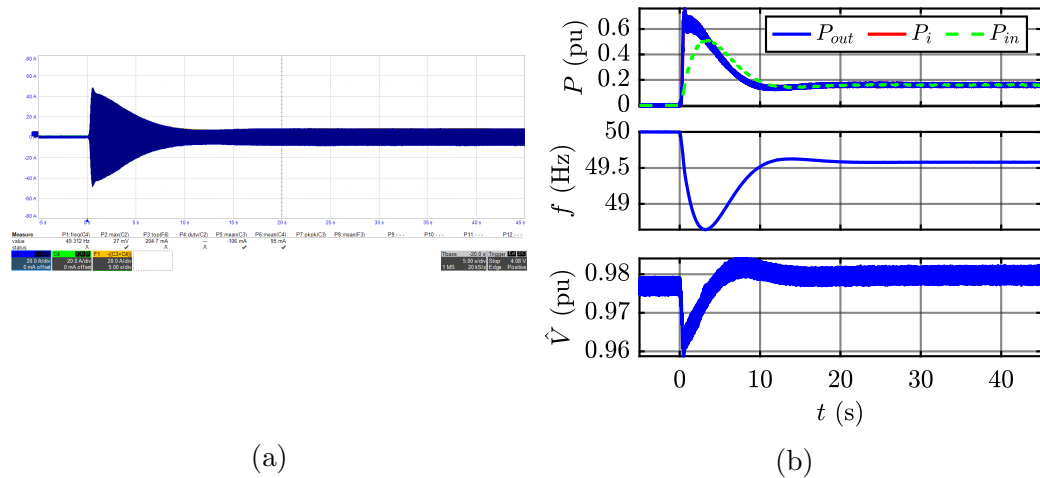


Figure 12.3.4: Osaka’s response to grid frequency variation of -0.42 Hz, from left to right:

- (a) Grid-side currents;
- (b) Active power (top), Osaka’s frequency (center) and PCC voltage amplitude (bottom).

12.3.3 Harmonic Distortion

In this test, 5% of fifth harmonic is added to the three phase grid voltage provided by the grid emulator. FFT of Fig. 12.3.5a shows that PCC voltage

has a contribution of circa 8.5 V for the fifth harmonic, when Osaka control is disabled. Then, enabling Osaka algorithm, this fifth harmonic term decreases, reaching a value of 6 V as can be observed from Fig. 12.3.6a. Even in this case, the distorted current (Fig. 12.3.6b) introduces a voltage drop on the filter impedance which leads to a better voltage quality.

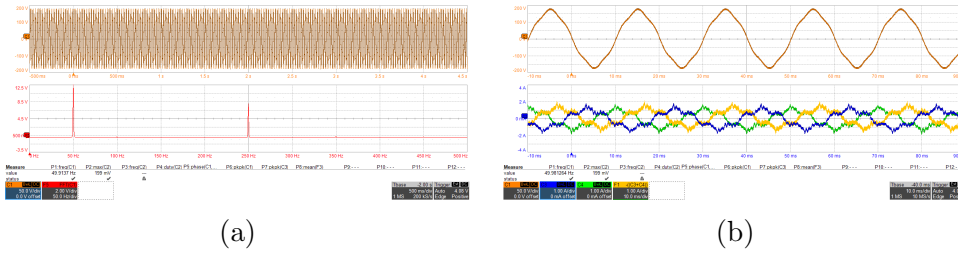


Figure 12.3.5: From left to right:
 (a) PCC Phase Voltage with 5% of fifth harmonic (top) and its FFT (bottom) with Osaka disabled;
 (b) PCC Phase Voltage with 5% of fifth harmonic (top) and grid-side currents (bottom).

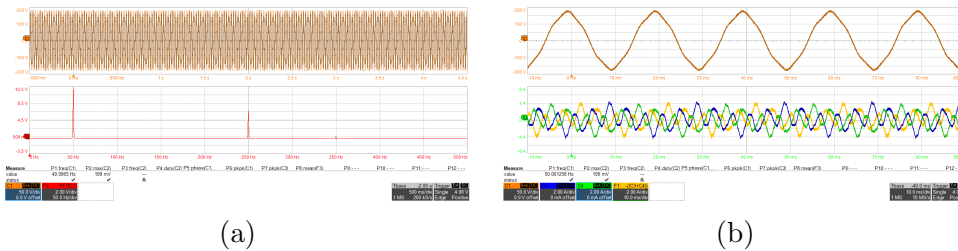


Figure 12.3.6: From left to right:
 (a) PCC Phase Voltage with 5% of fifth harmonic (top) and its FFT (bottom) with Osaka enabled;
 (b) PCC Phase Voltage with 5% of fifth harmonic (top) and grid-side currents (bottom).

12.3.4 Voltage Dips

For this test the current limit is set to the conventional value of 36 A, whereas the threshold is equal to 15 A. The difference between the two values has been chosen to guarantee a large safety margin. In fact, if they were equal, there would be a higher probability to perform the transition with a delay, risking to overcome the limit of 36 A.

Every voltage dip type, independently of reactive droop control, leads to currents higher than 36 A. Therefore, in every case the transition to the current model occurs. Powers must be calculated using current references not saturated, in order to guarantee the stability of the control.

As can be noticed from all outcomes, virtual reactive power always overcomes the limit of 1 pu, whereas the real power and currents are perfectly saturated. When droop control is disabled and the voltage dip disappears, the dynamic is influenced by the tuning of τ_e . Enabling droop control, electromotive force and power take less time to reach the steady state condition.

In all cases Osaka can support the grid during voltage dip, by means the injection of reactive power. Then, when the currents are continuously lower than 5 A for at least 500 ms, the control algorithm switches to the conventional mode. This transition leads to a variation of the electromotive force, as it is evident from Fig. 12.3.10b.

For each dip, it is indicated the instant when the transition occurs.

Finally, in the following charts, \hat{U} is the amplitude of the voltage provided by the grid emulator. It is not a physical measured quantity, but it is inserted to show the shape of the generated voltage dip.

Dip Type 1

This kind of voltage dip is too short to see the impact of reactive droop control. Reactive power oscillates when the voltage dip occurs and it has no sufficient time to complete the transient, as shown in Fig. 12.3.7b and Fig. 12.3.8b.

The instants of transition are similar for the two cases. They are respectively: 820 ms and 923 ms.

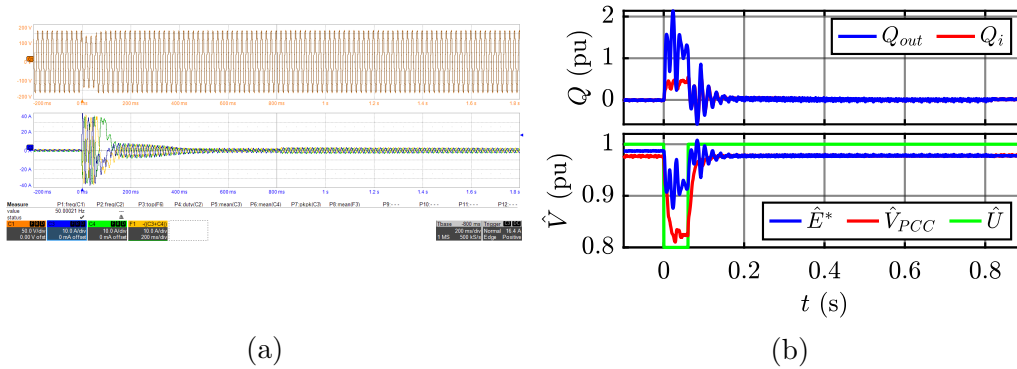


Figure 12.3.7: Osaka’s response to voltage dip type 1, with reactive droop control disabled, from left to right:
 (a) PCC line voltages (top) and grid-side currents (bottom);
 (b) Reactive power (top) and electromotive force (bottom).

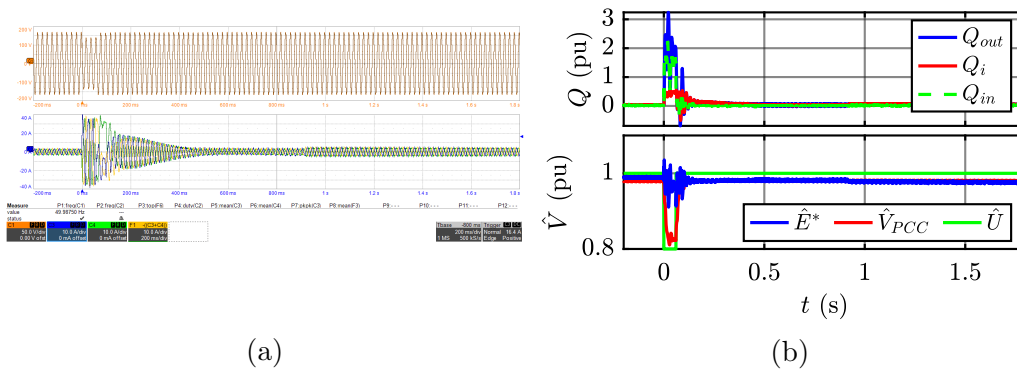


Figure 12.3.8: Osaka’s response to voltage dip type 1, with reactive droop control enabled, from left to right:
 (a) PCC line voltages (top) and grid-side currents (bottom);
 (b) Reactive power (top) and electromotive force (bottom).

Dip Type 2

This voltage dip lasts a sufficient time to allow reactive power to complete the oscillations and to observe the influence of reactive droop control. When it disabled, as shown in Fig. 12.3.9b, the electromotive force decreases and at the end of the dip it follows the dynamic imposed by the excitation time constant τ_e . At 2.43 s the transition to the conventional voltage control occurs.

Enabling the reactive droop control, the dynamic is faster and in fact the instant of transition is 1.33 s, as can be seen from Fig. 12.3.10b.

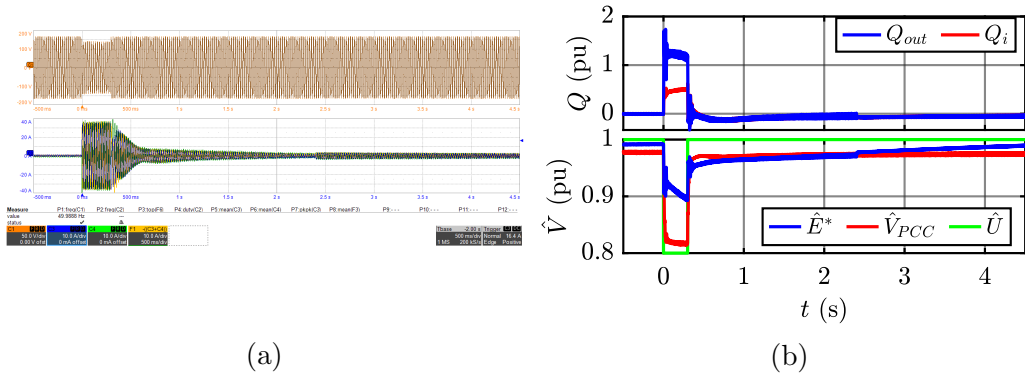


Figure 12.3.9: Osaka’s response to voltage dip type 2, with reactive droop control disabled, from left to right:

- (a) PCC line voltages (top) and grid-side currents (bottom);
- (b) Reactive power (top) and electromotive force (bottom).

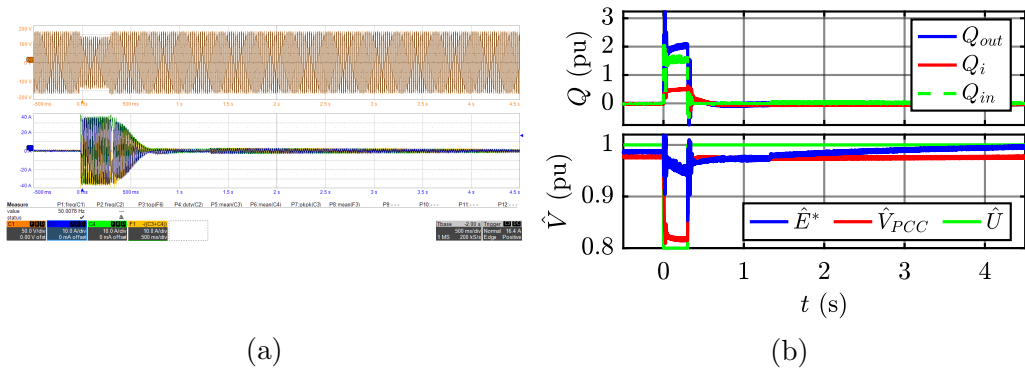


Figure 12.3.10: Osaka’s response to voltage dip type 2, with reactive droop control enabled, from left to right:

- (a) PCC line voltages (top) and grid-side currents (bottom);
- (b) Reactive power (top) and electromotive force (bottom).

Dip Type 3

All the observations for dip type 2 are also valid for this kind of dip. The only difference lies obviously in the values reached by the quantities. The transitions instances are larger, as can be seen from Fig. 12.3.11b and Fig. 12.3.12b. They are respectively: 4.37 s and 2.48 s.

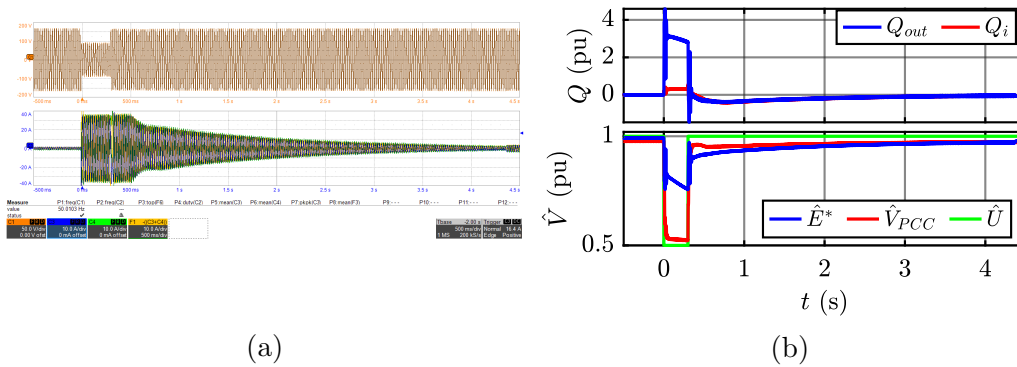


Figure 12.3.11: Osaka’s response to voltage dip type 3, with reactive droop control disabled, from left to right:
 (a) PCC line voltages (top) and grid-side currents (bottom);
 (b) Reactive power (top) and electromotive force (bottom).

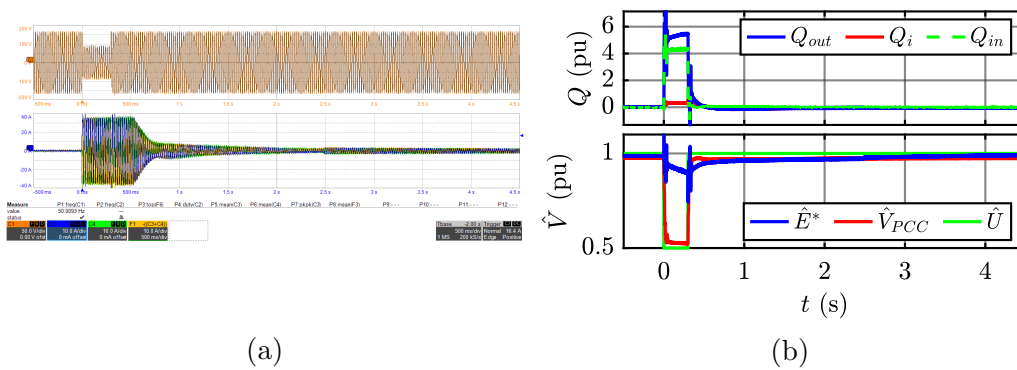


Figure 12.3.12: Osaka’s response to voltage dip type 3, with reactive droop control enabled, from left to right:
 (a) PCC line voltages (top) and grid-side currents (bottom);
 (b) Reactive power (top) and electromotive force (bottom).

12.4 VISMA

VISMA is built as a complete model of a real synchronous generator. Therefore, the outcomes are expected to be very similar respect to a conventional SG. It belongs to the voltage-input current output category, therefore the limitation of current can be performed by means of the PI regulator.

12.4.1 Active and Reactive Power References

Active Power Reference Step

As can be noticed from Fig. 12.4.1b, the response to active power step variations is underdamped, as happens for conventional SGs. The virtual and real power are very similar and the references is reached after circa 5 s.

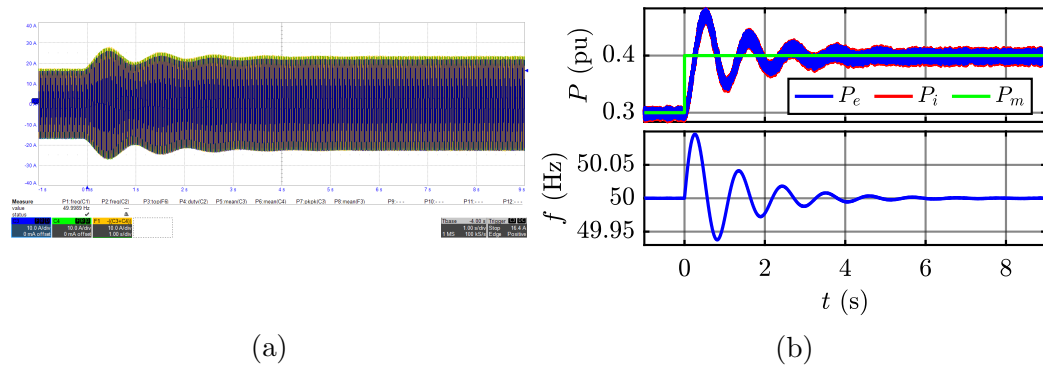


Figure 12.4.1: VISMA's response to active power reference step from 0.3 to 0.4 pu, from left to right:

- (a) Grid-side currents;
- (b) Active power (top) and VISMA's frequency (bottom).

Reactive Power Reference Step

In this case, the excitation part of the model is realised by means of a PI regulator. The dynamic is faster than other solutions. Excitation flux linkage and reactive power takes circa 1 s to reach the steady state condition. Virtual and real reactive power are practically the same. This is true both with reactive droop control disabled and not, as demonstrated by the results in Fig. 12.4.2b and Fig. 12.4.3b.

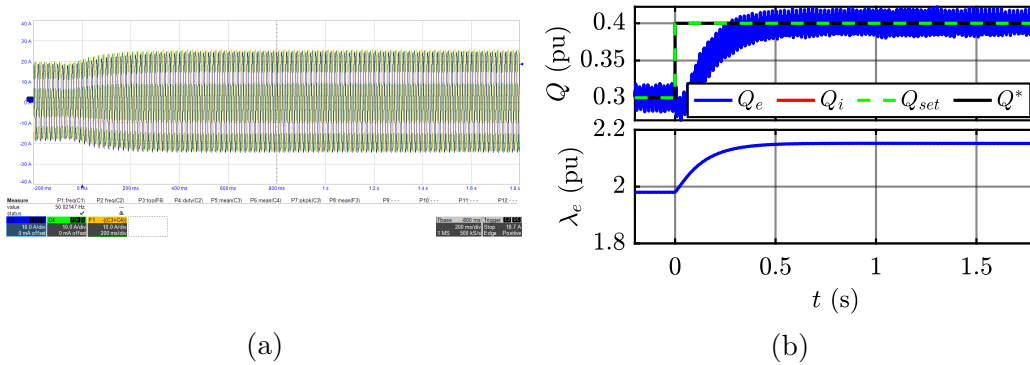


Figure 12.4.2: VISMA’s response to reactive power reference step from 0.3 to 0.4 pu with reactive droop control disabled, from left to right:
 (a) Grid-side currents;
 (b) Reactive power (top) and electromotive force (bottom).

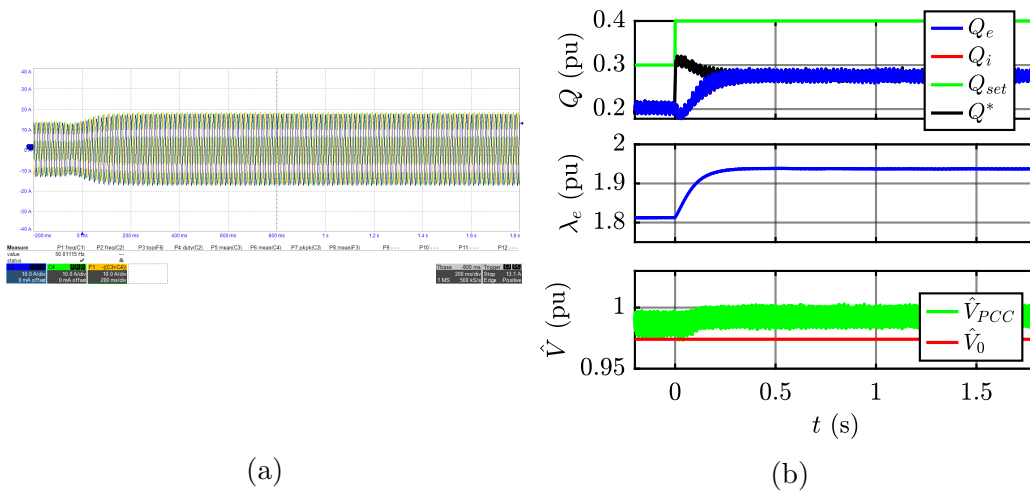


Figure 12.4.3: VISMA’s response to reactive power reference step from 0.3 to 0.4 pu with reactive droop control enabled, from left to right:
 (a) Grid-side currents;
 (b) Reactive power (top), excitation flux linkage (center), voltages (bottom).

The difference between the two cases is the value of the reactive power reference Q^* . The latter is characterised by $Q^* = Q_{set}$, whereas the former includes the droop control term ΔQ_d :

$$Q^* = Q_{set} + \Delta Q_d$$

ΔQ_d is zero when $Q_{set} = 0$, imposing $\widehat{V}_0 = 0.98$. It corresponds to the value of \widehat{V}_{PCC} when all references are set to zero.

Then, when non-zero Q_{set} is applied, currents starts to flow from the inverter to the grid and \widehat{V}_{PCC} increases. The consequence is a decrease of ΔQ_d and a total reference Q^* lower respect to the case without droop. The excitation flux will be obviously lower as well.

12.4.2 Inertial Response

This is the response with the lowest active power peak between all solutions. It is equal to 0.227 pu, whereas currents reach 13.7 A, as shown in Fig. 12.4.4. In steady state power goes to zero, because there is not any governor in this model.

Finally, even here, real and virtual power are the same.

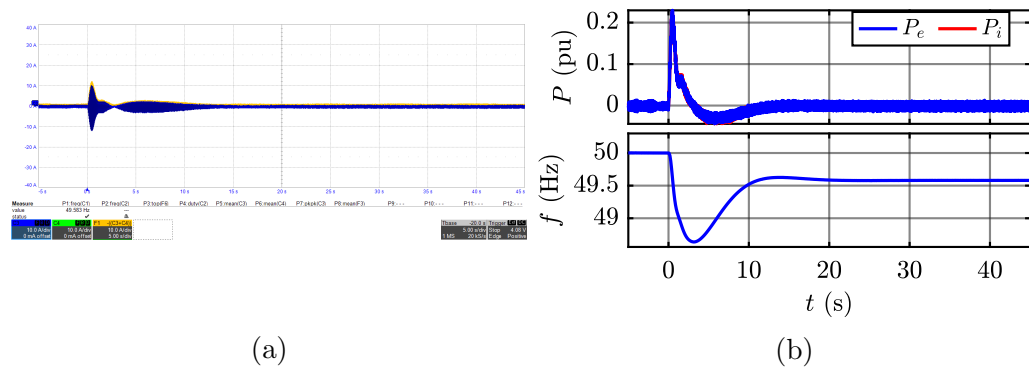


Figure 12.4.4: VISMA's response to grid frequency variation of -0.42 Hz, from left to right:

- (a) Grid-side currents;
- (b) Active power (top) and VISMA's frequency (bottom).

12.4.3 Harmonic Distortion

In this test, 5% of fifth harmonic is added to the three phase grid voltage provided by the grid emulator. When current references are disabled, the fifth harmonic introduces a contribution of 8.5 V, as can be seen from Fig. 12.4.5a. After the enabling of VISMA's references, a negligible reduction of the distortion can be observed from Fig. 12.4.6a. Therefore VISMA neither amplify nor reduces the impact of harmonic distortion into the grid.

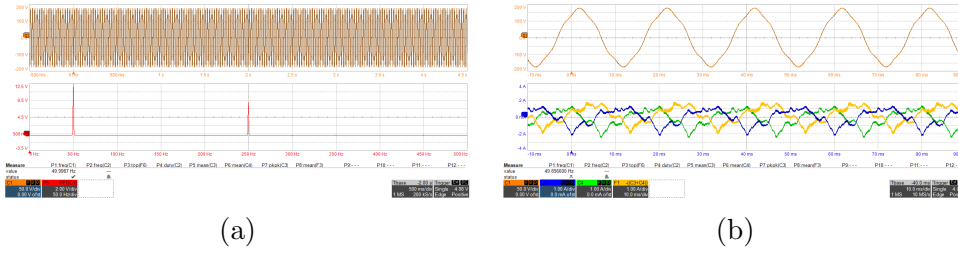


Figure 12.4.5: From left to right:
 (a) PCC Phase Voltage with 5% of fifth harmonic (top) and its FFT (bottom) with VISMA’s current references disabled;
 (b) PCC Phase Voltage with 5% of fifth harmonic (top) and grid-side currents (bottom) with VISMA’s current references disabled.

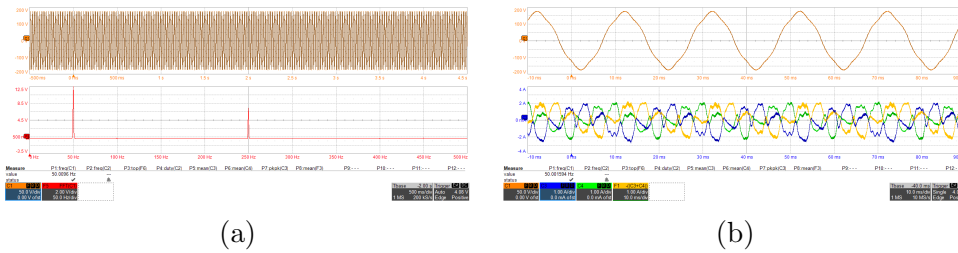


Figure 12.4.6: From left to right:
 (a) PCC Phase Voltage with 5% of fifth harmonic (top) and its FFT (bottom) with VISMA’s current references enabled;
 (b) PCC Phase Voltage with 5% of fifth harmonic (top) and grid-side currents (bottom) with VISMA’s current references enabled.

12.4.4 Voltage Dips

In the following charts, \hat{U} is the amplitude of the voltage provided by the grid emulator. It is not a physical measured quantity, but it is inserted to show the shape of the generated voltage dip.

For each voltage dip, currents are limited to 36 A and they are characterized by an evident unidirectional component. This leads to strong reactive power oscillations.

When the reactive droop control is disabled, this phenomenon is predominant. Immediately power and currents grow and then they return to the previous condition.

The case of reactive droop control enabled is different: the unidirectional

component is still present, but the droop control allows to also inject reactive power.

When the voltage dip disappears, virtual reactive power needs a certain time to return to zero. With droop control enabled, this time is larger respect to the other case.

In conclusion, VISMA can support grid during voltage dips by means of reactive droop control.

Dip Type 1

Dip Type 1 is too short to appreciate the influence of the reactive droop control on the reactive power and consequently on currents, as can be seen from Fig. 12.4.7 and Fig. 12.4.8.

This is no true for the excitation flux linkage, which decreases when the reactive droop control is disabled and increases in the other case.

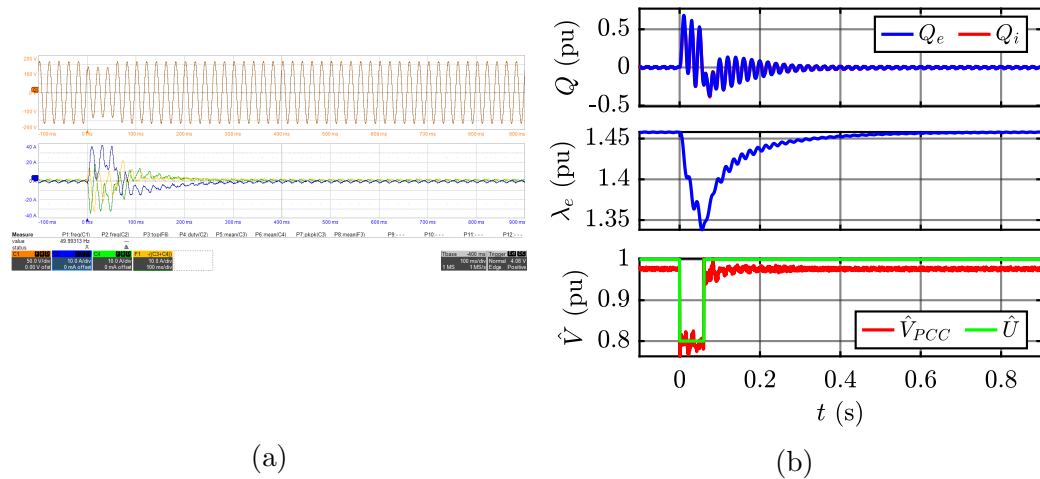


Figure 12.4.7: VISMA’s response to voltage dip type 1, with reactive droop control disabled, from left to right:

- (a) PCC line voltages (top) and grid-side currents (bottom);
- (b) Reactive power (top), excitation flux linkage (center), voltages (bottom).

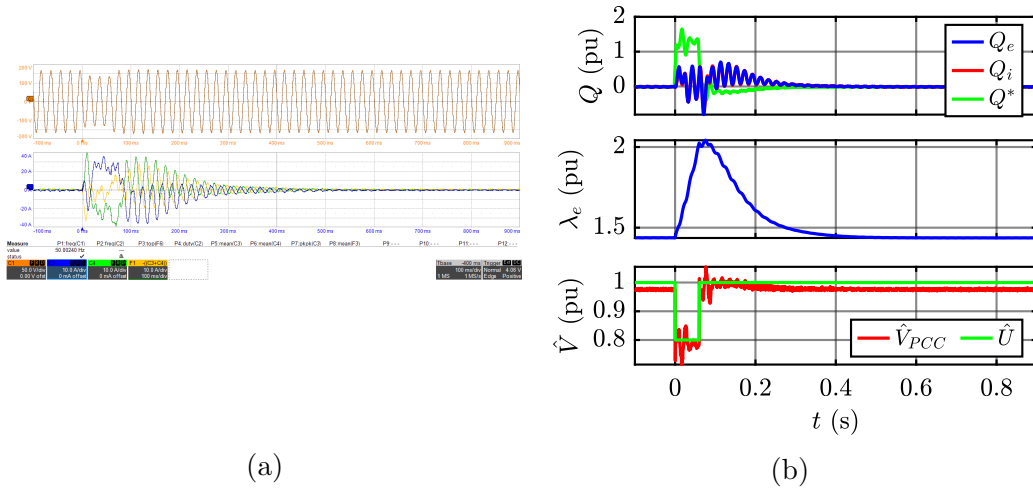


Figure 12.4.8: VISMA’s response to voltage dip type 1, with reactive droop control enabled, from left to right:

- (a) PCC line voltages (top) and grid-side currents (bottom);
- (b) Reactive power (top), excitation flux linkage (center), voltages (bottom).

Dip Type 2

Comparing Fig. 12.4.9a with Fig. 12.4.10a it can be noticed that when reactive droop control is disabled, currents goes to zero after the transient, whereas, with reactive droop control enabled, currents remain equal to 36 A during the voltage dip permanence.

At the end of the voltage dip, after a transient characterised by oscillations, reactive power return to zero.

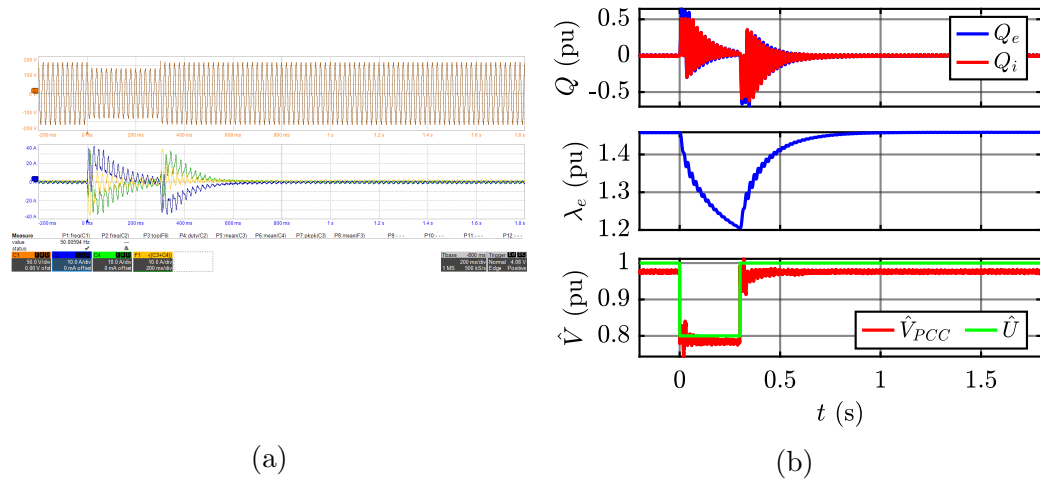


Figure 12.4.9: VISMA’s response to voltage dip type 2, with reactive droop control disabled, from left to right:

- (a) PCC line voltages (top) and grid-side currents (bottom);
- (b) Reactive power (top), excitation flux linkage (center), voltages (bottom).

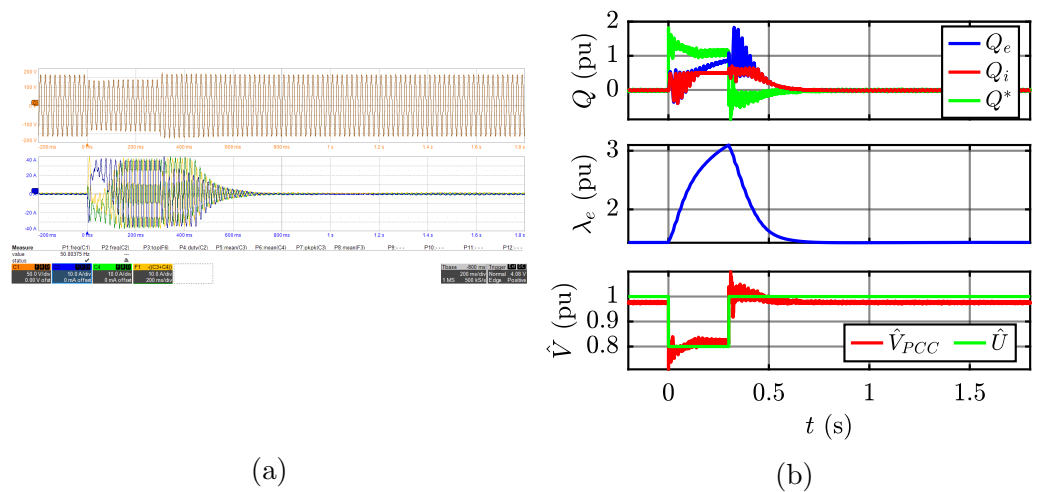


Figure 12.4.10: VISMA’s response to voltage dip type 2, with reactive droop control enabled, from left to right:

- (a) PCC line voltages (top) and grid-side currents (bottom);
- (b) Reactive power (top), excitation flux linkage (center), voltages (bottom).

Dip Type 3

Fig. 12.4.11b and Fig. 12.4.12b show the results for voltage dip type 3. All the observations for type 2 are also valid in this case. The only difference lies in the values of the quantities.

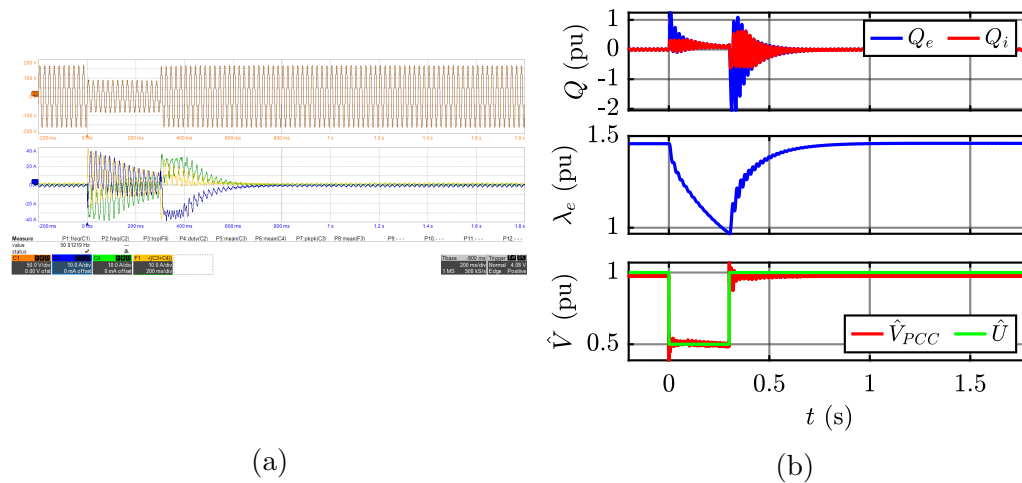


Figure 12.4.11: VISMA's response to voltage dip type 3, with reactive droop control disabled, from left to right:
 (a) PCC line voltages (top) and grid-side currents (bottom);
 (b) Reactive power (top), excitation flux linkage (center), voltages (bottom).

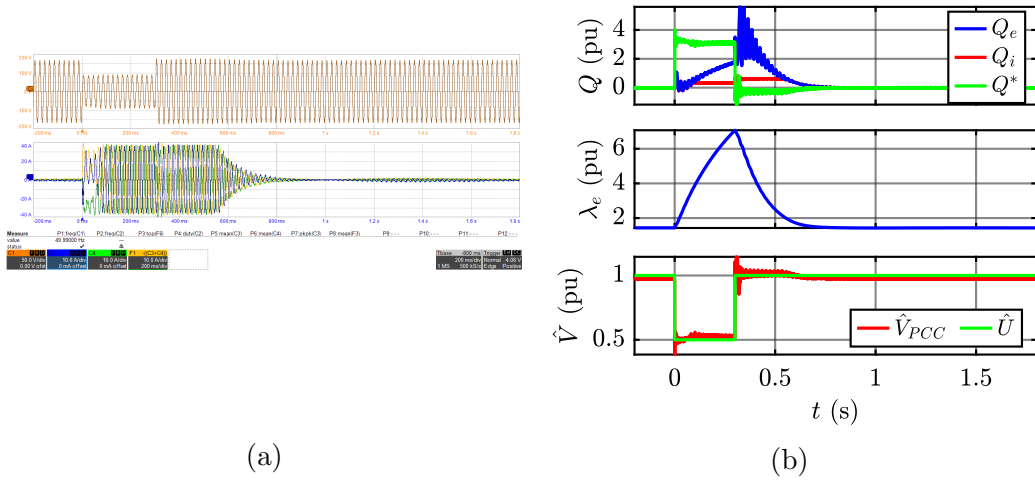


Figure 12.4.12: VISMA's response to voltage dip type 3, with reactive droop control enabled, from left to right:
 (a) PCC line voltages (top) and grid-side currents (bottom);
 (b) Reactive power (top), excitation flux linkage (center), voltages (bottom).

12.5 VISMA1

VISMA1 is one of the two simplified versions of VISMA and it belongs to the voltage-input current-output category. A PI regulator compares the current references with the measured ones to generate the voltage references for the PWM modulator. Therefore there is no need to introduce additional blocks to limit the currents, because the limitation can be implemented in the PI regulator's structure.

12.5.1 Stability Analysis

For each voltage-input current-output models, it has been chosen to use the same parameters for the virtual impedance used to retrieve current references. The chosen values are:

$$\begin{cases} r_v = 0.02 \text{ pu} \\ l_v = 0.1 \text{ pu} \end{cases}$$

Differently from other solutions, VISMA1 has instability problems with this choice of parameters. Imposing $Q^* = 0.1 \text{ pu}$, Fig. 12.5.1a and Fig. 12.5.1b show how strong is the difference between currents when virtual inductance is, respectively, $l_v = 0.1 \text{ pu}$ and $l_v = 0.2 \text{ pu}$. The former case is very close to diverge, whereas the latter is stable.

Another example is given to demonstrate the instability. Starting from $P_m = 0.1 \text{ pu}$ and $l_v = 0.1 \text{ pu}$, a step variation of P_m from 0.1 pu to 0.2 pu is applied. Currents before the step do not show evident problems, as can be seen in Fig. 12.5.2a, but when the step occurs power and currents grow exponentially and the protections turn off the system, as illustrated in Fig. 12.5.2b.

In conclusion, the more the value of the inductance, the better the filtering action against disturbances. For this reason, VISMA1 has been tested using the following parameters:

$$\begin{cases} r_v = 0.02 \text{ pu} \\ l_v = 0.2 \text{ pu} \end{cases}$$

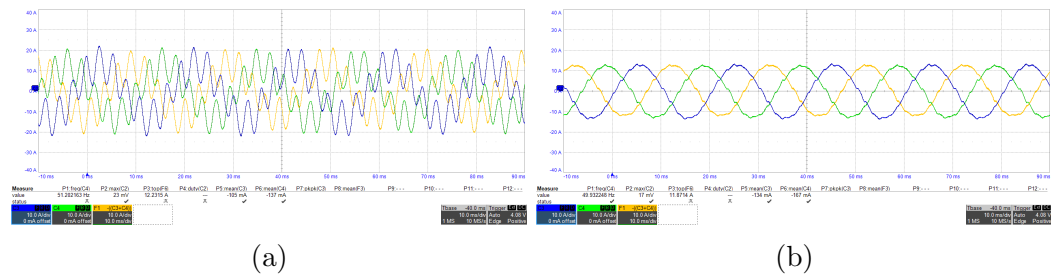


Figure 12.5.1: VISMA1’s response to reactive power reference equal to 0.1 pu, from left to right:

- (a) Grid-side currents with $l_v = 0.1$ pu;
- (b) inverter currents with $l_v = 0.2$ pu.

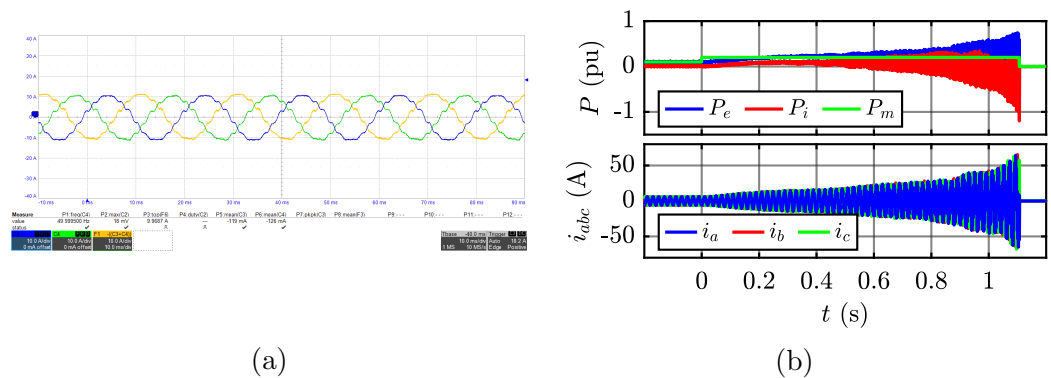


Figure 12.5.2: VISMA1’s response to active power reference step from 0.1 to 0.2 pu, with $l_v = 0.1$ from left to right:

- (a) Grid-side currents before the step;
- (b) Active power (top) and currents (bottom).

12.5.2 Active and Reactive Power References

Active Power Reference Step

A step variation of the active power reference from 0.3 to 0.4 pu is applied. It can be noticed, from Fig. 12.5.3b, that active power tracks the reference with high dynamic and a negligible overshoot. Finally, virtual and real active power are practically the same.

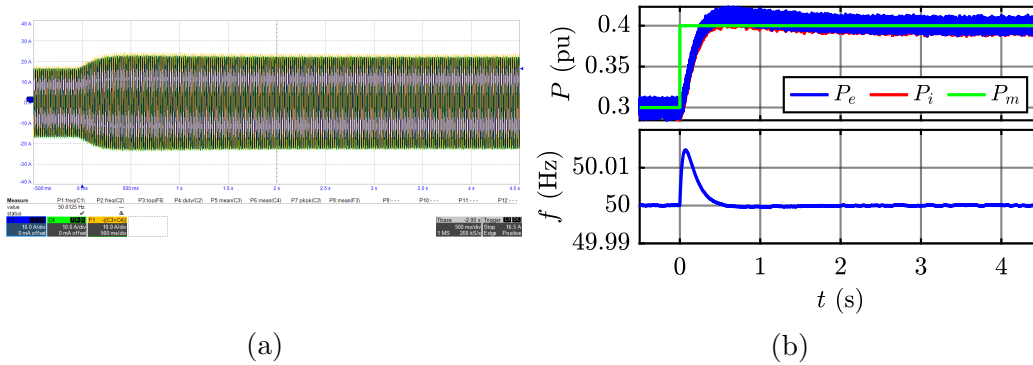


Figure 12.5.3: VISMA1's response to active power reference step from 0.3 to 0.4 pu:

- (a) Grid-side currents;
 (b) Active power (top) and VISMA1's frequency (bottom).

Reactive Power Reference Step

The excitation part is characterized by a pure integrator, where the excitation time constant τ_e is set to 1 s. According to control theory, quantities must take $4\tau_e - 5\tau_e$ to reach the new steady state condition. The results in Fig. 12.5.5a and Fig. 12.5.5b shows that, enabling or not the reactive droop control, the reactive power and the electromotive force take circa 5 s to reach the steady state, after the step variation. Therefore, the control theory is respected. In both cases the real reactive power does not reach the reference, but there is an error, due to a partial coupling with the active power.

When the reactive droop control is disabled, $Q^* = Q_{set}$ and Q_e reaches the value of 0.4 pu.

Turning on the reactive droop control, \widehat{V}_0 is set equal to \widehat{V}_{PCC} when $Q_{set} = 0$, in order to start with $Q^* = 0$. Then Q_{set} increases, current begins to circulate from the inverter to the grid and \widehat{V}_{PCC} grows as well. Consequently, the droop control operates, reducing the total reactive power reference respect to the case without droop:

$$Q^* = Q_{set} + \Delta Q_d$$

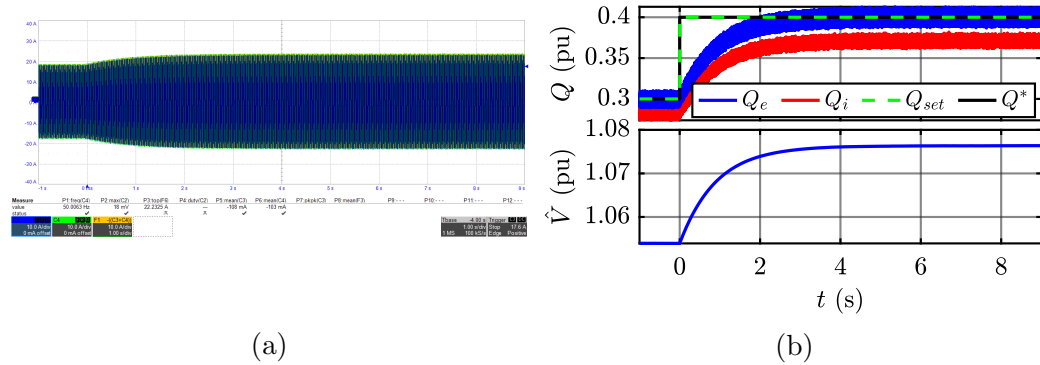


Figure 12.5.4: VISMA1’s response to reactive power reference step from 0.3 to 0.4 pu with reactive droop control disabled, from left to right:
 (a) Grid-side currents;
 (b) Reactive power (top) and electromotive force (bottom).

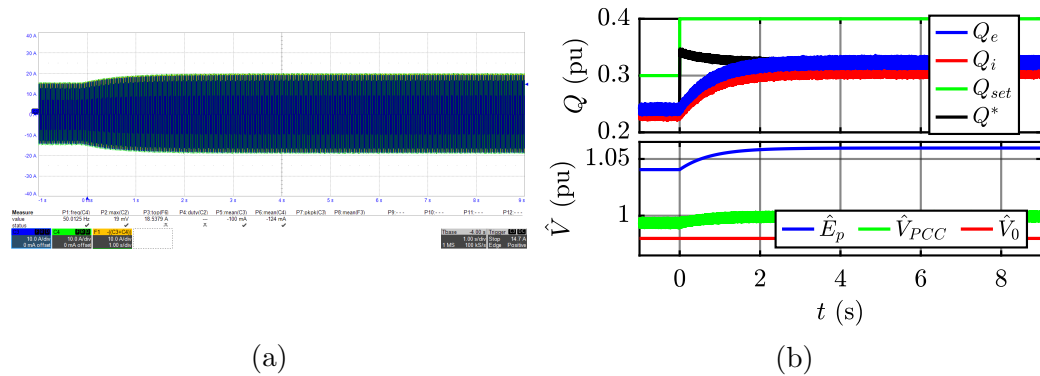


Figure 12.5.5: VISMA1’s response to reactive power reference step from 0.3 to 0.4 pu with reactive droop control enabled, from left to right:
 (a) Grid-side currents;
 (b) Reactive power (top) and electromotive force (bottom).

12.5.3 Inertial Response

The virtual active power increases up to 3 pu during the reduction of frequency, whereas the real power and current are limited to respectively 0.6 pu and 36 A, as shown in Fig. 12.5.6. At steady state the active power injected into the grid is zero, because this model does not embed a governor.

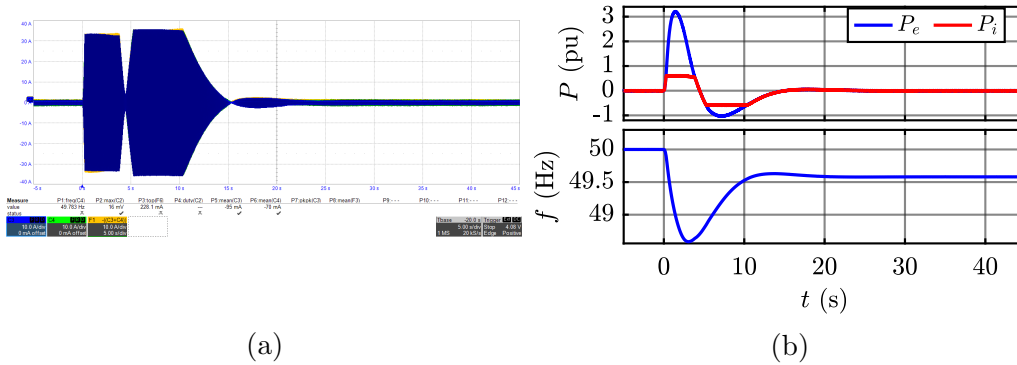


Figure 12.5.6: VISMA1’s response to grid frequency variation of -0.42 Hz, from left to right:
 (a) Grid-side currents;
 (b) Active power (top) and frequency (bottom).

12.5.4 Harmonic Distortion

In this test, 5% of fifth harmonic is added to the three phase grid voltage provided by the grid emulator. The contribution of distortion is equal to 8.5 V, as can be seen from FFT of Fig. 12.5.7a, when current references are disabled.

As soon as references are enabled, the fifth harmonic term decreases, reaching a value of 5.5 V (see Fig. 12.5.8a). Therefore, VISMA1 provides a filtering action, reducing the grid harmonic distortion. This result is due to the voltage drop across the grid impedance, introduced by the distorted inverter currents shown in Fig. 12.5.8b.

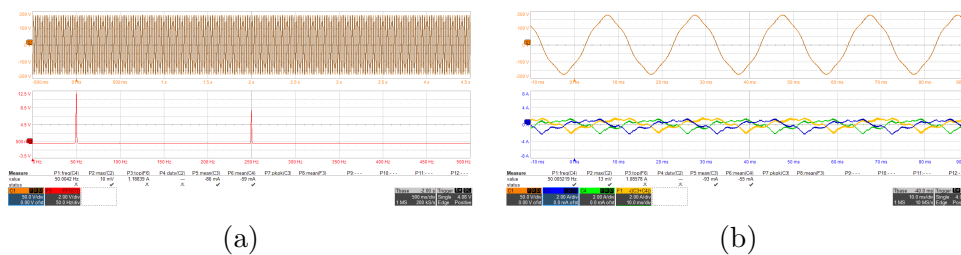


Figure 12.5.7: From left to right:
 (a) PCC Phase Voltage with 5% of fifth harmonic (top) and its FFT (bottom) with VISMA1’s current references disabled;
 (b) PCC Phase Voltage with 5% of fifth harmonic (top) and grid-side currents (bottom) with VISMA1’s current references disabled.

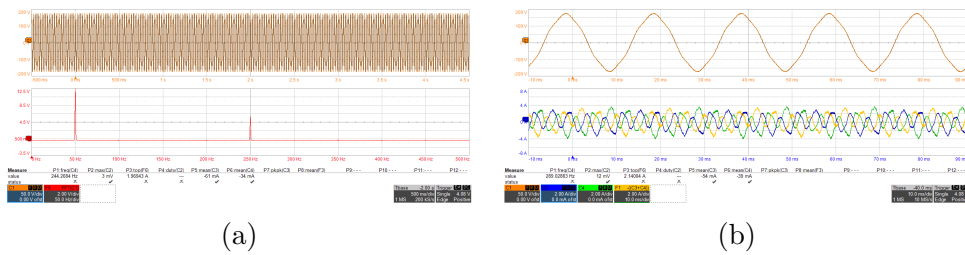


Figure 12.5.8: From left to right:
 (a) PCC Phase Voltage with 5% of fifth harmonic (top) and its FFT (bottom) with VISMA1's current references enabled;
 (b) PCC Phase Voltage with 5% of fifth harmonic (top) and grid-side currents (bottom) with VISMA1's current references enabled.

12.5.5 Voltage Dips

In the following charts, \hat{U} is the amplitude of the voltage provided by the grid emulator. It is not a physical measured quantity, but it is inserted to show the shape of the generated voltage dip.

For each voltage dip the current is saturated to 36 A. The virtual reactive power overcomes the limit whereas the real one is limited.

When the reactive droop control is disabled, the dynamic is dominated by the excitation time constant, set to 1 s. In fact, the reactive power and the electromotive force follow a transient, after the conclusion of the voltage dip, which takes circa 5 s to complete.

If the droop control is enabled, the electromotive force, the reactive power and so the currents reach the steady state condition in a shorter time, because of the presence of a non-zero reference of reactive power.

Finally, as can be observed from Fig. 12.5.9 to Fig. 12.5.14, VISMA1 can provide grid support during voltage dips, by means of the injection of reactive power.

Dip Type 1

This kind of dip is too short to appreciate the effect of the reactive droop control. In fact, comparing the results of Fig. 12.5.9b and Fig. 12.5.10b, no consistent differences can be noticed.

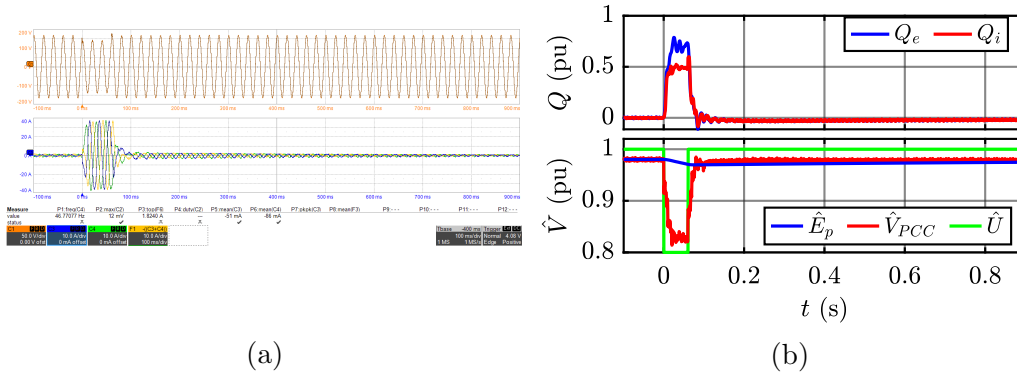


Figure 12.5.9: VISMA1's response to voltage dip type 1, with reactive droop control disabled, from left to right:
 (a) PCC line voltages (top) and grid-side currents (bottom);
 (b) Reactive power (top) and electromotive force (bottom).

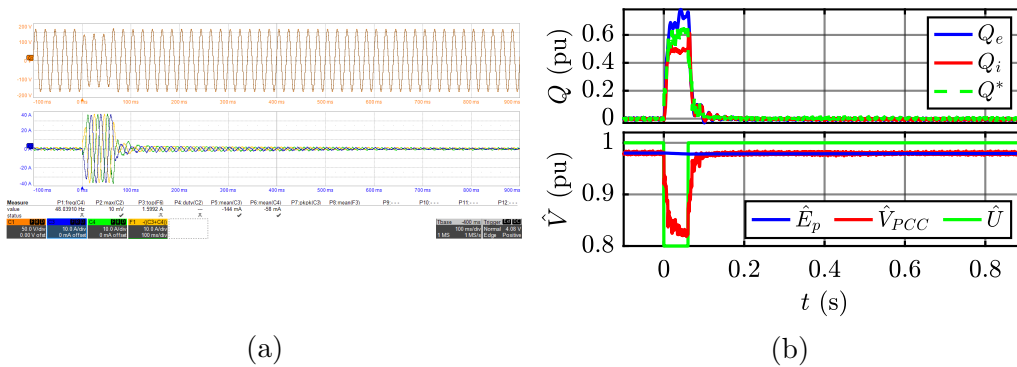


Figure 12.5.10: VISMA1's response to voltage dip type 1, with reactive droop control enabled, from left to right:
 (a) PCC line voltages (top) and grid-side currents (bottom);
 (b) Reactive power (top) and electromotive force (bottom).

Dip Type 2

Here the effect of the reactive droop control is visible. At the end of the voltage dip, the reactive power takes circa 4 s to returns to zero when the reactive droop control is disabled, as demonstrated by Fig. 12.5.11b. Enabling the reactive droop control, the transient is faster and the reactive power returns to zero in a few milliseconds, as shown in Fig. 12.5.12b.

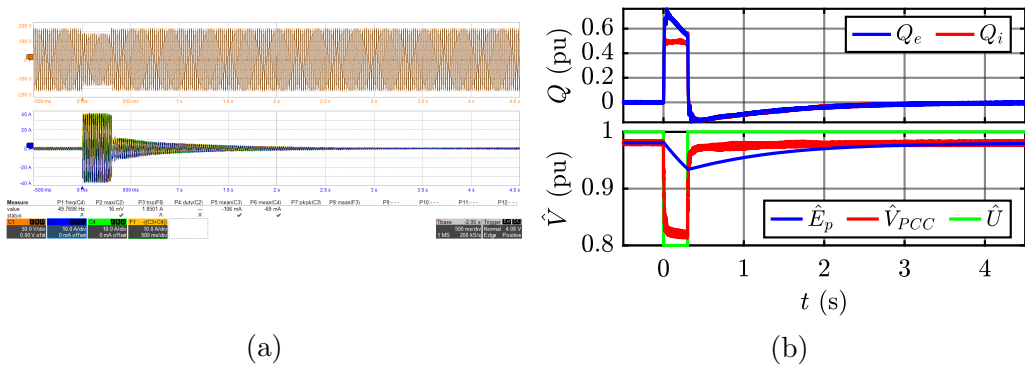


Figure 12.5.11: VISMA1’s response to voltage dip type 2, with reactive droop control disabled, from left to right:
 (a) PCC line voltages (top) and grid-side currents (bottom);
 (b) Reactive power (top) and electromotive force (bottom).

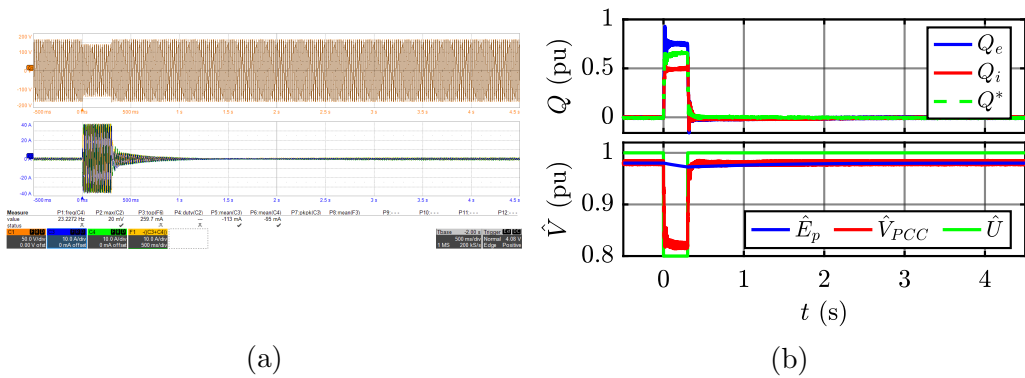


Figure 12.5.12: VISMA1’s response to voltage dip type 2, with reactive droop control enabled, from left to right:
 (a) PCC line voltages (top) and grid-side currents (bottom);
 (b) Reactive power (top) and electromotive force (bottom).

Dip Type 3

This result is very similar to what is obtained with voltage dip type 2. Even here the reactive power takes circa 4 s to return to zero without reactive droop control (Fig. 12.5.13b). In the opposite case, the dynamic is faster, as can be seen in Fig. 12.5.14b.

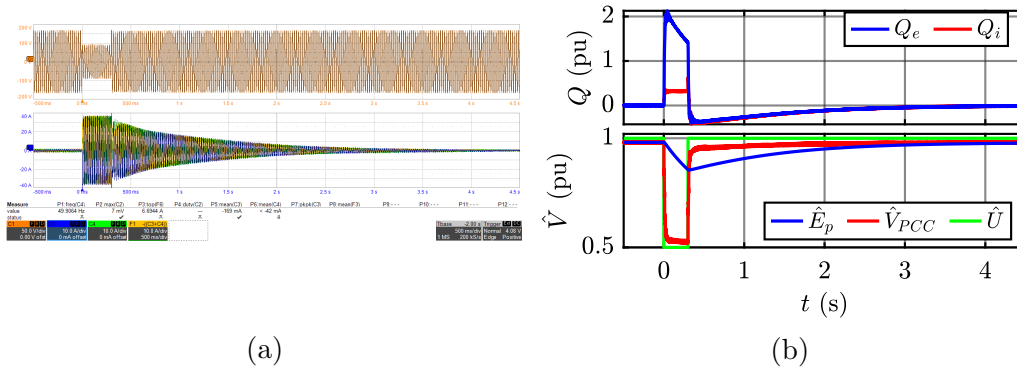


Figure 12.5.13: VISMA1's response to voltage dip type 3, with reactive droop control disabled, from left to right:
 (a) PCC line voltages (top) and grid-side currents (bottom);
 (b) Reactive power (top) and electromotive force (bottom).

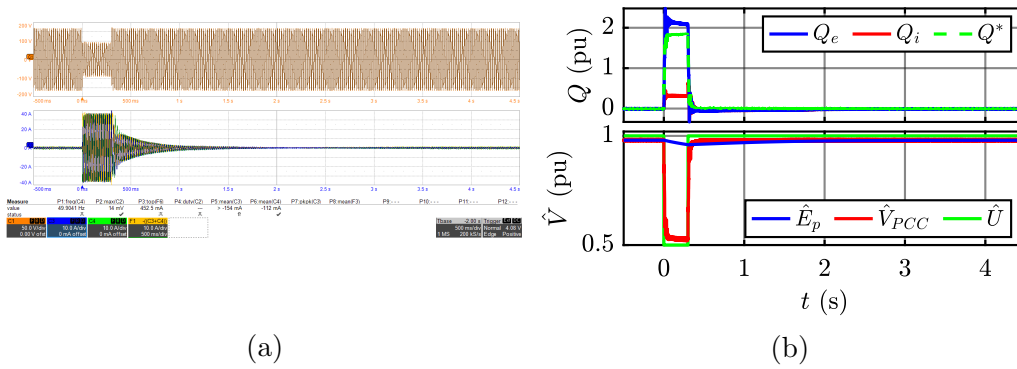


Figure 12.5.14: VISMA1's response to voltage dip type 3, with reactive droop control enabled, from left to right:
 (a) PCC line voltages (top) and grid-side currents (bottom);
 (b) Reactive power (top) and electromotive force (bottom).

12.6 VISMA2

VISMA2 is the second simplified version of VISMA, and it belongs to the category of current-input voltage-output VSG solutions, together with Synchroverter (base form) and Osaka. VISMA2 was born as an alternative to VISMA1 in order to overcome its limits, but it has yet disadvantages. The main one is the absence of a current limitation system, because its working principle is based on open-loop voltage control. In order to test the performance of this model, it has been necessary to introduce an addition part for the algorithm. The adaptation has been described in Subsection 2.5.5. Threshold has been set to different values according to the test.

12.6.1 Active and Reactive Power References

Even here, VISMA2’s active and reactive powers used for the control algorithm are different from the real ones. They can coincide or not, according to cases.

Active Power Reference Step

In these tests, only the conventional voltage control is used, because currents do not reach values dangerous for the system. Threshold is set to 30 A only for safety reasons. Therefore, no transition will occur.

The active power reference is properly reached without overshoot both by the virtual and the real powers, which are practically the same, as can be seen from Fig. 12.6.1b.

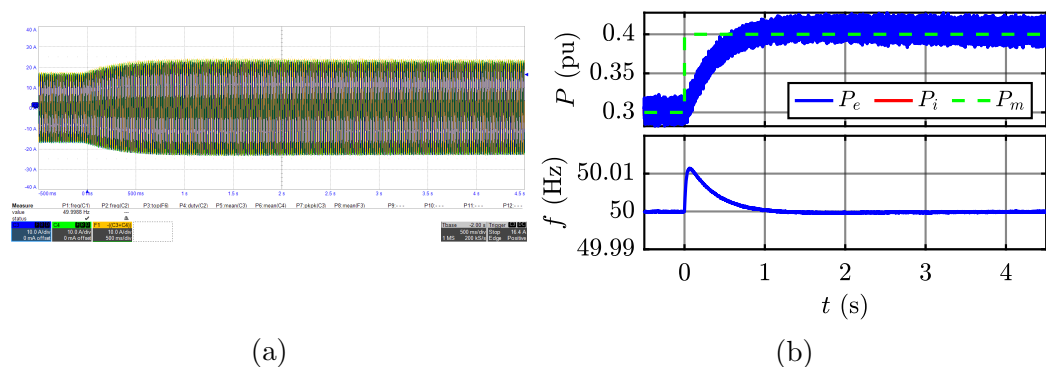


Figure 12.6.1: VISMA2’s response to active power reference step from 0.3 to 0.4 pu:

- (a) Grid-side currents;
- (b) Active power (top) and VISMA2’s frequency (bottom).

Reactive Power Reference Step

The excitation part of the model is based on a pure integrator, characterised by an excitation time constant τ_e set to 1 s. According to the control theory, after a step variation of the reference, it is expected to reach the steady state condition in a time of circa $4\tau_e - 5\tau_e$. The result matches with the theory because the steady state is reached in a time circa equal to 5 s.

Reference is reached both when droop control is disabled and when is enabled. In the first case, the reference Q^* is equal to 0.4 pu. Virtual reactive power reaches this value, whereas the real one is different. The former is calculated by means of the voltage references and the filtered inverter currents, whereas the latter is retrieved by the measurement of PCC voltage and inverter currents. Therefore, the difference is due to the impedance located between the two points of measure.

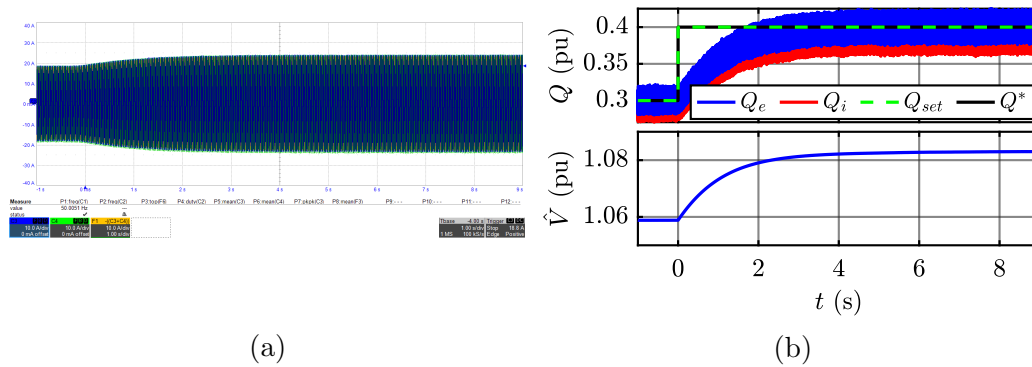


Figure 12.6.2: VISMA2's response to reactive power reference step from 0.3 to 0.4 pu with reactive droop control disabled, from left to right:
 (a) Grid-side currents;
 (b) Reactive power (top) and electromotive force (bottom).

In the second case, the droop control term ΔQ_d takes part in the definition of the total reactive power reference:

$$Q^* = Q_{set} + \Delta Q_d$$

Voltage reference is set to 0.97, the value of \widehat{V}_{PCC} when all the references are zero. In this way, when $Q_{set} = 0$, Q^* is zero as well.

The flowing of current from the inverter to the grid leads to a PCC voltage variation and consequently the droop control starts to limit the Q^* , respect to the case without droop control. The final result is a total reactive power

reference of circa 0.25 pu. This value is reached by the virtual reactive power, whereas the real one is slightly lower.

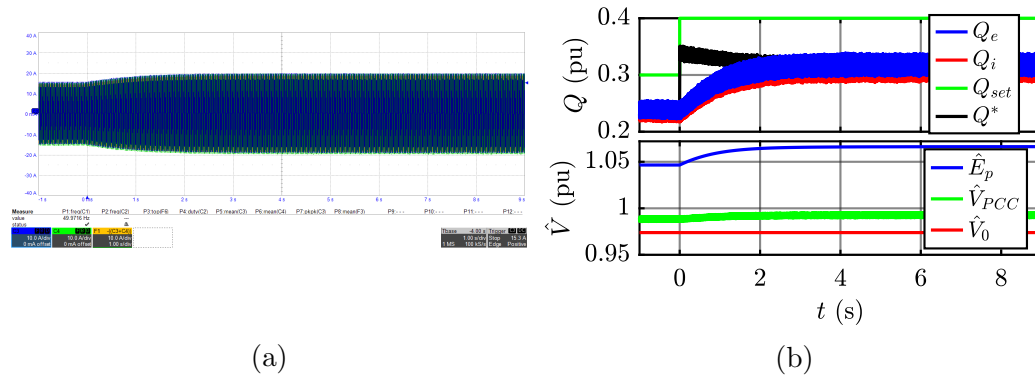


Figure 12.6.3: VISMA2's response to reactive power reference step from 0.3 to 0.4 pu with reactive droop control enabled, from left to right:

- (a) Grid-side currents;
- (b) Reactive power (top) and electromotive force (bottom).

12.6.2 Inertial Response

In this case the threshold is set to 15 A because the power is expected to reach a value unsustainable for the system. Current limit is the usual value of 36 A. Threshold is much lower than the current limit in order to guarantee a safety margin and avoid to perform the transition with values of currents close to the limit.

When the frequency variation occurs, active power starts to increase, up to circa 7 pu, whereas the real one is limited, thanks to the current saturation. The transition from the conventional control to the current one happens immediately because of the high dynamic of the active power.

Then, at 21.3 s the algorithm comes back to the conventional voltage-output configuration. The successive transient leads to the steady state condition where the active power is equal to zero, because of the absent of an active droop controller.

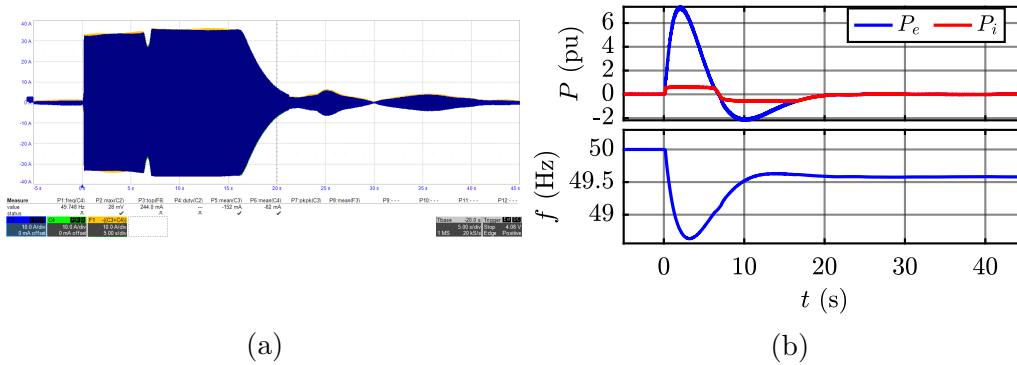


Figure 12.6.4: VISMA2’s response to grid frequency variation of -0.42 Hz, from left to right:
 (a) Grid-side currents;
 (b) Active power (top) and frequency (bottom).

12.6.3 Harmonic Distortion

In this test, 5% of fifth harmonic is added to the three phase grid voltage provided by the grid emulator. FFT of Fig. 12.6.5a shows the contribution of fifth harmonic is circa 8.5 V, when VISMA2 is disabled.

This terms decreases to 6 V when VISMA2 is enabled, as can be observed from Fig. 12.6.6a. Therefore, VISMA2 actuates a filtering action by means of the voltage drop on the grid impedance introduced by the distorted current of Fig. 12.6.6b.

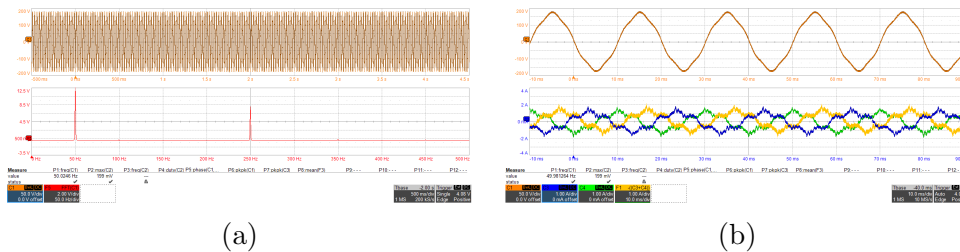


Figure 12.6.5: From left to right:
 (a) PCC Phase Voltage with 5% of fifth harmonic (top) and its FFT (bottom) with VISMA2 disabled;
 (b) PCC Phase Voltage with 5% of fifth harmonic (top) and grid-side currents (bottom) with VISMA2 disabled.

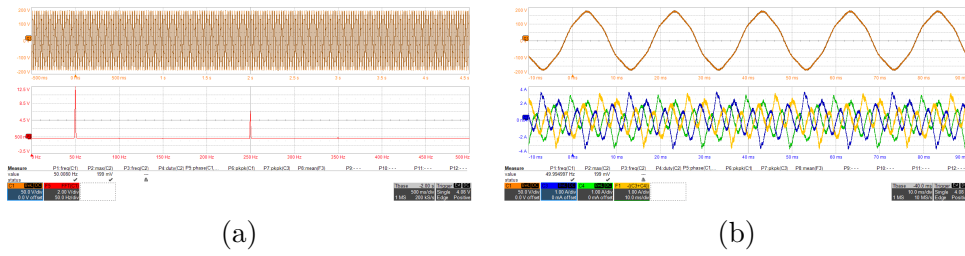


Figure 12.6.6: From left to right:
 (a) PCC Phase Voltage with 5% of fifth harmonic (top) and its FFT (bottom) with VISMA2 enabled;
 (b) PCC Phase Voltage with 5% of fifth harmonic (top) and grid-side currents (bottom) with VISMA2 enabled.

12.6.4 Voltage Dips

In the following charts, \hat{U} is the amplitude of the voltage provided by the grid emulator. It is not a physical measured quantity, but it is inserted to show the shape of the generated voltage dip.

Even here threshold is set to 15 A, whereas the limit of current is 36 A. The logic is the same of inertial response.

When the voltage dip occurs, independently of the case, the current is saturated and the virtual reactive power overcomes the value of 1 pu. When the reactive droop control is enabled, Q_e tracks the reference and the dynamic is faster respect to the case without reactive droop control. An evident difference can be found in the trend of the electromotive force for dip types 2 and 3. Without droop control, it takes much more time to reach the steady state value, comparing the same dip with droop control.

When the current is continuously lower than 5 A for at least 0.5 s, the control comes back to the voltage mode. For each dip the instant of transition has been indicated.

Dip Type 1

In this case the responses with and without reactive droop control are very similar, as can be noticed comparing Fig. 12.6.7b and Fig. 12.6.8b. Even the transition instants are practically the same: 656 ms without droop, against 644 ms with droop.

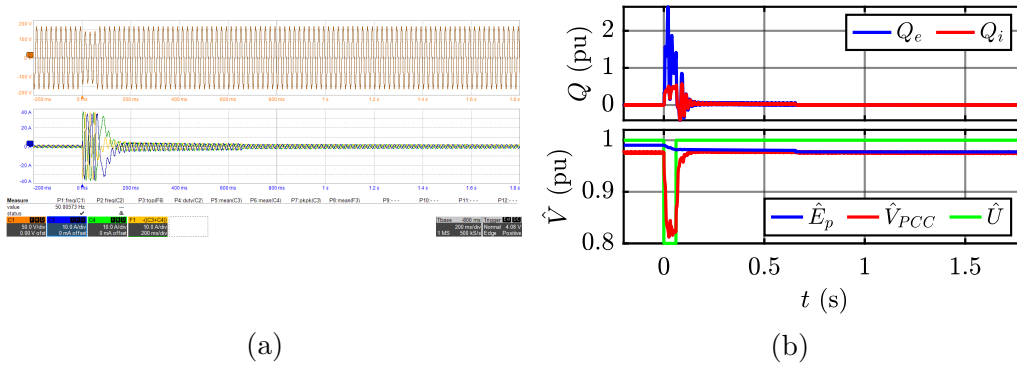


Figure 12.6.7: VISMA2's response to voltage dip type 1, with reactive droop control disabled, from left to right:
 (a) PCC line voltages (top) and grid-side currents (bottom);
 (b) Reactive power (top) and electromotive force (bottom).

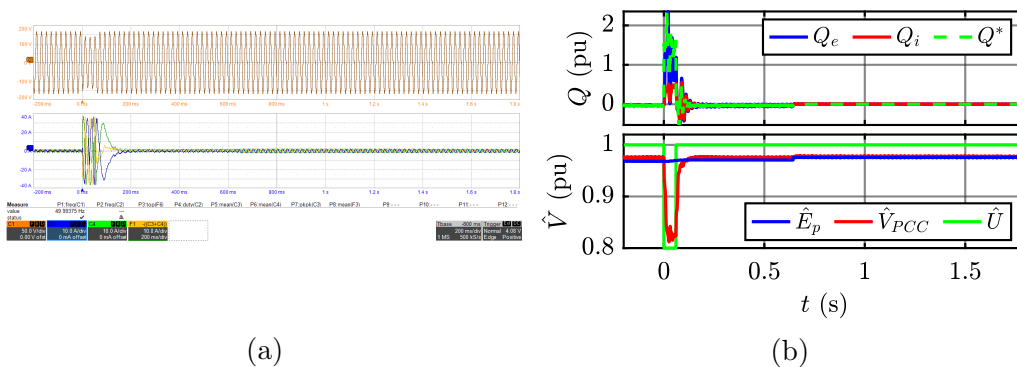


Figure 12.6.8: VISMA2's response to voltage dip type 1, with reactive droop control enabled, from left to right:
 (a) PCC line voltages (top) and grid-side currents (bottom);
 (b) Reactive power (top) and electromotive force (bottom).

Dip Type 2

With voltage dip type 2, the effect of the reactive droop control starts to be evident, as can be observed comparing Fig. 12.6.9b and Fig. 12.6.10b. In this case the two transition instants are respectively: 1.6 s and 1.41 s.

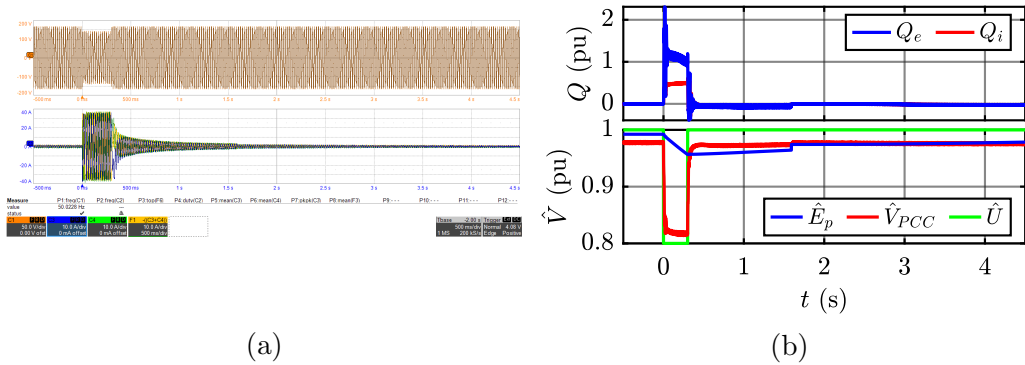


Figure 12.6.9: VISMA2's response to voltage dip type 2, with reactive droop control disabled, from left to right:

- (a) PCC line voltages (top) and grid-side currents (bottom);
- (b) Reactive power (top) and electromotive force (bottom).

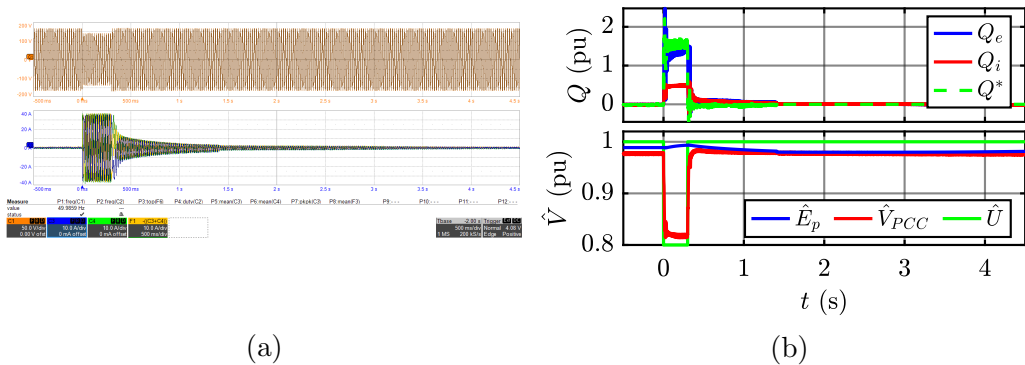


Figure 12.6.10: VISMA2's response to voltage dip type 2, with reactive droop control enabled, from left to right:

- (a) PCC line voltages (top) and grid-side currents (bottom);
- (b) Reactive power (top) and electromotive force (bottom).

Dip Type 3

In this case the reactive droop control introduces a consistent effect on the transient after the end of the voltage dip. As shown in Fig. 12.6.11b, the reactive power takes circa 5 s to return to zero after the end of the voltage dip. The transition instant is equal to 4.35 s. On the opposite, when the reactive droop control is enabled, the transient lasts circa 2 s and the transition instant is equal to 1.93 s.

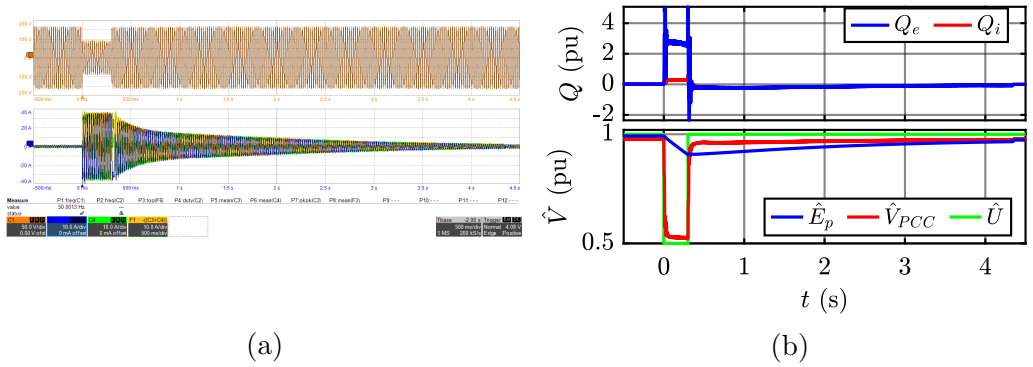


Figure 12.6.11: VISMA2's response to voltage dip type 3, with reactive droop control disabled, from left to right:
 (a) PCC line voltages (top) and grid-side currents (bottom);
 (b) Reactive power (top) and electromotive force (bottom).

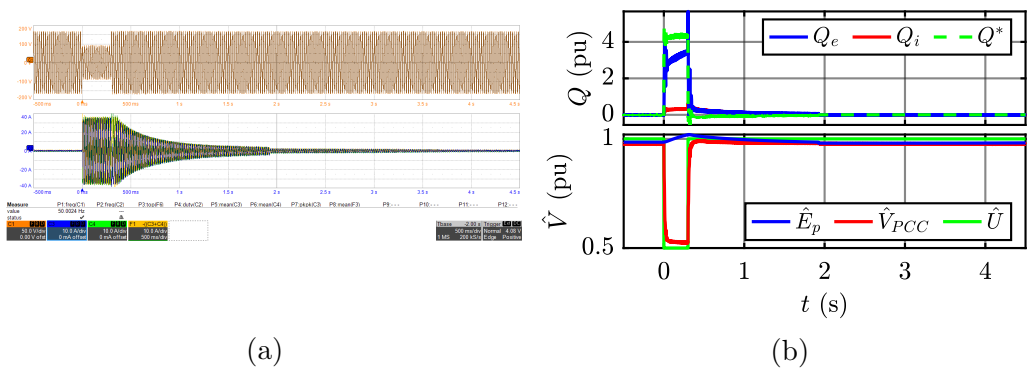


Figure 12.6.12: VISMA2's response to voltage dip type 3, with reactive droop control enabled, from left to right:
 (a) PCC line voltages (top) and grid-side currents (bottom);
 (b) Reactive power (top) and electromotive force (bottom).

12.7 SPC

SPC is a voltage-input current-output model. Current references are compared with the grid-side ones and the error is provided to a PI regulator. It allows to properly saturate the real currents flowing from the inverter to the grid.

For SPC, all three versions have been tested, in order to observe the differences among them. This model normally uses real powers to close the active and reactive power loops. Only during synchronization and saturation, powers are calculated using not saturated current references, in order to guarantee the stability of the control. Real powers will be saturated by means of the current limitation performed by the PI regulator.

In order to simplify the notation, the three versions will be indicated with the following names: SPC SG, SPC PI, SPC LL.

12.7.1 Active and Reactive Power References

Active Power Reference Step

For SPC PI the active power reference is obtained by the sum of the external reference and the droop active power:

$$P^* = P_{set} + P_w$$

Instead, for SPC SG and SPC LL $P^* = P_{set}$ because the external governor is not used.

The responses of the three versions to the active power step are very similar. Slight differences can be observed between SPC SG and the other two: for the first one the rising time is circa two times bigger respect to the other two. On the other hand, frequency peak is circa 50.02 Hz, whereas SPC PI and SPC LL reach a peak of about 50.06 Hz. The results are respectively shown in Fig. 12.7.1, Fig. 12.7.2 and Fig. 12.7.3.

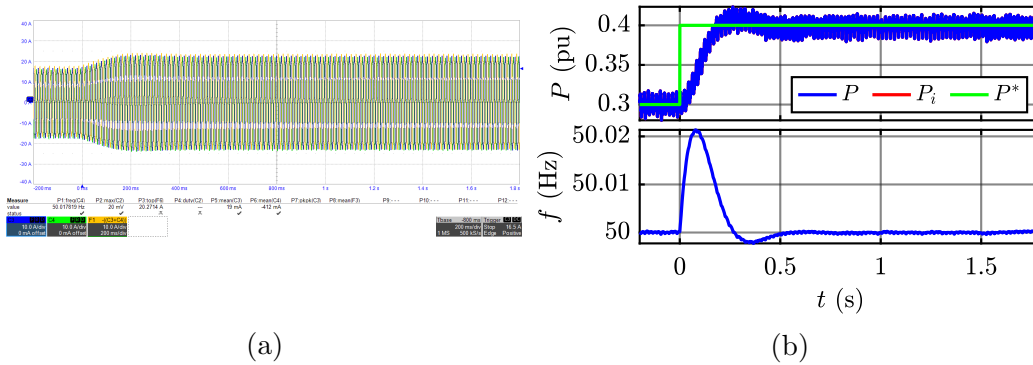


Figure 12.7.1: SPC SG's response to active power reference step from 0.3 to 0.4 pu, from left to right:
 (a) Grid-side currents;
 (b) Active power (top) and frequency (bottom).

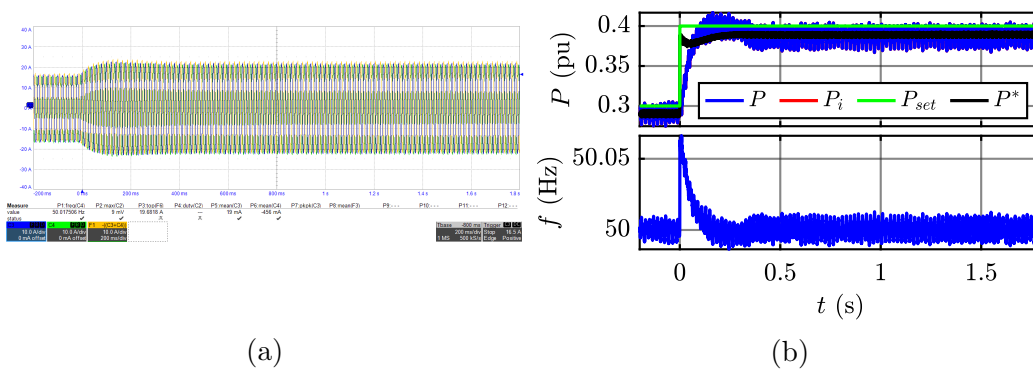


Figure 12.7.2: SPC PI's response to active power reference step from 0.3 to 0.4 pu, from left to right:
 (a) Grid-side currents;
 (b) Active power (top) and frequency (bottom).

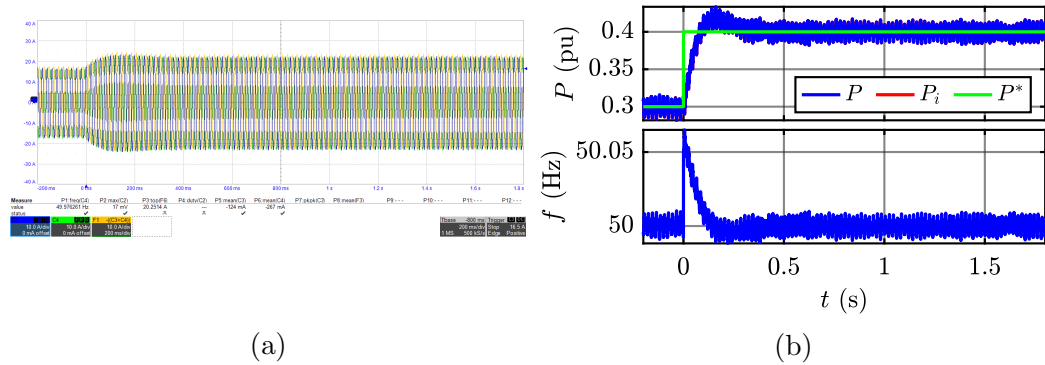


Figure 12.7.3: SPC LL's response to active power reference step from 0.3 to 0.4 pu, from left to right:
 (a) Grid-side currents;
 (b) Active power (top) and frequency (bottom).

Reactive Power Reference Step

The excitation part is the same for each version, therefore it is expected to obtain the same results. The control is based on a pure integrator and the dynamic depends on the excitation time constant τ_e , set to 1 s. Therefore, when a step variation of the reference occurs, it is expected to reach the steady state condition after $4\tau_e - 5\tau_e$ according to control theory.

The outcomes are in compliance with these statements. In fact, as can be seen from Fig. 12.7.4b, Fig. 12.7.5b and Fig. 12.7.6b, the transient takes circa 5 s to complete. When the the reactive droop control is enabled, the dynamic is faster. The results are shown in Fig. 12.7.7b, Fig. 12.7.8b and Fig. 12.7.9b. The difference between the employment of the droop control or not lies in the value of the reactive power reference Q^* .

When the reactive droop control is disabled $Q^* = Q_L$. Whereas, in the other case, the droop control term is added to Q_L :

$$Q^* = Q_L + \Delta Q_d$$

The voltage reference \hat{V}_0 is equal to 0.97, which is the value of PCC voltage amplitude when $Q_L = 0$. In this way, tests start with $Q^* = 0$. When $Q_L \neq 0$, inverter injects power and PCC voltage changes. Consequently, a no-zero droop control contribution will be also present. The result is a total reference $Q^* = 0$ lower respect to the first case.

Independently on the droop control, the reactive power reaches the reference for each version.

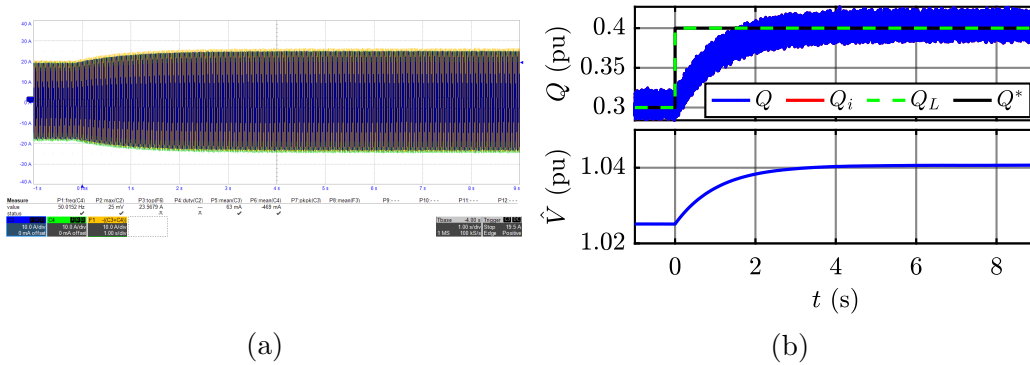


Figure 12.7.4: SPC SG's response to reactive power reference step from 0.3 to 0.4 pu with reactive droop control disabled, from left to right:
 (a) Grid-side currents;
 (b) Reactive power (top) and electromotive force (bottom).

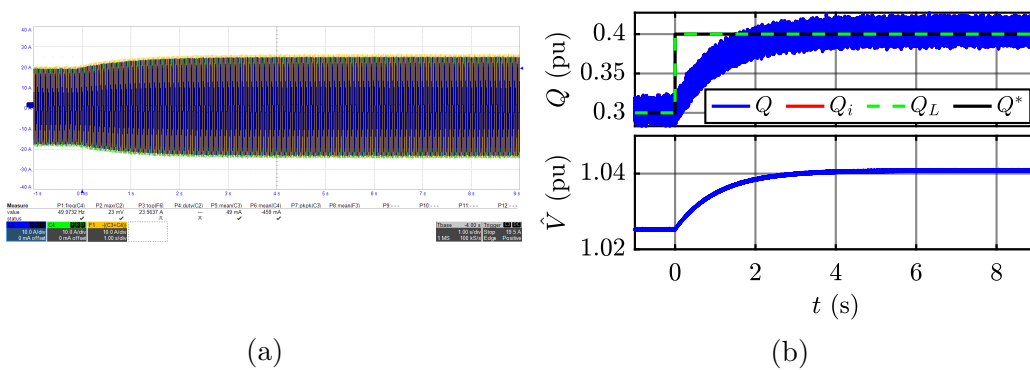


Figure 12.7.5: SPC PI's response to reactive power reference step from 0.3 to 0.4 pu with reactive droop control disabled, from left to right:
 (a) Grid-side currents;
 (b) Reactive power (top) and electromotive force (bottom).

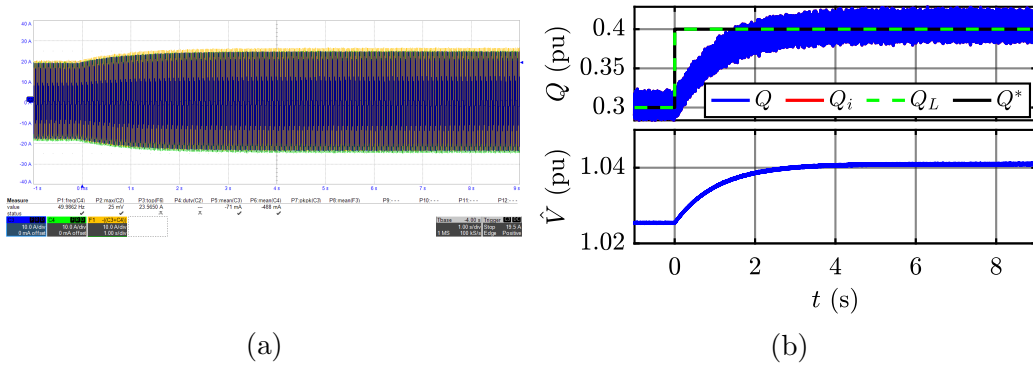


Figure 12.7.6: SPC LL's response to reactive power reference step from 0.3 to 0.4 pu with reactive droop control disabled, from left to right:
 (a) Grid-side currents;
 (b) Reactive power (top) and electromotive force (bottom).

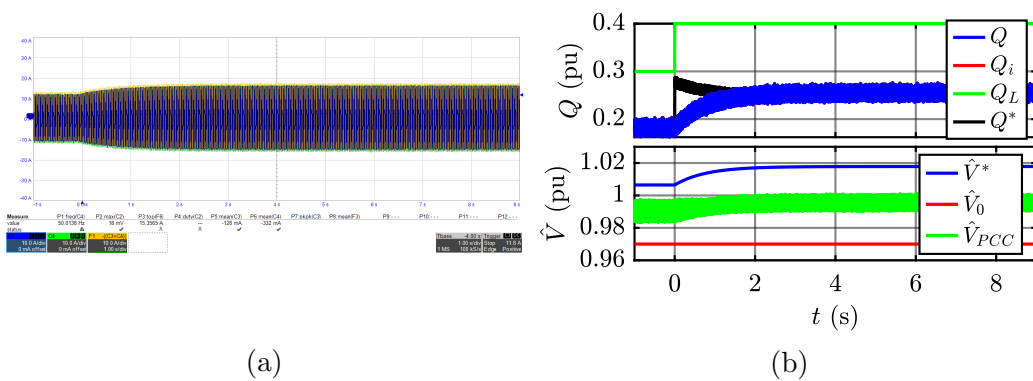


Figure 12.7.7: SPC SG's response to reactive power reference step from 0.3 to 0.4 pu with reactive droop control enabled, from left to right:
 (a) Grid-side currents;
 (b) Reactive power (top) and electromotive force (bottom).

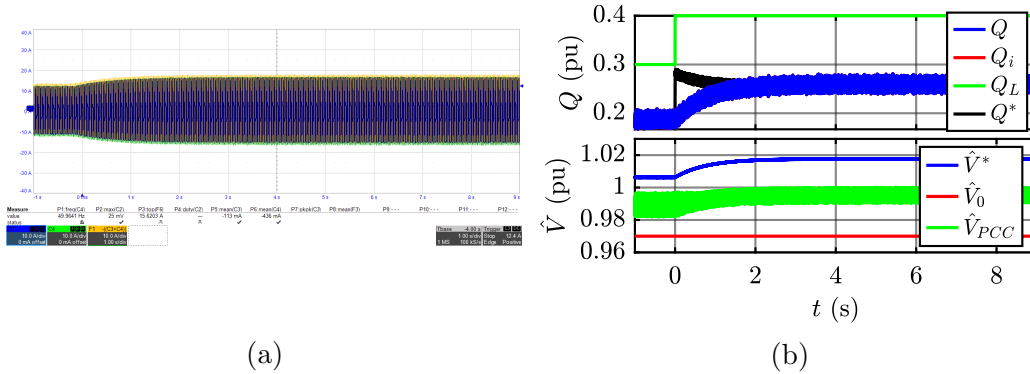


Figure 12.7.8: SPC PI's response to reactive power reference step from 0.3 to 0.4 pu with reactive droop control enabled, from left to right:
 (a) Grid-side currents;
 (b) Reactive power (top) and electromotive force (bottom).

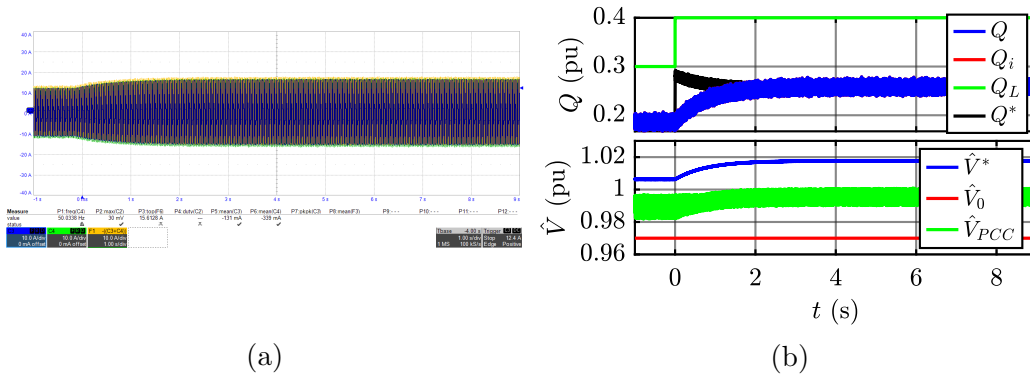


Figure 12.7.9: SPC LL's response to reactive power reference step from 0.3 to 0.4 pu with reactive droop control enabled, from left to right:
 (a) Grid-side currents;
 (b) Reactive power (top) and electromotive force (bottom).

12.7.2 Inertial Response

The variation of frequency leads to the injection of the active power from the inverter to the grid.

SPC SG is based on the conventional swing equation and the equivalent droop coefficient is equal to $k_d = 153$ pu according to the tuning. Therefore, in steady state, the SPC SG's active power is expected to be:

$$P = k_d \Delta\omega = k_d \cdot (\omega_r - \omega) = 153 \cdot \frac{0.42}{50} = 1.26 \text{ pu}$$

The result of Fig. 12.7.10b is perfectly in compliance with the forecast. Obviously, the real power is saturated by means of the current limitation.

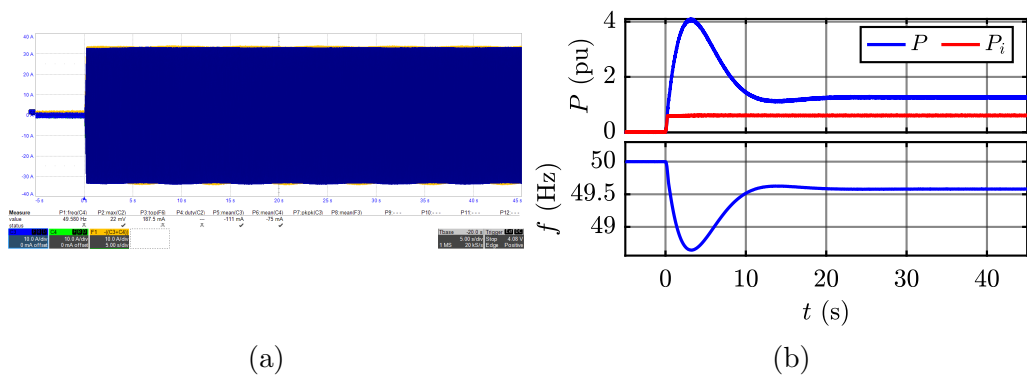


Figure 12.7.10: SPC SG's response to grid frequency variation of -0.42 Hz, from left to right:
 (a) Grid-side currents;
 (b) Active power (top) and frequency (bottom).

As regards SPC PI and SPC LL, a dedicated active droop control is used, eliminating the link between droop control and damping. The former has an external droop controller, whereas the latter inherently embeds this feature. In both cases, setting the droop coefficient to the conventional value of 5%, in steady state inverter injects an active power equal to:

$$P = -\frac{\Delta f}{b_p} = \frac{0.42}{50 \cdot 0.05} = 0.168 \text{ pu}$$

Results for SPC PI and SPC LL are respectively shown in Fig. 12.7.11b and Fig. 12.7.12b.

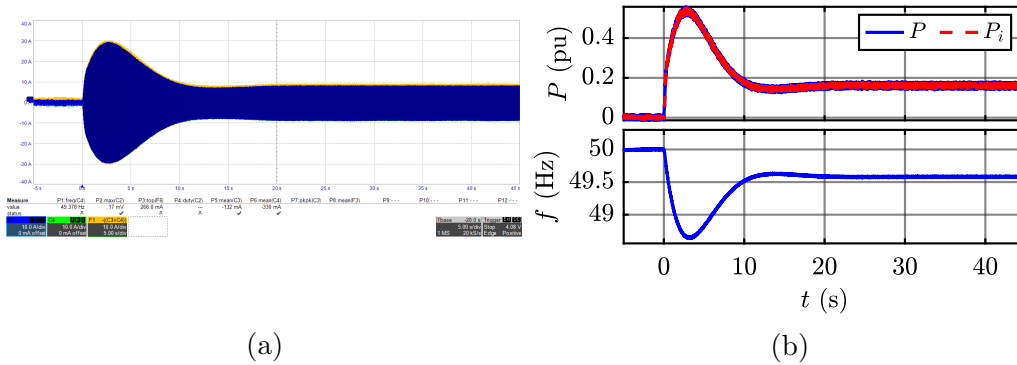


Figure 12.7.11: SPC PI's response to grid frequency variation of -0.42 Hz, from left to right:
 (a) Grid-side currents;
 (b) Active power (top) and frequency (bottom).

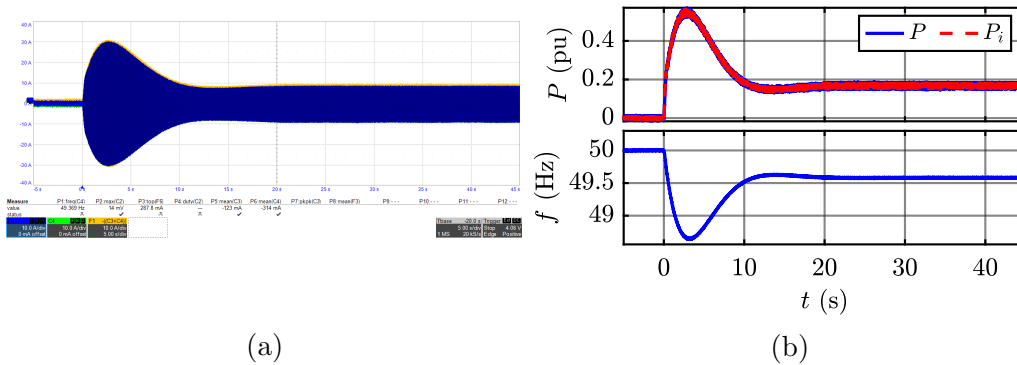


Figure 12.7.12: SPC LL's response to grid frequency variation of -0.42 Hz, from left to right:
 (a) Grid-side currents;
 (b) Active power (top) and frequency (bottom).

12.7.3 Harmonic Distortion

In this test, 5% of fifth harmonic is added to the three phase grid voltage provided by the grid emulator. The result is a contribution of 8.5 V, as shown in the FFT of Fig. 12.7.13a. Current references are still disabled, therefore this case is the same for all three version.

As soon as current references are enabled, the fifth harmonic term decreases to 4.5 V, independently on the PLC type. In this case, distorted currents

introduce a voltage drop on the grid impedance, performing a filtering action on the PCC voltage. Therefore, SPC can improve the power quality in presence of distortion, as demonstrated by the results in Fig. 12.7.14b, Fig. 12.7.15b and Fig. 12.7.16b

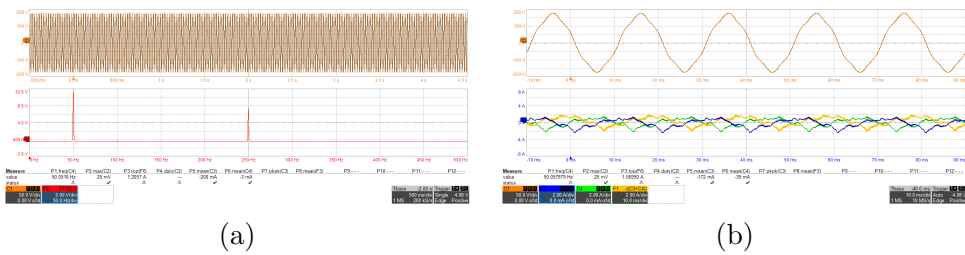


Figure 12.7.13: From left to right:
 (a) PCC Phase Voltage with 5% of fifth harmonic (top) and its FFT (bottom) with SPC's current references disabled;
 (b) PCC Phase Voltage with 5% of fifth harmonic (top) and grid-side currents (bottom).

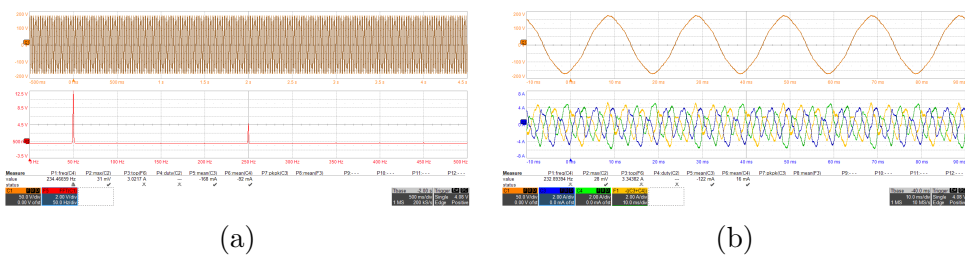


Figure 12.7.14: From left to right:
 (a) PCC Phase Voltage with 5% of fifth harmonic (top) and its FFT (bottom) with SPC SG's current references enabled;
 (b) PCC Phase Voltage with 5% of fifth harmonic (top) and grid-side currents (bottom).

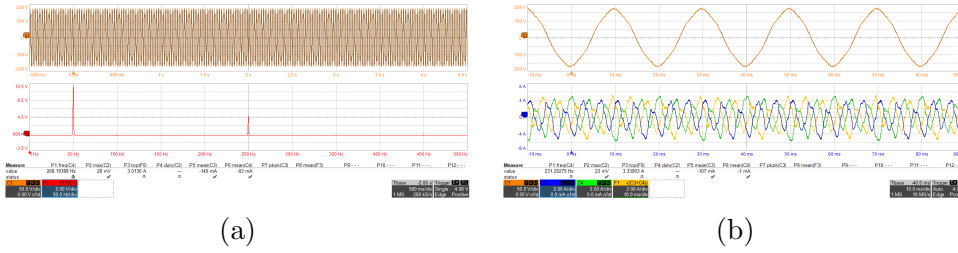


Figure 12.7.15: From left to right:
 (a) PCC Phase Voltage with 5% of fifth harmonic (top) and its FFT (bottom) with SPC PI's current references enabled;
 (b) PCC Phase Voltage with 5% of fifth harmonic (top) and grid-side currents (bottom).

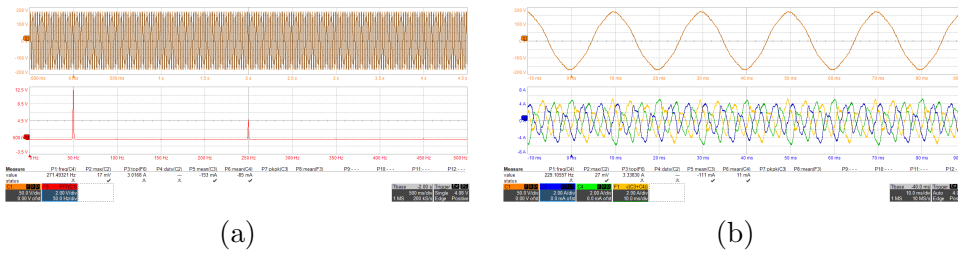


Figure 12.7.16: From left to right:
 (a) PCC Phase Voltage with 5% of fifth harmonic (top) and its FFT (bottom) with SPC LL's current references enabled;
 (b) PCC Phase Voltage with 5% of fifth harmonic (top) and grid-side currents (bottom).

12.7.4 Voltage Dips

In the following charts, \hat{U} is the amplitude of the voltage provided by the grid emulator. It is not a physical measured quantity, but it is inserted to show the shape of the generated voltage dip.

The only difference between the three versions of SPC is the active power controller, therefore it is expected to obtain the same results for each of them. In all cases currents are limited to 36 A and so the real reactive power is saturated. To guarantee the stability of the control, during saturation, powers are computed using the not saturated references. As can be seen from all results, when the voltage dip starts, virtual reactive power shows oscillations which damp in circa 100 ms.

Dip Type 1

When the voltage dip starts, reactive power shows oscillations which remain during all the dip. The time is too short to appreciate the effect of reactive droop control. Fig. 12.7.17, Fig. 12.7.18 and Fig. 12.7.19 show there are not particular differences between the three versions, and the same is true with reactive droop control, as demonstrated by Fig. 12.7.20, Fig. 12.7.21 and Fig. 12.7.22.

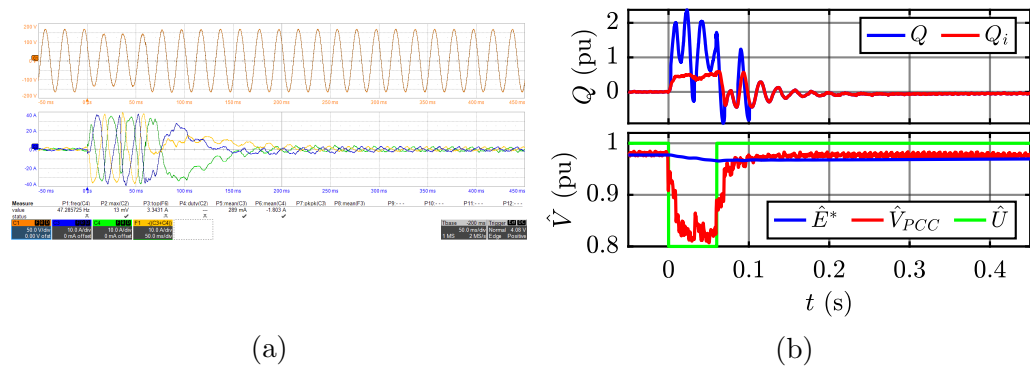


Figure 12.7.17: SPC SG's response to voltage dip type 1, with reactive droop control disabled, from left to right:
 (a) PCC line voltages (top) and grid-side currents (bottom);
 (b) Reactive power (top) and electromotive force (bottom).

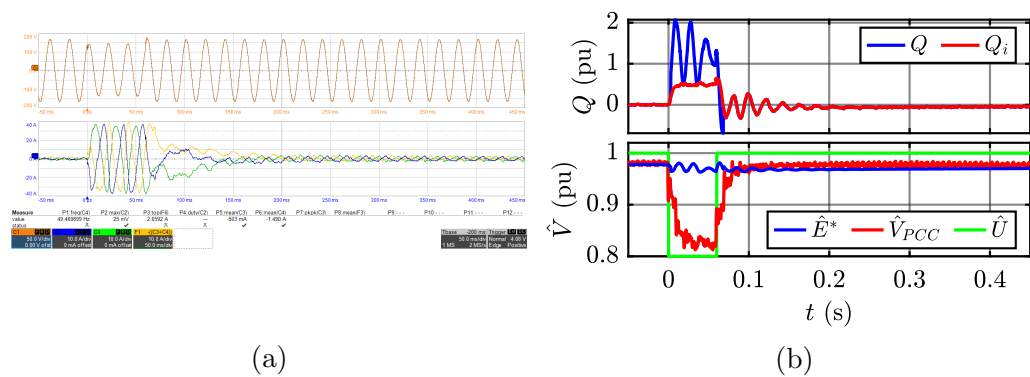


Figure 12.7.18: SPC PI's response to voltage dip type 1, with reactive droop control disabled, from left to right:
 (a) PCC line voltages (top) and grid-side currents (bottom);
 (b) Reactive power (top) and electromotive force (bottom).

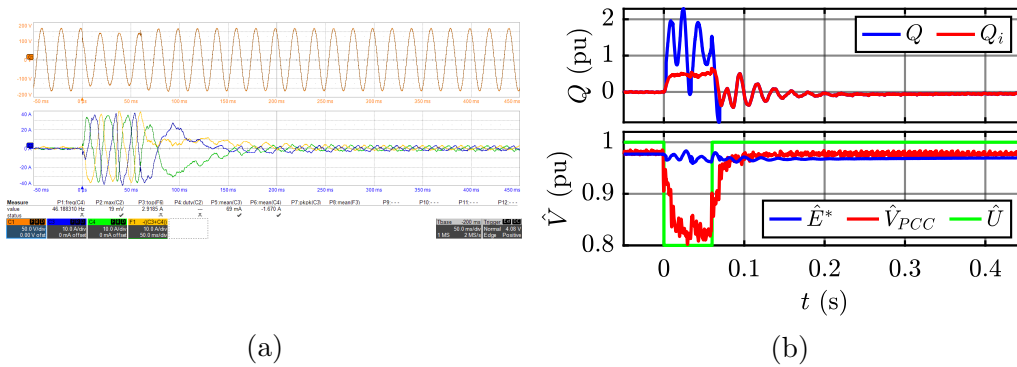


Figure 12.7.19: SPC LL's response to voltage dip type 1, with reactive droop control disabled, from left to right:
 (a) PCC line voltages (top) and grid-side currents (bottom);
 (b) Reactive power (top) and electromotive force (bottom).

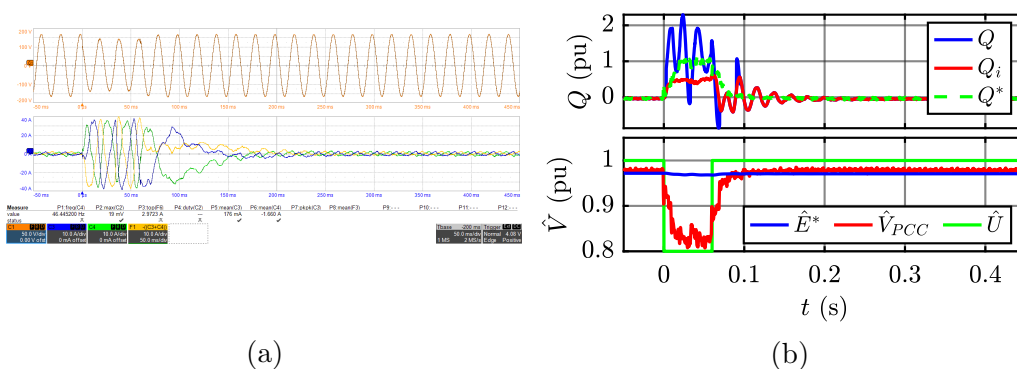


Figure 12.7.20: SPC SG's response to voltage dip type 1, with reactive droop control enabled, from left to right:
 (a) PCC line voltages (top) and grid-side currents (bottom);
 (b) Reactive power (top) and electromotive force (bottom).

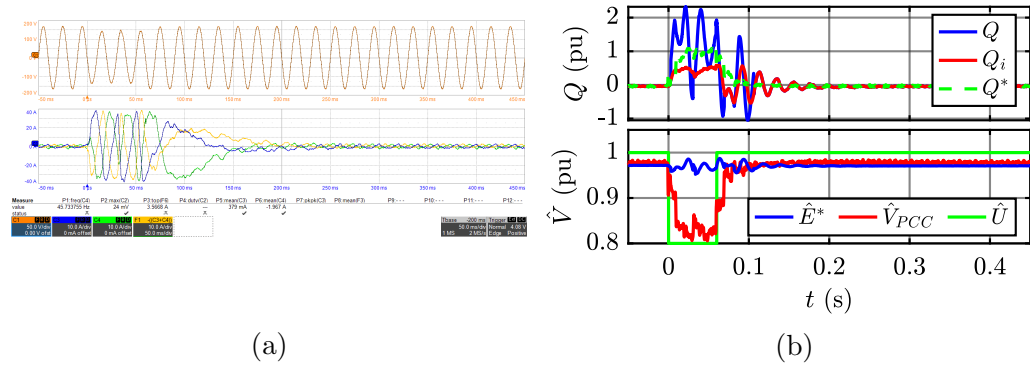


Figure 12.7.21: SPC PI's response to voltage dip type 1, with reactive droop control enabled, from left to right:
 (a) PCC line voltages (top) and grid-side currents (bottom);
 (b) Reactive power (top) and electromotive force (bottom).

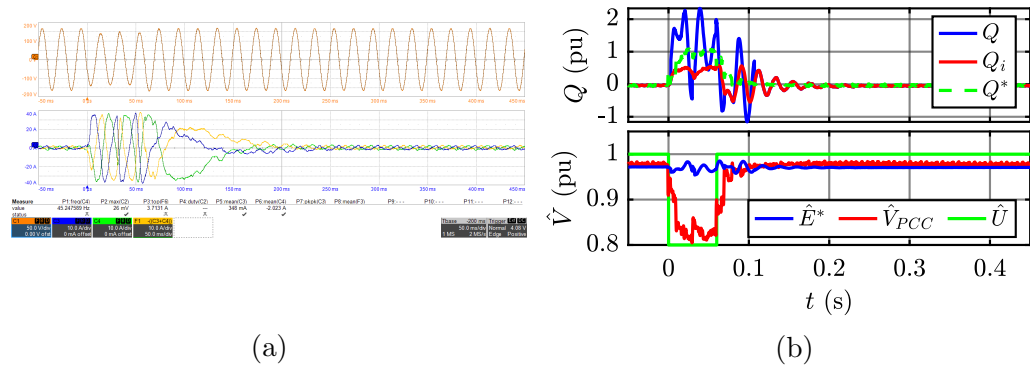


Figure 12.7.22: SPC LL's response to voltage dip type 1, with reactive droop control enabled, from left to right:
 (a) PCC line voltages (top) and grid-side currents (bottom);
 (b) Reactive power (top) and electromotive force (bottom).

Dip Type 2

In this case reactive power's oscillations have sufficient time to damp and the impact of reactive droop control can be observed. In circa 100 ms oscillations end and the virtual reactive power starts to decrease when the reactive droop control is disabled (Fig. 12.7.23, Fig. 12.7.24 and Fig. 12.7.25). The dynamic is dominated by the excitation time constant τ_e , set to 1 s. In fact, electromotive force takes circa 4 s to complete the transient.

Enabling the reactive droop control, after the oscillation transient, the virtual power is constant and tracks its reference, as can be observed from Fig. 12.7.26, Fig. 12.7.27 and Fig. 12.7.28. Finally, when the voltage dip ends, the electromotive force quickly comes back to the previous value. Even in this case, no evident differences can be appreciate between the three versions.

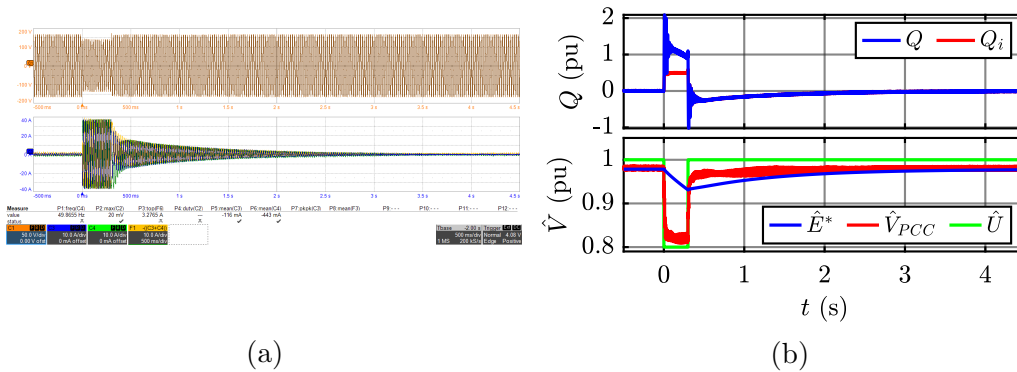


Figure 12.7.23: SPC SG's response to voltage dip type 2, with reactive droop control disabled, from left to right:

- (a) PCC line voltages (top) and grid-side currents (bottom);
- (b) Reactive power (top) and electromotive force (bottom).

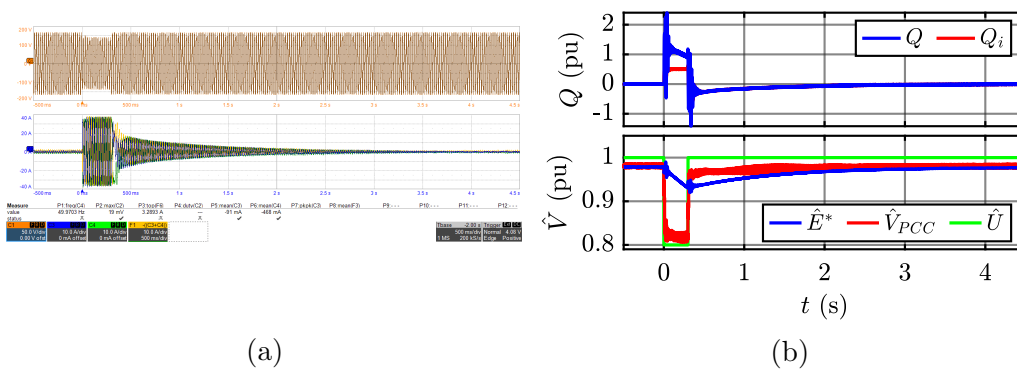


Figure 12.7.24: SPC PI's response to voltage dip type 2, with reactive droop control disabled, from left to right:

- (a) PCC line voltages (top) and grid-side currents (bottom);
- (b) Reactive power (top) and electromotive force (bottom).

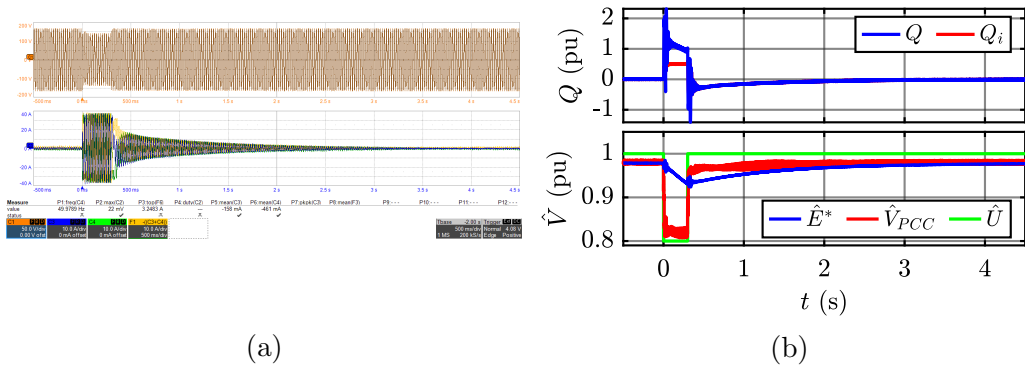


Figure 12.7.25: SPC LL's response to voltage dip type 2, with reactive droop control disabled, from left to right:
 (a) PCC line voltages (top) and grid-side currents (bottom);
 (b) Reactive power (top) and electromotive force (bottom).

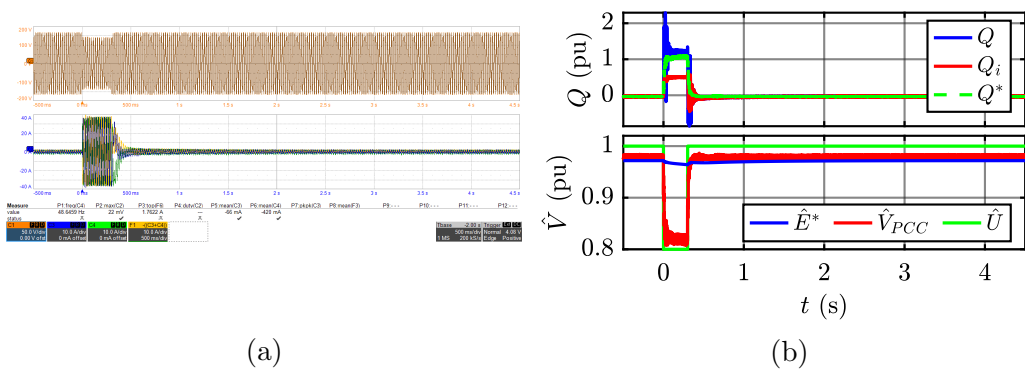


Figure 12.7.26: SPC SG's response to voltage dip type 2, with reactive droop control enabled, from left to right:
 (a) PCC line voltages (top) and grid-side currents (bottom);
 (b) Reactive power (top) and electromotive force (bottom).

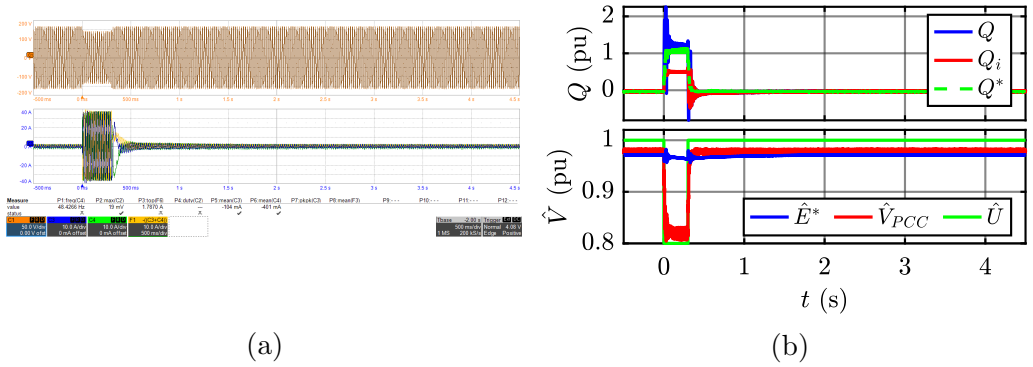


Figure 12.7.27: SPC PI's response to voltage dip type 2, with reactive droop control enabled, from left to right:
 (a) PCC line voltages (top) and grid-side currents (bottom);
 (b) Reactive power (top) and electromotive force (bottom).

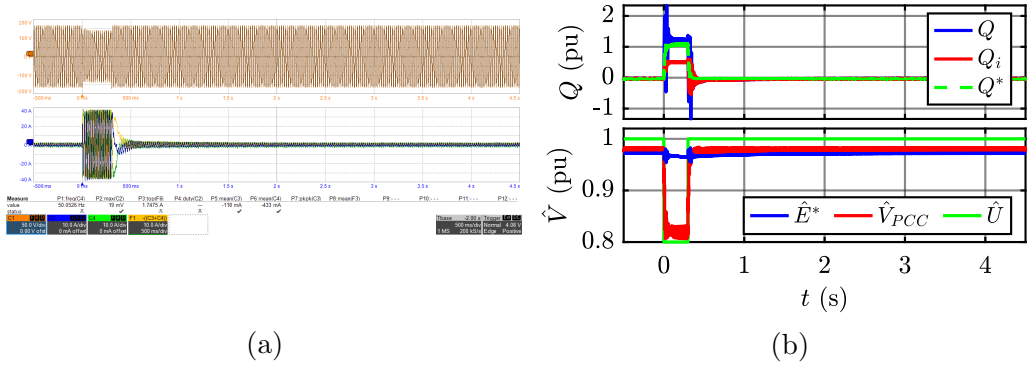


Figure 12.7.28: SPC LL's response to voltage dip type 2, with reactive droop control enabled, from left to right:
 (a) PCC line voltages (top) and grid-side currents (bottom);
 (b) Reactive power (top) and electromotive force (bottom).

Dip Type 3

All the statements for voltage dip 2 are valid. The only difference is in the values reached, but phenomena are the same. Even in this case, the three versions do not show evident differences, as demonstrated by from Fig. 12.7.29 to Fig. 12.7.34.

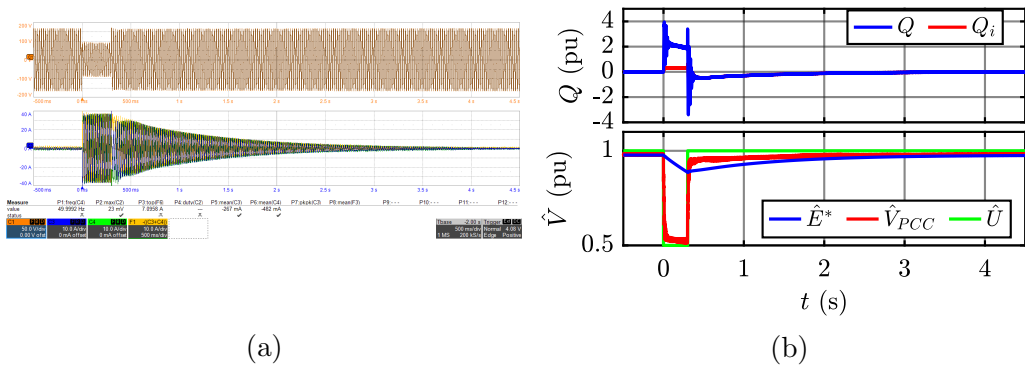


Figure 12.7.29: SPC SG's response to voltage dip type 3, with reactive droop control disabled, from left to right:
 (a) PCC line voltages (top) and grid-side currents (bottom);
 (b) Reactive power (top) and electromotive force (bottom).

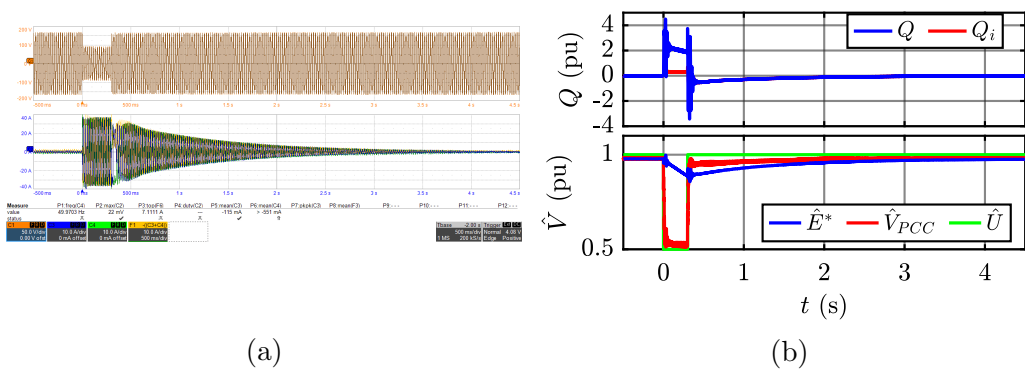


Figure 12.7.30: SPC PI's response to voltage dip type 3, with reactive droop control disabled, from left to right:
 (a) PCC line voltages (top) and grid-side currents (bottom);
 (b) Reactive power (top) and electromotive force (bottom).

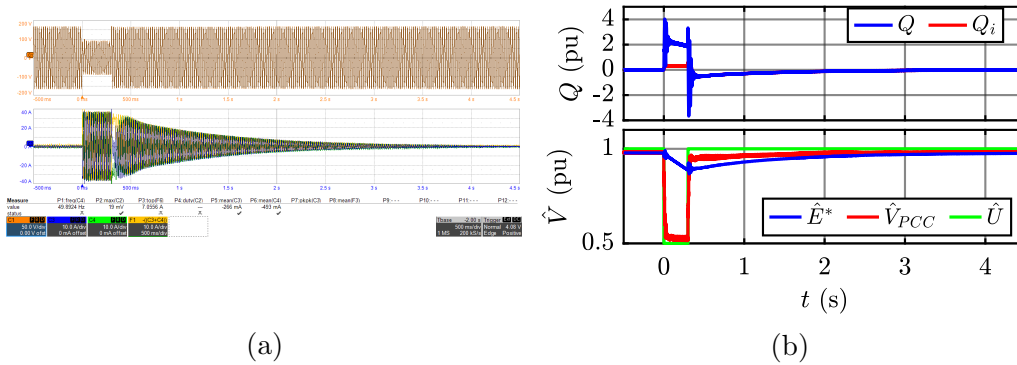


Figure 12.7.31: SPC LL's response to voltage dip type 3, with reactive droop control disabled, from left to right:
 (a) PCC line voltages (top) and grid-side currents (bottom);
 (b) Reactive power (top) and electromotive force (bottom).

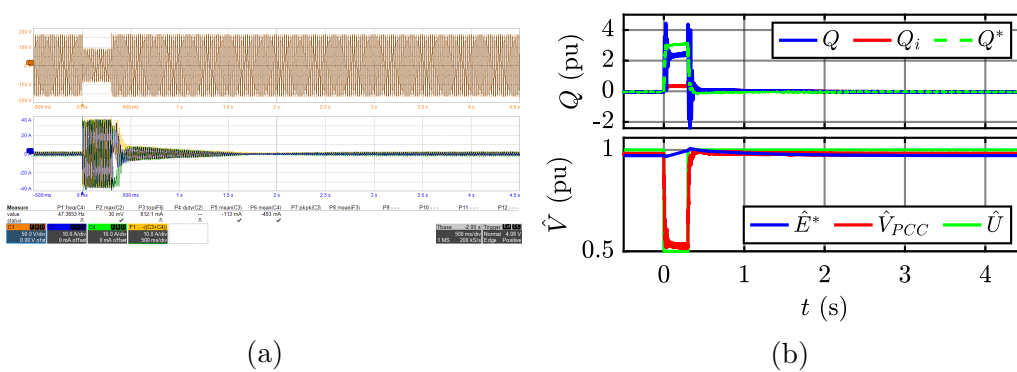


Figure 12.7.32: SPC SG's response to voltage dip type 3, with reactive droop control enabled, from left to right:
 (a) PCC line voltages (top) and grid-side currents (bottom);
 (b) Reactive power (top) and electromotive force (bottom).

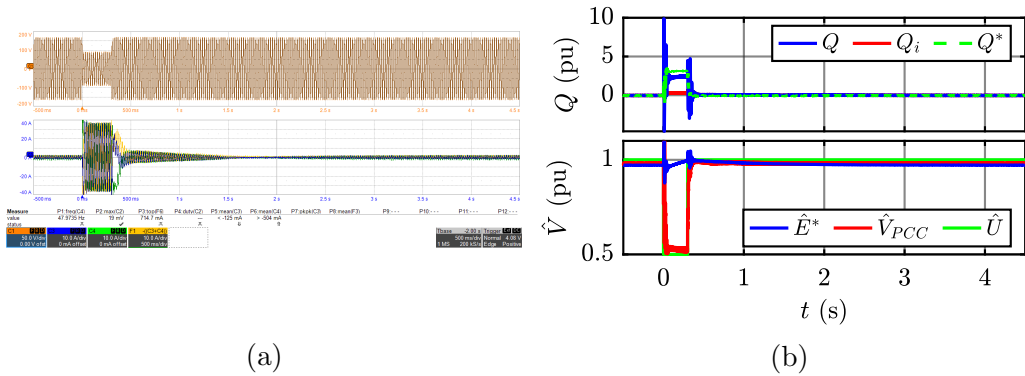


Figure 12.7.33: SPC PI's response to voltage dip type 3, with reactive droop control enabled, from left to right:
 (a) PCC line voltages (top) and grid-side currents (bottom);
 (b) Reactive power (top) and electromotive force (bottom).

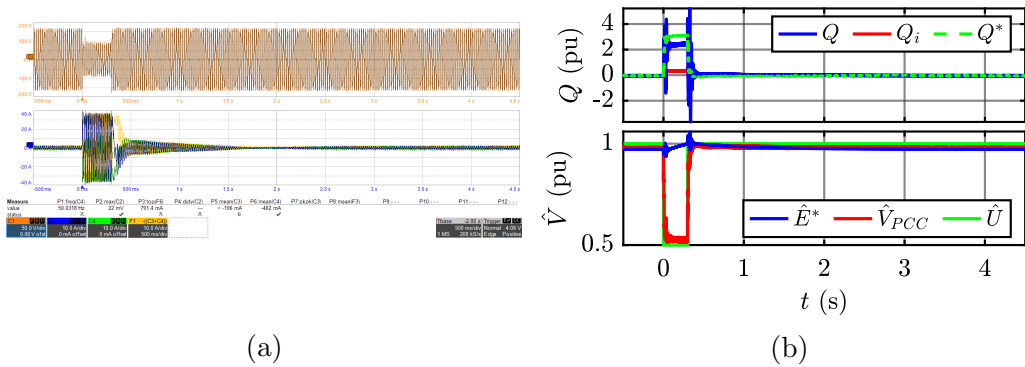


Figure 12.7.34: SPC LL's response to voltage dip type 3, with reactive droop control enabled, from left to right:
 (a) PCC line voltages (top) and grid-side currents (bottom);
 (b) Reactive power (top) and electromotive force (bottom).

12.8 VSYNC

VSYNC belongs to the voltage-input current-output category. Therefore, the model creates the current references which are compared with the measured currents. The error between them feeds a PI regulator, which provides the voltage references for the PWM modulator. The use of PI regulator allows to perform a reliable current limitation without additional blocks.

12.8.1 Active and Reactive Power References

VSYNC does not embed power loops, therefore virtual active and reactive powers do not exist. For the following results, only the real active and reactive power will be shown, with the symbols P and Q .

Active Power Reference Step

Applying a step variation of the active power reference P_{set} from 0.3 pu to 0.4 pu, VSYNC shows the second most underdamped response between all the VSG solutions, as illustrated in Fig. 12.8.1b. The first has been already seen in VISMA. The set point is reached after circa 2 s.

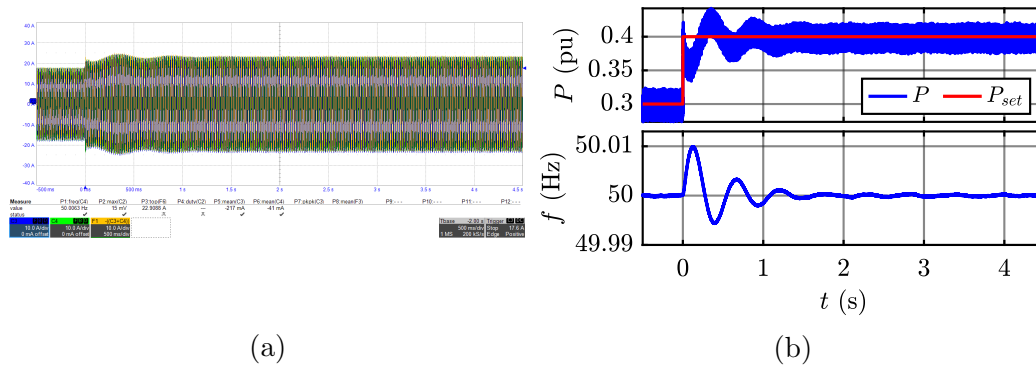


Figure 12.8.1: VSYNC's response to active power reference step from 0.3 to 0.4 pu:

- (a) Grid-side currents;
- (b) Active power (top) and VSYNC's frequency (bottom).

Reactive Power Reference Step

For VSYNC, the reactive power reference is directly used to compute the current references and there is not an excitation part. Therefore, the real reactive power follows immediately the step variation of the reference, as can

be noticed from Fig. 12.8.2b and Fig. 12.8.3b. The reactive power reference Q^* is obtained by the sum of two terms:

$$Q^* = Q_{set} + \Delta Q_d$$

When the reactive droop control is disabled, ΔQ_d is zero and $Q^* = Q_{set}$. In fact, as can be seen from Fig. 12.8.2b, Q^* is equal to 0.4 pu.

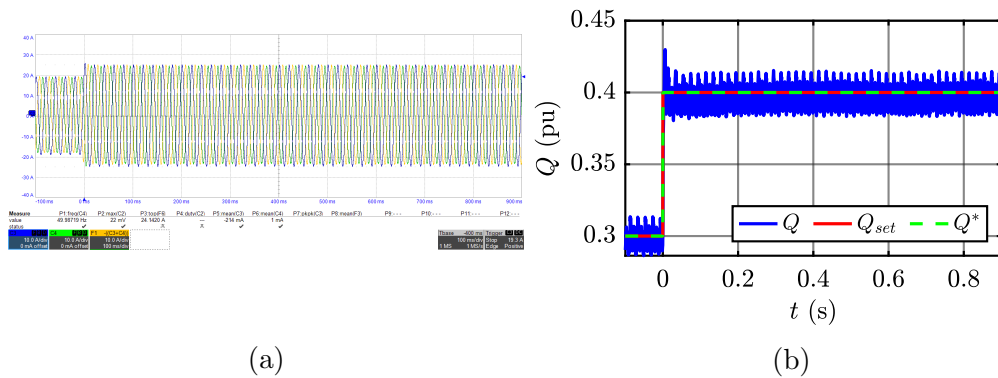


Figure 12.8.2: VSYNC's response to reactive power reference step from 0.3 to 0.4 pu with reactive droop control disabled, from left to right: (a) Grid-side currents; (b) Reactive power (top) and voltage reference amplitude (bottom).

As regard the case of reactive droop control enabled, the first step is to set the voltage reference \hat{V}^* equal to \hat{V}_{PCC} when $Q_{set} = 0$, in order to start the test with $Q^* = 0$. When $Q_{set} = 0.3$ pu, inverter injects current and the PCC voltage grows. Consequently, the reactive droop control introduces a negative term ΔQ_d to balance the voltage difference. The result is a total reactive reference Q^* lower than the case without droop control. In fact, as can be observed in Fig. 12.8.3b, it is circa 0.28 pu.

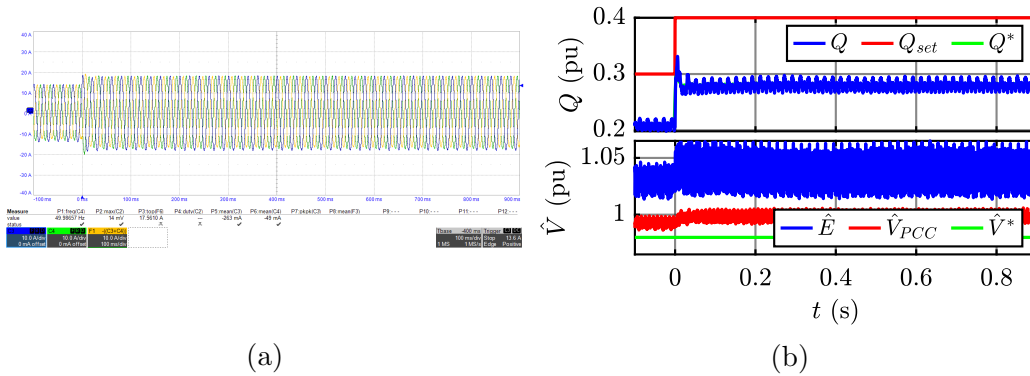


Figure 12.8.3: VSYNC’s response to reactive power reference step from 0.3 to 0.4 pu with reactive droop control enabled, from left to right:
 (a) Grid-side currents;
 (b) Reactive power (top) and voltage reference amplitude (bottom).

12.8.2 Inertial Response

When the frequency variation occurs, VSYNC injects active power and shows evident oscillations, as illustrated in Fig. 12.8.4b. After this transient, active power goes to zero because this model does not embed any active droop controller.

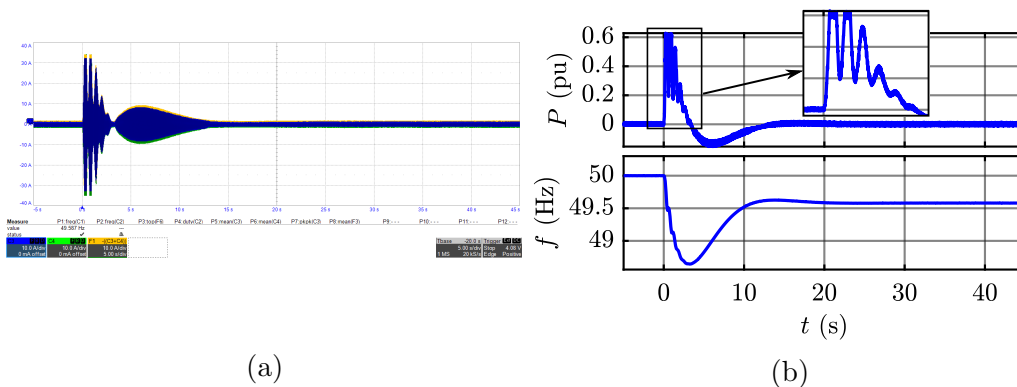


Figure 12.8.4: VSYNC’s response to grid frequency variation of -0.42 Hz, from left to right:
 (a) Grid-side currents;
 (b) Active power (top) and frequency (bottom).

12.8.3 Harmonic Distortion

In this test, 5% of fifth harmonic is added to the three phase grid voltage provided by the grid emulator. The FFT of Fig. 12.8.5a shows that, when the current references are disabled, the fifth harmonic contribution is equal to 8.5 V.

As soon as the current references are enabled, the grid-side currents become distorted, as shown in Fig. 12.8.6b. They introduce a voltage drop on the grid impedance which leads to an amplification of voltage distortion, as illustrated in Fig. 12.8.6a. In fact, the fifth harmonic term increases from 8.5 V to circa 14 V. Moreover, a seven harmonic contribution of about 7 V appears. In conclusion, VSYNC cannot improve the power quality in case of voltage grid distortion.

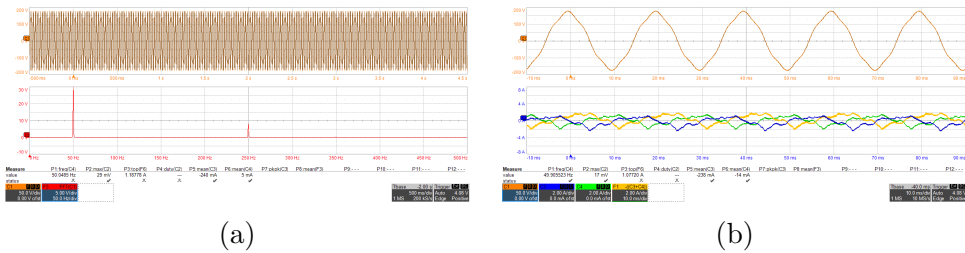


Figure 12.8.5: From left to right:

- (a) PCC Phase Voltage with 5% of fifth harmonic (top) and its FFT (bottom) with VSYNC's current references disabled;
- (b) PCC Phase Voltage with 5% of fifth harmonic (top) and grid-side currents (bottom) with VSYNC's current references disabled.

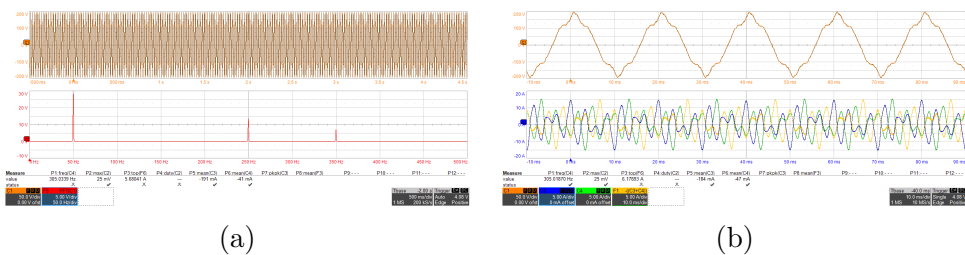


Figure 12.8.6: From left to right:

- (a) PCC Phase Voltage with 5% of fifth harmonic (top) and its FFT (bottom) with VSYNC's current references enabled;
- (b) PCC Phase Voltage with 5% of fifth harmonic (top) and grid-side currents (bottom) with VSYNC's current references enabled.

12.8.4 Voltage Dips

In the following charts, \hat{U} is the amplitude of the voltage provided by the grid emulator. It is not a physical measured quantity, but it is inserted to show the shape of the generated voltage dip.

In these tests the external reference Q_{set} is set to 0. The absence of an excitation part leads to a consistent difference between the employment or not of the reactive droop control.

In fact, when it is disabled, the total reference Q^* is zero and the real reactive power remains zero. It is only characterised by transient oscillations at the start and the end of the voltage dip, as shown in Fig. 12.8.7, Fig. 12.8.9 and Fig. 12.8.11.

If the reactive droop control is enabled, the reduction of the PCC voltage respect to the voltage reference leads to a request of positive reactive power. Therefore, in this case, VSYNC injects reactive power into the grid and it can support the grid during faults, as can be seen from all three type of dips, respectively in Fig. 12.8.8b, Fig. 12.8.10b and Fig. 12.8.12b.

Dip Type 1

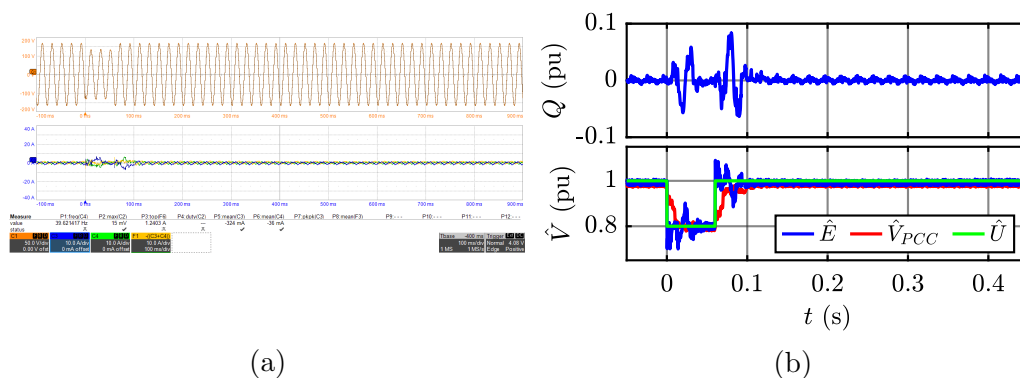


Figure 12.8.7: VSYNC’s response to voltage dip type 1, with reactive droop control disabled, from left to right:

- (a) PCC line voltages (top) and grid-side currents (bottom);
- (b) Reactive power (top) and voltage reference amplitude (bottom).

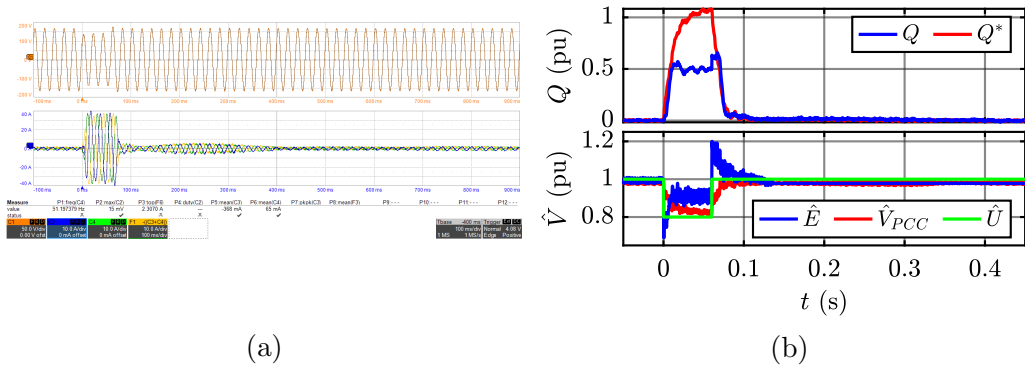


Figure 12.8.8: VSYNC’s response to voltage dip type 1, with reactive droop control enabled, from left to right:
 (a) PCC line voltages (top) and grid-side currents (bottom);
 (b) Reactive power (top) and voltage reference amplitude (bottom).

Dip Type 2

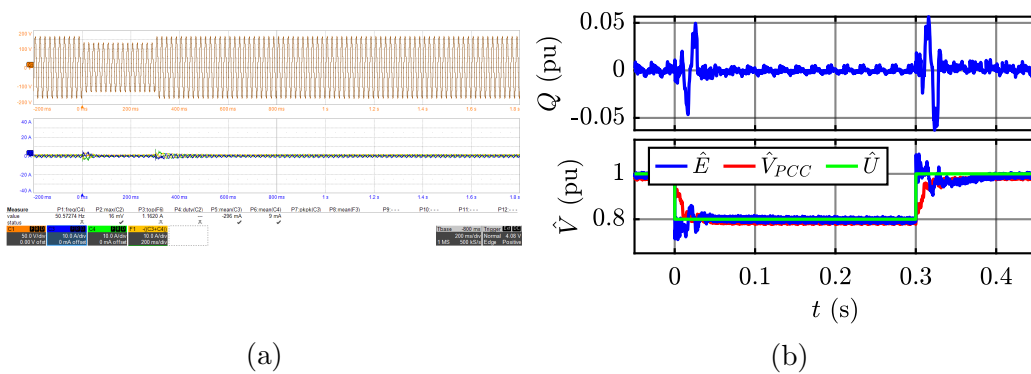


Figure 12.8.9: VSYNC’s response to voltage dip type 2, with reactive droop control disabled, from left to right:
 (a) PCC line voltages (top) and grid-side currents (bottom);
 (b) Reactive power (top) and voltage reference amplitude (bottom).

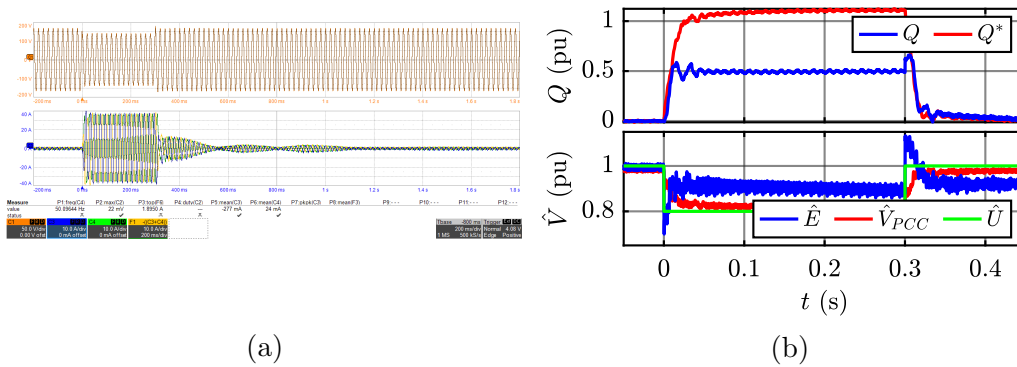


Figure 12.8.10: VSYNC's response to voltage dip type 2, with reactive droop control enabled, from left to right:
 (a) PCC line voltages (top) and grid-side currents (bottom);
 (b) Reactive power (top) and voltage reference amplitude (bottom).

Dip Type 3

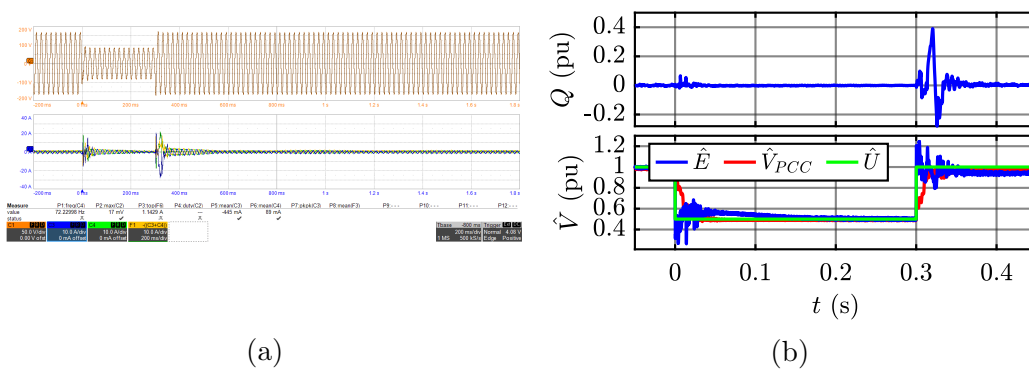


Figure 12.8.11: VSYNC's response to voltage dip type 3, with reactive droop control disabled, from left to right:
 (a) PCC line voltages (top) and grid-side currents (bottom);
 (b) Reactive power (top) and voltage reference amplitude (bottom).

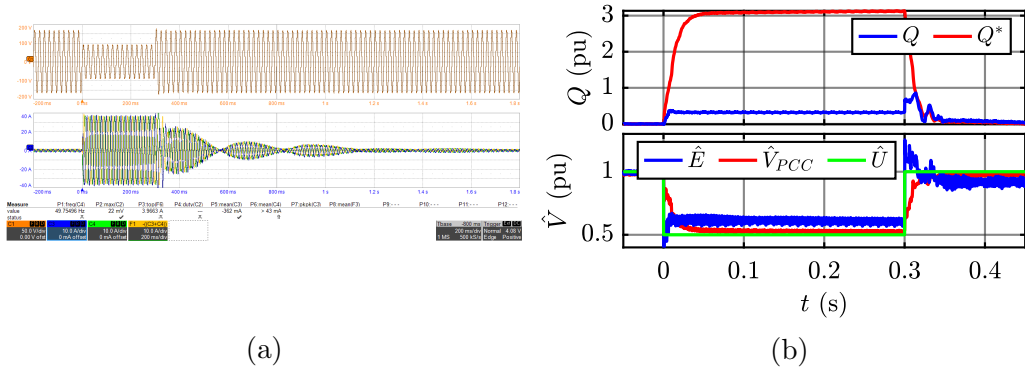


Figure 12.8.12: VSYNC's response to voltage dip type 3, with reactive droop control enabled, from left to right:
 (a) PCC line voltages (top) and grid-side currents (bottom);
 (b) Reactive power (top) and voltage reference amplitude (bottom).

12.9 Kawasaki

Kawasaki is a voltage-input current-output model. It provides as output the current references which feed a PI regulator. It allows to perform a reliable current limitation, without the employment of additional blocks.

12.9.1 Stability Analysis

For each voltage-input current-output VSG solution, the same parameters for the virtual impedance have been chosen:

$$\begin{cases} r_v = 0.02 \text{ pu} \\ x_v = 0.1 \text{ pu} \end{cases}$$

With these values, Kawasaki shows instability, as demonstrated by the result of Fig. 12.9.1. When a reactive power reference of 0.2 pu is asked, Kawasaki injects the current shown in Fig. 12.9.1a. Applying a step variation from 0.2 pu to 0.3 pu, the system diverges and the protections intervene, as can be seen from Fig. 12.9.1b. This instability is due to the too low inductance value. For this reason, it has been decided to increase it, up to 0.4 pu. All following tests will be performed with these parameters:

$$\begin{cases} r_v = 0.02 \text{ pu} \\ x_v = 0.4 \text{ pu} \end{cases}$$

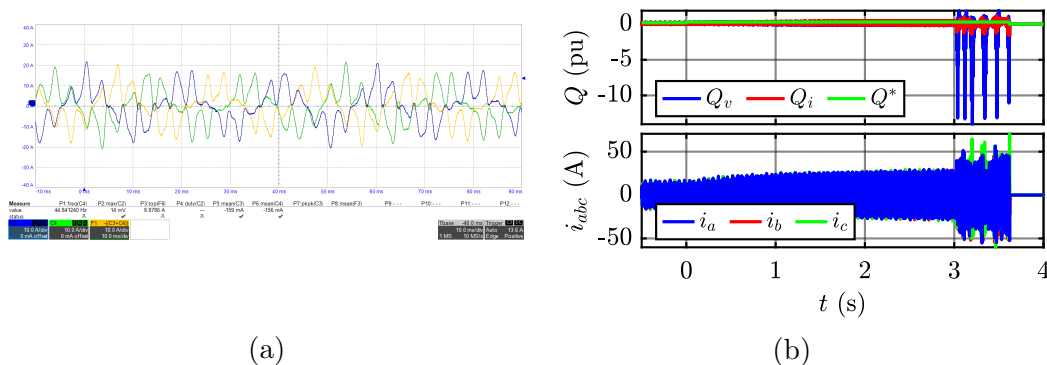


Figure 12.9.1: Kawasaki's response to reactive power reference step from 0.2 to 0.3 pu, with $x = 0.1$ from left to right:
 (a) Grid-side currents before the step;
 (b) Reactive power (top) and currents (bottom).

12.9.2 Active and Reactive Power References

Active Power Reference Step

When the active power reference step from 0.3 pu to 0.4 pu occurs, the active power tracks the reference with an underdamped response, as shown in Fig. 12.9.2b. The difference between the real and the virtual active power is negligible. The steady state condition is reached after circa 1.5 s.

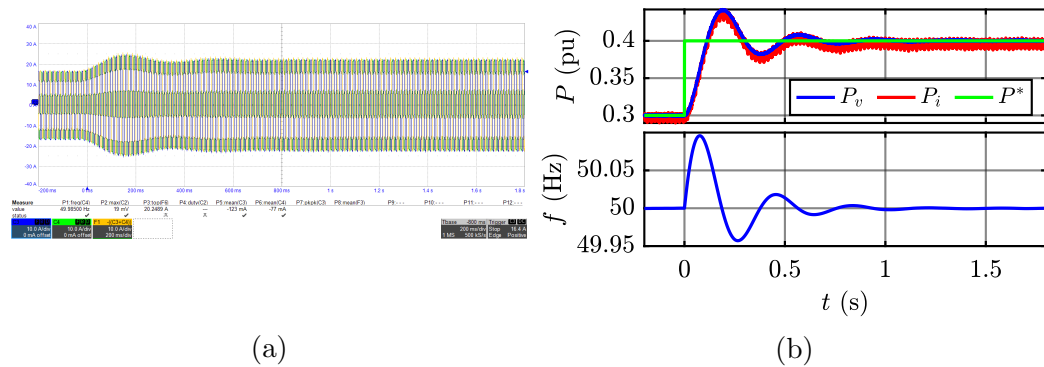


Figure 12.9.2: Kawasaki's response to active power reference step from 0.3 to 0.4 pu:

- (a) Grid-side currents;
- (b) Active power (top) and Kawasaki's frequency (bottom).

Reactive Power Reference Step

For this model, the response to the reactive power reference step variation can be evaluated only if the reactive droop control is enabled.

The voltage reference \hat{V}^* is set to 0.98 pu, the value of \hat{V}_{PCC} when $Q^* = 0$. With this choice, the inverter injects zero current when $Q^* = 0$.

Imposing a step variation from 0.3 pu to 0.4 pu, the virtual and the real reactive power do not reach the reference $Q^* = 0.4$ pu, because of the difference between the voltage reference \hat{V}^* and the PCC voltage \hat{V}_{PCC} , as can be observed from Fig. 12.9.3b.

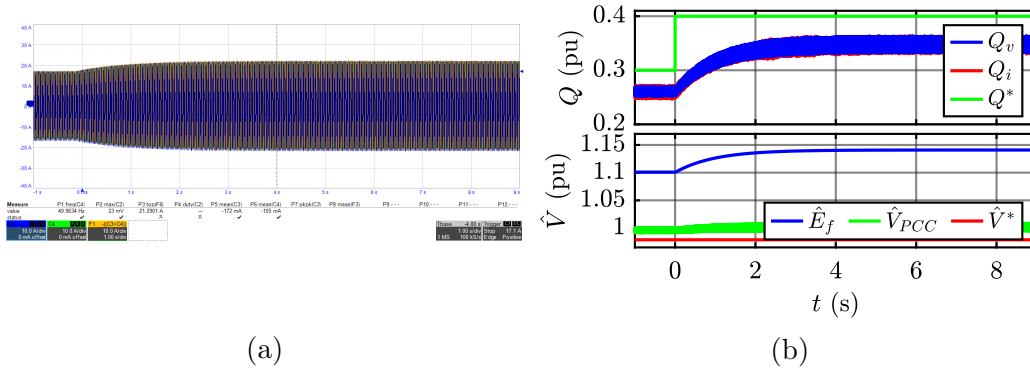


Figure 12.9.3: Kawasaki’s response to reactive power reference step from 0.3 to 0.4 pu with reactive droop control enabled, from left to right:
 (a) Grid-side currents;
 (b) Reactive power (top) and electromotive force (bottom).

12.9.3 Inertial Response

Applying a grid frequency variation, Kawasaki responds injecting active power into the grid. After a transient, when an active power peak of 0.54 pu is reached, the steady state value depends on the frequency variation and on the droop coefficient chosen for the governor:

$$P_v = \frac{\Delta\omega}{K_{gd}} = \frac{0.42}{50 \cdot 0.05} = 0.168 \text{ pu}$$

The result is shown in Fig. 12.9.4.

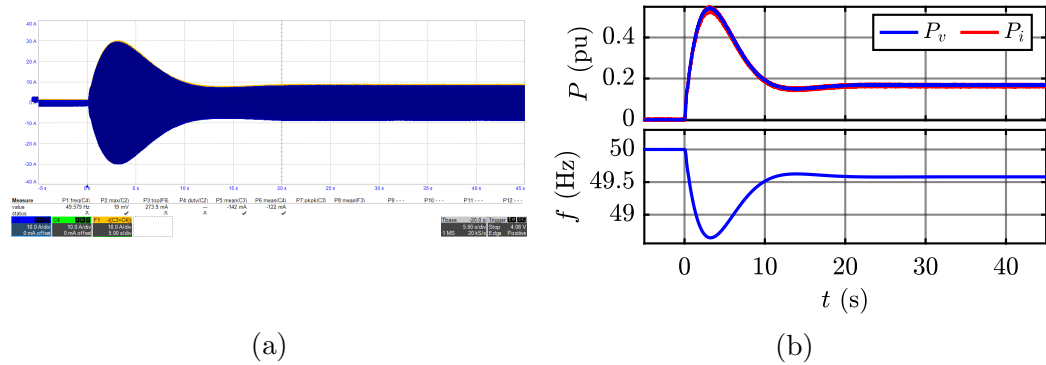


Figure 12.9.4: Kawasaki’s response to grid frequency variation of -0.42 Hz, from left to right:
 (a) Grid-side currents;
 (b) Active power (top) and frequency (bottom).

12.9.4 Harmonic Distortion

In this test, 5% of fifth harmonic is added to the three phase grid voltage provided by the grid emulator. The contribution of distortion, when the current references are disabled, is equal to 8.5 V, as can be observed from Fig. 12.9.5a.

This model is built using an algebraic impedance, which is equal for each frequency. Therefore it is expected to observe an amplification of the distortion when the current references are enabled. In fact, as can be seen from Fig. 12.9.6a, the fifth harmonic term increases from 8.5 V to circa 10 V and, moreover, a seventh harmonic contribution of about 4 V appears. In conclusion, Kawasaki cannot provide harmonic compensation in case of distortions.

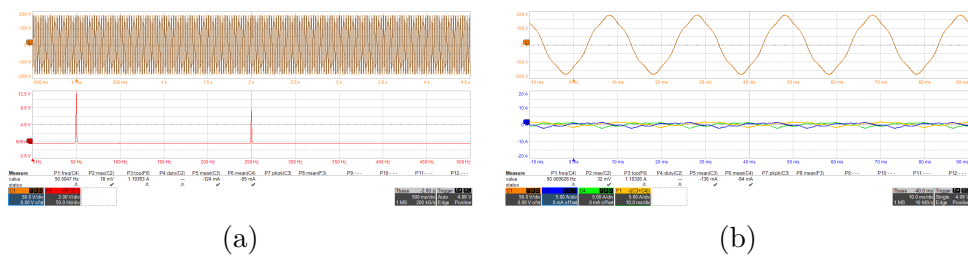


Figure 12.9.5: From left to right:
 (a) PCC Phase Voltage with 5% of fifth harmonic (top) and its FFT (bottom) with Kawasaki’s current references disabled;
 (b) PCC Phase Voltage with 5% of fifth harmonic (top) and grid-side currents (bottom) with Kawasaki’s current references disabled.

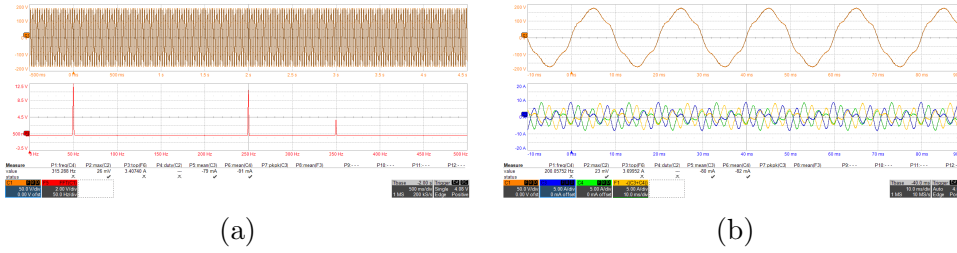


Figure 12.9.6: From left to right:
 (a) PCC Phase Voltage with 5% of fifth harmonic (top) and its FFT (bottom) with Kawasaki's current references enabled;
 (b) PCC Phase Voltage with 5% of fifth harmonic (top) and grid-side currents (bottom) with Kawasaki's current references enabled.

12.9.5 Voltage Dips

In the following charts, \hat{U} is the amplitude of the voltage provided by the grid emulator. It is not a physical measured quantity, but it is inserted to show the shape of the generated voltage dip.

The electromotive force \hat{E}_f is obtained by the employment of a PI regulator, which receives as input the error ϵ_V .

When the reactive droop control is disabled, ϵ_V is equal to the difference between the voltage reference \hat{V}^* and the PCC voltage amplitude. At the start of the voltage dip, the reactive power grows with high dynamic in all cases, as can be observed in Fig. 12.9.7b, Fig. 12.9.9b and Fig. 12.9.11b.

The electromotive force increases during the dip permanence because the error is constant and positive. At the end of the dip, \hat{E}_f comes back to the previous value and the reactive power goes to zero with slow dynamic.

If the reactive droop control is enabled, the error becomes:

$$\epsilon_v = \hat{V}^* - \hat{V}_{PCC} - K_{ad}Q_v$$

Therefore, the error decreases and consequently the electromotive force grows with a slower dynamic, as demonstrated by the results in Fig. 12.9.8b, Fig. 12.9.10b and Fig. 12.9.12b.

The different choice of parameters leads to obtain lower values of reactive power, compared to the other solutions. In fact, the saturation limit is reached only with the voltage dip type 3, as can be observed in Fig. 12.9.11b

and Fig. 12.9.12b.

Dip Type 1

In this case the voltage dip is too short to see differences between one case and the other, as demonstrated by the results of Fig. 12.9.7b and Fig. 12.9.8b. At the end of the voltage dip in both cases the steady state condition is quickly reached.

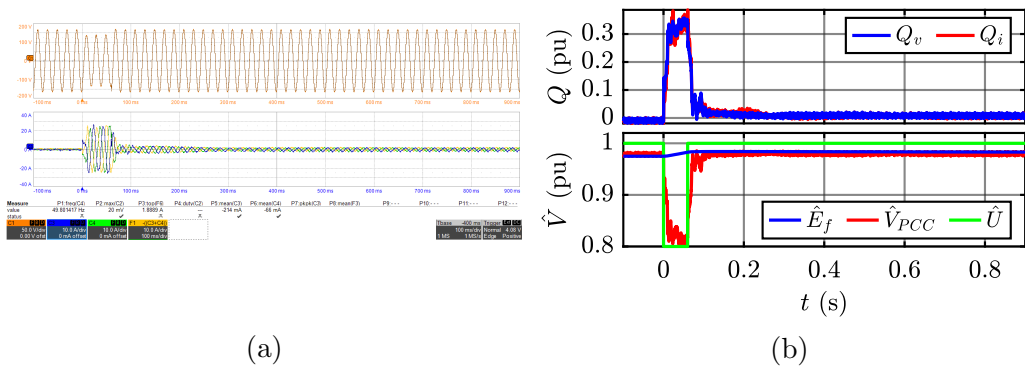


Figure 12.9.7: Kawasaki's response to voltage dip type 1, with reactive droop control disabled, from left to right:

- (a) PCC line voltages (top) and grid-side currents (bottom);
- (b) Reactive power (top) and electromotive force (bottom).

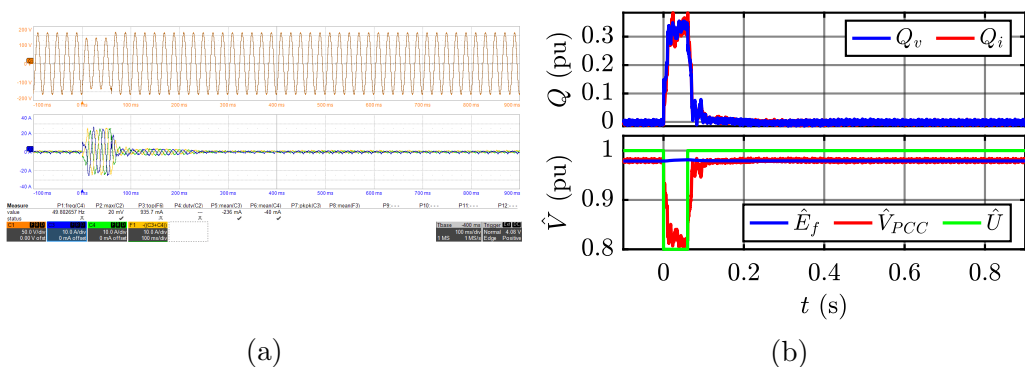


Figure 12.9.8: Kawasaki's response to voltage dip type 1, with reactive droop control enabled, from left to right:

- (a) PCC line voltages (top) and grid-side currents (bottom);
- (b) Reactive power (top) and electromotive force (bottom).

Dip Type 2

Here the effect of the reactive droop control is evident. During the voltage dip, the electromotive force shows a consistent increase when the reactive droop control is disabled, as can be noticed from the Fig. 12.9.9b. Then it takes several seconds to come back to previous value. On the opposite, when the reactive droop control is enabled, Fig. 12.9.10b shows the very fast dynamic of the reactive power and the electromotive force. They immediately reach the steady state condition.

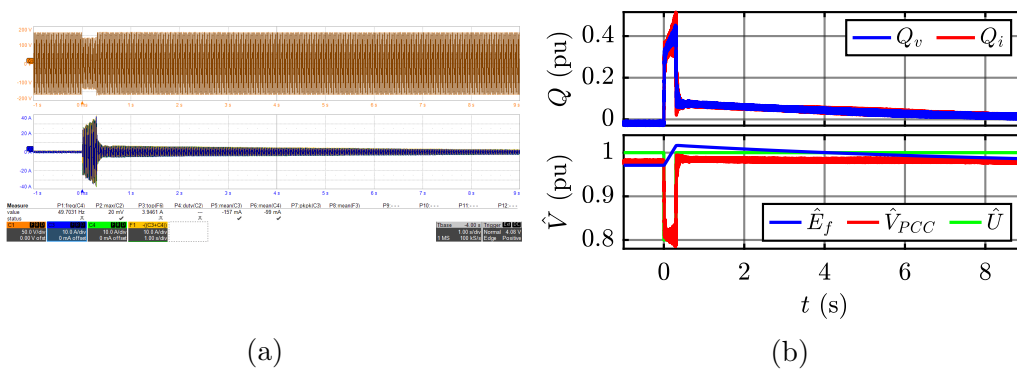


Figure 12.9.9: Kawasaki's response to voltage dip type 2, with reactive droop control disabled, from left to right:
 (a) PCC line voltages (top) and grid-side currents (bottom);
 (b) Reactive power (top) and electromotive force (bottom).

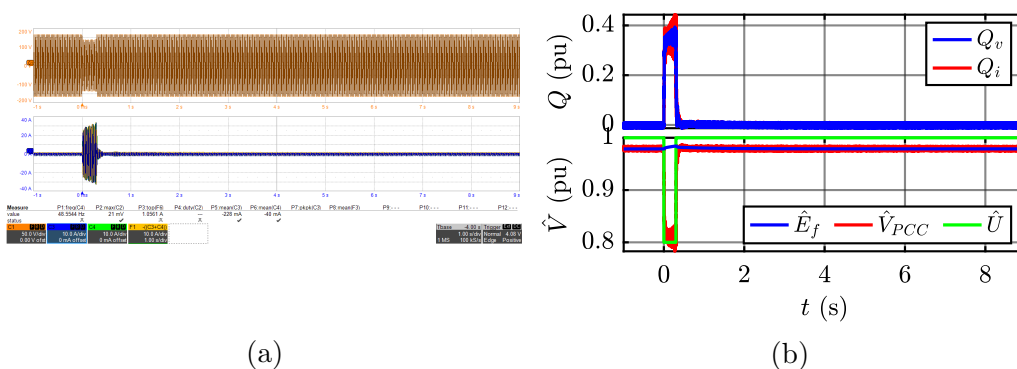


Figure 12.9.10: Kawasaki's response to voltage dip type 2, with reactive droop control enabled, from left to right:
 (a) PCC line voltages (top) and grid-side currents (bottom);
 (b) Reactive power (top) and electromotive force (bottom).

Dip Type 3

In this last case the transient at the end of the voltage dip takes more than 10 seconds to finish, as demonstrated by the result in Fig. 12.9.11b. The reactive droop control forces the transient to end in circa 2 s.

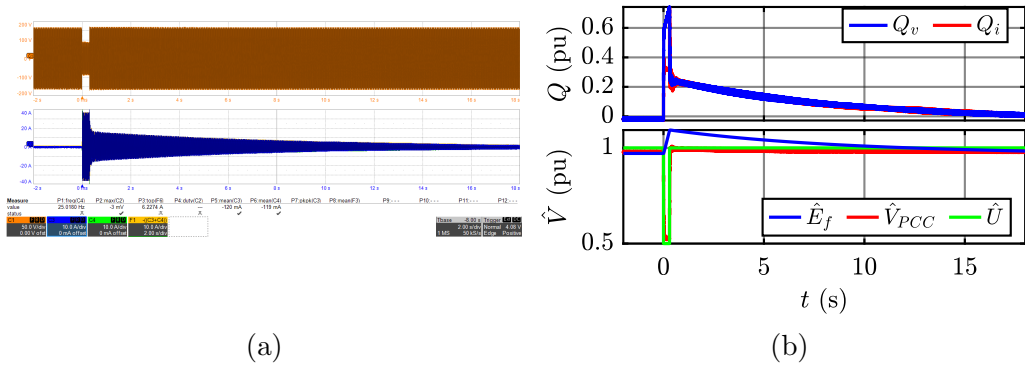


Figure 12.9.11: Kawasaki’s response to voltage dip type 3, with reactive droop control disabled, from left to right:

- (a) PCC line voltages (top) and grid-side currents (bottom);
- (b) Reactive power (top) and electromotive force (bottom).

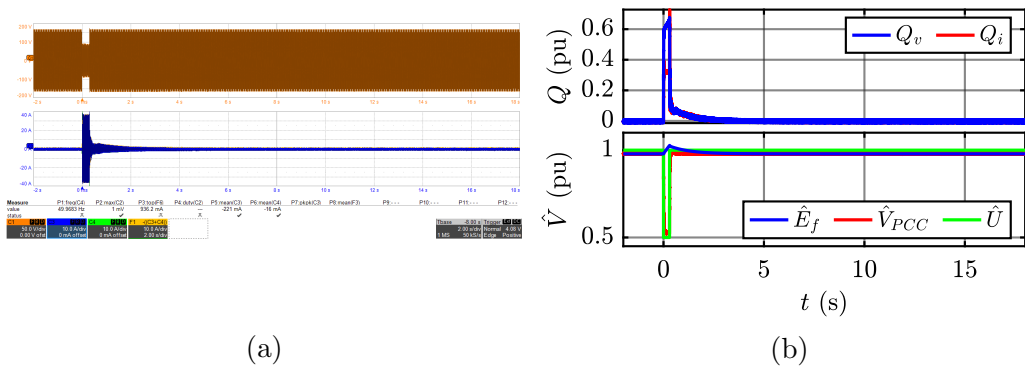


Figure 12.9.12: Kawasaki’s response to voltage dip type 3, with reactive droop control enabled, from left to right:

- (a) PCC line voltages (top) and grid-side currents (bottom);
- (b) Reactive power (top) and electromotive force (bottom).

12.10 CVSM

CVSM is a model characterised by the cascaded voltage and current controllers. It provides the current references to a PI regulator, which compares them with the feedback currents, obtaining the voltage references for the PWM modulator. The current limitation is inherently embedded in the working principle of the PI regulator.

12.10.1 Active and Reactive Power References

CVSM always uses real active and reactive power as feedback for power control loops. They are indicated with the symbol P and Q_m .

Active Power Reference Step

Applying an active power reference step from 0.3 pu to 0.4 pu, the active power quickly reaches the new value with a slight overshoot, as can be observed from Fig. 12.10.1b.

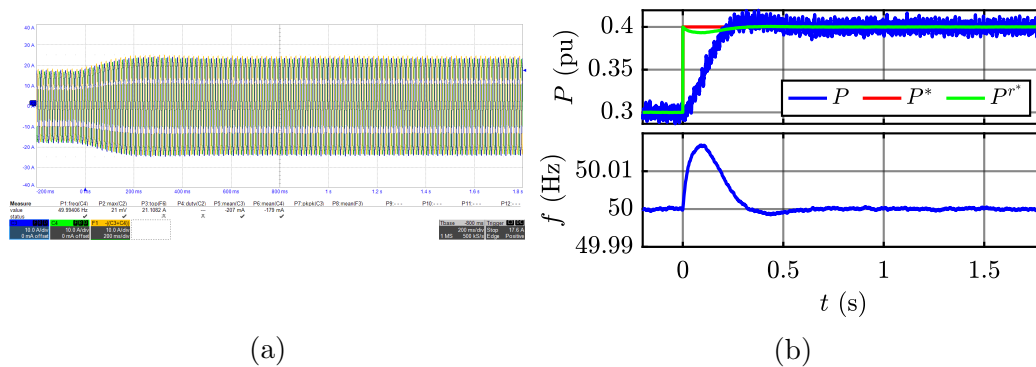


Figure 12.10.1: CVSM's response to active power reference step from 0.3 to 0.4 pu:

- (a) Grid-side currents;
- (b) Active power (top) and CVSM's frequency (bottom).

Reactive Power Reference Step

This test can be performed only if the reactive droop control is enabled. Voltage external reference \hat{v}^* is set equal to the value of the PCC voltage when Q^* is zero, in order to start the test with zero current.

Applying a step variation of Q^* from 0.3 pu to 0.4 pu, reactive power reaches a value of circa 0.18 pu, as shown in Fig. 12.10.2b. It cannot match the

reference because the reactive power droop controller does not embed an integrator able to zero the error between Q_m and Q^* .

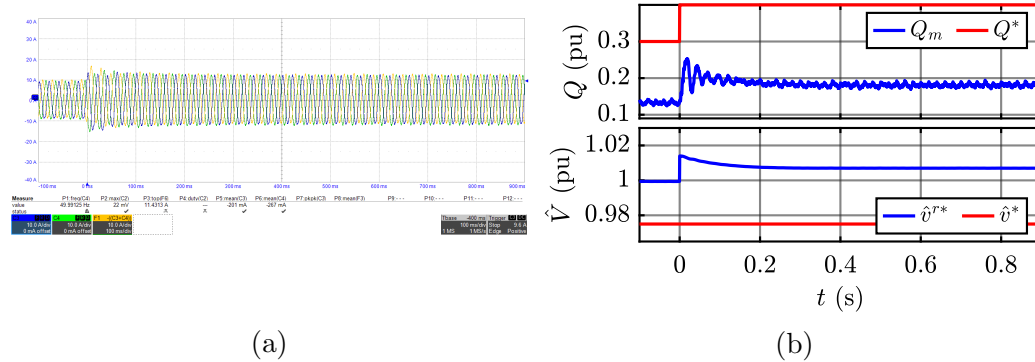


Figure 12.10.2: CVSM's response to reactive power reference step from 0.3 to 0.4 pu with reactive droop control enabled, from left to right:

- (a) Grid-side currents;
- (b) Reactive power (top) and electromotive force (bottom).

12.10.2 Inertial Response

When the frequency variation occurs, CVSM injects active power, as shown in Fig. 12.10.3. During the transient active power reaches a peak of almost 0.6 pu and currents remain under the limit of 36 A. In steady state, the injected active power depends on the frequency variation and the droop coefficient k_ω chosen for the frequency droop block:

$$P_\omega = k_\omega \cdot (\omega_{VSM}^* - \omega_{VSM}) = \frac{1}{0.05} \cdot \left(1 - \left(1 - \frac{0.42}{50} \right) \right) = 0.168 \text{ pu}$$

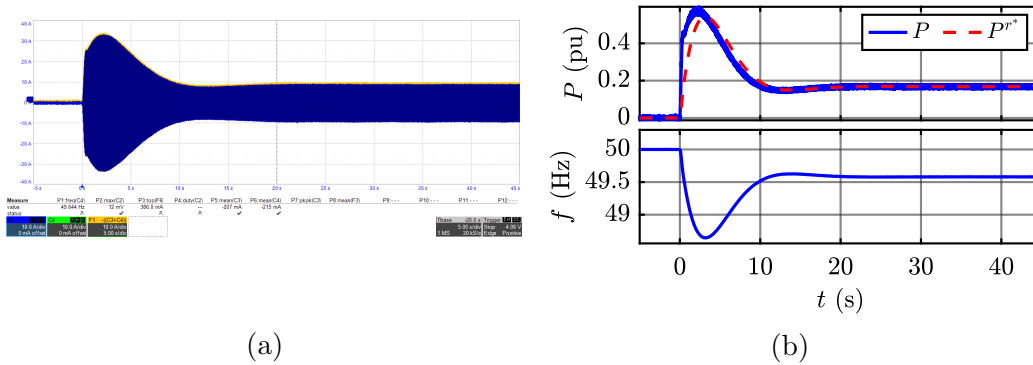


Figure 12.10.3: CVSM's response to grid frequency variation of -0.42 Hz, from left to right:

- (a) Grid-side currents;
 (b) Active power (top) and CVSM's frequency (bottom).

12.10.3 Harmonic Distortion

In this test, 5% of fifth harmonic is added to the three phase grid voltage provided by the grid emulator. The FFT of Fig. 12.10.4a shows that, when CVSM is disabled, the fifth harmonic contribution is equal to 8.5 V.

When CVSM is enabled, the fifth harmonic terms decreases from 8.5 V to circa 5.5 V, as can be observed from Fig. 12.10.5a. The distorted currents of Fig. 12.10.5b introduce a voltage drop on the grid impedance, which leads, in this case, to an improvement of the power quality. This is actually a fortuitous situation, because in this model the virtual reactance is calculated by means of the product between the virtual inductance and the speed. No integration is performed. Therefore, according to the nature of distortion, CVSM can actuate a positive or negative action.

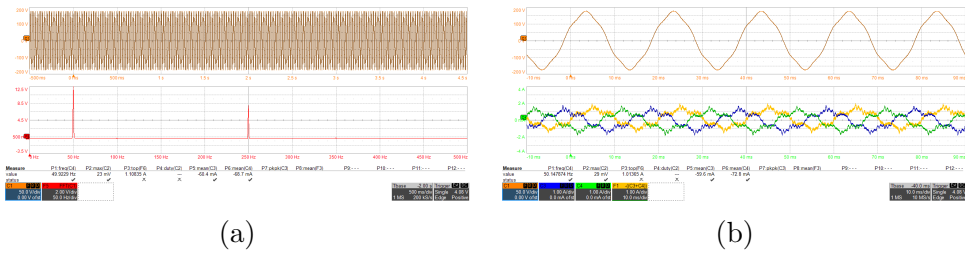


Figure 12.10.4: From left to right:
 (a) PCC Phase Voltage with 5% of fifth harmonic (top) and its FFT (bottom) with CVSM disabled;
 (b) PCC Phase Voltage with 5% of fifth harmonic (top) and grid-side currents (bottom) with CVSM disabled.

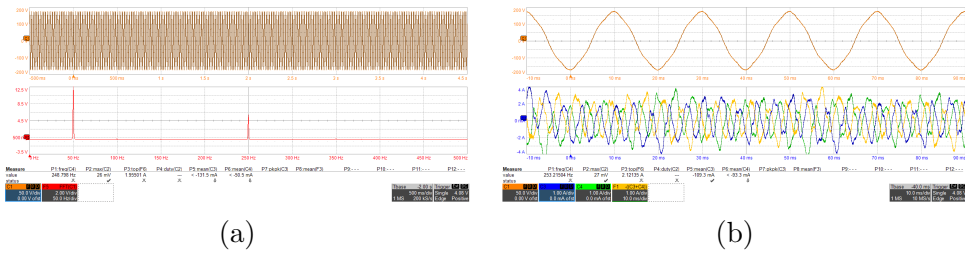


Figure 12.10.5: From left to right:
 (a) PCC Phase Voltage with 5% of fifth harmonic (top) and its FFT (bottom) with CVSM enabled;
 (b) PCC Phase Voltage with 5% of fifth harmonic (top) and grid-side currents (bottom) with CVSM enabled.

12.10.4 Voltage Dips

In the following charts, \hat{U} is the amplitude of the voltage provided by the grid emulator. It is not a physical measured quantity, but it is inserted to show the shape of the generated voltage dip.

When the voltage dip starts, independently on the case, current saturates to the limit of 36 A. This saturation leads to a peculiar characteristic of this model: when the current is limited, the total apparent power is equally divided in reactive and active power, independently on the case. Therefore, when the voltage dip starts, CVSM will inject both reactive and active power. It has been decided to test the CVSM’s response in a fourth case: voltage depth of 0.95 pu for 300 ms, in order to observe CVSM’s behaviour when currents do not saturate.

Finally, when the reactive droop control is disabled, it is expected to observe a constant electromotive force \hat{v}^{r*} because it is equal to \hat{v}^* . In turn, \hat{v}^* is set to the PCC voltage value before the dip.

If the reactive droop control is enabled, \hat{v}^{r*} will be:

$$\hat{v}^{r*} = \hat{v}^* + k_q(Q^* - Q_m)$$

Q^* will be always zero. Therefore the reactive power will influence the electromotive force during the dip.

Dip Type 1

Considering the case without reactive droop control, from Fig. 12.10.6b and Fig. 12.10.8a it can be observed the equal division of apparent power in reactive and active power during the voltage dip permanence. When it ends, CVSM shows high oscillations and then all powers go to zero. Electromotive force remains constant. This is no true when the reactive droop control is enabled. In fact, as can be observed from Fig. 12.10.7b, it decreases because of the presence of the term $k_q Q_m$. In terms of coupling with the active power there are no evident differences respect to the previous case, as can be observed comparing Fig. 12.10.7b with Fig. 12.10.8b.

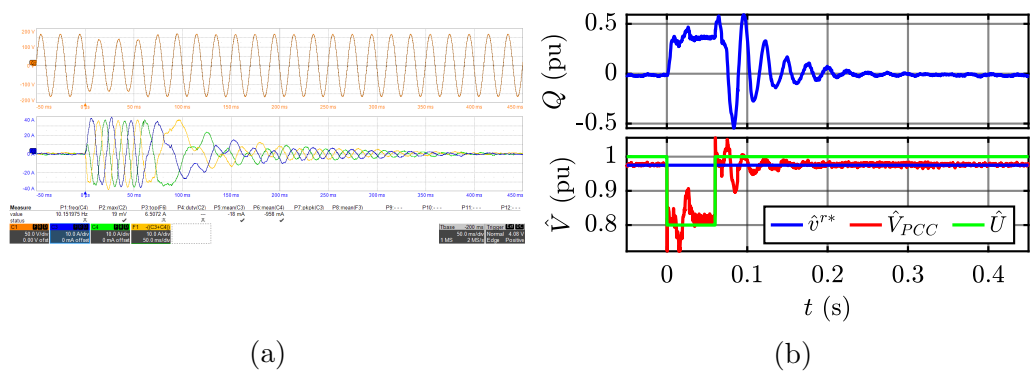


Figure 12.10.6: CVSM's response to voltage dip type 1, with reactive droop control disabled, from left to right:

- (a) PCC line voltages (top) and grid-side currents (bottom);
- (b) Reactive power (top) and electromotive force (bottom).

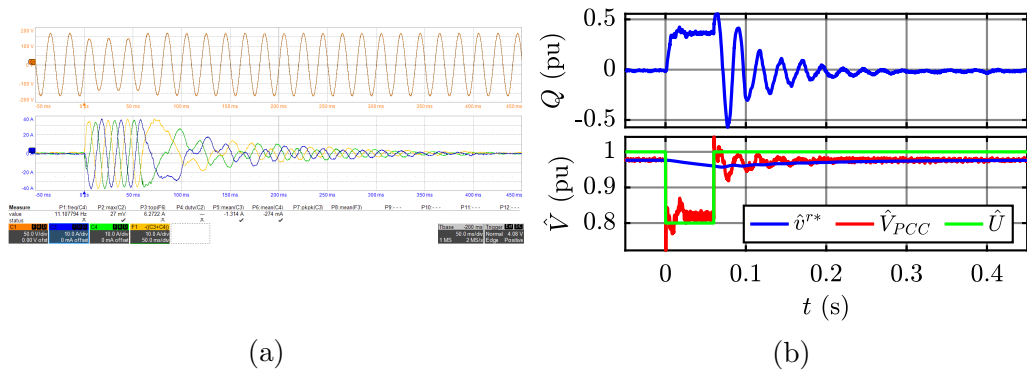


Figure 12.10.7: CVSM's response to voltage dip type 1, with reactive droop control enabled, from left to right:

- (a) PCC line voltages (top) and grid-side currents (bottom);
- (b) Reactive power (top) and voltage amplitude (bottom).

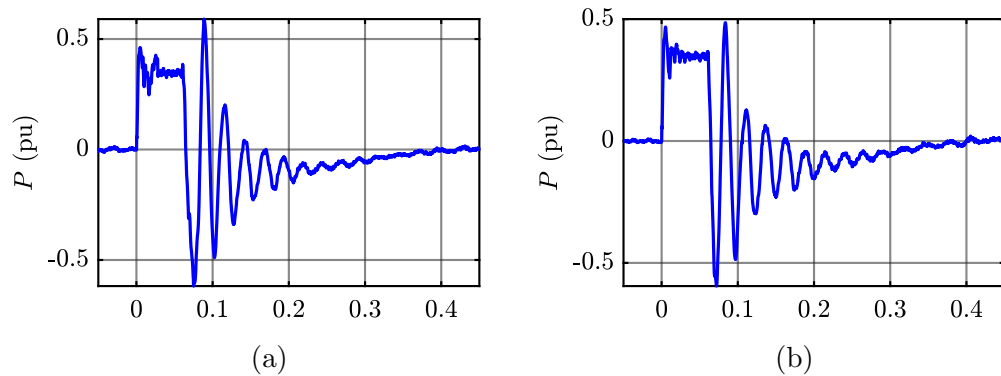


Figure 12.10.8: CVSM's response to voltage dip type 1, from left to right:

- (a) Active power with reactive droop control disabled;
- (b) Active power with reactive droop control enabled.

Dip Type 2

Considering the case without reactive droop control, from the comparison between Fig. 12.10.9b and Fig. 12.10.11a it can be observed the same coupling of dip type 1. Now, the oscillations have sufficient time to complete. At the end of the dip, active power jumps from one limit to the opposite and then it remains constant for circa 200 ms like reactive power. Then they return to zero.

The case of reactive droop control enabled is different, as can be seen from Fig. 12.10.10b and Fig. 12.10.11b. In fact, at the end of the dip, reactive

power quickly goes to zero, whereas active power, after the jumps, returns to zero. The other difference lies in the profile of the electromotive force, which decreases because of the presence of the term $k_q Q_m$.

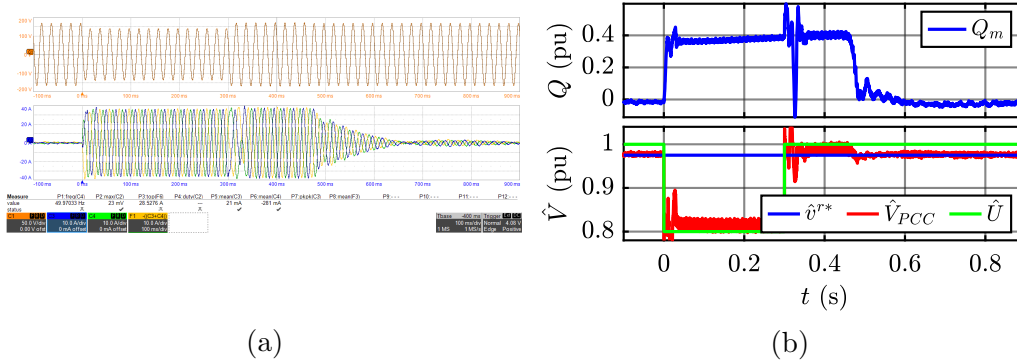


Figure 12.10.9: CVSM’s response to voltage dip type 2, with reactive droop control disabled, from left to right:
 (a) PCC line voltages (top) and grid-side currents (bottom);
 (b) Reactive power (top) and voltage amplitude (bottom).

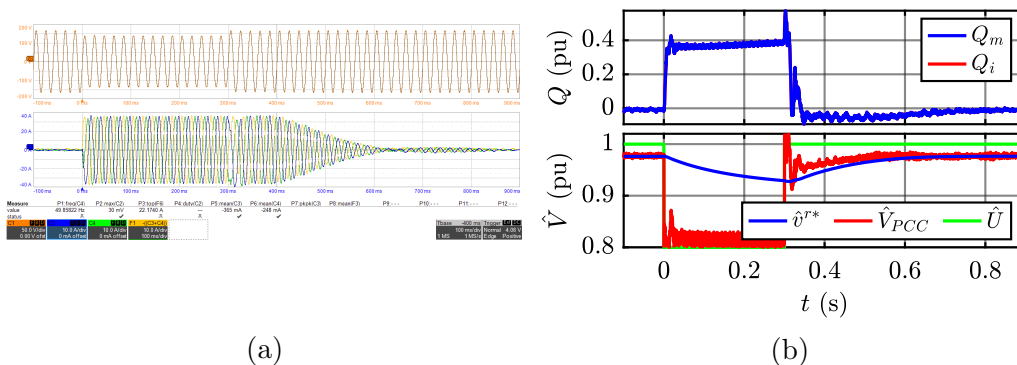


Figure 12.10.10: CVSM’s response to voltage dip type 2, with reactive droop control enabled, from left to right:
 (a) PCC line voltages (top) and grid-side currents (bottom);
 (b) Reactive power (top) and electromotive force (bottom).

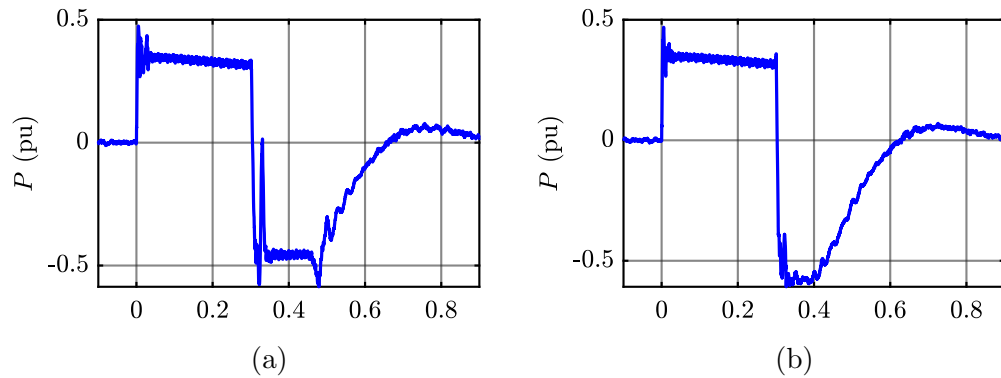


Figure 12.10.11: CVSM’s response to voltage dip type 2, from left to right:
 (a) Active power with reactive droop control disabled;
 (b) Active power with reactive droop control enabled.

Dip Type 3

Voltage dip 3 is characterised by lower values of active and reactive powers, because the current is limited at the same value, but this time the dip is deeper and so the PCC voltage is lower. Fig. 12.10.12b and Fig. 12.10.14a show the response of CVSM when the reactive droop control is disabled, whereas in Fig. 12.10.13b and Fig. 12.10.14b it can be observed the influence of the reactive droop control. The behaviour is very similar to voltage dip type 2, expect for what happens at the end of the dip. Here, with and without the reactive droop control, powers immediately start to decrease with evident oscillations.

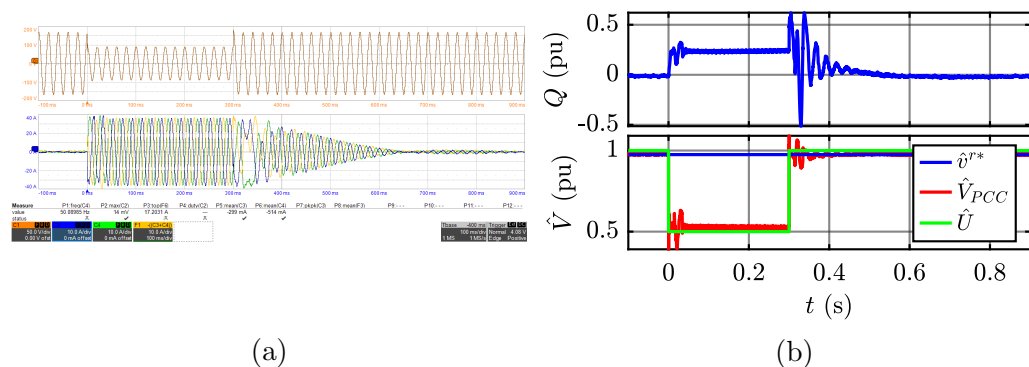


Figure 12.10.12: CVSM’s response to voltage dip type 3, with reactive droop control disabled, from left to right:
 (a) PCC line voltages (top) and grid-side currents (bottom);
 (b) Reactive power (top) and electromotive force (bottom).

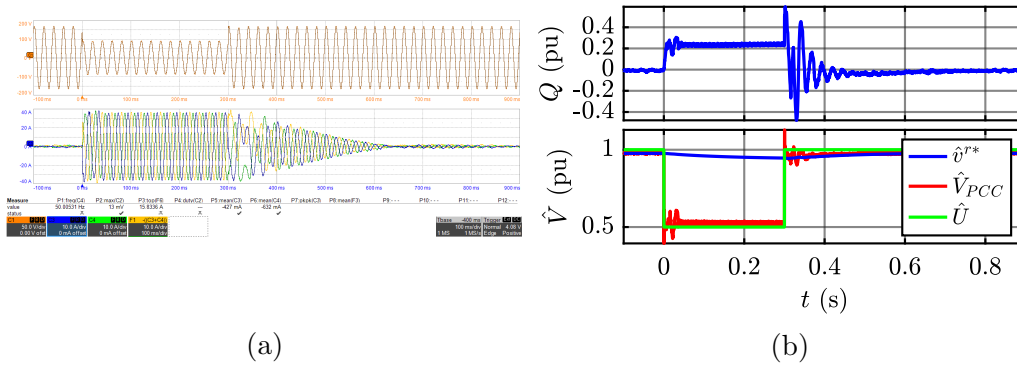


Figure 12.10.13: CVSM's response to voltage dip type 3, with reactive droop control enabled, from left to right:
 (a) PCC line voltages (top) and grid-side currents (bottom);
 (b) Reactive power (top) and electromotive force (bottom).

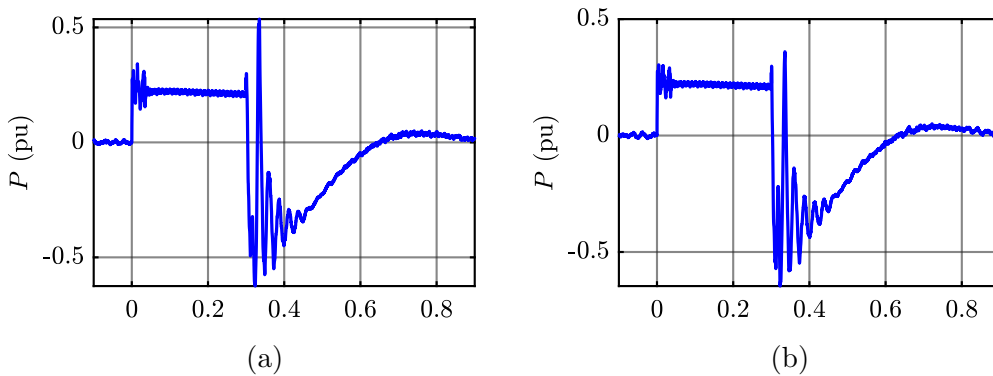


Figure 12.10.14: CVSM's response to voltage dip type 3, from left to right:
 (a) Active power with reactive droop control disabled;
 (b) Active power with reactive droop control enabled.

Fourth Case

Finally, this fourth case is useful to observe the behaviour of CVSM when current does not saturate. Considering the case without reactive droop control, Fig. 12.10.15b shows a constant profile of reactive power around 0.3 pu, whereas it can be seen from Fig. 12.10.17a that active power, after a transient, comes back to zero. Reactive power remains constant because the electromotive force is constant. At the end of the voltage reduction, reactive power goes to zero and active power shows a transient with oscillation. As regards the case of reactive droop control enabled, as can be observed

from Fig. 12.10.16b and Fig. 12.10.17b, the two transients are characterised by more evident oscillation. Moreover, when the voltage is 0.95 pu, the reactive power decreases with slow dynamic, because this time the electromotive force decreases.

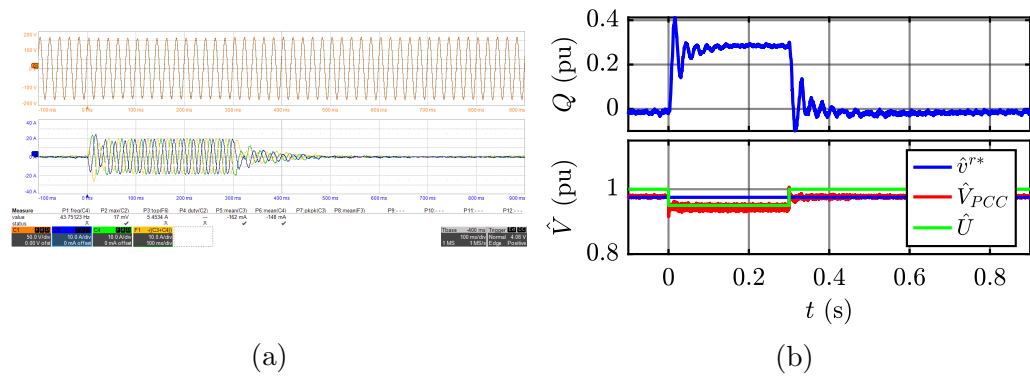


Figure 12.10.15: CVSM’s response to the fourth case, with reactive droop control disabled, from left to right:
 (a) PCC line voltages (top) and grid-side currents (bottom);
 (b) Reactive power (top) and electromotive force (bottom).

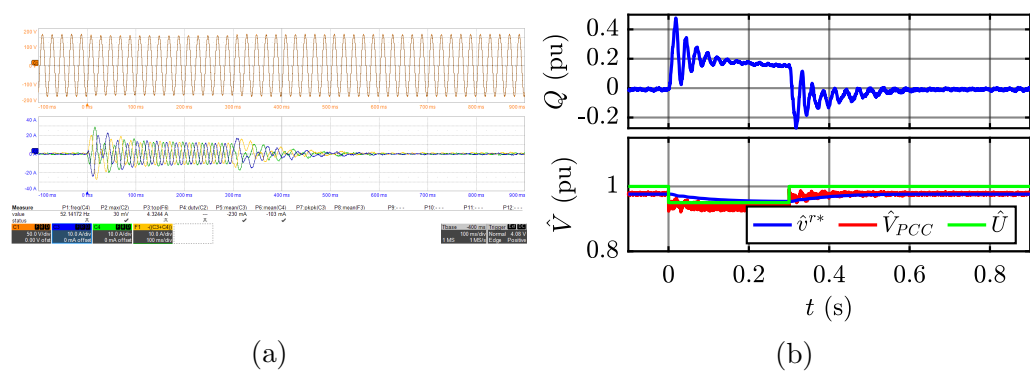


Figure 12.10.16: CVSM’s response to the fourth case, with reactive droop control enabled, from left to right:
 (a) PCC line voltages (top) and grid-side currents (bottom);
 (b) Reactive power (top) and electromotive force (bottom).

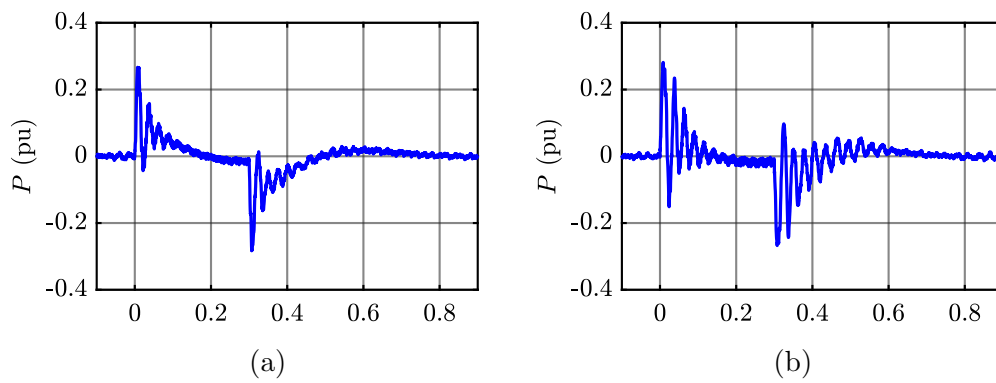


Figure 12.10.17: CVSM's response to the fourth case, from left to right:
(a) Active power with reactive droop control disabled;
(b) Active power with reactive droop control enabled.

Chapter 13

Comparison of VSG Solutions

After the theoretical description of each VSG solution and the analysis of their behaviour by means of experimental tests, the final comparison between all of them can be actuated.

For each kind of test, the main aspects of the solutions will be highlighted and summarised in tables.

In order to singularly evaluate each aspect of a test, the following notation is adopted:

- "+" stands for "positive";
- "-" stands for "negative";
- "0" stands for "neutral".

Moreover, a final vote will be given to each VSG solution, summing the results of the singular evaluations. This can be: 1 in case of "+", -1 in case of "-" and 0 in case of "0".

13.1 Active Power Reference

For each VSG solution the active power tracks the reference with no steady state error.

Most of them show a high quality response in terms of settling time and damping.

For Osaka and VISMA2 the profile is damped, whereas for Synchronverter, VISMA1, the three SPC versions and CVSM the response is underdamped with a slight overshoot. In all cases the set point is reached in at most 1 s. As regards the frequency variation, in almost all cases it does not overcome the value of 20 mHz. The exceptions are SPC PI and SPC LL, which show a maximum value of circa 60 mHz, due to the presence of a proportional gain.

Then, VISMA, VSYNC, Kawasaki show a consistent underdamped profile. Obviously VISMA is characterised by the most underdamped response, because it represents a complete model of a conventional synchronous generator. As regards VSYNC and Kawasaki, in both cases active power reaches a peak of about 0.5 pu and the transient ends after circa 1.5 s. A difference lies in the frequency variation: for VSYNC it is circa 10 mHz, much lower than the value of 100 mHz reached by Kawasaki. This is the highest value of frequency variation reached between all solutions.

Table 13.1.1 summarises the results for each solution.

Table 13.1.1: Active Power Reference: comparison.

Model	Damping	Steady State Error	Frequency Peak
Synchronverter	+	+	+
Osaka	+	+	+
VISMA	-	+	-
VISMA 1	+	+	+
VISMA 2	+	+	+
SPC SG	+	+	+
SPC PI	+	+	-
SPC LL	+	+	-
VSYNC	-	+	+
Kawasaki	-	+	-
CVSM	+	+	+

13.2 Reactive Power Reference

For this kind of test, the analysed VSG solutions show different responses according to the nature of their reactive part.

Synchronverter, Osaka, VISMA1, VISMA2 and SPC embed a reactive power controller in their excitation block. The reactive power reference is compared with the feedback of the reactive power (real reactive power for Osaka and SPC, virtual reactive power for the others). The error between them is provided to a PI regulator (Osaka) or a pure integrator (the other four VSGs). These structures guarantee zero error at steady state, as observed from the experimental results.

The excitation parts of Synchronverter, VISMA1, VISMA2 and SPC are based on a pure integrator, with a gain which depends on the category (volt-

age or current output) and a time constant τ_e set to 1 s for all of them. Therefore, it is expected to observe similar responses, where the reference is reached after $4\tau_e - 5\tau_e$. In fact, the experimental tests have been demonstrated the validity of this tuning procedure.

The same happens for Osaka. Nevertheless the excitation block is constituted by a PI regulator, the integral part is defined as the pure integrator of the previous described solutions and consequently, the Osaka's response is similar to the other models.

As VISMA completely emulates the behaviour of a synchronous generator, it has a specific part for the generation of the excitation flux linkage. The response to the reactive power reference step is faster than the other solutions. The effect of the reactive droop control is the reduction of the external reactive power reference.

For each case, with and without the reactive droop control, the reference is reached with a damped behaviour by both the virtual and the real reactive power, with the exception of VISMA1's real reactive power. In fact, the slight coupling with the active power leads to a steady state error.

The remaining solutions to compare are: VSYNC, Kawasaki and CVSM. They do not embed a reactive power controller. In the VSYNC there is no excitation part and the reactive power reference is directly used to compute the current references. Therefore, when a step variation occurs, the real reactive power immediately tracks the reference. When the reactive droop control is disabled, the reference is reached by the real reactive power. Enabling the reactive droop control, the real reactive power still tracks the reference reactive power, which is lower than the external reactive reference because of the droop control effect.

The Kawasaki model embeds an AVR model, which cannot guarantee zero error in steady state, as demonstrated by experimental tests. In this case the response to reactive power reference step can be evaluated only when reactive droop control is enabled, since when it is disabled the output of AVR is zero. Finally, CVSM is characterised by a reactive power droop controller which cannot zero the steady error between reactive power reference and the real reactive power because it is a simple reactive droop control, without any integrator.

Table 13.2.1 summarises the comparison between the VSG solution in terms of steady state error.

Table 13.2.1: Reactive Power Reference: comparison.

Model	Steady State Error
Synchronverter	+
Osaka	+
VISMA	+
VISMA1	+
VISMA2	+
SPC	+
VSYNC	+
Kawasaki	-
CVSM	-

13.3 Inertial Response

The inertial response strongly depends on how the active droop control is implemented.

Osaka, SPC PI, Kawasaki and CVSM use a governor model to regulate the frequency. In steady state, by setting the droop coefficient to the conventional value of 5%, these VSGs inject the same active power, equal to 0.168 pu. During the transient, the SPC PI and Kawasaki show practically the same behavior. The active power grows with the same dynamic, reaches a peak of almost 0.6 pu and then decreases.

As regards the Osaka's response, it is characterised by higher dynamic than SPC PI and Kawasaki. In fact, comparing the results, Osaka's active power trend shows a higher slope. Since it is a voltage-output model, its damping coefficient is higher than the damping coefficient of current-output models, as can be observed from Table 2.5.3. In the first instants, the damping coefficient amplifies the frequency difference and gives its contribution together with the governor. The higher is the damping coefficient, the higher is the active power peak. In fact, in this case the active power peak is about 0.7 pu.

Finally, even the CVSM shows a faster dynamic respect to SPC PI and Kawasaki. Here, the reasons is the lack of a low pass filter in the frequency controller. There is only a gain corresponding to the droop coefficient of 5%. The active power peak is around 0.6 pu.

Then, there are some models which do not embed a dedicated governor, but still can inject active power after grid frequency variations. They are the Synchronverter and the SPC LL. During the first instants, the former shows

a virtual active power peak of 3 pu, since high pass term P_{HF} is not saturated and in the first instants it is equal to:

$$P_{HF} = k_d(\omega - \omega_{PLL}) = 269 \frac{0.42}{50} = 2.26 \text{ pu}$$

In steady state this term is zero and the only contribution comes from P_{LF} . It is saturated to the maximum transferable active power with a droop coefficient of 5%:

$$P_{droop,max} = D_p \Delta\omega = \frac{1}{0.05} \frac{0.42}{50} = 20 \frac{0.42}{50} = 0.168 \text{ pu} \quad (13.3.1)$$

SPC LL shows a peculiar behavior: the active power trend is the same of SPC PI and Kawasaki, even if there is no dedicated governor model. The reason lies in the structure of lead lag. There is an additional freedom degree which can be used to decouple the damping effect and the droop control. The frequency control is an embedded feature of this solution.

The other models to study are: VISMA, VISMA1, VISMA2, SPC SG and VSYNC. They do not implement a governor.

VISMA completely emulates the behaviour of a synchronous generator. The active power trend in this case is much lower than the others. The peak is 0.227 pu. In steady state active power is zero because no governor is implemented.

For VISMA1, VISMA2 and SPC SG the active power grows surpassing the limit of 1 pu during the first part of the frequency variation. Then, in steady state, active power goes to zero.

VSYNC, instead, does not embed an active power loop. Active power is measured and observed. It is not used as feedback. When the frequency variation occurs, VSYNC active power grows and when the limit of current of 36 A is reached, VSYNC starts to oscillate. In steady state active power goes to zero because of the absence of a governor model.

Table 13.3.1 summarises the results to the inertial response for each VSG solution.

Table 13.3.1: Inertial Response: comparison.

Model	Damping-Droop Coupling	Frequency Regulation
Synchronverter	–	+
Osaka	+	+
VISMA	0	–
VISMA1	–	–
VISMA2	–	–
SPC SG	–	–
SPC PI	+	+
SPC LL	+	+
VSYNC	0	–
Kawasaki	+	+
CVSM	+	+

13.4 Harmonic Distortion

The response to the fifth harmonic distortion depends on the VSG category (voltage or current output) and how the virtual impedance is implemented. Many models can actuate a filtering action in case of distortion. In this case, the distorted grid current introduces a voltage drop across the grid impedance which reduces the distortion of the grid voltage.

These models are: Synchronverter, Osaka, VISMA1, VISMA2 and SPC. When the VSG is disabled, the distortion is quantified by a contribution of 8.5 V on the fifth harmonic. As soon as they are enabled, it decreases from 8.5 V to:

- 4.5 V for the Synchronverter;
- 6 V for the Osaka;
- 5.5 V for the VISMA1;
- 6 V for the VISMA2;
- 4.5 V for the SPC.

It can be noticed that for voltage-output models (Osaka and VISMA2) the voltage amplitude is higher respect to the other cases.

The difference between the Synchronverter and the VISMA1 lies in the increase of the virtual inductance for the VISMA1. The more is the value of the impedance, the lower is the current and the consequently filtering effect.

VISMA does not shows evident changes and the response can be assumed

neutral.

As regards the CVSM, the voltage amplitude decreases from 8.5 V to 5.5 V. This positive result is actually fortuitous. The virtual impedance is not completely emulated. In fact the value of reactance is equal for all frequencies. Therefore, even in this case the result is positive, CVSM cannot be considered a model able to actuate harmonic compensation.

The remaining models (VSYNC and Kawasaki) amplify the distortion. The VSYNC model does not embed a virtual impedance, therefore no filtering effect can be actuated.

Finally, the Kawasaki's response is due to the choice to use an algebraic virtual impedance. This does not change when the frequency changes, leading to the amplification of the distortion.

Finally, in Table 13.4.1 a summary of the comparison for this test is given.

Table 13.4.1: Harmonic Distortion: comparison.

Model	Filtering Capability
Synchronverter	+
Osaka	+
VISMA	0
VISMA1	+
VISMA2	+
SPC	+
VSYNC	-
Kawasaki	-
CVSM	-

13.5 Voltage Dips

This test has been chosen to evaluate the capability of VSGs to support the grid during faults. When a voltage dip occurs, the inverter can inject reactive power (and so current) to limit the decrease of voltage.

With some exceptions, each VSG solution shows the same trend: when the voltage dip occurs, the real reactive power injected by the inverter into the grid grows and saturates because the current limit of 36 A is reached. Therefore the grid supporting is feasible. This happens independently on the use

of reactive droop control.

The exceptions, or the models which deserve a more detailed description are: VISMA, VSYNC and CVSM.

Since the VISMA completely emulates the behaviour of a synchronous generator, its current shows evident unipolar component both at start and at end of the voltage dip. When the reactive droop control is disabled, the unipolar component is dominant. In this case, the VISMA can inject current only during the time needed to zero the unipolar component. Enabling the reactive droop control, the grid supporting can be actuated. In fact, after a transient, the currents remain constant at the limit value for all the dip duration.

When the reactive droop control is disabled, the VSYNC does not inject reactive power and so current. The reference voltage for the PWM modulator immediately tracks the new value of the grid voltage. No grid supporting is performed. On the opposite, when the reactive droop control is enabled, the VSYNC injects reactive power and the current saturates to the limit of 36 A.

Finally, the CVSM's response is peculiar because of the coupling between the active and reactive power. When the current is limited, active power and reactive power are equally divided. The grid supporting is performed, but a consistent active power contribution is also present.

All the other not mentioned VSG solutions guarantee grid support in both cases and show similar responses. Slight differences can be observed, in particular as regards the oscillations in the first instants at the start and the end of the voltage dip. The Osaka and the SPC show high oscillations, whereas the remaining (Synchronverter, VISMA1, VISMA2 and Kawasaki) have a more damped response.

In conclusion, in Table 13.5.1 the main aspects of the VSG solutions regarding the voltage dips are collected.

Table 13.5.1: Voltage Dips: comparison.

Model	Active - Reactive Coupling	Grid Supporting
Synchronverter	+	+
Osaka	+	+
VISMA	+	+
VISMA1	+	+
VISMA2	+	+
SPC	+	+
VSYNC	+	+
Kawasaki	+	+
CVSM	-	+

13.6 Final Result

Nine aspects have been considered and evaluated. The tenth is the current limitation system. In this case, only the Osaka and VISMA2 show a negative result, because of the higher complexity to actuate a reliable current saturation.

Finally, in Table 13.6.1 the final results for each VSG solution are listed.

Table 13.6.1: Final comparison.

Model	Final Result
Synchronverter	8/10
Osaka	8/10
VISMA	2/10
VISMA1	6/10
VISMA2	4/10
SPC SG	5/10
SPC PI	8/10
SPC LL	8/10
VSYNC	3/10
Kawasaki	2/10
CVSM	4/10

Chapter 14

Conclusions

Virtual Synchronous Generators represent a promising solution to facilitate the spread and the penetration of the renewable energy plants into the electric system. In fact, by means of this control approach, renewable power generators can provide ancillary services, guaranteeing the grid stability.

In this master thesis the analysis of the VSG solutions proposed in the literature has been conducted, both theoretically and practically. The main characteristics of each solution have been highlighted, by means of PLECS simulations and experimental tests.

The former allowed to understand the working principles of each solution and to properly tune the parameters of the control algorithm. The latter showed how VSGs works on the field of application, what are their points of weakness and strengths.

Table 14.0.1 summarises the main pros and cons of the analysed VSG solutions.

Table 14.0.1: Main pros and cons of the analysed VSG solutions.

Model	Pros	Cons
Synchron- verter	<ul style="list-style-type: none"> • No PLL needed • Current limitation • Harmonic filtering ac- tion • Grid support during faults • Open-loop voltage control 	<ul style="list-style-type: none"> • Damping-droop cou- pling
Osaka	<ul style="list-style-type: none"> • Damping-droop de- coupling • Harmonic filtering ac- tion • Grid support during faults 	<ul style="list-style-type: none"> • PLL needed • Complex current limi- tation
VISMA	<ul style="list-style-type: none"> • Current limitation • Grid support during faults 	<ul style="list-style-type: none"> • Many parameters • PLL needed • Underdamped re- sponse • No harmonic filtering action

Table 14.0.1 (Continued)

Model	Pros	Cons
VISMA1	<ul style="list-style-type: none"> • Current limitation • Harmonic filtering action • Grid support during faults 	<ul style="list-style-type: none"> • PLL needed
VISMA2	<ul style="list-style-type: none"> • Open-loop voltage control • Harmonic filtering action • Grid support during faults 	<ul style="list-style-type: none"> • PLL needed • Current derivation • Complex current limitation
SPC SG	<ul style="list-style-type: none"> • No PLL needed • Current limitation • Harmonic filtering action • Grid support during faults 	<ul style="list-style-type: none"> • Damping-droop coupling

Table 14.0.1 (Continued)

Model	Pros	Cons
SPC PI	<ul style="list-style-type: none"> • No PLL needed • Current limitation • Damping-droop decoupling • Harmonic filtering action • Grid support during faults 	<ul style="list-style-type: none"> • High sensibility to disturbs
SPC LL	<ul style="list-style-type: none"> • No PLL needed • Current limitation • Damping-droop decoupling • Harmonic filtering action • Grid support during faults 	<ul style="list-style-type: none"> • High sensibility to disturbs

Table 14.0.1 (Continued)

Model	Pros	Cons
VSYNC	<ul style="list-style-type: none"> • No PLL needed • Current limitation • Grid support during faults 	<ul style="list-style-type: none"> • Underdamped response • Harmonic amplification
Kawasaki	<ul style="list-style-type: none"> • Current limitation • Damping-droop decoupling • Grid support during faults 	<ul style="list-style-type: none"> • PLL needed • Harmonic amplification (algebraic impedance)
CVSM	<ul style="list-style-type: none"> • Current limitation • Damping-droop decoupling • Grid support during faults 	<ul style="list-style-type: none"> • Complex tuning • Wrong harmonic compensation (partial impedance emulation)

For the realisation of this master thesis, I carried out the following main activities, which can be considered my personal contributions:

- Bibliography research and study of VSG solutions available in the literature;
- Implementation and tuning of each VSG control algorithm by means of PLECS simulations;
- Realisation of C-codes for the discrete-time version of each solution;
- Adaptation of C-codes for dSPACE environment and the real setup;
- Experimental testing of every VSG model by means of a setup at the laboratory of Power Electronics Innovation Center.

Appendix A

Base Values

In order to facilitate the comparison between the VSG models, it is useful to adopt the per unit notation. Therefore, the base values must be defined. The base values used for the per unit representation are the following:

- Power base value S_b :

$$S_b = 15 \text{ kVA} \quad (\text{A.0.1})$$

It corresponds to the nominal power of the inverter;

- Voltage base value V_b :

$$V_b = 120\sqrt{2} \text{ V} \quad (\text{A.0.2})$$

It corresponds to the peak phase voltage of the grid emulator;

- Frequency base value f_b :

$$f_b = 50 \text{ Hz} \quad (\text{A.0.3})$$

It corresponds to the nominal frequency of the system;

- Speed base value ω_b :

$$\omega_b = 2\pi f_b = 314 \text{ rad/s} \quad (\text{A.0.4})$$

- Current base value I_b :

$$I_b = \frac{2}{3} \cdot \frac{S_b}{V_b} = 58.93 \text{ A} \quad (\text{A.0.5})$$

- Impedance base value Z_b :

$$Z_b = \frac{V_b}{I_b} = 2.88 \Omega \quad (\text{A.0.6})$$

Bibliography

- [1] “IPCC, 2014: Climate Change 2014: Synthesis Report. Contribution of Working Groups I, II and III to the Fifth Assessment Report of the Intergovernmental Panel on Climate Change [Core Writing Team, R.K. Pachauri and L.A. Meyer (eds.)]. IPCC, Geneva, Switzerland, 151 pp.”
- [2] International Energy Agency, “Electricity generation by fuel and scenario, 2018-2040.”
<https://www.iea.org/data-and-statistics/charts/electricity-generation-by-fuel-and-scenario-2018-2040>.
- [3] T. Esum and P. L. Chapman, “Comparison of photovoltaic array maximum power point tracking techniques,” *IEEE Transactions on Energy Conversion*, vol. 22, no. 2, pp. 439–449, 2007.
- [4] European Commission, “Commission Regulation (EU) 2016/631,” 2016.
<http://data.europa.eu/eli/reg/2016/631/oj>.
- [5] Terna - Rete Elettrica Nazionale S.p.A., “Codice di Rete,” 2020.
https://download.terna.it/terna/Codice%20di%20rete%20completo_20200424_8d7e8496cd24dd5.pdf.
- [6] Terna - Rete Elettrica Nazionale S.p.A., “Allegato A.17,” 2019.
https://download.terna.it/terna/Allegato%20A.17_8d787c9c8a17ba6.pdf.
- [7] Terna - Rete Elettrica Nazionale S.p.A., “Allegato A.68,” 2019.
https://download.terna.it/terna/Allegato%20A.68_8d787c9e10c227c.pdf.
- [8] Q. Zhong and G. Weiss, “Static synchronous generators for distributed generation and renewable energy,” in *2009 IEEE/PES Power Systems Conference and Exposition*, pp. 1–6, 2009.

- [9] Q. Zhong and G. Weiss, "Synchronverters: Inverters That Mimic Synchronous Generators," *IEEE Transactions on Industrial Electronics*, vol. 58, pp. 1259–1267, Apr. 2011.
- [10] M. Blau and G. Weiss, "Synchronverters used for damping inter-area oscillations in two-area power systems," *Renewable Energy and Power Quality Journal*, pp. 45–50, 04 2018.
- [11] K. Sakimoto, Y. Miura, and T. Ise, "Stabilization of a power system with a distributed generator by a virtual synchronous generator function," in *8th International Conference on Power Electronics - ECCE Asia*, pp. 1498–1505, 2011.
- [12] Jia Liu, Y. Miura, and T. Ise, "Dynamic characteristics and stability comparisons between virtual synchronous generator and droop control in inverter-based distributed generators," in *2014 International Power Electronics Conference (IPEC-Hiroshima 2014 - ECCE ASIA)*, pp. 1536–1543, 2014.
- [13] H. Beck and R. Hesse, "Virtual synchronous machine," in *2007 9th International Conference on Electrical Power Quality and Utilisation*, pp. 1–6, 2007.
- [14] R. Hesse, D. Turschner, and H.-P. Beck, "Micro grid stabilization using the virtual synchronous machine (VISMA)," *Renewable energy & power quality journal*, vol. 1, pp. 676–681, 2009.
- [15] Y. Chen, R. Hesse, D. Turschner, and H.-P. Beck, "Dynamic properties of the virtual synchronous machine (VISMA)," *Renewable energy & power quality journal*, pp. 755–759, 2011.
- [16] Y. Chen, R. Hesse, D. Turschner, and H. Beck, "Improving the grid power quality using virtual synchronous machines," in *2011 International Conference on Power Engineering, Energy and Electrical Drives*, pp. 1–6, 2011.
- [17] Y. P. Chen, R. Hesse, D. Turschner, and H.-P. Beck, "Comparison of methods for implementing virtual synchronous machine on inverters," *Renewable energy & power quality journal*, pp. 734–739, 2012.
- [18] P. Rodriguez, I. Candela, and A. Luna, "Control of pv generation systems using the synchronous power controller," in *2013 IEEE Energy Conversion Congress and Exposition*, pp. 993–998, 2013.

- [19] W. Zhang, D. Remon, A. Mir, A. Luna, J. Rocabert, I. Candela, and P. Rodriguez, "Comparison of different power loop controllers for synchronous power controlled grid-interactive converters," in *2015 IEEE Energy Conversion Congress and Exposition (ECCE)*, pp. 3780–3787, 2015.
- [20] J. Driesen and K. Visscher, "Virtual synchronous generators," in *2008 IEEE Power and Energy Society General Meeting - Conversion and Delivery of Electrical Energy in the 21st Century*, pp. 1–3, July 2008.
- [21] M. P. N. van Wesenbeeck, S. W. H. de Haan, P. Varela, and K. Visscher, "Grid tied converter with virtual kinetic storage," in *2009 IEEE Bucharest PowerTech*, pp. 1–7, 2009.
- [22] Y. Hirase, K. Abe, K. Sugimoto, and Y. Shindo, "A grid connected inverter with virtual synchronous generator model of algebraic type," *IEEE Transactions on Power and Energy*, vol. 132, pp. 371–380, 01 2012.
- [23] S. D'Arco, J. A. Suul, and O. B. Fosso, "Control system tuning and stability analysis of virtual synchronous machines," in *2013 IEEE Energy Conversion Congress and Exposition*, pp. 2664–2671, 2013.
- [24] S. D'Arco, J. A. Suul, and O. B. Fosso, "Small-signal modeling and parametric sensitivity of a virtual synchronous machine in islanded operation," *International Journal of Electrical Power & Energy Systems*, vol. 72, pp. 3 – 15, 2015. The Special Issue for 18th Power Systems Computation Conference.
- [25] *Grid Synchronization in Single-Phase Power Converters*, ch. 4, pp. 43–91. John Wiley & Sons, Ltd, 2010.
- [26] *Grid Synchronization in Three-Phase Power Converters*, ch. 8, pp. 169–204. John Wiley & Sons, Ltd, 2010.
- [27] P. Kundur, N. Balu, and M. Lauby, *Power System Stability and Control*. EPRI power system engineering series, McGraw-Hill Education, 1994.
- [28] H. Bevrani, T. Ise, and Y. Miura, "Virtual synchronous generators: A survey and new perspectives," *International Journal of Electrical Power & Energy Systems*, vol. 54, pp. 244 – 254, 2014.

- [29] F. Mandrile, E. Carpaneto, and R. Bojoi, "Virtual synchronous generator with simplified single-axis damper winding," in *2019 IEEE 28th International Symposium on Industrial Electronics (ISIE)*, pp. 2123–2128, 2019.
- [30] F. Mandrile, E. Carpaneto, E. Armando, and R. Bojoi, "Simple tuning method of virtual synchronous generators reactive control," in 2020 IEEE Energy Conversion Congress and Exposition, 2020, In press.
- [31] G. Delille, B. Francois, and G. Malarange, "Dynamic frequency control support by energy storage to reduce the impact of wind and solar generation on isolated power system's inertia," *IEEE Transactions on Sustainable Energy*, vol. 3, no. 4, pp. 931–939, 2012.
- [32] B. S. Institution, "Electromagnetic compatibility (EMC). Environment. Voltage dips and short interruptions on public electric power supply systems with statistical measurement results," tech. rep., 2003.